FLUORESCENCE-GUIDED THERAPY IN ONCOLOGY

TARGETED IMAGING AND PHOTODYNAMIC THERAPY

Pieter B. A. A. van Driel

Fluorescence-guided Therapy in Oncology

Targeted imaging and photodynamic therapy

Pieter Bastiaan Arie Antonius van Driel

Fluorescence-Guided Therapy in Oncology

Targeted imaging and photodynamic therapy

Fluorescentie-geleide oncologische therapie

Gerichte beeldvorming en fotodynamische therapie

Proefschrift

ter verkrijging van de graad van doctor aan de
Erasmus Universiteit Rotterdam
op gezag van de Rector magnificus
Prof. dr. R.C.M.E. Engels

en volgens besluit van het College voor Promoties.
De openbare verdediging zal plaatsvinden op

24 - 10 - 2018 om 09:30 uur

Door

Pieter Bastiaan Arie Antonius van Driel

geboren te Arnhem

Promotor: Prof. dr. C.W.G.M. Löwik

Overige leden: Prof. dr. ir. M. Hendriks- de Jong
                 Prof dr. C. Verhoef
                 Prof. dr. R.J. Baatenburg de Jong

Copromotor:en: Dr. A.L. Vahrmeijer
                 Dr. S. Keereweer

Contents

CHAPTER 1

General introduction and outline of the thesis

Introduction

Over the last century, preoperative imaging has been of major importance for pre -operative planning of surgical procedures. At the end of the nineteenth century, Wilhelm Conrad Rontgen created the x-ray Radiograph for which he received the Nobel Prize in 1901. Not long thereafter, Franz Konig was the first to describe tumour imaging when he reported the detection of a sarcoma of the tibia. Imaging modalities further evolved with the development of the computerized tomography in 1972 by Hounsfiels who received the Nobel Price in 1979 and with magnetic resonance imaging in 1973. Both of major importance for the field of cancer imaging. Since then, many developments have been made including PET and SPECT (Beaney, 1984; Jaszczak and Coleman, 1985). In clinical practice, the various non-invasive imaging modalities including ultrasonography, x-ray, CT, MRI, positron emission tomography and singlephoton-emission computed tomography enable early detection, staging, and treatment evaluation of cancer.

Although many preoperative imaging modalities are currently available, during surgery the surgeon is only incidentally assisted by intraoperative imaging modalities such as ultrasonography and x-ray fluoroscopy for further analysis of tissue (Flum et al., 2003; Leen et al., 2006). Presently, surgeons mostly discriminate healthy tissue from cancerous tissue by means of visual inspection and palpation, and subsequently resect the tumour with an adequate tumour-free margin. High percentages of non-radical tumour resections have been described in clinically (based on vision and palpation) radical resected tumours (McMahon et al., 2003). To illustrate, local recurrence after curative primary surgery of cancer in the oral cavity has been reported to be 22% (Rusthoven et al., 2010). Postoperative radiotherapy is therefore usually administered to prevent local recurrence. However, despite such radiotherapy following treatment of tongue tumours, many patients have been observed to redevelop tumours locally (Brown et al., 2007; Rusthoven et al., 2010). The inability to adequately detect the tumour border could be of importance in the high rate of non-radical resections. Therefore, intraoperative imaging may promise an improvement of radical resections of tumours, thus increasing patients' survival rates. Fluorescence imaging is a highly potential imaging modality that provides the surgeon with necessary real-time information and could therefore have major impact in future surgical oncology. Although fluorescence imaging gained some interest in the early twentieth century, this technology was not further developed due to the absence of necessary knowledge and technical support at that time. With the advent of knowledge and technical support in the 1980s, optical imaging regained interest. Exciting research became available because optical imaging made it possible to image processes at molecular level in real time. Several wavelengths were used but particularly, the advantages of the use of near-infrared light (NIR 700-900 nm, **Figure 1**), that is

the closest in wavelength to visible light were important for the potential use of fluorescence intra-operatively (Patterson et al 1989).
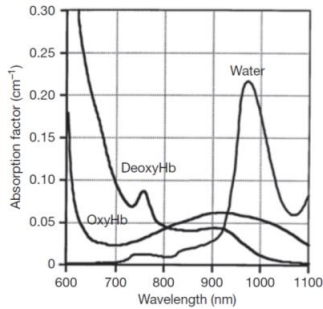

Figure 1; Illustrating the 'NIR window,' delimiting on the one side by the increasing absorbance of blood and on the other side by the increasing absorbance of water. Reproduced from Chance B. (1998) Near-infrared images using continuous, phase-modulated, and pulsed light with quantitation of blood and blood oxygenation. Annals of the New York Academy of Sciences 838: 29–45.

NIR light appeared to be much less absorbed and thus penetrate tissue much deeper than visible light or light above 900 nm. Furthermore, lower autofluorescence was observed using NIR light compared to that with visible light where autofluorescence hampered a good contrast (Frangioni 2003). Finally, for an adequate intra-operative implementation it was of importance not to alter the regular surgical field. As the human eye is not sensitive to NIR fluorescent light the surgical field remains unstained. On the other hand, it raised the challenge of developing NIR fluorescence camera systems. When imaging modalities became available, acquisition time in the millisecond range was possible, enabling real-time imaging. Altogether this paved the way for the development of real-time intra-operative fluorescence imaging (Vahrmeijer et al. 2013).

In practice, NIR fluorescent contrast agents are administered intravenously, topically or intraparenchymally. During surgery the contrast agent is visualized using a NIR fluorescence camera system (**Figure 2)**. For intraoperative imaging purposes that do not require a specific molecular target, such as in sentinel lymph node (SLN) mapping or vascular imaging, a single contrast agent (fluorophore) can be used. Indocyanine green (ICG) and methylene blue are currently the only NIR fluorophores registered by the Food and Drug Administration (FDA) or the European Medicines Agency (EMA). Although ICG has been used since 1950, initially it was primary used in hepatic function diagnostics and cardiology. But, as soon as intra-operative imaging systems became available many clinical trials on SLN mapping were undertaken (Schaafsma et al. 2011). In contrast to SLN or vascular imaging, in tumour imaging mainly specific molecular targets are used. In this, a contrast agent is conjugated to a targeting moiety that targets one of the hallmarks of cancer. In the past decade many research has been devoted to find the optimal probe that offers the ultimate tumour-to-background ratio (TBR). Whether a probe adequately detects a tumour cell intra-operatively depends on many variables.
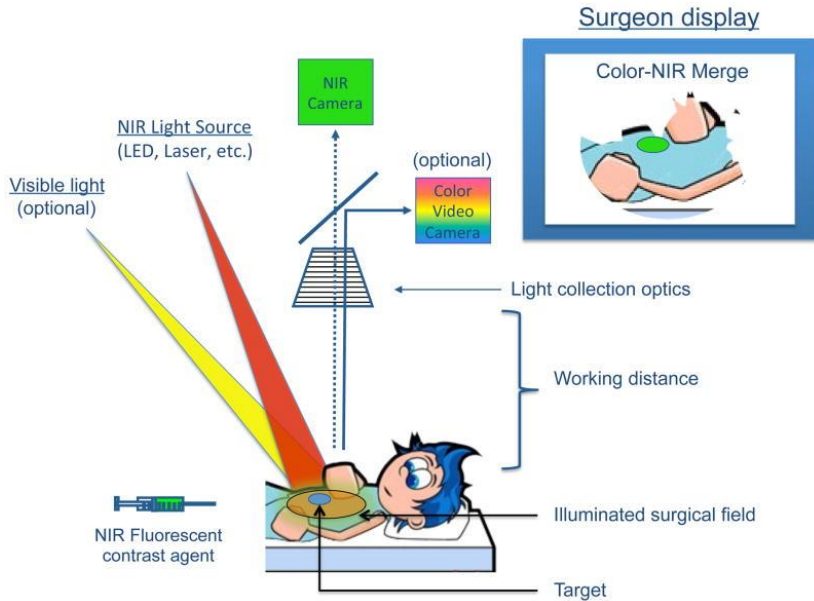
Figure 2; The mechanics of NIR fluorescence imaging. A NIR fluorescent contrast agent is administered intravenously, topically, or intraparenchymally. During surgery, the agent is visualized using a NIR fluorescence imaging system of the desired form factor, i.e., above the surgical field for open surgery or encased within a fiberscope for minimally-invasive and robotic surgery (open surgery form factor shown). All systems must have adequate NIR excitation light, collection optics and filtration, and a camera sensitive to NIR fluorescence emission light. An optimal imaging system includes simultaneous visible (i.e., white) light illumination of the surgical field, which can be merged with NIR fluorescence images. The surgeon display can be one of several forms factors including a standard computer monitor, goggles, or a wall projector (monitor form factor shown). Current imaging systems operate at a sufficient working distance that enables the surgeon to operate and illuminates a sizable surgical field.

Target

The growing insight in cancer is increasingly pointing toward multifactorial processes[1, 2]. In 2000, Hanahan and Weinberg (2000) reported six essential alterations in cell physiology that collectively dictate malignant growth. In 2011 the hallmarks were revised and two emerging hallmarks and enabling characteristics were added. Preclinically, many targeting moieties of these hallmarks have been explored in the past decennium (Keereweer et al. 2011). Nonetheless, cancer targeting with high sensitivity and specificity remains challenging, mostly because of a great extent of intra- and intertumoral heterogeneity (Gerlinger et al., 2012; Marusyk et al., 2012). Hence, the search for a universal tumour-specific target remains to be ongoing.

1

Probe efficiency

The efficiency of agents to specifically target a single tumour cell is essential when distinguishing tumour cells from healthy tissue. Several factors influence the ability of the probe to reach its target. A first important factor in probe efficiency that has a large influence on the TBR is the number of receptors or epitopes per cell (Gioux et al., 2010). On average, a cancer cell expresses 10^3–10^4 surface receptors to which the NIR fluorescent probe can bind (Frangioni, 2008; Hilderbrand and Weissleder, 2010). High expression of the antigen allows more fluorophores to accumulate, resulting in higher concentrations and signal (Thurber et al., 2010). Also, the process of endocytosis can amplify the fluorescence signal, partly depending on the tumour size (Gioux et al., 2010; Kovar et al., 2009). In larger tumours, TBRs ranging from 3 to 12 are often reported. However, smaller tumours often have much higher ratios due to more efficient diffusion and endocytosis (Thurber et al., 2010). Secondly, probe concentrations in the tumour ranging from picomolar to low nanomolar levels are required to generate sufficient TBR for image-guided surgery (Gioux et al., 2010). The dose of the probe is highly important to obtain an adequate TBR. With saturating doses the extent of antibody uptake is dependent on antigen expression levels. Nonetheless, at subsaturating doses, it is mostly the delivery which hampers the fluorescent signal (Thurber and Weissleder, 2011). A third factor in probe efficiency is the biodistribution of the probe. Although in fact an intrinsic property of the probe, the biodistribution has great influence on detection thresholds and the TBR. An adequate vascularization of the tumour is indispensable for probe delivery. Tumours exceeding the size of 1 mm are in need of their own vascularization to supply oxygen and nutrients (Naumov et al., 2006). However, tumours smaller than 1 mm usually have inadequate vascularization which hampers the delivery of probes. Once the probe is nearby tumour tissue, the wall of a blood vessel serves as a barrier between tumour cells and the intravascular environment. Most tumours induce disorganized and abnormal neovascularization, resulting in leaky blood vessels. In addition, lymphatic drainage architecture of the tumour is disordered. This results in enhanced permeability and retention (EPR effect), a universal effect of tumours that causes passive passage over endothelium and accumulation of the probe in the interstitium of tumour tissue (Fang et al., 2011). After the extracellular matrix is traversed, the probe needs sufficient time to interact with the target for binding to occur and the unbounded probe to be cleared from the circulation (Fang et al., 2011; Frangioni, 2003). Clearance from circulation occurs through the liver and/or kidneys via excretion into bile/feces and urine, respectively. The best time of optimal imaging with low background signal present is greatly dependent on clearance route and clearance rate (Gioux et al., 2010).

Fluorescent Dye

The chemical properties of the probe, consisting of a targeting moiety and fluorophore, form an alternative important cluster of factors in fluorescence imaging abilities. In principle, a fluorophore should not alter the biodistribution and efficiency of the targeting moiety. The fluorophore's high fluorescent signal at the site of interest is subject to several criteria: wavelength, quantum yield (QY), photobleaching, clearance, nonspecificity, solubility, and toxicity. First, as mentioned earlier, the most efficient wavelength for clinical applications is the NIR region. In this region, the influence of autofluorescence is limited, and due to diminished absorption, maximum penetration depth is achieved. An extensively used chemical structure to achieve absorption and emission in the NIR region is the polymethine backbone (e.g., used in ICG and Cy5) (Gioux et al., 2010). The second criterion is the QY. The efficiency of the fluorescence process is determined by the QY of the fluorophore that is defined as the ratio of the number of photons emitted divided by the number of photons absorbed. When every absorbed photon results in a photon emitted, maximum QY is obtained. Heptamethine dyes (emission 800 nm) generally have a serum QY between 10% and 20% (Gioux et al., 2010). Third, photobleaching refers to the permanent loss of the ability to fluoresce due to photochemical damage. Photobleaching can occur when a dye-specific photobleaching threshold is reached. Rapid photobleaching restrains the use of a higher fluence rate that potentially can improve the TBR (Frangioni, 2003). The ideal fluorescent dye should further be cleared rapidly, preferentially through renal clearance and should not bind to any proteins. Nonspecific background binding of the dye to proteins, cellular membranes, and extracellular matrix materials will increase background fluorescence and degrade the TBR (Kairdolf et al., 2008). Moreover, a high uptake of a fluorescent dye in the liver will result in contamination of the gastrointestinal tract and decrease the ability to detect primary tumours or metastases in this area. Therefore, rapid renal clearance is preferential. Recently, Choi et al. found that rapid clearance by the kidneys and low background binding was achieved when fluorescent dyes had a neutral surface charge, were geometrically balanced and polyionic (Choi et al., 2011). Finally, for practical use, a fluorescent dye has to be soluble and nontoxic. When a fluorophore meets all these criteria, the targeting moiety will account for the greater part of the efficiency of the probe.

Camera

In order to be used inside an operation room, high fundamental requirements are set for the NIR image-guided camera system. The camera system has to comply with current standard surgical procedures and (logistic) protocols, as well as provide sufficient freedom of motion for the surgeon. Also, transillumination and light-conducting liquid media cannot be used intraoperatively with the current state of the art technology. Gioux et al. (2010) offer a comprehensive overview of requirements and limitations of an intraoperative imaging system,

including the required field of view, the fluorescence excitation light source, the NIR excitation fluence rate, simultaneous imaging of color 'white light' video, and collection optics and cameras. For lesions located at the surface, the detection threshold is a function of TBR and magnification (Thurber et al., 2010). In order to accommodate various surgical applications, a field of view of 10–20 cm (4–8 in.) is required (Gioux et al., 2010). However, in order to increase the detection threshold, as well as for surgical resection of small tumour volumes and avoidance of thin nerves, adjustable field of view by either zoom or fixed magnification lensing is necessary (Gioux et al., 2010).

Autofluorescence

Fluorescence imaging is based on the concept of signal-to-background ratio, which is usually called tumour-to-background ratio (TBR) in the case of cancer imaging. For the targeted cancer cells to be detected, the tumour-specific signal must be significantly discriminated from the nonspecific surrounding signal. However, cells contain endogenous fluorophores which fluoresce when excited with light of the appropriate wavelength. Autofluorescence refers to this intrinsic fluorescence of the tissue that induces a nonspecific background signal (Keereweer et al., 2011). When autofluorescence is high, the TBR is decreased, which hampers the identification of fluorescence signals with lower intensity. In the visible light region, autofluorescence is the main limiting factor of most in vivo optical imaging applications. Although the use of invisible NIR light solves a great deal of this problem, NIR autofluorescence signals still occur and may vary between different tissues (Frangioni, 2003). Therefore, the influence of autofluorescence on the TBR is an important determinant of detection thresholds in optical imaging. The effect of autofluorescence can be reduced by separating the signal of the targeted fluorophores from the background signal during optical imaging in vivo. Two methods are used to achieve such disjunction of signals, namely, by unmixing the fluorescence spectrum (i.e., 'spectral unmixing') of each fluorophore or by imaging the lifetime of a fluorophore (Akers et al., 2008; Mansfield, 2010). These are useful techniques when distinguishing a specific signal, for example, a molecular event, or highlighting a signal against background autofluorescence.

Optical properties

Although optical properties of the imaged tissue have significant influence on the acquired fluorescent light intensity, the influence of these properties is often unappreciated in optical image-guided cancer surgery. Light must travel through tissue to reach a fluorescent contrast agent. The degree in which such photons actually reach the target depends on the tissue's absorption and scattering properties, which both become more hindering factors with increasing light penetration depth (Frangioni, 2003)(**Figure 3**). After excitation, the photon emitted by the fluorophore is subject to the same influences once more as they travel back to the surface.
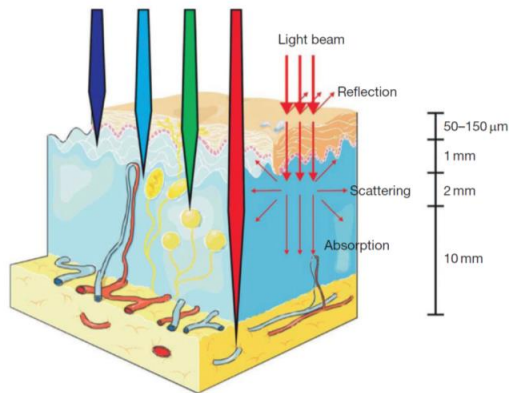
Figure 3; Light propagation through the tissues. Light traveling through tissue will undergo reflection, scattering, and absorption..

In this manner, fluorescence intensity is modulated by the tissue optical properties of absorption, scattering, and tissue penetration depth, which are important to consider when quantification of the signal is required (Themelis et al., 2009). The NIR range is the most suitable range for clinical applications due to deep penetration of light into tissue. Despite this advantageous quality of NIR light, it is still subject to absorption and scattering. Absorption denotes that photons traveling through tissue can be absorbed by intrinsic components of that tissue. The main light absorbers in tissue, responsible for the minimal cumulative absorbance of NIR fluorescence, are oxyhemoglobin, deoxyhemoglobin, water, and lipids (Chance, 1998). However, the most important contributor to absorbance of NIR wavelengths in regular tissues (containing 8% blood volume and 29% lipid content) is hemoglobin, as it accounts for 39–64% of the total light absorbance (Frangioni, 2003). This explains why fluorescent signals in organs or tissues with high blood volumes, such as the liver (Hutteman et al., 2011), highly vascularized tumours, or tumour cells that co-opt host vessels (Holash et al., 1999), may appear lower than surrounding, less-absorbing tissue (even if they contain larger amounts of contrast agent compared to the surrounding tissue) (Themelis et al., 2009). This shows how absorption may prove an important confounder of TBR and how it results in a lower detection threshold. Another challenge to the use of NIR light in optical imaging is posed by scattering. Due to refractive index mismatches between tissue components the direction of a photon will vary during its journey through tissue. This phenomenon is known as scattering. Although a single scatter event may not have a large effect on photon direction by itself, the cumulative effect of multiple consecutive scatter events may result in a significant photon deflection. In tissues, this effect can have a 100- to a 1000-fold higher distortion of the fluorescence signal than absorption. However, despite the probability of such a change in direction, forward movement of the photon is most likely to occur

1

(Ntziachristos, 2010). Scatter and absorption coefficients vary between locations and tissues due to the different components within the heterogeneous tissue. Intratumour heterogeneity could even induce different TBRs between the same population of tumours (Marusyk et al., 2012). The net effect of scattering and absorption on fluorescence imaging depends on the exact optical properties of the tissue under scrutiny.

Effects on light at greater penetration depths

Both absorption and scattering are important influences on the assessment of detection thresholds of the NIR-fluorescent signal. The influence of these effects on the fluorescence signal will be greater when tissue depth increases. Using visible light, penetration depth is limited to a few millimeters due to light absorption by biological chromophores (Keereweer et al., 2011). With light emitted in the NIR spectrum, penetration depth of higher wavelengths is increased to over a centimeter (Frangioni, 2008; Hilderbrand and Weissleder, 2010; Weissleder and Pittet, 2008). Although the absorption and scattering of light varies significantly between tissues, in general, fluorescence intensity has a strong nonlinear dependence on the depth of the fluorescence activity (Frangioni, 2003; Themelis et al., 2009; Thurber et al., 2010). A clear correlation has been demonstrated between increased penetration depth, increased scattering, and decreased fluorescence signal (Pleijhuis et al., 2011). Hence, superficial lesions will appear brighter than an identical lesion that is located deeper in the tissue.

Despite the aforementioned challenges in probe development and limitations of fluorescence-guided surgery due to optical properties, clinical application is still very appealing. During surgery, tumours can be explored after resection and the remaining surroundings can be scanned for residual tumour cells, indicating irradical margins. When an area is found with persisting fluorescence signal, this can subsequently be excised until no signal is detected any longer, similar to the technique of Mohs' surgery (Mohs, 1957). Nevertheless, although in the future even a single cell can be imaged on the surface, optical properties will probably hamper detection of cancer cells situated under the surface. This may require the need of adjuvant therapy. Further, high-risk pathological characteristics could justify adjuvant therapy. In these selected cases, intra-operative photodynamic therapy (PDT) could be of great value after fluorescence-guided surgery.

Adjuvant targeted photodynamic therapy

In PDT, photosensitizers are used that produce cytotoxic reactive oxygen species after excitation by light with a specific wavelength. As a result, cancer cells are killed by apoptosis and/or necrosis, and tumour microvasculature is obliterated (Agostinis et al. 2011; Castano et al. 2006). Specific damage of the tissue of interest is obtained by local illumination. Furthermore, the very short half-life of cytotoxic reactive oxygen species ensures that damage only occurs in the immediate vicinity of its formation. Although conventional adjuvant treatments (i.e., radiotherapy, chemotherapy, or a combination) can induce immunosuppression, PDT-induced immunogenic cell death induces a local inflammatory reaction and stimulates the host immune system (Castano et al. 2006). In addition, formation of a tumour specific immune response (e.g., production of tumour-specific cytotoxic T-cells) offers opportunities to treat distant metastases (Castano et al. 2006). Compared to other adjuvant therapeutic modalities, PDT has the potential to induce low toxicity in normal tissue, produce negligible systemic effects, and reduce acute and long-term morbidity (Agostinis et al. 2011). Furthermore, PDT does not compromise future treatment options for patients with residual or recurrent disease and can be repeated with perpetual efficacy. Wavelength-specific excitation of photosensitizers could technically be performed using the same imaging systems as those used for optical image-guided surgery, emphasizing its practical advantages as an adjuvant therapeutic modality in the surgical theatre. In order to fully exploit the advantages of both modalities, a tumour-specific NIR fluorescent photosensitizer is required (Bugaj, 2011). A tumour-specific photosensitizer has the potential to be much more efficient and cause less damage to surrounding normal tissue than a non-specific photosensitizer (Bugaj, 2011). The increasing amount of photosensitizer that is expected to accumulate in the tissue of interest ensures that less light is required to induce a cytotoxic reaction. Consequently, even light that penetrates deeper into tissue (>1 cm) will result in specific damage of tumour cells that are deeper located. Moreover, such an agent could be used for both NIR fluorescence image-guided surgery and adjuvant PDT (i.e., a **"theranostic"**).

1

Outline of the thesis

In **part I** the current modalities of fluorescence-guided surgery and the challenges in optical imaging are reviewed. **Chapter 2** gives an extensive overview of the preclinical and clinical data in fluorescence-guided oncologic surgery to reflect its current status. In particular, it focuses on specific targeting of primary tumours by organic fluorescent agents that target the alterations in cell physiology in cancer. Data is presented per hallmark of cancer as described by Hannahan and Weinberg (2000, 2011) In **Chapter 3** the fundamental basic principles of optical imaging are studied. Here, the consequences of these principles on FGS and the influence on clinical decision-making are discussed in more detail. It illustrates how the technique can be a very powerful tool in guiding the surgeon to radical tumour resections, as long as the intrinsic limitations of this technique are taken into account.

In **Part II**, preclinical studies are performed using probes that target two different receptors in oncology.   Multiple clinically relevant tumour models are used to validate FGS in primary tumours, lymph node metastases and distant metastases. The first target that was explored is the epidermal growth factor receptor (EGFR) in **chapter 4**. The EGFR is a transmembrane glycoprotein that is involved in DNA synthesis and cell proliferation and overexpression contributes to oncogenesis. Because EGFR is highly overexpressed in oral squamous cell carcinomas (OSCC), an orthotopic OSCC of the tongue that metastasises to the cervical lymph nodes was used. In this study, a nanobody was conjugated to the fluorophore IRDye-800CW. A nanobody is the smallest functional antigen-binding fragment derived from naturally occurring heavy-chain-only antibodies. They show very specific binding to their targets and their size ensures efficient distribution and tissue penetration, as well as rapid clearance from the body. The FLARE NIR fluorescence camera was used for NIR fluorescence imaging. The camera was compared to preclinical cameras where measurements are performed in an ultimate environment that is created by imaging in a 'black box' to shield interfering ambient light. In search for an even more universal receptor, the epithelial cell adhesion molecule was evaluated in **chapter 5**. EpCAM is a transmembrane glycoprotein involved in cell-cell interactions and cell-stroma adhesion. Its expression is restricted to epithelial cells and is highly up-regulated in virtually all epithelial carcinomas. To assess the value of this target in FGS the monoclonal chimeric antibody 323/A3 was conjugated to the IRDye 800CW.   Four clinically relevant orthotopic tumour models, i.e. colorectal cancer, breast cancer, head and neck cancer, and peritonitis carcinomatosa were used to evaluate the performance of the anti-EpCAM agent with the clinically validated Artemis imaging system. Next, in **chapter 6,** the performance of the new Artemis camera was evaluated preclinically as well as clinically. In this article the Artemis camera was presented in literature for the first time. The minimal detectable dose of pure ICG and IRDye 800CW was

searched for *in vitro*. Subsequently, the lower limit of cells targeted by the EGFR targeting nanobody 7D12-800CW was determined. *In vivo,* the camera was evaluated in two procedures namely sentinel lymph node imaging and tumour specific FGS. Two head and neck cancer cell lines were used in combination with 7D12-800CW and the minimal size of tumour mass that could be visualized was explored. Further, for the first time, clinical evaluation of cancer patients using the NIR Artemis camera was described. Fluorescence imaging of ICG was performed in three patients with liver metastases.

In **part III** the focus was on the future of fluorescence-guided surgery. In **chapter 7** three major challenges in FGS were described and subsequently possible solutions were postulated. The challenges in FGS described here comprise imaging tumour heterogeneity, invasive tumour strands and dealing with the tissue optical properties. Tissue optical properties ensure that it is most unlikely that the last residual tumour cells will be visualized using FGS. Mainly in invasive tumour strands this could hamper radical tumour resections. To overcome the hurdle of optical properties and detect the last tumour cells, intrinsic fluorescence measurements can be performed intra-operatively. It was described how point reflectance and fluorescence spectroscopy using fiber optic probes can be used to overcome the effects of tissue optical properties and detect residual tumour cells. A second promising solution to detect and treat the remaining tumour cells is adjuvant photodynamic therapy. PDT is a promising minimally invasive approach that is being used for the local treatment of premalignant and malignant lesions. Despite the potential advantages of PDT, collateral damage to normal tissue remains a significant side effect, particularly in the treatment of large tumours. Targeted PDT, in which photosensitizers (PS) are selectively delivered to the tumour, could greatly enhance the efficacy of PDT. In **chapter 8**, a feasibility study is reported at the pre-clinical level on a recently introduced format of targeted PDT which employs nanobodies as targeting agents and a water-soluble PS (IRDye700DX) that can be used as fluorescence agent as well. The photosensitizer IRDye700DX was conjugated to the EGFR targeting nanobody 7D12 and the selectivity and phototoxicity was explored in an orthotopic head and neck cancer model. In **chapter 9**, the steps required for successful and safe implementation of intraoperative fluorescence imaging in the clinic were identified. The major topics on the critical path of implementation were identified and the possible actions discussed to overcome them. A main driving conclusion remained that intraoperative fluorescence imaging has great clinical potential and that with the community working together the clinical implementation of FGS could be substantially accelerated. Finally, in **chapter 10** the results of the studies in this thesis were summarized followed by a discussion on future perspectives of fluorescence-guided therapy in oncology.

1

This thesis demonstrates the use of fluorescence-guided therapy in oncology. First it shows the preclinical validation of two different targets and probes for fluorescence-guided surgery, results that pave the way towards clinical implementation. Next, the utility of the NIR fluorescence Artemis camera is described. Lastly, the first steps are made towards fluorescence theranostics in oncology: NIR fluorescence-guided surgery and intra-operative targeted photodynamic therapy.

References

- Agostinis P, Berg K, Cengel KA et al. (2011) Photodynamic therapy of cancer: an update. A Cancer Journal for Clinicians 61 (4):250-81

- Akers WJ, Berezin MY, Lee H, and Achilefu S (2008) Predicting in vivo fluorescence lifetime behavior of near-infrared fluorescent contrast agents using in vitro measurements. Journal of Biomedical Optics 13: 054042.

- Beaney RP (1984) Positron emission tomography in the study of human tumours. Seminars in Nuclear Medicine 14: 324–341.

- Brown JS, Blackburn TK, Woolgar JA, et al. (2007) A comparison of outcomes for patients with oral squamous cell carcinoma at intermediate risk of recurrence treated by surgery alone or with post-operative radiotherapy. Oral Oncology 43: 764–773.

- Bugaj AM (2011) Targeted photodynamic therapy – a promising strategy of tumour treatment. Photochemical & Photobiological Sciences 10(7):1097-109

- Castano AP, Mroz P, Hamblin MR (2006) Photodynamic therapy and anti-tumour immunity. Nature Review Cancer. 6(7):535-45

- Chance B (1998) Near-infrared images using continuous, phase-modulated, and pulsed light with quantitation of blood and blood oxygenation. Annals of the New York Academy of Sciences 838: 29–45.

- Choi HS, Nasr K, Alyabyev S, et al. (2011) Synthesis and in vivo fate of zwitterionic near-infrared fluorophores. Angewandte Chemie International Edition in English 50: 6258–6263.

- Fang J, Nakamura H, and Maeda H (2011) The EPR effect: Unique features of tumour blood vessels for drug delivery, factors involved, and limitations and augmentation of the effect. Advanced Drug Delivery Reviews 63: 136–151.

- Flum DR, Dellinger EP, Cheadle A, Chan L, and Koepsell T (2003) Intraoperative cholangiography and risk of common bile duct injury during cholecystectomy. JAMA: The Journal of the American Medical Association 289: 1639–1644.

- Frangioni JV (2003) In vivo near-infrared fluorescence imaging. Current Opinion in Chemical Biology 7: 626–634.

- Frangioni JV (2008) New technologies for human cancer imaging. Journal of Clinical Oncology 26: 4012–4021.

- Friedl P, Alexander S (2011) Cancer invasion and the microenvironment: plasticity and reciprocity. Cell 147(5):992-1009

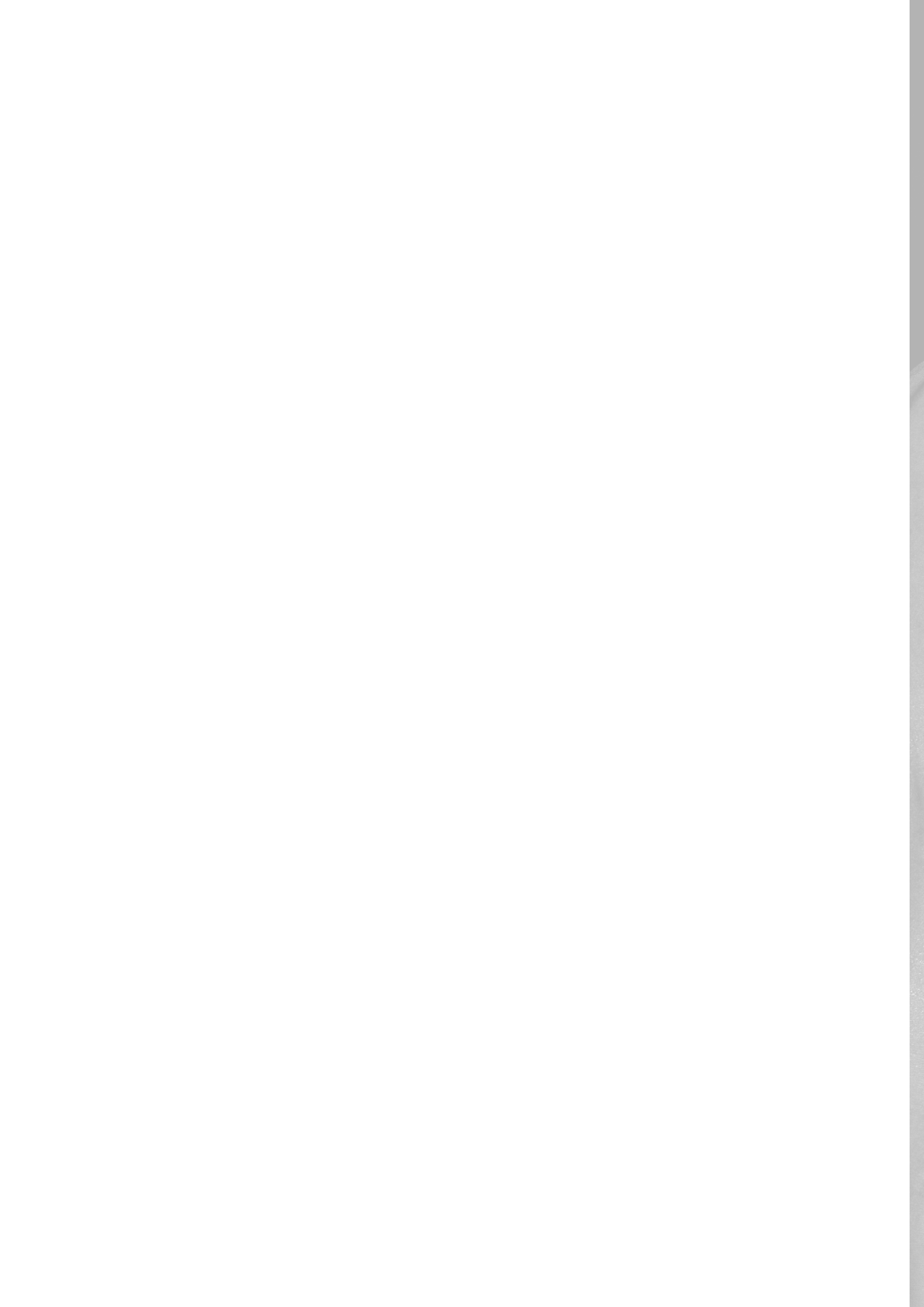- Gerlinger M, Rowan AJ, Horswell S, et al. (2012) Intratumour heterogeneity and branched

evolution revealed by multiregion sequencing. The New England Journal of Medicine 366: 883–892.

- Gioux S, Choi HS, and Frangioni JV (2010) Image-guided surgery using invisible nearinfrared light: Fundamentals of clinical translation. Molecular Imaging 9: 237–255.

- Hanahan D and Weinberg RA (2000) The hallmarks of cancer. Cell 100: 57–70.

- Hilderbrand SA and Weissleder R (2010) Near-infrared fluorescence: Application to in vivo molecular imaging. Current Opinion in Chemical Biology 14: 71–79.

- Holash J, Maisonpierre PC, Compton D, et al. (1999) Vessel cooption, regression, and growth in tumours mediated by angiopoietins and VEGF. Science 284: 1994–1998.

- Hutteman M, Mieog JS, van der Vorst JR, et al. (2011a) Intraoperative near-infrared fluorescence imaging of colorectal metastases targeting integrin alpha(v)beta(3) expression in a syngeneic rat model. European Journal of Surgical Oncology 37: 252–257.

- Jaszczak RJ and Coleman RE (1985) Single photon emission computed tomography (SPECT). Principles and instrumentation. Investigative Radiology 20: 897–910.

- Kairdolf BA, Mancini MC, Smith AM, and Nie S (2008) Minimizing nonspecific cellular binding of quantum dots with hydroxyl-derivatized surface coatings. Analytical Chemistry 80: 3029–3034.

- Keereweer S, Kerrebijn JD, van Driel PB, et al. (2011a) Optical image-guided surgery – Where do we stand? Molecular Imaging and Biology 13: 199–207.

- Kovar JL, Volcheck W, Sevick-Muraca E, Simpson MA, and Olive DM (2009) Characterization and performance of a near-infrared 2-deoxyglucose optical imaging agent for mouse cancer models. Analytical Biochemistry 384: 254–262.

- Leen E, Ceccotti P, Moug SJ, et al. (2006) Potential value of contrast-enhanced intraoperative ultrasonography during partial hepatectomy for metastases: An essential investigation before resection? Annals of Surgery 243: 236–240.

- Mansfield JR (2010) Distinguished photons: A review of in vivo spectral fluorescence imaging in small animals. Current Pharmaceutical Biotechnology 11: 628–638.

- Marusyk A, Almendro V, and Polyak K (2012) Intra-tumour heterogeneity: A looking glass for cancer? Nature Reviews. Cancer 12: 323–334.

- McMahon J, O'Brien CJ, Pathak I, et al. (2003) Influence of condition of surgical margins on local recurrence and disease-specific survival in oral and oropharyngeal cancer. British Journal of Oral and Maxillofacial Surgery 41: 224–231.

- Mohs FE (1957) Chemosurgical method for microscopically controlled excision of cancer. American Journal of Proctology 8: 273–282.

- Naumov GN, Akslen LA, and Folkman J (2006) Role of angiogenesis in human tumour dormancy: Animal models of the angiogenic switch. Cell Cycle 5: 1779–1787.

- Ntziachristos V (2010) Going deeper than microscopy: The optical imaging frontier in biology. Nature Methods 7: 603–614.

- Patterson MS, Chance B, and Wilson BC (1989) Time resolved reflectance and transmittance for the non-invasive measurement of tissue optical properties. Applied Optics 28: 2331–2336.

- Pleijhuis RG, Langhout GC, Helfrich W, et al. (2011) Near-infrared fluorescence (NIRF) imaging in breast-conserving surgery: Assessing intraoperative techniques in tissue-simulating breast phantoms. European Journal of Surgical Oncology 37: 32–39.

- Rusthoven KE, Raben D, Song JI, Kane M, Altoos TA, and Chen C (2010) Survival and patterns of relapse in patients with oral tongue cancer. Journal of Oral and Maxillofacial Surgery 68: 584–589.

- Schaafsma BE, Mieog JS, Hutteman M, et al. (2011) The clinical use of indocyanine green as a near-infrared fluorescent contrast agent for image-guided oncologic surgery. Journal of Surgical Oncology 104: 323–332.

- Themelis G, Yoo JS, Soh KS, Schulz R, and Ntziachristos V (2009) Real-time intraoperative fluorescence imaging system using light-absorption correction. Journal of Biomedical Optics 14: 064012.

- Thurber GM, Figueiredo JL, and Weissleder R (2010) Detection limits of intraoperative near infrared imaging for tumour resection. Journal of Surgical Oncology 102: 758–764.

- Thurber GM and Weissleder R (2011) Quantitating antibody uptake in vivo: Conditional dependence on antigen expression levels. Molecular Imaging and Biology 13: 623–632.

- Vahrmeijer AL, Hutteman M, van der Vorst JR, van de Velde CJ, Frangioni JV (2013) Image-guided cancer surgery using near-infrared fluorescence. Nature Review Clinical Oncology 10(9):507-18

- Weissleder R and Pittet MJ (2008) Imaging in the era of molecular oncology. Nature 452: 580–589.

I

Current modalities and challenges in optical fluorescence-guided surgery

CHAPTER 2

Fluorescence-guided surgery: a promising approach for future oncologic surgery

Pieter B.A.A. van Driel[1], Stijn Keereweer[2], Thomas J.A. Snoeks[2], Clemens W.G.M. Löwik[2]

1. Endocrinology and Molecular Imaging, Leiden University Medical Center, Leiden, The Netherlands.
2. Department of Otorhinolaryngology Head and Neck Surgery, Erasmus Medical Center, Rotterdam, The Netherlands.

ABSTRACT

Imaging is currently used for cancer detection, staging, and treatment evaluation. However, during surgery, surgeons rely mostly on visual inspection and palpation. Fluorescence imaging could provide the surgeon with necessary real-time information and could therefore revolutionize surgical oncology. This chapter gives an extensive overview of the current status of preclinical and clinical fluorescence-guided surgery. We will focus on specific targeting of the primary tumour by fluorescent agents that take aim of the alterations in cell physiology that denote cancer.

4.20.1 Introduction

2

This chapter will give an overview of preclinical and clinical data to reflect the current status of fluorescence-guided surgery. We will focus on specific targeting of the primary tumour by fluorescent agents that take aim of the alterations in cell physiology that denote cancer, as described by Hanahan and Weinberg (2000, 2011). Concretely, we will discuss the preclinical and clinical work of non-invasive NIR fluorescence imaging of cancer in relation to these hallmarks. Altogether, an extensive overview will be given to provide the knowledge of the current status of fluorescence-guided surgery.

4.20.4 Tumour Detection Using Organic Fluorescent Probes

Specific targeting of the primary tumour and metastases by fluorescent agents to intraoperatively identify the tumour margin is expected to be of great importance in future surgical oncology. Different targeting strategies can be used to visualize tumours and subsequently identify their margins for radical resection. Preclinically, many targeting moieties have been explored in the past decennium. Nonetheless, cancer targeting with high sensitivity and specificity remains challenging, mostly because of a great extent of intra- and intertumoral heterogeneity (Gerlinger et al., 2012; Marusyk et al., 2012). Hence, the quest for a universal tumour-specific target remains to be ongoing. In 2000, Hanahan and Weinberg (2000) reported six essential alterations in cell physiology that collectively dictate malignant growth, namely, tissue invasion and metastasis, sustained angiogenesis, limitless replicative potential, self-sufficiency in growth signals, insensitivity to growth-inhibitory signals, and evasion of programmed cell death (Keereweer et al., 2011a). In the following, the preclinical and clinical work of NIR fluorescence tumour imaging will be discussed, based on specific targeting of each of these hallmarks of cancer (see also Part I, Chapter 4.05).

4.20.4.1 Tumour Imaging: Preclinical Studies

4.20.4.1.1 Tissue invasion and metastasis

One of the six essential alterations in cell physiology of tumour cells is the capability of tissue invasion and metastasis. To escape the limiting nutrients and space available around the primary tumour, tumour cells colonize distant tissue in the body. Proteases play a major role in facilitating tumour cells to invade adjacent tissue and metastasize to distant sites. Many tumours have elevated levels of proteolytic enzymes (Keppler et al., 1996; Kim et al., 1998; Koblinski et al., 2000). Proteases can be classified by their mechanisms of action: serine, cysteine, threonine, aspartate, glutamic acid proteases, and metalloproteases (Yang et al., 2009a). The main focus of interest in targeting proteases for NIR fluorescence imaging has been in cathepsins, metalloproteases, and the urokinase plasminogen activator. Cysteine cathepsins are involved in protein degradation. They are a member of the family of papain-like cysteine proteases and were linked to cancer as long as 30 years ago (Sloane et al., 1981). An elevated cathepsin expression has been associated with poor prognosis and progression in a number of cancers (Turk et al., 2012). Moreover, high serum cathepsins have been correlated with metastases (Turk et al., 2012). Cathepsin expression is elevated in cancer cells as well as in macrophages and other host cells that are located within the tumour microenvironment (Mohamed and Sloane, 2006; Vasiljeva et al., 2006). Next to the well-known extracellular function of promoting migration and invasion of

cancer cells, cathepsins play a pro- and antitumorigenic intracellular role in tumour progression (Turk et al., 2012). Eleven human cathepsins are known (i.e., cathepsins B, C, F, h, K, L, O, S, V, X, and W) of which especially cathepsins B, D, and S are important because of the high expression in malignancies. Therefore, these particular cathepsins have been used as targets in optical imaging studies. Weissleder et al. (1999) were the first to image protease activity using the so-called 'smart probes' (Figure 9).
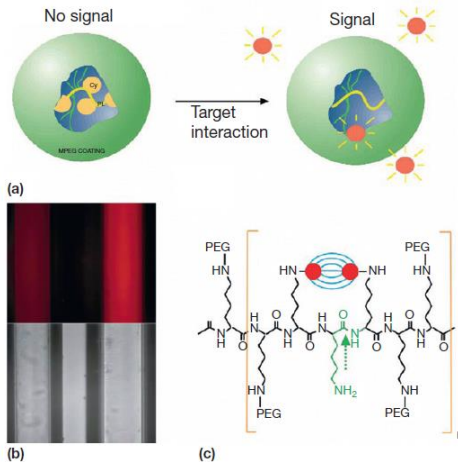

Figure 9 (a) Schematic diagram of probe activation. The initial proximity of the fluoro- chrome molecules to each other results in signal quenching. (b) NIRF image (top) and bright light image (bottom) of nonactivated probe (left) and activated probe (right). Note the difference in signal intensity between enzyme-activated and unactivated probe. (c) Chemical structure of repeating graft copolymer segment indicating quenching of fluorophore Cy and enzymatic degradation site (green arrow). Reproduced from Weissleder R, Tung CH, Mahmood U, and Bogdanov A Jr. (1999) In vivo imaging of tumours with protease-activated near-infrared fluorescent probes. Nature Biotechnology 17(4): 375–378.

(Further information about 'smart probes' can also be found in Part I, Chapter 4.05 and Part III, Chapter 4.15) The smart probes are based on multiple self-quenching (i.e., inactivated) fluorophores that are located close to each other. Until the probe is dequenched by the protease of interest, excited fluorophores will absorb energy from each other that would otherwise result in the emission of a photon (Kobayashi et al., 2010). Weissleder et al. (1999) coupled the fluorophore Cy5.5 to a synthetic graft copolymer consisting of poly-L-lysine sterically protected by multiple methoxypolyethylene glycol (MPEG) side chains. Selective in vivo accumulation of probe in a breast and small cell lung tumour was effectuated by the EPR effect (Fang et al., 2011). Intratumoral dequenching (i.e., activation) of the fluorophores resulted in a 12-fold increase in NIR fluorescent signal that allowed for the detection of tumours with submillimetre-sized diameters. The substrate-based probe was dequenched by a series of cysteine/serine proteases, including cathepsins B, H, and L. Shortly after the finding of the smart probe, Bremer et al. (2002) reported the use of aforementioned probe to differentiate the cathepsin B expression levels of breast cancer cell lines. Considering the presentation of both human and murine cathepsin B in this study, Bremer et al. (2005) conducted a second study in which a spontaneous breast tumour was used. Again, breast tumours could be detected. Many resembling probes, targeting different cathepsins and built around a reporter substrate, have been developed (Abd-Elgaliel and Tung, 2010; Cruz-Monserrate et al., 2011; Tung et al., 1999). Thereby, tumour-

specific imaging in pancreatic cancer, pancreatic intraepithelial neoplasia, peripheral lung cancer, breast cancer, oral squamous cell carcinoma, and lymph node metastases have been reported using the cathepsins B, H, L, and S sensitive and commercially available probe ProSense680 or ProSense780 (PerkinElmer, Waltham, Massachusetts) (Eser et al., 2011; Figueiredo et al., 2006; Keereweer et al., 2011b, 2012a; von Burstin et al., 2008; Xie et al., 2012). Mieog et al. (2011b) determined the accuracy of real-time NIR fluorescence imaging in obtaining tumour-free resection margins by using ProSense680 and ProSense780 (Figure 10).
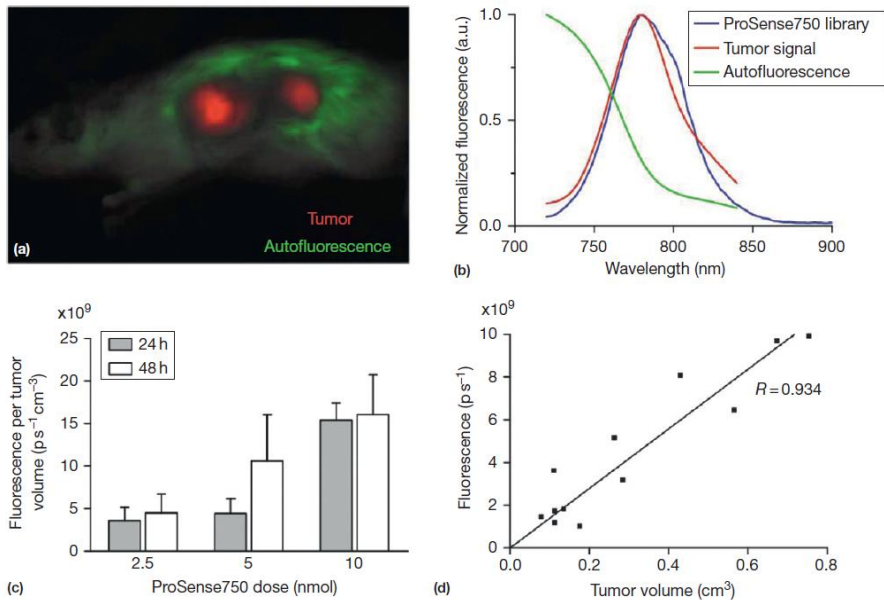
Figure 10; (a) In vivo activation of ProSense750 by syngeneic rat model of primary breast cancer: a typical example of a spectral unmixed image of an EMR86 tumour-bearing female WAG/Rij rat, acquired 24 h after intravenous administration of 10 nmol ProSense750. Shown is the separation of the autofluorescence signal (pseudocolored green) and the ProSense750 signal (pseudocolored red; IVIS spectrum). (b) Emission curve plot of the spectrally unmixed fluorescence signals from (a) demonstrates matching of the tumour signal (red line) with the predefined ProSense750 emission curve (blue line), confirming the localization of activated ProSense750 at the tumours. (c) In a dose-dependent and time-dependent experiment, nine tumor bearing rats (N¼35 tumours) were randomized to three ProSense750 dose groups and imaged 24 h (gray bars) and 48 h (open bars) after intravenous administration of ProSense750 using the IVIS Spectrum. Bars represent mean_SEM. (d) Scatter plot of fluorescence intensity and tumour volume of the 10 nmol dose group imaged 24 h after intravenous administration of ProSense750 (R¼0.934, P<0.0001, N¼12 tumours from three rats). Reproduced from Mieog JS, Hutteman M, van der Vorst JR, et al. (2011) Image-guided tumour resection using real-time near-infrared fluorescence in a syngeneic rat model of primary breast cancer. Breast Cancer Research and Treatment 128(3): 679–689.

2

Complete resection was attained in 17 out of 17 tumours with minimal excision of healthy tissue. Next to cathepsins, matrix metalloproteinases (MMPs) are important matrix-degrading proteinases involved in organ morphogenesis, wound healing, and embryonic development. Similar to the proteases mentioned above, MMPs are overexpressed in many tumours. Over 20 MMPs are known of which predominantly MMP-2, MMP-9, and MMP-7 are involved in the progression of cancer. Their complex role in carcinogenesis includes the stimulation of cancer cell growth, angiogenesis, migration, invasion, and metastasis. Like cathepsins, MMPs are overexpressed in cancer cells as well as tumour stromal cells (Egeblad and Werb, 2002; Hua et al., 2011; Overall and Lopez-Otin, 2002). The expression of MMPs correlates with advanced tumour stage, increased invasion, metastasis, and poor survival (Egeblad and Werb, 2002).

By modifying the aforementioned cathepsin-sensing probe, Bremer et al. (2001a) were the first to image MMP activity using NIR fluorescence imaging in vivo. Although cleavable by other MMPs, the peptide substrate was primarily cleaved by MMP-2. The probe allowed identification ofMMP-2-positive tumours and the assessment ofMMP-2 activity after treatment with the potent MMP inhibitor prinomastat (Bremer et al., 2001a,b). Next to imaging of nonmembrane-bound MMPs, Zhu et al. (2011a,b) explored the imaging of membrane-type MMPs (MT-MMP). Membrane type-1 matrix metalloproteinase (MMP-14), one of the six MT-MMPs, is highly expressed in different cancers (Zhu et al., 2011a). A nonsubstrate MT1-MMP-binding peptide was conjugated to the NIR-fluorescent dye Cy5.5 and targeted the high MT1-MMP that expressed MDA-MB-435 xenografts. In the line of research with the commercially available probes targeting cathepsins, a substrate-based MMP targeting probe, MMPSense680 (PerkinElmer, Waltham, Massachusetts) was developed and used in NIR fluorescence imaging of oncology (Keereweer et al., 2011b, 2012a; Xie et al., 2012). In healthy tissue, the urokinase-type plasminogen activator receptor (uPAR) is moderately expressed in variable tissues. Increased expression is related to extensive tissue remodelling through the regulation of extracellular proteolysis in healthy tissues, as well as in many pathological conditions including cancer, inflammation, and infections (Blasi and Sidenius, 2010). The nonproteolytic functions consist of the promotion of cell proliferation, spreading, migration, and invasion (Blasi and Sidenius, 2010). Although a variety of studies reported the use of radioactive or iron oxide labeled uPA-based peptides, reports on targeting uPAR by using a targeting moiety conjugated to a fluorophore are relatively rare (Li et al., 2008; Liu et al., 2009; Yang et al., 2009b,c). Law et al. (2004) described the development of a selective uPA activatable NIR fluorescence imaging probe in vitro. A copolymer of L-lysine and MPEG was used as a backbone for an uPA selective substrate and conjugated to Cy5.5 or Cy7. Upon addition of recombinant human uPA to the probe, a significant amplification of fluorescence was observed. No amplification was observed using the negative control probe or when uPA inhibitors were added. The same probe was used to assess the validation in animal models of human colon adenocarcinoma and fibrosarcoma (Hsiao et al.,

2006). A threefold higher signal intensity was reported, correlating with tumour-associated uPA activity. Dullin et al. (2009) published the use of a nonactivatable uPAR antibody conjugated to Cy5.5 to visualize breast carcinoma. In contrast to the nonspecific antibody that was used as a control, clear visualization of the breast tumour was observed. Next to the substrate-based probes described above, fluorescent activity-based probes (ABPs) have been reported (Blum et al., 2005, 2007). In contrast to the substrate-based probes, ABPs label target proteases through covalent binding (Figure 11). One of the major advantages of using a substrate as a reporter in 'smart probes' is that a single active protease can process many substrates resulting in the amplification of fluorescent signal over time. However, such substrates do usually not target a specific single protease, making it difficult to determine which particular protease is being imaged (Blum et al., 2009). ABPs allow direct biochemical analysis of targets after in vivo imaging and enable a direct link to the imaging data. Moreover, due to small molecules, ABPs have shorter half-lives and shorter elimination times, resulting in higher contrast images. ABPs targeting cathepsins B, L, S, and X have been synthesized and were reported to successfully delineate tumours in vivo (Blum et al., 2007; Paulick and Bogyo, 2011; Tedelind et al., 2011; Verdoes et al., 2012). Blum et al. (2009) compared the substrate-based probes to the ABPs in imaging of MDA-MB 231 MFP and C2C12ras tumours in vivo. They reported a more rapid and selective uptake of ABPs into tumours and a brighter overall signal and suggested that the lack of signal amplification for an ABP was compensated by more efficient kinetics and prolonged retention. The major advantage of proteases over other targets is the ubiquity of the expression in cancer cells which make them very appealing as a universal target for intraoperative NIR fluorescence molecular imaging of cancer (Boonstra et al., 2011; Egeblad and Werb, 2002; Mohamed and Sloane, 2006). On the other hand, the increased expression of proteases is not limited to tumours and the tumour microenvironment but can be found in inflammation and infections. The disadvantage of increased expression in inflammation and infections is often disregarded when tumour models are used in immune-compromised mice. A second advantage of proteases is the overexpression in tumour stromal cells. These are an interesting target to identify the tumour invasive border and subsequently resect the tumour in a radical way.
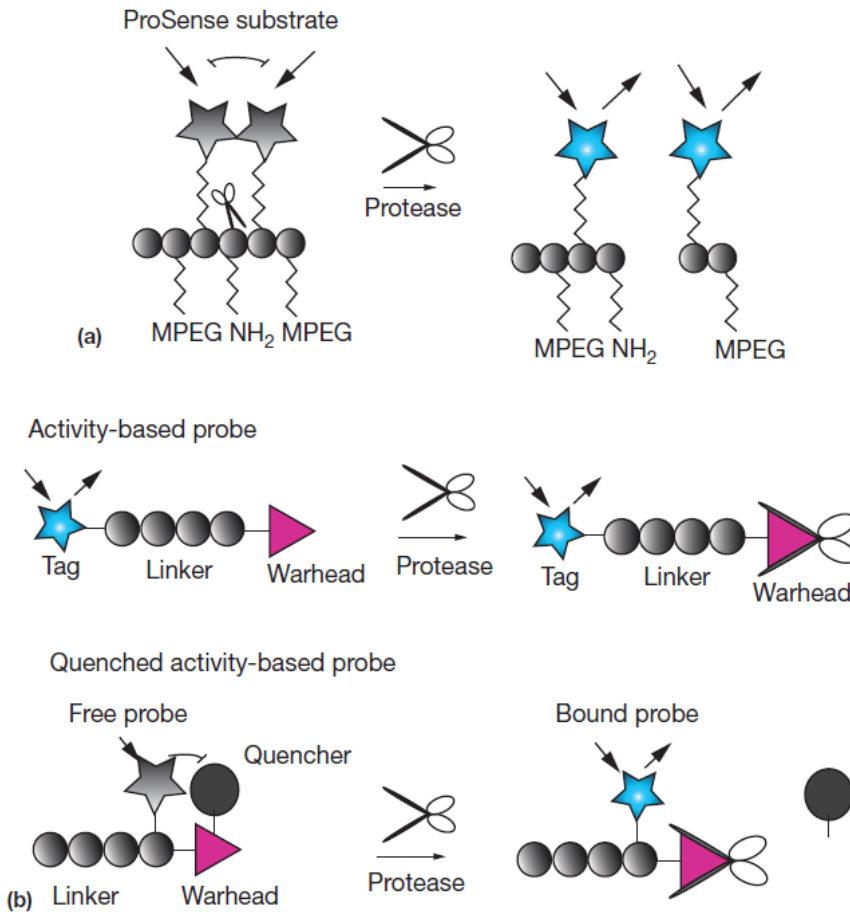
Figure 11; (a) Schematic diagram illustrating activation of the ProSense imaging probes by a target protease. The main backbone is made up of PEGylated poly-lysine modified with fluorophores that are quenched by close proximity (gray stars). Upon cleavage by a protease at free lysine residues, smaller fragments containing the unquenched fluorophore (blue stars) are released. (b) Schematic of fluorescent activity-based probes labeling a target protease. In both examples, the probe covalently binds in the active site of the protease target forming a permanent bond between the probe and the protease. In the top scheme, the probe contains a fluorescent reporter (blue start) that emits fluorescence even in the absence of protease. In the bottom scheme, the fluorophore (gray start) on the ABP is quenched by proximity to a quenching group (black circle) that is lost upon covalent modification of the target protease. Reproduced from Blum G, Weimer RM, Edgington LE, Adams W, and Bogyo M. (2009) Comparative assessment of substrates and activity based probes as tools for non-invasive optical imaging of cysteine protease activity. PLoS One. 4(7): e6374.

4.20.4.1.2 Sustained angiogenesis

An oncogenic event enables tumour cells to evade the immune system and enhance their survival. However, further growth of the tumour extending the size of 1 mm needs vascularization to supply oxygen and nutrients (Naumov et al., 2006). Hypoxia and nutrient deprivation shift the balance of pro- and antiangiogenic factors toward stimulatory angiogenic factors (Weis and Cheresh, 2011). Cytokines and growth factors are released in the tumour microenvironment allowing new blood vessels to grow by sprouting from preexisting blood vessels or by recruitment of endothelial progenitor cells (Avraamides et al., 2008). The defective architecture of newly formed blood vessels of most solid tumours ensures an enhanced vascular permeability, thereby offering sufficient supply of nutrients and oxygen for rapid growth (Fang et al., 2011). The vascular endothelial growth factor (VEGF) and integrins, both key regulators of tumour angiogenesis, provide targets to detect sustained angiogenesis of tumours. In addition, an interesting target in NIR fluorescence imaging is the enhanced vascular permeability and retention. These targets will be discussed separately in the following paragraphs. The VEGF represents a critical rate-limiting step in physiological angiogenesis. In physiological angiogenesis, VEGF has the ability to promote growth of vascular endothelial cells (ECs), acts as a survival factor for ECs, promotes monocyte chemotaxis, and is known as a vascular permeability factor (Ferrara et al., 2003). VEGF acts via two related receptor tyrosine kinases and is upregulated in many human tumours (Ferrara et al., 2003). In 2006, Backer et al. (2007) conjugated a single-chain Cys-tagged VEGF to Cy5.5 (scVEGF/Cy) and explored the specific focal uptake into the vasculature of tumours and surrounding host tissue. Compared to a functionally inactive control, scVEGF/Cy selectively accumulated in the tumour area. The intensity of NIRF images remained nearly constant for at least seven days after injection. Three other research groups conjugated bevacizumab, a humanized monoclonal antibody that neutralizes all isoforms of the ligand VEGF-A, to alexa fluor680, Cy5.5, and IRDye 800CW, respectively (Chang et al., 2008; Terwisscha van Scheltinga et al., 2011; Withrow et al., 2008). Detection of head and neck, ovarian, prostate, and pancreatic tumours and monitoring of VEGF expression could be obtained.

Integrins are a group of structurally related, heterodimeric transmembrane receptors that compose of an alfa and a beta subunit (Avraamides et al., 2008). They are involved in signal transduction, cell–cell interaction, and adhesion to the extracellular matrix (Hood and Cheresh, 2002). Twenty-five intregrin heterodimers are known, of which a number has been implicated in the regulation of cell growth, survival, and migration during angiogenesis (Avraamides et al., 2008). Integrins and especially the avb3 integrin are widely expressed in tumour cells and blood vessels of many solid tumours, which make them very appealing as a target in NIR fluorescence molecular imaging (Robinson and Hodivala-Dilke, 2011). The avb3 integrin expression had been

studied well by using radionuclide imaging when Chen et al. (2004) performed the first NIR fluorescence imaging study that targeted avb3 integrin. Cyclic arginine–glycine–aspartate (cRGD) was conjugated to Cy5.5 which enabled clear visualization of a subcutaneous glioblastoma tumour (Chen et al., 2004; Hsu et al., 2006). Wang et al. (2004) synthesized an integrin avb3-targeted peptide cyclo (Lys-Arg-Gly-Asp-Phe) conjugated to Cy5.5 or IRDye 800CW and reported its accumulation in tumours expressing avb3. Soon after these exciting results, the commercial probe IntegriSense680 (PerkinElmer, Waltham, MA) became available. This targeting moiety consists of a small peptidomimetic antagonist conjugated to a NIR-fluorescent dye. A higher specificity toward avb3 compared to RGD-based probes could be obtained. Moreover, IntegriSense was internalized into avb3 positive tumour cells with subsequent slower clearance (Keereweer et al., 2012b; Kossodo et al., 2010; Themelis et al., 2011). To extend the blood circulation half-life of the small RGD-based probe, Chen et al. (2009) covalently conjugated a cyclic peptide, c(RGDyK), and an organic dye (IRDye 800CW or Cy5.5) to HSA. Higher tumour accumulation and TBRs were obtained using HSA–RGD–IRDye 800CW in a subcutaneous glioblastoma cancer cell line. Attention has to be paid that although the blood circulation time will extend, penetration into the tissue might diminish, resulting in the same or an even lower TBR. Two new, exciting approaches were reported to improve the specificity and increase the TBR. The use of 'smart probes' targeting avb3 was introduced by Jin et al. (2007). To improve the performance of their cRGD molecule RAFT-c(-RGDfK-)4, they developed a self-quenched probe by linking a fluorescence quencher to Cy5 via a disulfide bond. Fluorescence could be activated by RGD-mediated cellular internalization and a significant enhancement of fluorescent signal was obtained compared to the unquenched molecule. Lee et al. (2011) developed a pH activatable probe by conjugating a pH-sensitive cyanine dye to a cRGD peptide targeting avb3 integrin. The spectra were shifted to the visible region when the pH was above 6. Tumours exhibit a lower extracellular pH than normal tissue (Gerweck and Seetharaman, 1996; Thistlethwaite et al., 1985). Therefore, an increase in tumour specificity could be obtained using this probe. Cell microscopy indicated avb3 integrin facilitated endocytosismediated lysosomal accumulation and enhancement of the fluorescent signal. In vivo, similar enhancement of fluorescence was observed in an orthotopic breast cancer model. The defective architecture of blood vessels and extensive amounts of vascular permeability factors provide most solid tumours with an enhanced vascular permeability (Fang et al., 2011). The increased vascular permeability ensures macromolecules larger than 40 kDa to leak out from the tumour vasculature. Due to ineffective lymphatic drainage and subsequent abnormal fluid transport accumulation of thesemolecules in the interstitial space occurs (Fang et al., 2011). This effect and pathophysiological nature of tumour vasculature and lymphatic drainage are of essential value for anticancer drug design. Keereweer et al. (2012b) explored the EPR effect in NIR fluorescence molecular imaging using the nonspecific IRDye 800CW PEG (LI-COR Biosciences, Lincoln,

NE). Clear demarcation of an oral squamous cell carcinoma of the tongue could be obtained. Angiogenesis is essential for tumour growth and metastasis. The enhanced expression of angiogenic-related receptors and release of cytokines and growth factors are of universal importance for tumours. The relative ubiquity in this overexpression, as angiogenesis is essential for every tumour to grow, makes this hallmark very appealing as a target in NIR fluorescence molecular imaging.

4.20.4.1.3 Limitless replicative potential

The essence of carcinogenesis is the progression of changes in a normal cell that ultimately gains the ability of uncontrolled cell division. Three acquired capabilities are necessary to escape the normal growth program: growth signal autonomy, insensitivity to antigrowth signals, and resistance to apoptosis (Hanahan and Weinberg, 2000, 2011). To persevere the ability of limitless cell division, an increased metabolism and rapid DNA synthesis are required. An elevated rate of glycolysis and an increased expression of the folate receptor (FR) are two important targets in the limitless replicative potential of cancer. PET has become widely clinically available as a tool in cancer detection, staging, and monitoring the response after treatment (Gambhir, 2002; Stokkel et al., 1998, see also Volume 1). PET enables the imaging and quantification of cellular and molecular processes. One of the targets in PET, using the tracer 2-deoxy-2[18F]fluoro-D-glucose ([18F]FDG), is the increased glucose metabolism in malignant tissue (Rajendran et al., 2004). In the 1930s, Warburg et al. (1927) reported the increased glycolysis of malignant tissue compared to normal tissue. The increased demand for glucose in malignant tissue is usually associated with upregulation of the glucose transporters (GLUT 1 and GLUT 3) and hexokinase (Rajendran et al., 2004). The first in vivo study using a 2-deoxyglucose analog coupled to a NIR-fluorescent dye was done by Cheng et al. (2006). Encouraged by the GLUT-specific uptake of the recently synthesized 2-dexoyglucose analog 2-NBDG (O'Neil et al., 2005) in vitro, they conjugated Cy5.5 and D-glucosamine (Cy5.5–2DG). Tumour-specific uptake of Cy5.5–2DG was observed in a variety of tumours in vitro and in vivo. Nonetheless, the Cy5.5–NHS, used as a control, demonstrated the same tumour specificity. In addition, blocking of the GLUT and hexokinase pathway showed no decrease in fluorescent signal. Although tumour specific, the NIR-fluorescent glucose analog did not prove to target the tumour through the GLUT/hexokinase pathway. Kovar et al. (2009) conjugated 2-deoxyglucose to the IRDye 800CW (800CW 2-DG). Tumour-specific uptake was observed in epithelial and prostate carcinomas in vitro as well as in vivo. In contrast to Cheng et al. (2006), specific blocking of IRDye 800CW 2-DG uptake by an antibody against the GLUT 1 glucose transporter and by an excess of unlabeled 2-DG was reported. Shortly after these results, 800CW 2-DG (LI-COR Biosciences) became commercially available and Keereweer et al. (2012a,c) successfully used the probe to visualize an oral squamous cell carcinoma of the tongue and cervical lymph node metastases in animal models. Folate is a

generic name for a group of structurally related compounds like folic acid and vitamin B9. It plays an important role during one-carbon transfer reactions that are critical to the metabolism of nucleic acids and amino acids (Choi and Mason, 2000). The function of folate in DNA synthesis and replication, cell division, and growth and survival is of particular importance in rapid dividing cells (Choi and Mason, 2000). The high affinity FR is a glycosylphosphatidylinositolanchored protein that mediates folate uptake by endocytosis (Henderson, 1990). Four isoforms of the FR have been described of which FRa is of particular interest in NIR fluorescence imaging. The FRa is highly expressed in nonmucinous tumours of epithelial origin and its expression is restricted in normal cells (Parker et al., 2005). Moreover, the affinity of FR for folic acid is high, the excretion of folate from receptor negative tissue is fast, and the small size of folate facilitates its efficient penetration of solid tumours (Sega and Low, 2008). Numerous studies explored the use of the FR to visualize a variety of tumours. Tung et al. (2002) coupled the asymmetric NIR-fluorescent compound NIR2 to a amino-derivatized folic acid. The experiments were performed using the FR expressing OVCAR3 ovarian cancer cell line and the FR-negative human lung carcinoma A549. Competitive inhibition studies using folic acid and NIR2–folate revealed that fluorophore attachment did not interfere with binding to the FR. Subsequently, OVCAR3 tumours were implanted in the lower abdomen of nude mice. Successful NIR-fluorescent identification of the tumour was obtained as early as 1 h after administration of the conjugate and the fluorescent signal reached a plateau at 24 h. No enhancement of tumour fluorescence was observed in mice after the administration of NIR2 alone (Tung et al., 2002). Moon et al. (2003) used the same NIR2–folate probe in FR-positive nasopharyngeal epidermoid carcinomas and reported the inhibition of fluorescent signal after administration of unlabeled folate. Next to the fluorescence detection of primary tumours, the use of a folate–fluorescein conjugate enabled the visualization of metastatic loci of submillimeter size (Kennedy et al., 2003). Considering the undesirable optical qualities of fluorescein, two groups explored the conjugation of folate to ICG (Liu et al., 2010; Milstein et al., 2005). Liu et al. (2010) synthesized a folate–polyethylene glycol (PEG) complex conjugated to ICG. Four different cell lines were used and a TBR up to 20 was obtained. The limitless replicative potential is a very interesting target in the use of NIR fluorescence imaging. Many studies appraised the use of glucose analogs in noninvasive detection of tumours using PET imaging. Recently, Tseng et al. (2012) compared the use of NIR-conjugated 2-deoxyglucose to [18F]FDG and suggested that large bulky fluorophores disrupt the facilitated transport and retention of the 2-DG probes. Even though these results do not support the use of large fluorophores conjugated to a glucose analog, the general acceptance of tumour detection using PET imaging certainly makes increased glycolysis of tumours an interesting target. On the other hand, although not ubiquitously expressed, the FR holds as a very promising target for NIR molecular imaging. The upregulation in a large variety of epithelial tumours, the absence of the FR in most normal tissue, the high affinity of the FR for its ligand, and the small

size and subsequent rapid clearance of folate make the FR a promising target in NIR molecular imaging (Sega and Low, 2008).

4.20.4.1.4 Self-sufficiency in growth signals

The essence of cancer is the uncontrollable dividing and growth of cells and subsequent invasion of nearby tissue. Normal cells are dependent on mitogenic growth signals if the cells want to get into an active proliferative state. Tumour cells produce many of their own growth signals which reduce their dependence on growth signals from the microenvironment (Hanahan and Weinberg, 2000, 2011). The tumour cell has three available molecular strategies to acquire independency of growth signals from the microenvironment: alteration of extracellular growth signals, alteration of transcellular transducers of those signals, or alteration of intracellular circuits that translate those signals into action (Hanahan and Weinberg, 2000, 2011). Targets available within the hallmark of self-sufficiency in growth signals have been widely explored. The most promising tools for target-specific NIR fluorescence molecular imaging are antibody derivatives. Intact antibodies can provoke immunogenic reactions. Moreover, slow blood clearance via the liver results in high contrast images days after injection. These disadvantages encouraged the quest for new antibody derivatives. In this quest, many different antibody fragments have been synthesized (Figure 12).
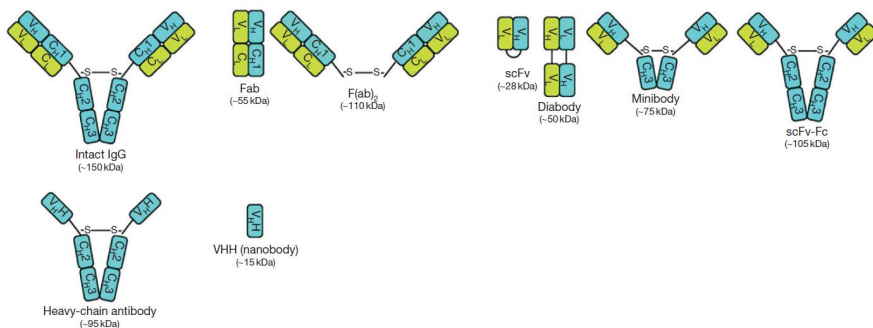

Figure 12; Schematic representation of antibody formats. Antibody fragments ranging from Fab fragments to nanobodies have been engineered. Reproduced from Romer T, Leonhardt H, and Rothbauer U (2011) Engineering antibodies and proteins for molecular in vivo imaging. Current Opinion in Biotechnology 22(6): 882–887.

2

The ideal antibody derivative should possess a high affinity to their target antigen and an optimal blood clearance to create high contrast imaging in a short time. Furthermore, they need to have a low immunogenicity and sufficient tissue penetration (Romer et al., 2011). In this paragraph, we will discuss the major preclinical work of NIR fluorescence imaging of cancer that has been performed targeting the epidermal growth factor receptor (EGFR), the HER2, the mesenchymal epithelial transition factor (cMET), and the insulin-like growth factor 1 (IGF1R). The epidermal growth factor (EGF) tyrosine kinase receptor family comprises four receptors: EGFR/ErbB-1, HER2/ErbB-2, HER3/ErbB-3, and HER4/ErbB-4. The signalling pathway is involved in cell proliferation, survival, adhesion, migration, and differentiation of normal tissue. Activating mutants and overexpression contribute to oncogenesis by proliferation, dedifferentiation, inhibition of apoptosis, invasiveness, and lack of adhesion dependence (Yarden, 2001). Of the four receptors, EGFR and HER2 are of particular interest in NIR fluorescence molecular imaging due to the overexpression in many different cancers (Modjtahedi and Dean, 1994). Soukos et al. (2001) were one of the first that conjugated a fluorescent dye (Cy5.5) to an anti-EGFR monoclonal antibody to detect an EGFR positive tumour. They reported a clear demarcation of an EGFR positive carcinogenesis model of a hamster's cheek pouch. The highest TBR was reached between four and eight days after injection of the probe. In 2006, the FDA approved two monoclonal antibodies raised against the EGFR. Soon, several studies reported the conjugation of a fluorescent dye to panitumumab and cetuximab (Barrett et al., 2007; Gleysteen et al., 2008; Heath et al., 2012; Koyama et al., 2007; Villaraza et al., 2010). Cetuximab is a recombinant, human/mouse chimeric monoclonal antibody that binds specifically to the extracellular domain of the human EGFR. It has an approximate molecular weight of 152 kDa and is an IgG1 antibody that competitively inhibits endogenous ligand binding (Gleysteen et al., 2008). Gleysteen et al. (2008) conjugated cetuximab to Cy5.5. Clear demarcation of primary tongue tumour and bilateral cervical nodes was demonstrated. In mice-bearing pulmonary metastases, stereomicroscopic fluorescence imaging demonstrated a distinct speckled fluorescence pattern and histopathological analysis was used to confirm the presence of metastases (Gleysteen et al., 2008). Panitumumab on the other hand is a fully humanized IgG2 monoclonal antibody with an approximate molecular weight of 147 kDa. Unlike cetuximab, it is not associated with infusion reactions (Kundu and Nestor, 2012). Heath et al. (2012) validated the use of the SPY imaging system to detect micrometastatic head and neck squamous cell carcinoma. Panitumumab was conjugated to the IRDye 800CW, and orthotopic tongue tumours were clearly delineated from normal tissue. Fluorescence intensity of the primary tumour was minimal using nonspecific IgG, and they were able to detect regional lymph node metastasis and microscopic areas of disease (Heath et al., 2012). To decrease the blood clearance time and improve the penetrating capability, smaller antibody mimetics were developed. The natural ligand

for EGFR has an approximate molecular weight of 6 kDa. Several groups used EGF to image EGFR expression in vivo (Ke et al., 2003; Keereweer et al., 2012a,c). Although clear demarcation of tumours could be achieved, the possible stimulation of the EGFR-mediated pathway is an unwanted property for in vivo imaging (Adams et al., 2007). Affibodies are single proteins composed of 58 amino acids derived from one of the IgG-binding domains of staphylococcal protein A. The high affinity toward their target protein and a molecular weight of approximately 6 kDa make them appealing antibody mimetics for NIR fluorescence imaging (Gong et al., 2010; Qi et al., 2012). Another promising antibody mimetic is the nanobody. Nanobodies are the smallest functional antigen-binding fragments of a naturally occurring single-chain antibody (Muyldermans et al., 1994). The nanobodies were derived from the fully functional heavy-chain antibodies of camels and llamas that contain a single variable domain and two constant domains. Like affibodies, they have a low molecular weight of 15 kDa and bind very specifically to their targets. Oliveira et al. (2011) tested an anti-EGFR nanobody conjugated to IRDye 800CW (7D12-IR) and compared it with cetuximab conjugated to the IRDye 800CW (Figure 13). 7D12–IR allowed visualization of the tumour 30-min postinjection when no signal above background was observed with cetuximab–IR. Quantification of the IR-conjugated proteins in the tumour revealed a significantly higher uptake of 7D12–IR compared to cetuximab–IR which could be explained by superior penetration and distribution of 7D12–IR (Oliveira et al., 2011). Using a phage display method, Jeong et al. (2012) found an EGFR-specific peptide (EGBP) and tested three linking groups for the conjugation to Cy5.5. Clear differences were observed between the different probes and EGBP–C-Cy5.5 turned out to be the optimized optical imaging agent for the detection of EGFR positive U87MG tumours. High TBRs were obtained as early as 30-min postinjection. To obtain a more specific fluorescent signal and a higher TBR, Hama et al. (2007) explored the target-specific activation of the optical signal. They described a two-step activation process. First, EGFR positive tumours were pretargeted with biotinylated cetuximab followed by a second agent, a neutravidin–BODIPY-FL fluorescent conjugate. The binding of this conjugate to biotinylated cetuximab resulted in a tenfold amplification of the optical fluorescence signal. To amplify the tumour-specific fluorescent signal, Ogawa et al. (2009a) took advantage of the property of ICG that loses its fluorescence after protein binding. After cell binding and internalization, ICG dissociated from panitumumab thus activating fluorescence. This quenching NIR probe using panitumumab and ICG successfully visualized the EGFR positive MDA-MB468 and A431 tumours.
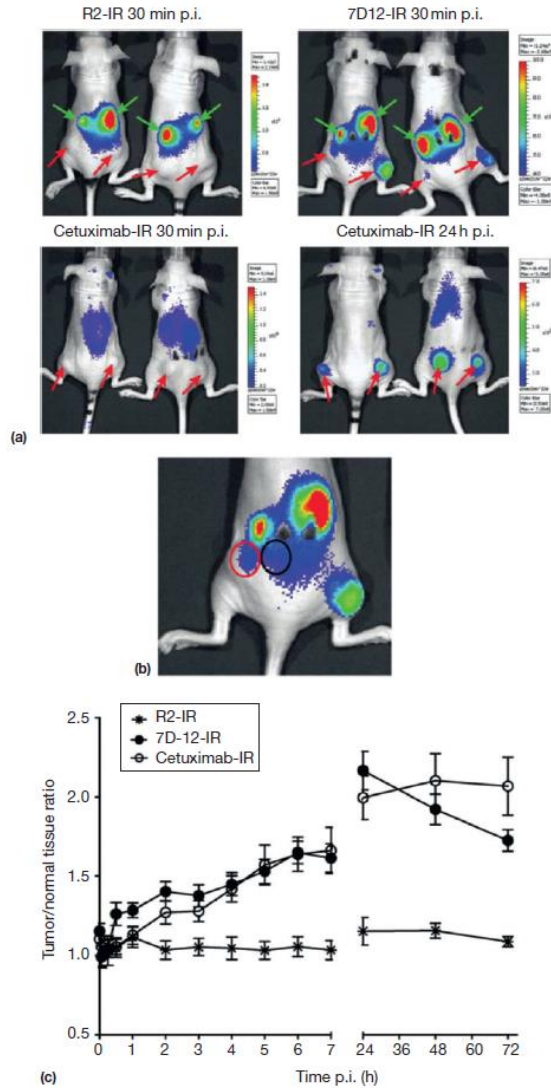
Figure 13; In vivo optical molecular imaging. Athymic nude mice bearing A431 human tumour xenografts at both hind legs were intravenously injected with 7D12–IR, R2–IR, or cetuximab–IR and imaged under anesthesia at several time points postinjection. (a) Images of mice taken with the optical imaging system at 30 min and 24 h postinjection (p.i.), in which tumours are indicated with red arrows and kidneys with green arrows. (b) For all of the images obtained, regions of interest were drawn around the tumour areas and in normal tissues (exemplified with red and black line, respectively), and the corresponding values of average fluoresence radiance (p/s/cm2/sr) were used to calculate tumour to normal tissue ratios 002EC. These values are plotted in time postinjection. Reproduced from Oliveira S, van Dongen GA, Stigter-van Walsum M, et al. (2011) Rapid visualization of human tumour xenografts through optical imaging with a near-infrared fluorescent anti-epidermal growth factor receptor nanobody. Molecular Imaging 2011 11(1): 33–46.

The second EGF receptor, HER2 (HER-2/neu, ErbB2), is as widely explored as a target in NIR fluorescence imaging as EGFR. Hilger et al. (2004) were one of the first that targeted HER2 using an anti-HER2 antibody conjugated to a fluorophore. They used the trastuzumab, an antibody that was approved by the FDA in 1998, and conjugated the antibody to Cy5.5. Distinct fluorescence imaging of the HER2 overexpressing tumour SK-BR-3 could be obtained compared to the normal-expressing PE/CA-PJ34 tumours. Several other groups conjugated trastuzumab or HER2-specific affibodies to a fluorophore for intraoperative tumour imaging, quantitative analysis of HER2 expression, or molecular imaging of drug susceptibility and dosing during HER2-targeted therapy (Chernomordik et al., 2010; Gee et al., 2008; Gong et al., 2010; Longmire et al., 2009; Terwisscha van Scheltinga et al., 2011). In the quest to higher TBRs and tumour-specific signal, Ogawa et al. (2009a) used the same quenching technique with ICG used in the conjugation to panitumumab to target the HER2. ICG conjugated to trastuzumab clearly demarked 3T3/HER2þ tumours. Next, Ogawa et al. (2009b) explored an in vivo targeted activatable optical imaging probe based on a fluorophore–quencher pair conjugated to a targeting moiety. Trastuzumab was labeled with the TAMRA (fluorophore)–QSY7 (quencher) pair. Upon internalization of the probe through the HER2, the probe was dequenched, resulting in high fluorescence intensities in the tumour and subsequent high TBRs. One group explored the use of NIR fluorescence imaging to, noninvasively, distinguish tumours by their cell surface expression profiles (Barrett et al., 2007; Koyama et al., 2007). Mice bearing A431 (overexpressing EGFR), NIH3T3/HER2þ (overexpressing HER2), and Balb3T3/DsRed (nonexpression control) tumours were injected with a cocktail of optically labeled antibodies: Cy5.5-labeled cetuximab and Cy7-labeled trastuzumab. Spectral fluorescence molecular imaging clearly differentiated tumours using the cocktail of optically labeled antibodies. cMET is a receptor tyrosine kinase, stimulated via its ligand hepatocyte growth factor, also known as scatter factor (HGF/ SF). The activation of the signaling pathway results in a number of biological effects in tumour cells including scattering, branching morphogenesis, cell motility, invasion, migration, and metastasis (Maulik et al., 2002). As cMET has been shown to be overexpressed and mutated in a variety of malignancies, it serves as a promising target in NIR fluorescence molecular imaging (Maulik et al., 2002). By immunizing rabbits with a HGF–cMET complex, Kim et al. (2007) generated a monoclonal antibody (SFN68). They screened out an epitopemimicking peptide from a phage display of a combinatorial peptide library and conjugated the peptide to the fluorophore Cy5.5 (cMBP–AOC–Cy5.5). Clear demarcation of the subcutaneous injected U87MG tumour was obtained. A coinjection with free peptide resulted in a 35% decrease of florescent intensity. Although several studies reported the use of antibodies to target cMET, no further studies have been performed using NIR fluorescence imaging (Perk et al., 2008; Towner et al., 2008). The insulin-like growth factor signaling system plays a key role in the growth and development of several cancers by stimulating cellular proliferation and survival (Pollak, 2004, 2012). The IGF1R

is a tyrosine kinase cell surface receptor that binds either the insulin-like growth factor 1 (IGF1) or the insulin-like growth factor 2 (IGF2). Expression of the IGF1R family (IIRF) is seen widely in both neoplastic and normal tissue. Although IIRF can be overexpressed in malignant tissues, gene amplification that is associated with large increases in receptor number is rare (Pollak, 2012). Nonetheless extensive research has been done, including phase III clinical trials, to explore the treatment of IGF1R-specific antibodies. Zhang et al. (2009) assessed the use of a humanized anti-IGF1R monoclonal antibody (AVE-1642) conjugated to the fluorophore Alexa 680 to detect IGF1R expression and its downregulation by antibodies. The IGF1Rtargeted probe was able to visualize the tumour and detect the downregulation of IGF1R. The overexpression of growth factor receptors in malignancies has been widely studied over the last decades. NIRfluorescent probes in many different sizes with a variety of fluorophores have been studied, mainly targeting the EGFR family. Although not ubiquitously expressed in malignancies, preclinical results have shown that the EGFR family is of great interest in NIR fluorescence imaging in overexpressing cancers. cMET, even though not many studies appraised the use of a cMET-targeted antibody conjugated to a fluorophore, does look promising as well. IIRF seems to be less attractive due to the moderate gene amplification. Nevertheless, more research is needed to explore this target in NIR fluorescence imaging of cancer. Although promising results were achieved targeting the self-sufficiency in growth signals so far, the quest for the most efficient antibody (mimetic) will continue.

4.20.4.2 Clinical Detection of Tumours

Although considerable preclinical research in NIR fluorescence imaging of tumours has been performed in the past decades, clinical studies are still awaited. The main reason holds the lack of FDA-approved fluorescent dyes and to a lesser extent the targeting moieties. At the end of 2011, the first and to date only tumour-specific in-human study had been published by van Dam et al. (2011). They systemically administered folate conjugated to fluorescein isothiocyanate (folate–FITC) to visualize ovarian cancer. The FRa provides a promising target in epithelial ovarian cancer (EOC) as 90–95% of patients with EOC revealed to overexpress the FRa (Markert et al., 2008). Currently, the overall 5-year survival rate of EOC is 45% and tumour-specific detection could aid in improved staging and possibly survival (van Dam et al., 2011). A total of ten patients were included of which four patients were diagnosed with a malignant epithelial ovarian tumour, one patient with a serous borderline tumour, and five patients with a benign ovarian tumour. Fluorescence imaging was done using a real-time multispectral intraoperative fluorescence imaging system. Fluorescence was detectable in all patients with a malignant tumour and FRa expression. One patient with a malignant tumour did not have any overexpression of FRa and

subsequently no fluorescence could be detected. No fluorescent signal was detected in the patients with benign tumours. The fluorescent dye FITC has an excitation wavelength of 495 and emits light at 520 nm. These are suboptimal fluorescent properties for clinical use. Nevertheless, this study provides the first in-human proof-ofprinciple of intraoperative tumour-specific fluorescence imaging for ovarian cancer. Although one study comprised the clinical use of a tumourspecific fluorescent probe, several clinical studies reported the use of ICG in the real-time NIR fluorescence visualization of hepatobiliary cancer. Intravenously injected ICG is excreted exclusively by the liver. Initially, Gotoh et al. (2009) used ICG for intraoperative NIR-fluorescent cholangiography. During cholangiography procedures in patients with hepatocellular carcinoma (HCC), they discovered that HCCs fluoresced strongly. The hypothesis was that cancerous tissue retained intravenously injected ICG through a disorder in biliary excretion. Intraoperative visualization of hepatobiliary cancer could be of great value because the intrahepatic recurrence rates after resection of CRC metastases range from 11% to 37.5% (Schaafsma et al., 2011b). The current procedure comprises preoperative diagnostic imaging with subsequent intraoperative ultrasound imaging. However, 3–17% of HCCs and metastases of CRC can be detected only by microscopic examination (Ishizawa et al., 2009). Gotoh et al. (2009) included ten patients who underwent curative hepatic resection for HCC. All of the primary tumours were identified with a NIR fluorescence imaging system and could be removed radically guided by the fluorescent signal. In four cases (40%) new HCC nodules were detected that could not be detected by eye, palpation, or with intraoperative ultrasonography. Soon afterward, several other studies reported the use of ICG in intraoperative NIR fluorescence imaging of hepatobiliary cancer (Harada et al., 2010; Ishizawa et al., 2009; Uchiyama et al., 2010, 2011). Imaging of ICG has to occur at least 24 h after injection. In this window, healthy liver parenchyma will wash out ICG and adequate TBRs can be obtained. The relatively unfavorable optical properties of the liver allow a limited penetration depth of NIR-fluorescent signal (Ishizawa et al., 2009). Ishizawa et al. (2009) described three fluorescent patterns on the cut surfaces of the surgical specimens: a total fluorescent type, a partial fluorescent type, and a rim fluorescent type. They suggested that, in contrast to well-differentiated HCC, poorly differentiated HCC and CRC metastases produce rim fluorescence because of biliary excretion disorders in the surrounding noncancerous liver tissue that have been compressed by the tumour (Ishizawa et al., 2009). So far, promising results were reported using ICG in realtime NIR fluorescence imaging of hepatobiliary cancer. Due to the limited penetration depth of fluorescent signal, ultrasound is still required to detect tumours located at greater depth. Nevertheless, real-time NIR fluorescence imaging is a promising tool for the detection of superficially located tumours of the liver and guidance of their resection.

2

4.20.4.3 Conclusion and Future Directions

In cancer surgery, radical resection of the tumour is pivotal for the prognosis of the patient. Delineation of the tumour border and assessment of the tumour-free margin are essential to reach complete resection of the tumour. NIR fluorescence imaging could be of great value in this field of oncological surgery. The ideal probe would require the accurate size to penetrate tumour tissue and a high affinity for a target that is only expressed in tumours. Finally, excretion should be quick enough to rapidly obtain high contrast images. The intra- and intertumoural heterogeneity challenges the quest to find the optimal probe (Gerlinger et al., 2012; Marusyk et al., 2012). Targeting strategies that target the universal hallmarks of cancer could circumvent the difficulty of heterogeneity. Two promising universal hallmarks that have been explored as a possible target are tumour angiogenesis and degradation of the extracellular matrix (Keereweer et al., 2011b, 2012b). Nonetheless, the intra- and intertumoural heterogeneity could also lead to a personal approach of probe selection. Depending on the characteristics of a single tumour, a cocktail of probes could be selected to target a tumour in its best way. Recently, some interesting targets have been reported. Increased expression of the follicle-stimulating hormone (FSH) receptor has been found in tumour blood vessels in a great variety of tumours (Radu et al., 2010). The increased expression was found at the periphery of the tumours in a layer of approximately 10 mm. Since the FSH receptor is only expressed on the granulosa cells of the ovary and sertoli cells of the testis in adult humans, high specificity of the probe could be expected. Although the pathogenic mechanism of increased FSH receptor expression is yet unknown, the FSH receptor holds great promise as a target for NIR fluorescence imaging. Tissue optical properties and autofluorescence can have great influence on the final image that is presented to the surgeon. In the NIR- fluorescent range, the absorbance is limited compared to visible light. Nevertheless, the surgeon needs to be aware of the limitation in depth. With 3 cm of adipose tissue overlying the tissue of interest no fluorescent signal will appear. Highly vascularized tissue, containing many absorbers, will mask the tissue of interest in a greater extent than overlying tissues that are composed of less-absorbing molecules. Moreover, the possible randomization of photons due to scattering can result in a decrease in accuracy of probe localization. As NIR fluorescence imaging is going toward clinical application, this is essential knowledge for oncological surgeons. Enriched by basic knowledge of fluorescence, surgeons will be able to give the accurate interpretation of NIR-fluorescent images presented during operation. NIR fluorescence imaging can provide the surgeon with real-time imaging of the tumour. When the tumour is located, the fluorescent signal can be excised until no signal is detected any longer. Pre- and intraoperative diagnosis of small tumours and metastatic nodules remains challenging. As in SLN mapping, the use of multimodal tracers that are both radioactive and fluorescent could be of interest to overcome these challenges (Azhdarinia et al., 2012). The combination of tracers enables

preoperative localization with nuclear imaging, intraoperative detection of tumours using a gamma camera and intraoperative visualization, and real-time resection of the tumour with NIR fluorescence. The step toward clinical application of tumour-specific NIR fluorescence imaging has to be made yet. Although a variety of monoclonal antibodies are in clinical use (e.g., cetuximab, panitumumab, trastuzumab), apart from ICG, no organic fluorophores are FDA proved yet. The FDA approval will give rise to a major increase in clinical research and will answer whether or not and to what extent the prognosis of cancer patients will increase with the use of real-time NIR fluorescence imaging. Although we are waiting for the clinical use of NIRfluorescent probes, the quest to find efficient probes will continue. Future preclinical studies will focus on the exploration of new hallmarks of cancer and the improvement of (dual labeled) probes targeting known hallmarks. Clinical research needs to focus on the patients' benefit of this promising modality that gives visibility to the oncological field.

References

- Abd-Elgaliel WR and Tung CH (2010) Selective detection of cathepsin E proteolytic activity. Biochimica et Biophysica Acta 1800: 1002–1008.

- Adams KE, Ke S, Kwon S, et al. (2007) Comparison of visible and near-infrared wavelength-excitable fluorescent dyes for molecular imaging of cancer. Journal of Biomedical Optics 12: 024017.

- Avraamides CJ, Garmy-Susini B, and Varner JA (2008) Integrins in angiogenesis and lymphangiogenesis. Nature Reviews. Cancer 8: 604–617.

- Azhdarinia A, Ghosh P, Ghosh S, Wilganowski N, and Sevick-Muraca EM (2012) Dual-labeling strategies for nuclear and fluorescence molecular imaging: A review and analysis. Molecular Imaging and Biology 14: 261–276.

- Backer MV, Levashova Z, Patel V, et al. (2007) Molecular imaging of VEGF receptors in angiogenic vasculature with single-chain VEGF-based probes. Nature Medicine 13: 504–509.

- Barrett T, Koyama Y, Hama Y, et al. (2007) In vivo diagnosis of epidermal growth factor receptor expression using molecular imaging with a cocktail of optically labelled monoclonal antibodies. Clinical Cancer Research: An official journal of the American Association for Cancer Research 13: 6639–6648.

- Blasi F and Sidenius N (2010) The urokinase receptor: Focused cell surface proteolysis, cell adhesion and signaling. FEBS Letters 584: 1923–1930.

- Blum G, Mullins SR, Keren K, et al. (2005) Dynamic imaging of protease activity with fluorescently quenched activity-based probes. Nature Chemical Biology 1: 203–209.

- Blum G, von Degenfeld G, Merchant MJ, Blau HM, and Bogyo M (2007) Noninvasive optical imaging of cysteine protease activity using fluorescently quenched activity-based probes. Nature Chemical Biology 3: 668–677.

- Blum G, Weimer RM, Edgington LE, Adams W, and Bogyo M (2009) Comparative assessment of substrates and activity based probes as tools for non-invasive optical imaging of cysteine protease activity. PLoS One 4: e6374.

- Boonstra MC, Verspaget HW, Ganesh S, et al. (2011) Clinical applications of the urokinase receptor (uPAR) for cancer patients. Current Pharmaceutical Design 17: 1890–1910.

- Bremer C, Bredow S, Mahmood U, Weissleder R, and Tung CH (2001a) Optical imaging of matrix metalloproteinase-2 activity in tumours: Feasibility study in a mouse model. Radiology 221: 523–529.

- Bremer C, Ntziachristos V, Weitkamp B, Theilmeier G, Heindel W, and Weissleder R (2005) Optical imaging of spontaneous breast tumours using protease sensing 'smart' optical probes. Investigative Radiology 40: 321–327.

- Bremer C, Tung CH, Bogdanov A Jr., and Weissleder R (2002) Imaging of differential protease expression in breast cancers for detection of aggressive tumour phenotypes. Radiology 222: 814–818.

- Bremer C, Tung CH, and Weissleder R (2001b) In vivo molecular target assessment of matrix metalloproteinase inhibition. Nature Medicine 7: 743–748.

- Chang SK, Rizvi I, Solban N, and Hasan T (2008) In vivo optical molecular imaging of vascular endothelial growth factor for monitoring cancer treatment. Clinical Cancer Research 14: 4146–4153.

- Chen X, Conti PS, and Moats RA (2004) In vivo near-infrared fluorescence imaging of integrin alphavbeta3 in brain tumour xenografts. Cancer Research 64: 8009–8014.

- Chen K, Xie J, and Chen X (2009) RGD–human serum albumin conjugates as efficient tumour targeting probes. Molecular Imaging 8: 65–73.

- Cheng Z, Levi J, Xiong Z, et al. (2006) Near-infrared fluorescent deoxyglucose analogue for tumour optical imaging in cell culture and living mice. Bioconjugate Chemistry 17: 662–669.

- Chernomordik V, Hassan M, Lee SB, et al. (2010) Quantitative analysis of Her2 receptor expression in vivo by near-infrared optical imaging. Molecular Imaging 9: 192–200.

- Choi SW and Mason JB (2000) Folate and carcinogenesis: An integrated scheme. The Journal of Nutrition 130: 129–132.

- Cruz-Monserrate Z, Abd-Elgalie WR, Grote T, et al. (2011) Detection of pancreatic cancer tumours and precursor lesions by cathepsin E activity in mouse models. Gut 61(9): 1315–1322.

- Dullin C, Zientkowska M, Napp J, et al. (2009) Semiautomatic landmark-based twodimensional–three-dimensional image fusion in living mice: Correlation of nearinfrared fluorescence imaging of Cy5.5-labeled antibodies with flat-panel volume computed tomography. Molecular Imaging 8: 2–14.

- Egeblad M and Werb Z (2002) New functions for the matrix metalloproteinases in cancer progression. Nature Reviews. Cancer 2: 161–174.

- Eser S, Messer M, Eser P, et al. (2011) In vivo diagnosis of murine pancreatic intraepithelial neoplasia and early-stage pancreatic cancer by molecular imaging. Proceedings of the National Academy of Sciences of the United States of America 108: 9945–9950.

- Fang J, Nakamura H, and Maeda H (2011) The EPR effect: Unique features of tumour blood vessels for drug delivery, factors involved, and limitations and augmentation of the effect. Advanced Drug Delivery Reviews 63: 136–151.

- Ferrara N, Gerber HP, and LeCouter J (2003) The biology of VEGF and its receptors. Nature Medicine 9: 669–676.

- Figueiredo JL, Alencar H, Weissleder R, and Mahmood U (2006) Near infrared thoracoscopy of tumoural protease activity for improved detection of peripheral lung cancer. International Journal of Cancer 118: 2672–2677.

- Gambhir SS (2002) Molecular imaging of cancer with positron emission tomography. Nature Reviews. Cancer 2: 683–693.

- Gee MS, Upadhyay R, Bergquist H, et al. (2008) Human breast cancer tumour models: Molecular imaging of drug susceptibility and dosing during HER2/neu-targeted therapy. Radiology 248: 925–935.

- Gerlinger M, Rowan AJ, Horswell S, et al. (2012) Intratumour heterogeneity and branched evolution revealed by multiregion sequencing. The New England Journal of Medicine 366: 883–892.

- Gerweck LE and Seetharaman K (1996) Cellular pH gradient in tumour versus normal tissue: Potential exploitation for the treatment of cancer. Cancer Research 56: 1194–1198.

- Gleysteen JP, Newman JR, Chhieng D, Frost A, Zinn KR, and Rosenthal EL (2008) Fluorescent labeled anti-EGFR antibody for identification of regional and distant metastasis in a preclinical xenograft model. Head & Neck 30: 782–789.

- Gong H, Kovar J, Little G, Chen H, and Olive DM (2010) In vivo imaging of xenograft tumours using an epidermal growth factor receptor-specific affibody molecule labeled with a near-infrared fluorophore. Neoplasia 12: 139–149.

- Gotoh K, Yamada T, Ishikawa O, et al. (2009) A novel image-guided surgery of hepatocellular carcinoma by indocyanine green fluorescence imaging navigation. Journal of Surgical Oncology 100: 75–79.

- Hama Y, Urano Y, Koyama Y, Choyke PL, and Kobayashi H (2007) Activatable fluorescent molecular imaging of peritoneal metastases following pretargeting with a biotinylated monoclonal antibody. Cancer Research 67: 3809–3817.

- Hanahan D and Weinberg RA (2011) Hallmarks of cancer: the next generation. Cell 144: 646–674.

- Hanahan D and Weinberg RA (2000) The hallmarks of cancer. Cell 100: 57–70.

- Harada N, Ishizawa T, Muraoka A, et al. (2010) Fluorescence navigation hepatectomy by visualization of localized cholestasis from bile duct tumour infiltration. Journal of the American College of Surgeons 210: e2–e6.

- Heath CH, Deep NL, Sweeny L, Zinn KR, and Rosenthal EL (2012) Use of panitumumab–IRDye800 to image microscopic head and neck cancer in an orthotopic surgical model. Annals of Surgical Oncology 19(12): 3879–3887.

- Henderson GB (1990) Folate-binding proteins. Annual Review of Nutrition 10: 319–335.

- Hermanek P, Hutter RV, Sobin LH, and Wittekind C (1999) International Union Against Cancer. Classification of isolated tumour cells and micrometastasis. Cancer 86: 2668–2673.

- Hilger I, Leistner Y, Berndt A, et al. (2004) Near-infrared fluorescence imaging of HER-2 protein over-expression in tumour cells. European Radiology 14: 1124–1129.

- Hood JD and Cheresh DA (2002) Role of integrins in cell invasion and migration. Nature Reviews. Cancer 2: 91–100.

- Hsiao JK, Law B, Weissleder R, and Tung CH (2006) In-vivo imaging of tumour associated urokinase-type plasminogen activator activity. Journal of Biomedical Optics 11: 34013.

- Hsu AR, Hou LC, Veeravagu A, et al. (2006) In vivo near-infrared fluorescence imaging of integrin alphavbeta3 in an orthotopic glioblastoma model. Molecular Imaging and Biology 8: 315–323.

- Hua H, Li M, Luo T, Yin Y, and Jiang Y (2011) Matrix metalloproteinases in tumourigenesis: An evolving paradigm. Cellular and Molecular Life Sciences 68: 3853–3868.

- Hutteman M, Mieog JS, van der Vorst JR, et al. (2011a) Intraoperative near-infrared fluorescence imaging of colorectal metastases targeting integrin alpha(v)beta(3) expression in a syngeneic rat model. European Journal of Surgical Oncology 37: 252–257.

- Ishizawa T, Fukushima N, Shibahara J, et al. (2009) Real-time identification of liver cancers by using indocyanine green fluorescent imaging. Cancer 115: 2491–2504.

- Jeong MH, Kim K, Kim EM, et al. (2012) In vivo and in vitro evaluation of Cy5.5 conjugated epidermal growth factor receptor binding peptide. Nuclear Medicine and Biology 39(6): 805–812.

- Jin ZH, Razkin J, Josserand V, et al. (2007) In vivo noninvasive optical imaging of receptor-mediated RGD internalization using self-quenched Cy5-labeled RAFT-c(-RGDfK-)(4). Molecular Imaging 6: 43–55.

- Josephson L, Mahmood U, Wunderbaldinger P, Tang Y, and Weissleder R (2003) Pan and sentinel lymph node visualization using a near-infrared fluorescent probe. Molecular Imaging 2: 18–23.

- Kanitakis J (2007) Mammary and extramammary Paget's disease. Journal of the European Academy of Dermatology and Venereology 21: 581–590.

- Ke S, Wen X, Gurfinkel M, et al. (2003) Near-infrared optical imaging of epidermal growth factor receptor in breast cancer xenografts. Cancer Research 63: 7870–7875.

- Keereweer S, Kerrebijn JD, van Driel PB, et al. (2011a) Optical image-guided surgery – Where do we stand? Molecular Imaging and Biology 13: 199–207.

- Keereweer S, Mieog JS, Mol IM, et al. (2011b) Detection of oral squamous cell carcinoma and cervical lymph node metastasis using activatable near-infrared fluorescence agents. Archives of tolaryngology – Head & Neck Surgery 137: 609–615.

- Keereweer S, Mol IM, Vahrmeijer AL, et al. (2012a) Dual wavelength tumour targeting for detection of hypopharyngeal cancer using near-infrared optical imaging in an animal model. International Journal of Cancer 131(7): 1633–1640.

- Keereweer S, Mol IM, Kerrebijn JD, et al. (2012b) Targeting integrins and enhanced permeability and retention (EPR) effect for optical imaging of oral cancer. Journal of Surgical Oncology 105: 714–718.

- Keereweer S, Kerrebijn JD, Mol IM, et al. (2012c) Optical imaging of oral squamous cell carcinoma and cervical lymph node metastasis. Head & Neck 34: 1002–1008.

- Kennedy MD, Jallad KN, Thompson DH, Ben-Amotz D, and Low PS (2003) Optical imaging of metastatic tumours using a folate-targeted fluorescent probe. Journal of Biomedical Optics 8: 636–641.

- Keppler D, Sameni M, Moin K, Mikkelsen T, Diglio CA, and Sloane BF (1996) Tumour progression and angiogenesis: Cathepsin B & Co. Biochemistry and Cell Biology 74: 799–810.

- Kim J, Yu W, Kovalski K, and Ossowski L (1998) Requirement for specific proteases in cancer cell intravasation as revealed by a novel semiquantitative PCR-based assay. Cell 94: 353–362.

- Kim K, Hur Y, Ryu EK, et al. (2007) A neutralizable epitope is induced on HGF upon its interaction with its receptor cMet. Biochemical and Biophysical Research Communications 354: 115–121.

- Kobayashi H, Ogawa M, Alford R, Choyke PL, and Urano Y (2010) New strategies for fluorescent probe design in medical diagnostic imaging. Chemical Reviews 110: 2620–2640.

- Koblinski JE, Ahram M, and Sloane BF (2000) Unraveling the role of proteases in cancer. Clinica Chimica Acta; International Journal of Clinical Chemistry 291: 113–135.

- Kossodo S, Pickarski M, Lin SA, et al. (2010) Dual in vivo quantification of integrintargeted and protease-activated agents in cancer using fluorescence molecular tomography (FMT). Molecular Imaging and Biology 12: 488–499.
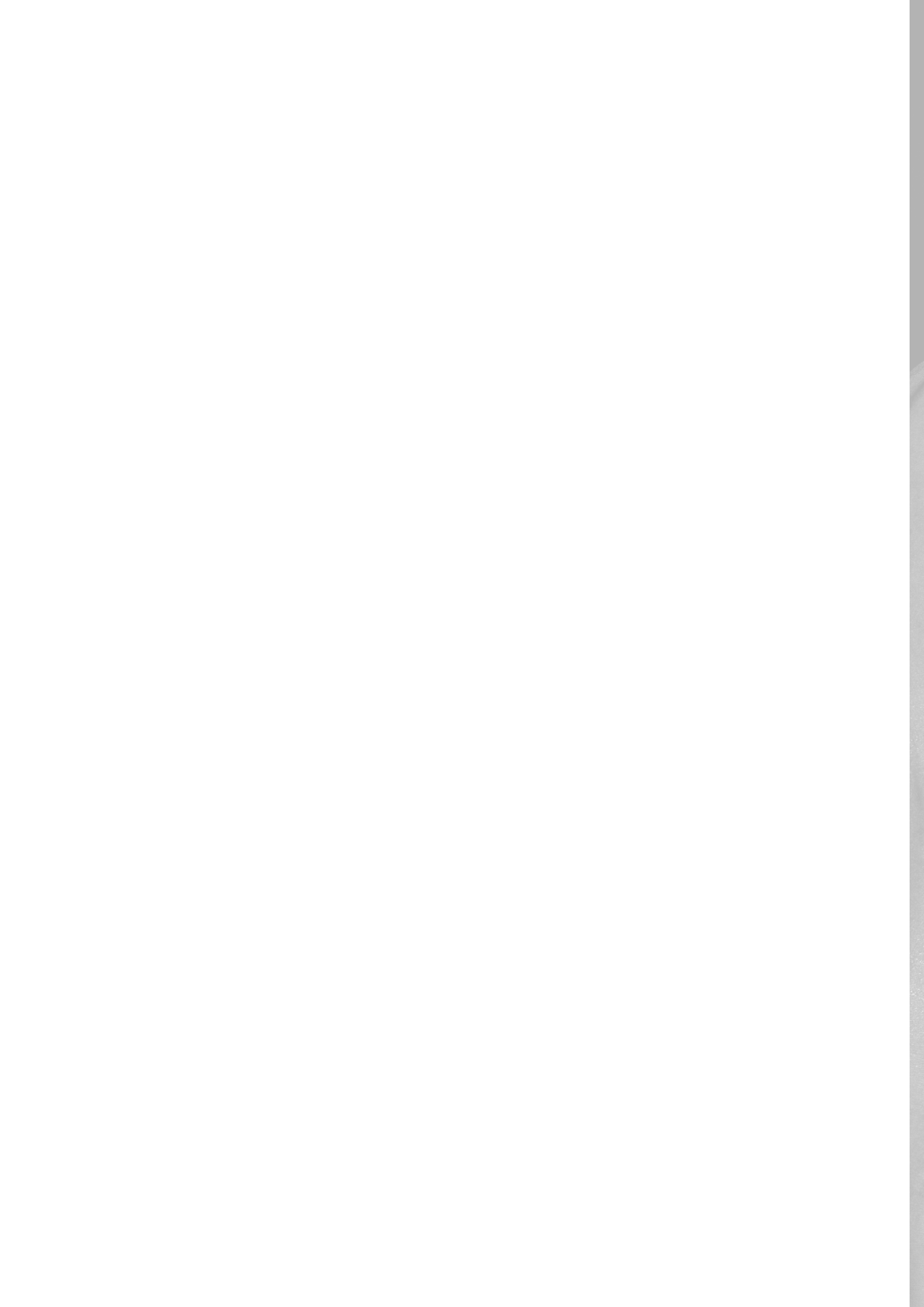
2

- Kovar JL, Volcheck W, Sevick-Muraca E, Simpson MA, and Olive DM (2009) Characterization and performance of a near-infrared 2-deoxyglucose optical imaging agent for mouse cancer models. Analytical Biochemistry 384: 254–262.

- Koyama Y, Barrett T, Hama Y, Ravizzini G, Choyke PL, and Kobayashi H (2007) In vivo molecular imaging to diagnose and subtype tumours through receptor-targeted optically labeled monoclonal antibodies. Neoplasia 9: 1021–1029.

- Kruijt B, Kascakova S, de Bruijn HS, et al. (2009) In vivo quantification of chromophore concentration using fluorescence differential path length spectroscopy. Journal of Biomedical Optics 14: 034022.

- Kundu SK and Nestor M (2012) Targeted therapy in head and neck cancer. Tumour Biology 33: 707–721.

- Law B, Curino A, Bugge TH, Weissleder R, and Tung CH (2004) Design, synthesis, and characterization of urokinase plasminogen-activator-sensitive near-infrared reporter. Chemistry & Biology 11: 99–106.

- Lee H, Akers W, Bhushan K, et al. (2011) Near-infrared pH-activatable fluorescent probes for imaging primary and metastatic breast tumours. Bioconjugate Chemistry 22: 777–784.

- Li ZB, Niu G, Wang H, et al. (2008) Imaging of urokinase-type plasminogen activator receptor expression using a 64Cu-labeled linear peptide antagonist by microPET. Clinical Cancer Research 14: 4758–4766.

- Liu D, Overbey D, Watkinson L, and Giblin MF (2009) Synthesis and characterization of an (111)In-labeled peptide for the in vivo localization of human cancers expressing the urokinase-type plasminogen activator receptor (uPAR). Bioconjugate Chemistry 20: 888–894.

- Liu F, Deng D, Chen X, Qian Z, Achilefu S, and Gu Y (2010) Folate-polyethylene glycol conjugated near-infrared fluorescence probe with high targeting affinity and sensitivity for in vivo early tumour diagnosis. Molecular Imaging and Biology 12: 595–607.

- Longmire M, Kosaka N, Ogawa M, Choyke PL, and Kobayashi H (2009) Multicolor in vivo targeted imaging to guide real-time surgery of HER2-positive micrometastases in a two-tumour coincident model of ovarian cancer. Cancer Science 100: 1099–1104.

- Markert S, Lassmann S, Gabriel B, et al. (2008) Alpha-folate receptor expression in epithelial ovarian carcinoma and non-neoplastic ovarian tissue. Anticancer Research 28: 3567–3572.

- Marusyk A, Almendro V, and Polyak K (2012) Intra-tumour heterogeneity: A looking glass for cancer? Nature Reviews. Cancer 12: 323–334.

- Maulik G, Shrikhande A, Kijima T, Ma PC, Morrison PT, and Salgia R (2002) Role of the hepatocyte growth factor receptor, c-Met, in oncogenesis and potential for therapeutic inhibition. Cytokine & Growth Factor Reviews 13: 41–59.

- Mieog JS, Hutteman M, van der Vorst JR, et al. (2011b) Image-guided tumour resection using real-time near-infrared fluorescence in a syngeneic rat model of primary breast cancer. Breast Cancer Research and Treatment 128: 679–689.

- Milstein AB, Kennedy MD, Low PS, Bouman CA, and Webb KJ (2005) Statistical approach for detection and localization of a fluorescing mouse tumour in intralipid. Applied Optics 44: 2300–2310.

- Modjtahedi H and Dean C (1994) The receptor for EGF and its ligands – Expression, prognostic value and target for therapy in cancer (review). International Journal of Oncology 4: 277–296.

- Mohamed MM and Sloane BF (2006) Cysteine cathepsins: Multifunctional enzymes in cancer. Nature Reviews. Cancer 6: 764–775.

- Moon WK, Lin Y, O'Loughlin T, et al. (2003) Enhanced tumour detection using a folate receptor-targeted near-infrared fluorochrome conjugate. Bioconjugate Chemistry 14: 539–545.

- Muyldermans S, Atarhouch T, Saldanha J, Barbosa JA, and Hamers R (1994) Sequence and structure of VH domain from naturally occurring camel heavy chain immunoglobulins lacking light chains. Protein Engineering 7: 1129–1135.

- Ogawa M, Kosaka N, Choyke PL, and Kobayashi H (2009a) In vivo molecular imaging of cancer with a quenching near-infrared fluorescent probe using conjugates of monoclonal antibodies and indocyanine green. Cancer Research 69: 1268–1272.

- Ogawa M, Kosaka N, Longmire MR, Urano Y, Choyke PL, and Kobayashi H (2009b) Fluorophore–quencher based activatable targeted optical probes for detecting in vivo cancer metastases. Molecular Pharmaceutics 6: 386–395.

- Ohnishi S, Lomnes SJ, Laurence RG, Gogbashian A, Mariani G, and Frangioni JV (2005) Organic alternatives to quantum dots for intraoperative near-infrared fluorescent sentinel lymph node mapping. Molecular Imaging 4: 172–181.

- Oliveira S, van Dongen GA, Stigter-van Walsum M, et al. (2011) Rapid visualization of human tumour xenografts through optical imaging with a near-infrared fluorescent anti-epidermal growth factor receptor nanobody. Molecular Imaging 11(1): 33–46.

- O'Neil RG, Wu L, and Mullani N (2005) Uptake of a fluorescent deoxyglucose analog (2-NBDG) in tumour cells. Molecular Imaging and Biology 7: 388–392.

- Overall CM and Lopez-Otin C (2002) Strategies for MMP inhibition in cancer: Innovations for the post-trial era. Nature Reviews. Cancer 2: 657–672.

- Parker N, Turk MJ, Westrick E, Lewis JD, Low PS, and Leamon CP (2005) Folate receptor expression in carcinomas and normal tissues determined by a quantitative radioligand binding assay. Analytical Biochemistry 338: 284–293.

- Paulick MG and Bogyo M (2011) Development of activity-based probes for cathepsin X. ACS Chemical Biology 6: 563–572.

- Perk LR, Stigter-van Walsum M, Visser GW, et al. (2008) Quantitative PET imaging of Met-expressing human cancer xenografts with 89Zr-labelled monoclonal antibody DN30. European Journal of Nuclear Medicine and Molecular Imaging 35: 1857–1867.

- Pollak MN (2004) Insulin-like growth factors and neoplasia. Novartis Foundation Symposium 262: 84–98 discussion 98–107, 265–108.

- Pollak M (2012) The insulin and insulin-like growth factor receptor family in neoplasia: An update. Nature Reviews. Cancer 12: 159–169.

- Qi S, Miao Z, Liu H, Xu Y, Feng Y, and Cheng Z (2012) Evaluation of four affibody-based near-infrared fluorescent probes for optical imaging of epidermal growth factor receptor positive tumours. Bioconjugate Chemistry 52(supplement 1): 1556.

- Radu A, Pichon C, Camparo P, et al. (2010) Expression of follicle-stimulating hormone receptor in tumour blood vessels. The New England Journal of Medicine 363: 1621–1630.
- Rajendran JG, Mankoff DA, O'Sullivan F, et al. (2004) Hypoxia and glucose metabolism in malignant tumours: Evaluation by [18F]fluoromisonidazole and [18F] fluorodeoxyglucose positron emission tomography imaging. Clinical Cancer Research 10: 2245–2252.
- Robinson SD and Hodivala-Dilke KM (2011) The role of beta3-integrins in tumour angiogenesis: Context is everything. Current Opinion in Cell Biology 23: 630–637.
- Romer T, Leonhardt H, and Rothbauer U (2011) Engineering antibodies and proteins for molecular in vivo imaging. Current Opinion in Biotechnology 22: 882–887.
- Sega EI and Low PS (2008) Tumour detection using folate receptor-targeted imaging agents. Cancer Metastasis Reviews 27: 655–664.
- Sloane BF, Dunn JR, and Honn KV (1981) Lysosomal cathepsin B: Correlation with metastatic potential. Science 212: 1151–1153.
- Soukos NS, Hamblin MR, Keel S, Fabian RL, Deutsch TF, and Hasan T (2001) Epidermal growth factor receptor-targeted immunophotodiagnosis and photoimmunotherapy of oral precancer in vivo. Cancer Research 61: 4490–4496.
- Stokkel MP, ten Broek FW, and van Rijk PP (1998) The role of FDG PET in the clinical management of head and neck cancer. Oral Oncology 34: 466–471.
- Tedelind S, Jordans S, Resemann H, et al. (2011) Cathepsin B trafficking in thyroid carcinoma cells. Thyroid Research 4(supplement 1): S2.
- Terwisscha van Scheltinga AG, van Dam GM, Nagengast WB, et al. (2011) Intraoperative near-infrared fluorescence tumour imaging with vascular endothelial growth factor and human epidermal growth factor receptor 2 targeting antibodies. Journal of Nuclear Medicine 52: 1778–1785.
- Themelis G, Harlaar NJ, Kelder W, et al. (2011) Enhancing surgical vision by using realtime imaging of alphavbeta3-integrin targeted near-infrared fluorescent agent. Annals of Surgical Oncology 18: 3506–3513.
- Thistlethwaite AJ, Leeper DB, Moylan DJ 3rd, and Nerlinger RE (1985) pH distribution in human tumours. International Journal of Radiation Oncology, Biology, Physics 11: 1647–1652.
- Towner RA, Smith N, Doblas S, et al. (2008) In vivo detection of c-Met expression in a rat C6 glioma model. Journal of Cellular and Molecular Medicine 12: 174–186.
- Tseng JC, Wang Y, Banerjee P, and Kung AL (2012) Incongruity of imaging using fluorescent 2-DG conjugates compared to (18)F-FDG in preclinical cancer models. Molecular Imaging and Biology 14(5): 553–560.
- Tung CH, Bredow S, Mahmood U, and Weissleder R (1999) Preparation of a cathepsin D sensitive near-infrared fluorescence probe for imaging. Bioconjugate Chemistry 10: 892–896.
- Tung CH, Lin Y, Moon WK, and Weissleder R (2002) A receptor-targeted near-infrared fluorescence probe for in vivo tumour imaging. ChemBioChem 3: 784–786.
- Turk V, Stoka V, Vasiljeva O, et al. (2012) Cysteine cathepsins: From structure, function and regulation to new frontiers. Biochimica et Biophysica Acta 1824: 68–88.

2

- Uchiyama K, Ueno M, Ozawa S, Kiriyama S, Shigekawa Y, and Yamaue H (2010) Combined use of contrast-enhanced intraoperative ultrasonography and a fluorescence navigation system for identifying hepatic metastases. World Journal of Surgery 34: 2953–2959.

- Uchiyama K, Ueno M, Ozawa S, et al. (2011) Combined intraoperative use of contrastenhanced ultrasonography imaging using a sonazoid and fluorescence navigation system with indocyanine green during anatomical hepatectomy. Langenbeck's Archives of Surgery/Deutsche Gesellschaft fur Chirurgie 396: 1101–1107.

- van Dam GM, Themelis G, Crane LM, et al. (2011) Intraoperative tumour-specific fluorescence imaging in ovarian cancer by folate receptor-alpha targeting: First inhuman results. Nature Medicine 17: 1315–1319.

- Vasiljeva O, Papazoglou A, Kruger A, et al. (2006) Tumour cell-derived and macrophagederived cathepsin B promotes progression and lung metastasis of mammary cancer. Cancer Research 66: 5242–5250.

- Verdoes M, Edgington LE, Scheeren FA, et al. (2012) A nonpeptidic cathepsin s activitybased probe for noninvasive optical imaging of tumour-associated macrophages. Chemistry & Biology 19: 619–628.

- Villaraza AJ, Milenic DE, and Brechbiel MW (2010) Improved speciation characteristics of PEGylated indocyanine green-labeled Panitumumab: Revisiting the solution and spectroscopic properties of a near-infrared emitting anti-HER1 antibody for optical imaging of cancer. Bioconjugate Chemistry 21: 2305–2312.

- von Burstin J, Eser S, Seidler B, et al. (2008) Highly sensitive detection of early-stage pancreatic cancer by multimodal near-infrared molecular imaging in living mice. International Journal of Cancer 123: 2138–2147.

- Wang W, Ke S, Wu Q, et al. (2004) Near-infrared optical imaging of integrin alphavbeta3 in human tumour xenografts. Molecular Imaging 3: 343–351.

- Warburg O, Wind F, and Negelein E (1927) The metabolism of tumours in the body. The Journal of General Physiology 8: 519–530.

- Weis SM and Cheresh DA (2011) Tumour angiogenesis: Molecular pathways and therapeutic targets. Nature Medicine 17: 1359–1370.

- Weissleder R, Tung CH, Mahmood U, and Bogdanov A Jr. (1999) In vivo imaging of tumours with protease-activated near-infrared fluorescent probes. Nature Biotechnology 17: 375–378.

- Withrow KP, Newman JR, Skipper JB, et al. (2008) Assessment of bevacizumab conjugated to Cy5.5 for detection of head and neck cancer xenografts. Technology in Cancer Research & Treatment 7: 61–66.

- Xie BW, Mol IM, Keereweer S, et al. (2012) Dual-wavelength imaging of tumour progression by activatable and targeting near-infrared fluorescent probes in a bioluminescent breast cancer model. PLoS One 7: e31875.

- Yang Y, Hong H, Zhang Y, and Cai W (2009a) Molecular imaging of proteases in cancer. Cancer Growth and Metastasis 2: 13–27.

- Yang L, Peng XH, Wang YA, et al. (2009b) Receptor-targeted nanoparticles for in vivo imaging of breast cancer. Clinical Cancer Research 15: 4722–4732.
- Yang L, Mao H, Cao Z, et al. (2009c) Molecular imaging of pancreatic cancer in an animal model using targeted multifunctional nanoparticles. Gastroenterology 136: 1514–1525 e1512.
- Yarden Y (2001) The EGFR family and its ligands in human cancer. Signalling mechanisms and therapeutic opportunities. European Journal of Cancer 37(supplement 4): S3–S8.
- Zhang H, Zeng X, Li Q, Gaillard-Kelly M, Wagner CR, and Yee D (2009) Fluorescent tumour imaging of type I IGF receptor in vivo: Comparison of antibody-conjugated quantum dots and small-molecule fluorophore. British Journal of Cancer 101: 71–79.
- Zhu L, Wang H, Wang L, et al. (2011a) High-affinity peptide against MT1-MMP for in vivo tumour imaging. Journal of Controlled Release 150: 248–255.
- Zhu L, Zhang F, Ma Y, et al. (2011b) In vivo optical imaging of membrane-type matrix metalloproteinase (MT-MMP) activity. Molecular Pharmaceutics 8: 2331–2338.

2

CHAPTER 3

Optical image-guided cancer surgery: challenges and limitations

Stijn Keereweer[1], Pieter B.A.A. Van Driel[2], Thomas J.A. Snoeks[2], Jeroen D.F. Kerrebijn[1], Robert J. Baatenburg de Jong[1], Alexander L. Vahrmeijer[3], Henricus J.C.M. Sterenborg[4], Clemens W.G.M. Löwik[2]

3. Department of Otorhinolaryngology Head and Neck Surgery, Erasmus Medical Center, Rotterdam, The Netherlands.
4. Endocrinology and Molecular Imaging, Leiden University Medical Center, Leiden, The Netherlands.
5. Department of Surgery, Leiden University Medical Center, Leiden, The Netherlands.
6. Center of Optical Diagnostics and Therapy, Erasmus Medical Center, Rotterdam, The Netherlands.

ABSTRACT

Purpose

To provide a clear overview of the various components that play an essential role in the conundrum of optical imaging for application in cancer surgery.

Background

Optical image-guided cancer surgery is a promising technique to adequately determine tumour margins by tumour-specific targeting, potentially resulting in complete resection of tumour tissue with improved survival. However, identification of the photons coming from the fluorescent contrast agent is complicated by autofluorescence, optical tissue properties, and accurate fluorescent targeting agents and imaging systems. These factors all have an important influence on the image that is presented to the surgeon.

Results

Considering the clinical consequences at stake, it is a prerequisite to answer the questions that are essential for the surgeon. What is optical image-guided surgery and how can it improve patient care? What should the oncologic surgeon know about the fundamental principles of optical imaging to understand which conclusions can be drawn from the images? And how do the limitations influence the clinical decision-making? This manuscript discusses these questions and provides a clear overview of the basic principles and practical applications.

Conclusion

Although there are limitations to the intrinsic capacity of the technique, when practical and technical surgical possibilities are considered, optical imaging can be a very powerful intraoperative tool in guiding the future oncologic surgeon towards radical resection and optimal clinical results.

Introduction

For cancer surgery with curative intentions, radical resection (i.e., removal of all cancer cells) is a sine qua non. To achieve this, the surgeon has to adequately assess the tumour resection margin during the operation. Optical molecular imaging using near-infrared (NIR) fluorescence introduces a revolutionary new approach to address this basic challenge in surgical oncology (1–3). The field of optical imaging emerged in the early 20th century with the observation of porphyrin fluorescence in certain tumours, but a lack of fundamental knowledge and suitable optical equipment prevented further development at the time (4). The finding that photons in the NIR range (650–900 nm) travel through tissue much deeper than photons in the visible light range (5) was essential for the advancement of optical imaging toward clinical practice, and further development gained momentum over the past decade (1, 6). To use optical imaging for visualization of cancer, fluorescent agents are injected that emit light in the NIR range and are tumour specific using a variety of targeting strategies (2). Because the human eye is not sensitive for light in the NIR region, dedicated camera systems are required to detect the fluorescence emission from these molecules (2). With real-time intraoperative fluorescence imaging of tumour margins, the technique promises to guide the oncologic surgeon toward optimal radical resection and clinical results. Preclinically, optical imaging has been used in tumour identification, image-guided resection, therapy monitoring, and detection of sentinel lymph nodes. Because tumourspecific agents were not yet approved for clinical use, the first clinical studies were conducted using nonspecific fluorescent agents that had long been approved for different applications and could therefore be used for sentinel lymph node mapping (6, 7). Clinical trials of tumour imaging using indocyanine green have been reported in hepatobiliary and colorectal cancer (8). Recently, a milestone step was completed when the first-in-human trial using tumour-specific targeting was reported (9), marking the beginning of a new phase of optical image-guided surgery. However, although it is very likely that the technique will deliver an important contribution to surgical oncology, this approach has fundamental limitatioins that influence the ability to differentiate the targeted tissue from its surroundings. Nowthat the first clinical trial has been reported, the group of oncologic surgeons that gets acquainted with the flourishing field of optical image-guided surgery is increasing day by day, with clinical consequences at stake. As we show in this review, it is essential for the clinician to understand which phenomena occur when photons travel through tissues and how these phenomena influence the optical image that is acquired. We therefore believe that it is now, more than ever, of paramount importance to provide the surgical oncologist a clear overview of the basic principles of optical image-guided surgery to be able to understand how these limitations influence the sensitivity of this technique. Awareness of these limitations and focusing research on solving these challenges are of utmost

importance for proper implementation and evaluation of the clinical value of this new technology.

The basic principle of fluorescence imaging

The geometric principle of fluorescence imaging is illustrated in Fig. 1A. A light source is required that sends out a bundle of light with a specific wavelength that is able to excite the fluorophore (i.e., excitation photons). Because the targeted fluorophore is located under the tissue surface, this excitation light has to enter and travel through tissue to reach the fluorophore. Light entering the tissue is partly influenced by reflection and refraction at the tissue surface. The direction of photons that travel through the tissue can be changed due to scattering. In addition, photons can be absorbed by various components in the tissue.
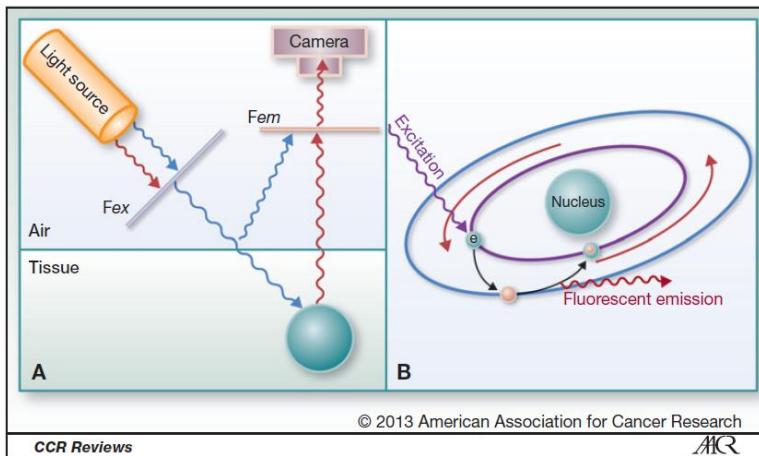

Figure 1; Geometric and basic principle of fluorescence imaging. A, light of the appropriate excitation wavelength is selected using a filter (Fex), which is located between a light source and the tissue. The excitation light travels through the tissue and is absorbed by a fluorophore, which subsequently emits light of a different wavelength. A small portion of this emitted light will exit the tissue and can be detected with a camera. A filter (Fem) is placed in front of the camera, which allows only the emitted light to pass into the camera. B, absorbed light by the fluorophore instigates an electron (e) in the ground state toward an electronically excited state. Upon return to the ground state, the fluorophore emits a photon. The wavelength of this emitted photon is specific for the fluorophore. Fex, excitation filter; Fem, emission filter.

Only when such a component is a fluorophore, which can be either an intrinsic tissue component (i.e., autofluorescence) or an injected external fluorescent agent, absorption of a photon results in a gain in energy of the fluorophore, which then enters an excited state (Fig. 1B).

3

The electrons remain in this state for about 10 _8 seconds depending on the molecule, which is called the lifetime of the fluorophore. After this phase, the system returns to its ground state and emits the photon, which could be heading into all directions (Fig. 1B). The change in energy between the absorbed and the emitted photon results in a change in wavelength. This shift of shorter wavelengths (higher energy) of the absorption spectrum to longer wavelengths (lower energy) of the emitted fluorophores is called the Stokes shift. After excitation of the fluorophore, emission photons will also be influenced by scattering and absorption, and the photons that reach the tissue surface will subsequently be influenced again by reflection and refraction at the surface.

Finally, in a clinical geometry, only part of these photons can eventually be detected by the camera system. Although optical imaging is based on the detection of photons, Fig. 2 illustrates that the path that photons travel through the imaged tissue is influenced by optical properties of the components in the tissue (i.e., absorption and scattering). As a result, fluorescence images will display intensities that are strongly influenced by varying absorption properties of the tissue and the images may be blurred due to scattering of light. The following paragraphs explain in detail how these phenomena influence the acquired image.
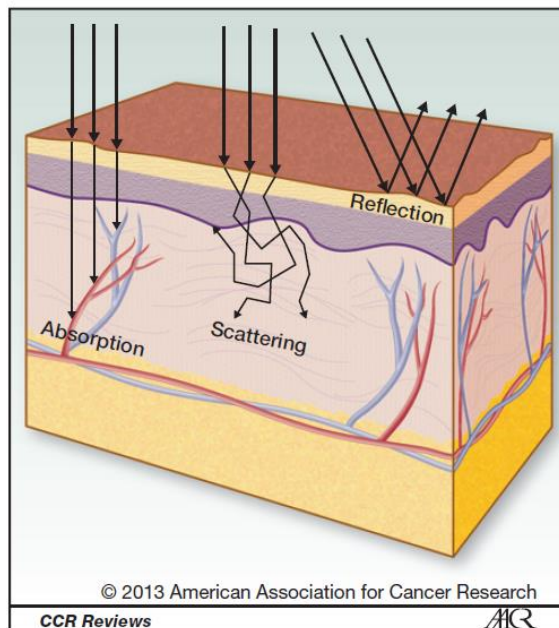

Figure 2; Light propagation through tissue. Light travelling through tissue is subject to reflection, scattering, and absorption.

What happens when light travels through tissue?

Absorption

All tissues contain components that can absorb photons that travel through them. The composition of these components varies between different tissue types and organs, but also within these tissues, and may vary in time (10). In general, the most relevant absorbers of photons are water, lipids, oxyhemoglobin, and deoxyhemoglobin (Fig. 3A) (11). Blood is the main absorber in the visible region, and the absorption of light by blood is the highest in the blue-green region. This fact can be illustrated by illuminating the human skin with white light. Because of the absorption of photons with shorter wavelengths, a reddish reflection returns from the skin. In this way, absorbers influence the color of the light that exits imaged tissues. In the NIR range, the absorbance per volume of these components is much lower than in other parts of the spectrum, allowing for deeper penetration of photons into the tissue (Fig. 3).
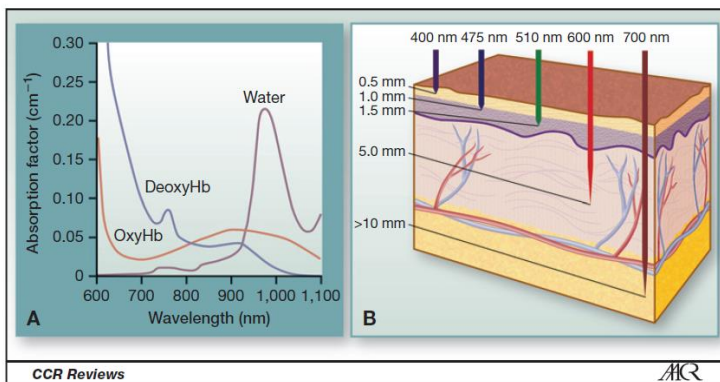
Figure 3; Absorption of light. A, absorption of light by various components varies over the wavelength spectrum, resulting in an optimal window for fluorescence imaging in the NIR light region between 650 and 900 nm. Figure 3A is reprinted from ref. 11, with permission, from John Wiley & Sons. B, penetration of light range from 0.5 mm to more than 10 mm contingent to the wavelength. OxyHb, oxygenated hemoglobin; DeoxyHb, deoxygenated hemoglobin.

Scattering

Next to absorption of the photon, a change in photon direction can occur, an effect known as scattering (Fig. 4). In most parts of the visible and NIR region, scattering events occur much more frequently than absorption events. Even though a forward direction of scattering photons is most likely to occur in tissues, the accumulation of multiple consecutive scatter events will result in a gradual randomization of the propagation direction (i.e., diffuse light, Fig. 4; ref. 12). Randomization of the direction of light reduces the signal strength as well as the accuracy of determination of the source localization. However, scattering can also have a positive effect on the fluorescence signal intensity because of its effect on the excitation light. The photons that

3

excite the fluorophore follow a similar contorted light path as the emission light. In highly scattering tissue, the contorted light path causes retention of photons in that specific area. In other words, in a highly scattering medium, the photons bounce around locally for a longer time, increasing the chance for a fluorescence event. Consequently, there can be increased fluorescence intensity in tissues with more scattering compared with tissues with less scattering (13). The net effect of scattering on fluorescence imaging depends on the exact optical properties of the tissue at hand.
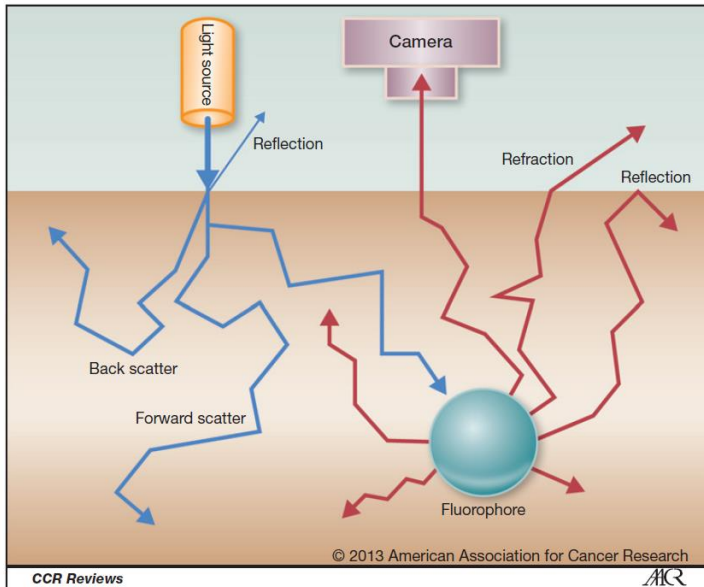
Figure 4; Photons change direction multiple times when traveling through tissue. In the case of forward scatter, a photon travels more or less in the same direction before and after the scattering event. In the case of backscatter, the photon will end up traveling in the opposite direction after the scattering event. During fluorescence imaging, the direction of both the excitation light and the emitted light is randomized due to scattering. Only a small portion of the excitation light will reach a fluorophore, and only the camera will capture a small portion of the emitted light. As a result, it is often difficult to pinpoint the exact origin of the detected fluorescent signal.

Influence of optical properties on light penetration depth

Scattering and absorption coefficients vary between locations and tissues due to the different components within the heterogeneous tissue. Importantly, the influence of these phenomena on the fluorescence signal will be higher when fluorescent light has to emerge from larger tissue depths and consequently has to pass more absorbers and scattering events. In the visible light region, absorption by biologic chromophores limits the penetration depth to a few millimeters with a maximum of 10 millimeters. Because of less absorption and scattering, penetration depth is

increased to more than a centimeter in the NIR region (14, 15); however, this measurement strongly depends on the type of tissue (refs. 1, 3, 16; Fig. 5).
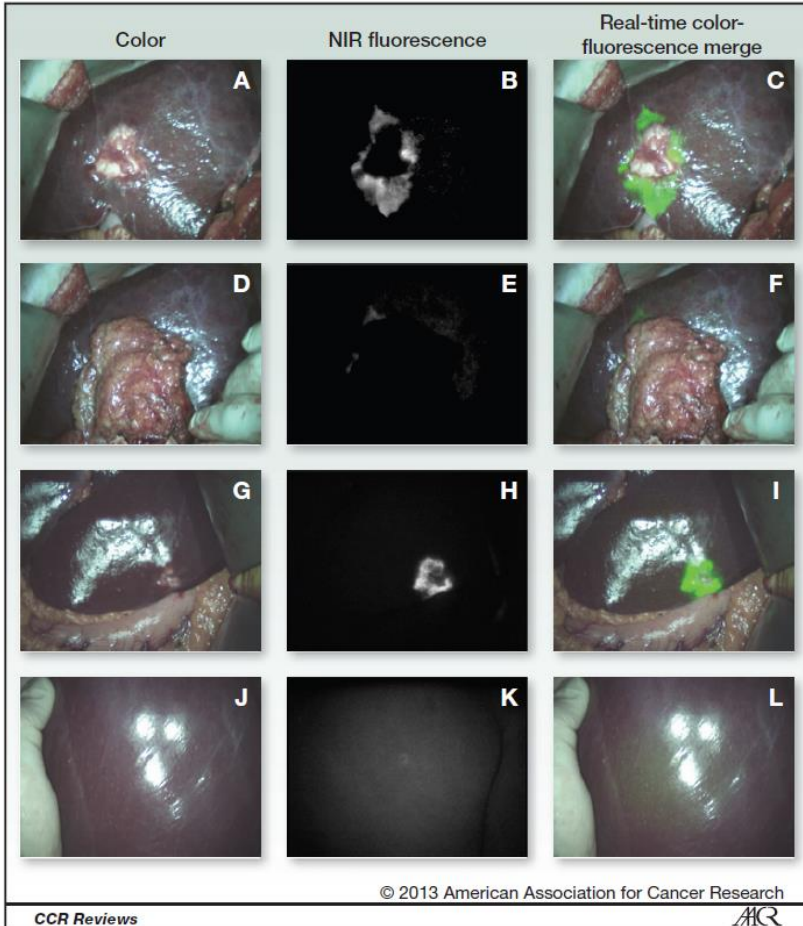
Figure 5; Effect of optical tissue properties during real-time intraoperative optical imaging of liver metastases in humans. The consequences of absorption and scattering on the image are essential for understanding the limitations of optical image-guided surgery: At the surface, fluorescent agents will appear as a bright and sharply delineated spot. However, the target will always be surrounded by a halo of fluorescent light that was directed into the tissue after emission, scattered around locally, and emitted from the surface at some distance from the target location. Moreover, due to absorption and scattering, an identical fluorescent agent that is located deeper within the tissue will have lower signal intensity and will be imaged as an indistinct blob. An example is shown of a liver metastasis that is delineated by fluorescence signal (A–C). When a thick layer of greater omentum covers the area of interest, fluorescence signal is not detected (D–F). A second liver metastasis is indicated in a different patient (G–I). However, when the liver is flipped around and the opposite side is imaged, high absorption of the liver that is saturated with blood results in an indistinct fluorescent blob (J–L).

3

Reflection and refraction

As imaging during surgery always focuses on a surface, the mismatch between the indices of refraction of tissue and air is unavoidable, resulting in a change in direction of the photons. This mismatch in index of refraction causes reflections to occur at the surface. The excitation light will be partially reflected from the surface, like the sun on a water surface. When the light is nearly perpendicular to the surface of the tissue, the surface reflection is not more than a few percent. However, emitted fluorescent light that is generated inside the tissue is diffuse and partly reaches the surface under large angles, resulting in complete reflection within the tissue. This internal diffuse reflection coefficient at the surface can be in the order of 50%. Consequently, the emitted fluorescent light is even more diffuse, and the amount of light that escapes the surface and can be detected by the fluorescence camera is further decreased.

Fluorescence imaging and autofluorescence

The goal of fluorescence imaging is to detect a target by its specific fluorescence signal. Detection of the fluorescent signal of the targeted fluorophore is hampered because all cells contain various endogenous fluorophores that become fluorescent when excited by UV, visible, or NIR radiation of suitable wavelength. This intrinsic fluorescence of the tissue induces a nonspecific background signal. The number of endogenous fluorophores varies strongly between tissue types. Moreover, the autofluorescence can change in time because of bleaching of the endogenous fluorophores and because some of the endogenous fluorophores are related to metabolism (e.g., NADH, NAD, FAD, and FADH). Because we can see cancerous lesions with our eyes, the optical properties of these lesions are changed by definition, and a difference in autofluorescence signal compared with the surroundings can be detected. This effect has been used for autofluorescence-guided surgery (17). However, due to the aforementioned effects, "tumourspecific" autofluorescence signals can vary over time, making it an unreliable target. Furthermore, other benign visible changes (e.g., scar formation) also result in a change in autofluorescence, limiting the specificity of this technique (18). Most importantly, despite positive correlations that have been reported in a number of studies that use autofluorescence to detect and remove the tumour (17), it is not clear which biologic aspects are responsible for the change in autofluorescence signal in the imaged lesions. Studies to assess these aspects are compromised because of artifacts as a result of color changes in cancer tissue (18). The surgeon should therefore approach changes in autofluorescence with the same level of uncertainty as visible clues of cancerous tissue. If high correlation of autofluorescence and tumour tissue is consistently reported, they can be used to aid the surgeon in assessing the tumour margins but should not be considered as tumour-specific proof of tumour margins. As a good alternative, a target-specific

agent that contains a fluorophore is usually injected intravenously. Now that we understand how optical properties can influence the optical path of the photon, we are confronted with a second challenge: How can we determine if the photon that we detect has been excited by the targeted fluorophore, and not by its surrounding autofluorescent components? For the targeted cancer cells to be detected, the signal of the target-specific fluorescence agent must be significantly higher than the nonspecific autofluorescence. Although autofluorescence is much lower when NIR light is used, the signal-to-background ratio (SBR) must be sufficient to distinguish the photons of the target-specific fluorescent agent from the autofluorescence signal.

What are the consequences of these effects for fluorescence imaging of cancer?

We have now set the stage for optical imaging in tissues and gained a clear picture of the problems that we face when we aim to detect a minimal amount of tumour-specific fluorescence agent within this diffuse heterogeneous medium containing absorbers, scatter events, and endogenous fluorophores. First, the fluorescence intensity is not only influenced by the concentration and fluorescence quantum yield of the fluorescent agent but also by the tissue optical properties that are involved. For example, as a result of absorption by blood, fluorescence signals in organs with high blood volumes, such as the liver (19) or highly vascularized tumours, or in tumour cells that co-opt host vessels (20) may appear lower than surrounding less-absorbing tissue, even if they contain larger amounts of contrast agent compared with the surrounding tissue (21). Similarly, less absorbing lesions (e.g., cysts and lymph nodes) may seem brighter in a heterogeneous environment. The variability in absorption and scattering between different tissues or even tissue components should be taken into account during the process of image-guided surgery. Second, intraoperative camera systems will not only detect the fluorescence signal of the fluorescent agent but also the autofluorescence in the scanned region, and therefore a sufficient SBR is required. At present, various strategies are being evaluated that represent attempts to improve adequate identification and quantification of the targeted photons.

Strategies to reduce the influence of absorption and scattering on the image

With the state-of-the-art technological advancements, it remains impossible to determine all absorbers and scatter events within a diffuse, inhomogeneous medium. However, calculation methods have been developed that try to estimate the perturbation caused by optical tissue properties and improve the image by partly correcting for these properties (14). An intraoperative fluorescence imaging system has been developed that implements such a correction scheme for

light intensity variation in tissues (21). Improved accuracy was shown within phantoms and postmortem tissues, independently of optical property variation in tissues. At a 5-fold change of absorption variation within the fluorescent lesions, quantification errors were reduced from 25% in uncorrected images to 8% using the correction scheme (21). A second new technology being investigated in this field is fluorescence differential path length spectroscopy, which determines fluorophore concentration based on the fluorescence intensity corrected for absorption (22). This facilitates quantitative concentration measurements even for strong variations in either background absorption or scattering. However, currently this method can only be conducted using fiber-optic measurement at a single point. An imaging version and subsequent intraoperative applications have not been developed yet. Finally, tomographic reconstruction techniques (23), Raman spectroscopy (24), and photoacoustic imaging (12, 25) may play important roles in the future, although currently they are not suited for real-time imaging in the surgical theater. Raman spectroscopy is based on inelastic scattering: the effect on the frequency of excitation photons that changes upon interaction with tissue, which is independent of optical tissue properties or autofluorescence (24, 26). In surface-enhanced Raman spectroscopy (SERS), tumour-specific nanobodies are injected that are able to increase the intrinsically very low Raman effect, thereby improving detectability. Promising preclinical results of brain tumour resection guided by SERS have been reported (27). In photoacoustic imaging (also referred to as optoacoustic imaging), thermoelastic expansion of molecules resulting from laser pulse irradiation causes emission of acoustic waves that can be measured by photoacoustic spectroscopy. The resolution in photoacoustic imaging is not limited by tissue scattering but by the attenuation of acoustic frequencies by tissue (12, 25). This technique improves deep-tissue imaging but is less suitable for image-guided surgery.

Strategies to distinguish the target-specific fluorescence signal from autofluorescence

Two methods are now under investigation that represent attempts to separate the target-specific fluorescence signal from the nonspecific autofluorescence. The first is based on differences in the fluorescence spectrum between photons from these two fluorescent sources (i.e., spectral unmixing), and the second method exploits differences in the fluorescence lifetime of the fluorophores (i.e., lifetime imaging). The concept of spectral unmixing is based on the "signature" emission intensity that each fluorophore has at certain wavelengths, providing the fluorophore with its own specific emission spectrum (28). Using spectral unmixing, the signal is decomposed into a collection of predefined spectra that is used to determine the individual contribution of each fluorophore. Using calculation models combined with the fluorophore-specific emission spectrum as reference (i.e., linear unmixing), the contribution of each

fluorophore in a total fluorescent signal can be extracted (29). When spectral signatures of the fluorophore of interest and the autofluorescence are known, unmixing these specific fluorescence spectra may result in a more accurate SBR. The first-inhuman trial on intraoperative tumour-specific fluorescence imaging was conducted using a camera system that was based on spectral unmixing technology (9, 21). There are, however, fundamental problems with this approach. Linear unmixing is based on the assumption that the measured spectrum consists of the sum of the fluorescence spectra of all the components in the tissue, that is, linear mixing. As mentioned earlier, inhomogeneous optical properties influence the path that photons travel through the imaged tissue and therefore not only put their own signatures on the fluorescence spectrum but may also do so nonlinearly owing to the inhomogeneous nature of tissue. Furthermore, the unmixing procedure is a very complex process that requires all components contributing to the spectrum to be known, as well as all of their specific "signature" spectra, which also need to be sufficiently distinctive from one another. The second method, fluorescence lifetime imaging, distinguishes individual fluorophores by their specific temporal decay after excitation. This fluorescence decay (i.e., lifetime) is a fluorophore-specific characteristic that is not influenced by the local concentration of fluorophores, the optical path, the local excitation intensity, or the local fluorescence detection efficiency. To acquire the characteristic decay curves, a picosecond laser pulse is used for excitation and fluorescence is measured as a function of time. On the basis of the specific lifetime of the fluorophores, the target-specific fluorescence signal can be distinguished from the nonspecific autofluorescence. In addition, the temporal response at which photons emerge from the tissue can be measured (i.e., time-domain imaging), which is used to estimate the concentration and depth of the fluorescent source. Lifetime imaging requires specific conditions in terms of pulsed excitation and data capturing with complex data processing, which currently makes it a time consuming technique. Although intraoperative lifetime based techniques are being developed at a strong pace and hold promising advantages, it will take some time before they can be used in a real-time intraoperative setting where mobility of the equipment and speed of data processing and interpretation are of the essence (30).

What is required for a target-specific fluorescence image?

So far, we have assumed that the fluorescent agent has been able to specifically target the tissue of interest with subsequent colocalization between the fluorescent signal and tumour cells. However, to gain a complete insight into the different phenomena that can influence the optical image, it is necessary to understand the challenges of tumour-specific targeting. On the basis of the hallmarks of cancer (31), a growing variety of tumour-specific targets are available for imaging of cancer (2). The efficiency of target-specific agents to reach their intended target is

defined by many variables, including affinity of the agent and abundance of the target receptors or epitopes (16). To achieve target-specific fluorescence imaging, the contrast agent has to be delivered to the target, requires adequate contact time with the target for binding to occur, and has to be retained by the target while nonbound agents are cleared from the circulation (10). It has been reported that at saturating doses of the agent, high-affinity antibody uptake is dependent on antigen expression levels. However, at subsaturating doses, the signal is generally limited by delivery of the agent (32). For the agent to be effectively delivered to the target, many barriers in the human body have to be passed. Next to inhibitor proteins present in plasma that can non-specifically bind to the agent (1), walls of blood vessels provide a first barrier for drug delivery to targeted tumour tissues. In most cases, abnormal neovascularization of the tumour occurs [i.e., enhanced permeability and retention (EPR) effect] resulting in leaky tumour blood vessels (33). As a result, macromolecular drugs can traverse the endothelium of these leaky blood vessels and passively accumulate in the interstitium of tumour tissues (33). However, the EPR effect is largely dependent on the size of the agent; larger agents are less efficient in crossing the endothelial barrier (34). Tumour growth beyond the size of approximately 1 mm is dependent on oxygen and supply of nutrients and therefore requires angiogenesis (35). However, in smaller lesions, the angiogenic switch may not have occurred and drug delivery could be hampered due to the lack of adequate vascularization. In other cases, tumour cells may grow alongside pre-existent host vasculature, a process known as vessel co-option (20). In these cases, in which angiogenesis-directed targeting may not yet be possible, indirect indicators of tumour growth could be useful for tumour detection, even in the earliest stages of carcinogenesis. For example, NIR fluorescence agents that detect proteases that are involved immigration of tumour cells and degradation of the extracellular matrix can allow for imaging of the invasive tumour front (36–38), and preneoplastic lesions in Barrett esophagus can be identified by targeting changed patterns of lectin binding (39). Once extravascular, two barriers for adequate binding of the agent remain. First, the agent has to cross extracellular matrix tissue surrounding the target cells (33). At this point, diffusion into the tumour is sometimes impeded by high hydrostatic pressure of many solid tumours, preventing homogeneous infiltration of the agent (1). Second, binding of the agent to specific epitopes of the cancer cell has to occur, and internalization of the agent can further amplify the fluorescence signal (23, 40, 41). Therefore, the cellular basement membrane is the third barrier, which can be passed using the transporter system of the cell by receptor-mediated endocytosis (33). Finally, clearance of non-bound agent from the circulation is required to provide sufficient SBRs. This occurs through the liver (i.e., excretion into bile and feces) and/or the kidney (i.e., excretion into urine). Both the route of clearance and the clearance rate are important determinants for the blood half-life time and consequently the background signal and optimal imaging time of contrast agents (40).

How relevant is all this for the clinical practice of surgical oncology?

Optical imaging is a complicated process. To adequately interpret the intraoperative fluorescent image of the tumour that is presented, the surgeon should comprehend that the target-specific fluorescent agent had to get to and stay at the tumour, that part of the signal was reduced and distorted by absorbers and scatter events, and that the signal had to be subtracted from its autofluorescent surroundings. Considering all these influences that could hamper detection of cancer cells that are located under the surface, the additional value of NIR fluorescence imaging over conventional surgery could be questioned. After all, after a mere 3 decades of extensive research, the fundamental principles of optical imaging still leave room for error, and it currently seems that this approach will never be unambiguous. To determine the additional value of intraoperative optical imaging, we need to ask ourselves what the fundamental purpose of this tool should be for surgical oncology. In essence, the goal of surgery is to remove all cancer cells while minimizing damage to surrounding healthy tissues. Considering the small size of a single cancer cell or group of cells, the limited target epitopes available for the fluorescent agent and the optical tissue properties and autofluorescence, detection of the last cancer cells under a surface will not always be possible. Nevertheless, it is very likely that the current technique of optical imaging, with its limitations, will offer improvement of the conventional surgical practice to successfully treat the patient and could provide a final solution to the conundrum of irradical resection. The most obvious reason is that, although there are limitations when considering the cellular level, optical imaging allows for a more detailed delineation of the tumour margins than the conventional practice of assessment by palpation and visual aspects of the tumour. It was repeatedly shown in animal models that tumour margins can be clearly demarcated by optical imaging (10, 38, 42). Consequently, the surgeon can resect the tumour based on these images with the required tumour-free margin outside the fluorescent tissue. Moreover, in some cases that have thin tumour strands that are invisible to the naked eye, a tumourfree margin of up to several centimeters is required for local control using conventional surgical practice. Although effects of scattering could result in a fluorescent halo of up to several millimeters under certain conditions, detection of these tumour strands using optical imaging would still largely reduce the need of these large tumour-free margins, resulting in improved postoperative functionality. Although yet to be proven in large clinical trials, it is anticipated that this approach will already lead to a decrease in the local recurrence rate and improved patient survival and functionality. Second, it has been suggested that penetration depth limitations might not be relevant for surgical practice because the surgeon will, by definition, bring the area of interest closer to the surface during the surgical procedure (34, 43). When, after resection of the tumour mass, an area is found with persisting fluorescence signal indicating irradical margins, this could be resected subsequently until no more signal is found in a "cut the light-procedure," similar to the technique

of Mohs surgery. Although a similar procedure, optical imaging will be much more efficient than Mohs surgery due to real-time acquisition and the fact that intraoperative pathologic evaluation is not required. At the surface, the influence of optical properties will be minimized, improving the sensitivity even in cases of perineural or perivascular growth, as long as the photons from the contrast agent can be differentiated from autofluorescence. Finally, although it is currently impossible to completely correct for an unknown variability in optical properties of the tissue, we should not forget that a very advanced system is available that has the capability to identify distinct tissue components (e.g., blood vessels) during the surgical process: the surgeon him or herself. The true additional value of this technique will become clear once the surgical expertise to distinguish tissue components becomes incorporated into the interpretation of the images. For example, the surgeon would preferably reinvestigate a suspicious region that has no fluorescence signal if it is covered by a blood vessel as long as the surgeon realizes that vessels can be highly absorbent. Using the knowledge about the tissues at hand, optical image-guided surgery will result in a dynamic and flexible process providing the surgeon with valuable additional information during the entire operation. This will likely require a learning curve that would follow the encouraging example of pioneer work in resection of malignant gliomas using 5-aminolevulinic acid. Preliminary intraoperative studies in this field provide detailed reports on these learning processes (44, 45). These studies showed that photons are highly absorbed by blood or cauterized tissue debris after monopolar cautery resection and that suction of these layers or rinsing the surface with saline is required for unperturbed assessment of tissue fluorescence. Furthermore, necrotic tumour centers accumulated little fluorescence, which was not a problem because necrosis could easily be distinguished under white light and therefore did not impair fluorescence-guided tumour resection. Tissues were not falsely labeled by fluorescence from blood contaminating the tumour cavity, which might have been expected if plasma had contained substantial amounts of fluorescent agent. Photobleaching after overexposure was minimized with improved development of fluorophores. Finally, the fluorescent source could be located by manipulation of the tissues, as illustrated in Fig. 5. The success of this approach has led to a randomized controlled multicenter phase III trial showing improved progression-free survival in patients with malignant glioma using fluorescence-guided surgery (46).

What level of accuracy is required for the routine of surgical practice?

Considering the intraoperative flexibility of a trained surgeon and the practice of exploration of the area of interest during surgery, we believe that optical image-guided surgery has the potential to greatly reduce the tumour-free safety margin. If a tumour-free margin could be minimized, postoperative functional outcome could be drastically improved in many cases where the tumour is surrounded by important anatomical structures. This would require tumour imaging with optimal sensitivity and specificity of the tumour-specific agent, followed by resection of the fluorescent tissue without any excess margin of healthy tissue. It is anticipated that sensitivity and specificity of the target-specific agent will be optimized by simultaneously targeting multiple tumour characteristics at different wavelengths (42, 47). To adequately assess the fluorescent border, high accuracy of the imaging technique is demanded. This would require high-resolution images that can be acquired at higher magnifications than the regular macroscopic field of view. Although not suitable for intraoperative use, a system that incorporates both macroscopic and microscopic imaging has been tested in an experimental setting of cancer detection (23). In the macroscopic field of view, the smallest lesion detectable with a highly expressed antigen (e.g., several million antigens/cell) was approximately 600 mm, a volume that approaches pixel resolution of the macroscopic images (110 mm/pixel). Higher magnification of this tumour revealed images down to the single cell level due to higher resolution (23). These results suggest that incorporation of zoom function into the intraoperative camera system would improve surgical accuracy by using a combination of macroscopic imaging (to survey the tissue and guide tumour resection) and microscopic imaging (to verify clean resection margins; ref. 40). However, scattering generally determines the sharpness of the in vivo fluorescence image, especially for deeply located fluorescent sources, and not the imaging equipment. Furthermore, microsurgical or robotic camera systems are only used in some oncological surgical specialties (e.g., neurosurgery). Therefore, in daily routine and logistics of surgical practice in most other cases, the tremor of the surgical hand will limit removal of the tumour with accuracy smaller than 0.5 mm. As a result, the accuracy of removing the fluorescent tissue will not only be limited by the resolution of optical imaging but also by the practical limitations of the surgical hand. As long as microscopic or robotic surgery is not a routine practice, the discussion on the level of resolution will lie within the margin of technical surgical possibilities. In analogy to highly accurate stereotactic radiotherapy using Cyberknife that has a technical error margin of 0.5 to 2 mm (48), it is very likely that this level of accuracy will be sufficient to adequately treat the patient with minimal unnecessary loss of functionality.

Challenges for clinical translation

Although a rapidly increasing amount of data is supporting the additional value of optical image-guided surgery for cancer therapy, challenges remain in translation of the preclinical experimental setup into routine clinical practice (2, 6). The technique requires development of tumour-specific fluorescence agents and dedicated intraoperative camera systems. Important progress has been made over the past few years in both fields, but it is essential to identify the hurdles that are still impeding successful clinical translation. An intrinsic limitation of development of fluorescence tumour-specific agents is the fact that such drugs are used as diagnostic tools instead of therapeutic drugs that require administration over a longer period of time. Development of diagnostic drugs is therefore subject to lower financial incentives for pharmaceutical companies. The first obvious steps were taken by conjugation of already clinically available tumour-specific agents (e.g., cetuximab) to fluorophores (2, 49). Until the technique will become available at a large scale, further development of these agents will have to be carried out by non-profit (i.e., academic) organizations. Furthermore, dedicated imaging systems will have to become easily available for a large group of surgeons to stimulate adoption of the technique. Currently, the most advanced systems are still only available in the research setting of clinical trials (7, 9), whereas other systems are already commercially available (50, 51). These economic and implementation issues are critical for successful adoption of surgical optical imaging.

Conclusions

Optical imaging has the potential to revolutionize cancer surgery by real-time fluorescence guidance in discriminating between healthy and diseased tissues and identifying vital structures. However, absorption, scattering, and autofluorescence are fundamental optical tissue properties that influence the images and limit the ability to differentiate the targeted tissue from its surroundings. In pursuit of removing all cancer cells by resection of the total tumour-specific fluorescence signal, the oncologic surgeon should carefully consider these limitations during the process of image-guided cancer surgery. Although there are limitations to the intrinsic capacity of the technique, when practical and technical surgical possibilities are considered, optical imaging can be a very powerful intraoperative tool in guiding the future oncologic surgeon toward radical resection and optimal clinical results.

References

1. Frangioni JV. New technologies for human cancer imaging. J Clin Oncol 2008;26:4012–21.

2. Keereweer S, Kerrebijn JD, van Driel PB, Xie B, Kaijzel EL, Snoeks TJ, et al. Optical image-guided surgery–where do we stand? Mol Imaging Biol 2011;13:199–207.

3. Weissleder R, Pittet MJ. Imaging in the era of molecular oncology. Nature 2008;452:580–9.

4. Rassmussen-Taxdal DS, Ward GE, Figge FH. Fluorescence of human lymphatic and cancer tissues following high doses of intravenous hematoporphyrin. Cancer 1955;8:78–81.

5. Patterson MS, Chance B, Wilson BC. Time resolved reflectance and transmittance for the non-invasive measurement of tissue optical properties. Appl Opt 1989;28:2331–6.

6. Keereweer S, Hutteman M, Kerrebijn JD, van de Velde CJ, Vahrmeijer AL, Lowik CW. Translational optical imaging in diagnosis and treatment of cancer. Curr Pharm Biotechnol 2012;13:498–503.

7. Mieog JS, Troyan SL, Hutteman M, Donohoe KJ, van der Vorst JR, Stockdale A, et al. Toward optimization of imaging system and lymphatic tracer for near-infrared fluorescent sentinel lymph node mapping in breast cancer. Ann Surg Oncol 2011;18:2483–91.

8. Schaafsma BE, Mieog JS, Hutteman M, van der Vorst JR, Kuppen PJ, Lowik CW, et al. The clinical use of indocyanine green as a nearinfrared fluorescent contrast agent for image-guided oncologic surgery. J Surg Oncol 2011;104:323–32.

9. van Dam GM, Themelis G, Crane LM, Harlaar NJ, Pleijhuis RG, Kelder W, et al. Intraoperative tumour-specific fluorescence imaging in ovarian cancer by folate receptor-alpha targeting: first in-human results. Nat Med 2011;17:1315–9.

10. Frangioni JV. In vivo near-infrared fluorescence imaging. Curr Opin Chem Biol 2003;7:626–34.

11. Chance B. Near-infrared images using continuous, phase-modulated, and pulsed light with quantitation of blood and blood oxygenation. Ann N Y Acad Sci 1998;838:29–45.

12. Ntziachristos V. Going deeper than microscopy: the optical imaging frontier in biology. Nat Methods 2010;7:603–14.

13. Star WM. Light dosimetry in vivo. Phys Med Biol 1997;42:763–87.

14. Bogaards A, Sterenborg HJCM, Wilson BC. In vivo quantification of fluorescent molecular markers in real-time: a review to evaluate the performance of five existing methods. Photodiagnosis Photodynamic Ther 2007;4:170–78.

15. Farrell TJ, Patterson MS. Diffusion modeling of fluorescence in tissue. In: Mycek M, Pogue BW, editors. Handbook of biomedical fluorescence. New York: Marcel Dekker Inc.; 2003. p. 29–60.

16. Hilderbrand SA, Weissleder R. Near-infrared fluorescence: application to in vivo molecular imaging. Curr Opin Chem Biol 2010;14:71–9. 17.

17. Poh CF, Zhang L, Anderson DW, DurhamJS, Williams PM, Priddy RW, et al. Fluorescence visualization detection of field alterations in tumour margins of oral cancer patients. Clin Cancer Res 2006;12:6716–22.

18. De Veld DC, Witjes MJ, Sterenborg HJ, Roodenburg JL. The status of in vivo autofluorescence spectroscopy and imaging for oral oncology. Oral Oncol 2005;41:117–31.
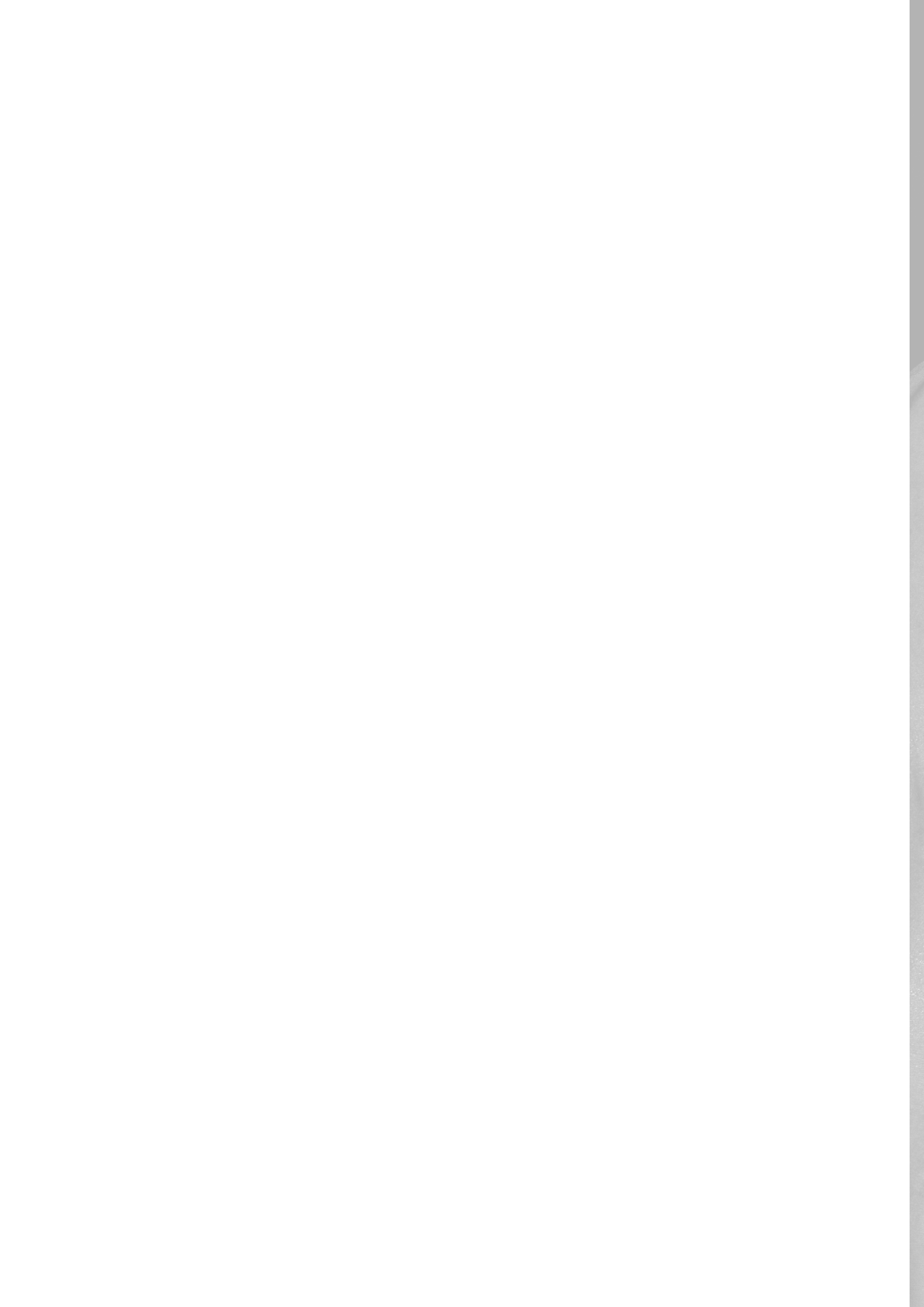
3

19. Hutteman M, Mieog JS, van der Vorst JR, Dijkstra J, Kuppen PJ, van der Laan AM, et al. Intraoperative near-infrared fluorescence imaging of colorectal metastases targeting integrin alpha(v)beta(3) expression in a syngeneic rat model. Eur J Surg Oncol 2011;37:252–7.

20. Holash J, Maisonpierre PC, Compton D, Boland P, Alexander CR, Zagzag D, et al. Vessel cooption, regression, and growth in tumours mediated by angiopoietins and VEGF. Science 1999;284:1994–8.

21. Themelis G, Yoo JS, Soh KS, Schulz R, Ntziachristos V. Real-time intraoperative fluorescence imaging system using light-absorption correction. J Biomed Opt 2009;14:064012.

22. Kruijt B, Kascakova S, de Bruijn HS, van der Ploeg-van den Heuvel A, Sterenborg HJ, Robinson DJ, et al. In vivo quantification of chromophore concentration using fluorescence differential path length spectroscopy. J Biomed Opt 2009;14:034022.

23. Thurber GM, Figueiredo JL, Weissleder R. Detection limits of intraoperative near infrared imaging for tumour resection. J Surg Oncol 2010;102:758–64.

24. Nijssen A, Koljenovic S, Bakker Schut TC, Caspers PJ, Puppels GJ. Towards oncological application of Raman spectroscopy. J Biophotonics 2009;2:29–36.

25. Ntziachristos V, Ripoll J, Wang LV, Weissleder R. Looking and listening to light: the evolution of whole-body photonic imaging. Nat Biotechnol 2005;23:313–20.

26. Zavaleta CL, Kircher MF, Gambhir SS. Raman's "effect" on molecular imaging. J Nucl Med 2011;52:1839–44.

27. Kircher MF, de la Zerda A, Jokerst JV, Zavaleta CL, Kempen PJ, Mittra E, et al. A brain tumour molecular imaging strategy using a new triplemodality MRI-photoacoustic–Raman nanoparticle. Nat Med 2012;18: 829–34.

28. Mansfield JR. Distinguished photons: a review of in vivo spectral fluorescence imaging in small animals. Curr Pharm Biotechnol 2010; 11:628–38.

29. Zimmermann T. Spectral imaging and linear unmixing in light microscopy. Adv Biochem Eng Biotechnol 2005;95:245–65.

30. Sun Y, Hatami N, Yee M, Phipps J, Elson DS, Gorin F, et al. Fluorescence lifetime imaging microscopy for brain tumour image-guided surgery. J Biomed Opt 2010;15:056022.

31. Hanahan D, Weinberg RA. The hallmarks of cancer. Cell 2000;100: 57–70.

32. Thurber GM, Weissleder R. Quantitating antibody uptake in vivo: conditional dependence on antigen expression levels. Mol Imaging Biol 2011;13:623–32.

33. Fang J, Nakamura H, Maeda H. The EPR effect: unique features of tumour blood vessels for drug delivery, factors involved, and limitations and augmentation of the effect. Adv Drug Deliv Rev 2011;63:136–51.

34. Olafsen T, Wu AM. Antibody vectors for imaging. Semin Nucl Med 2010;40:167–81.

35. Naumov GN, Akslen LA, Folkman J. Role of angiogenesis in human tumour dormancy: animal models of the angiogenic switch. Cell Cycle 2006;5:1779–87.

36. Blum G, von Degenfeld G, Merchant MJ, Blau HM, Bogyo M. Noninvasive optical imaging of cysteine protease activity using fluorescently quenched activity-based probes. Nat Chem Biol 2007;3:668–77.

37. Keereweer S, Mieog JS, Mol IM, Van Driel PB, Snoeks TJ, Baatenburg de Jong RJ, et al. Detection of oral squamous cell carcinoma and cervical lymph node metastasis using activatable near-infrared fluorescence agents. Arch Otolaryngol Head Neck Surg 2011;137:609–15.

38. Weissleder R, Tung CH, Mahmood U, Bogdanov A Jr. In vivo imaging of tumours with protease-activated near-infrared fluorescent probes. Nat Biotechnol 1999;17:375–8.

39. Bird-Lieberman EL, Neves AA, Lao-Sirieix P, O'Donovan M, Novelli M, Lovat LB, et al. Molecular imaging using fluorescent lectins permits rapid endoscopic identification of dysplasia in Barrett's esophagus. Nat Med 2012;18:315–21.

40. Gioux S, Choi HS, Frangioni JV. Image-guided surgery using invisible near-infrared light: fundamentals of clinical translation. Mol Imaging 2010;9:237–55.

41. Kovar JL, Volcheck W, Sevick-Muraca E, Simpson MA, Olive DM. Characterization and performance of a near-infrared 2-deoxyglucose optical imaging agent for mouse cancer models. Anal Biochem 2009; 384:254–62.

42. Keereweer S, Mol IM, Vahrmeijer AL, Van Driel PB, Baatenburg de Jong RJ, Kerrebijn JD, et al. Dual wavelength tumour targeting for detection of hypopharyngeal cancer using near-infrared optical imaging in an animal model. Int J Cancer 2012;131:1633–40.

43. Pleijhuis RG, Langhout GC, Helfrich W, Themelis G, Sarantopoulos A, Crane LM, et al. Near-infrared fluorescence (NIRF) imaging in breastconserving surgery: assessing intraoperative techniques in tissuesimulating breast phantoms. Eur J Surg Oncol 2011;37:32–9.

44. Stummer W, Stepp H, Moller G, Ehrhardt A, Leonhard M, Reulen HJ. Technical principles for protoporphyrin-IX-fluorescence guided microsurgical resection of malignant glioma tissue. Acta Neurochir (Wien) 1998;140:995–1000.

45. Stummer W, Stocker S, Wagner S, Stepp H, Fritsch C, Goetz C, et al. Intraoperative detection of malignant gliomas by 5-aminolevulinic acid-induced porphyrin fluorescence. Neurosurgery 1998;42:518–25; discussion 25–6.

46. Stummer W, Pichlmeier U, Meinel T, Wiestler OD, Zanella F, Reulen HJ. Fluorescence-guided surgery with 5-aminolevulinic acid for resection of malignant glioma: a randomised controlled multicentre phase III trial. Lancet Oncol 2006;7:392–401.

47. Xie BW, Mol IM, Keereweer S, van Beek ER, Que I, Snoeks TJ, et al. Dual-wavelength imaging of tumour progression by activatable and targeting near-infrared fluorescent probes in a bioluminescent breast cancer model. PLoS One 2012;7:e31875.

48. Kilby W, Dooley JR, Kuduvalli G, Sayeh S, Maurer CR Jr. The Cyber-Knife Robotic Radiosurgery Systemin 2010. Technol Cancer Res Treat 2010;9:433–52.

49. Rosenthal EL, Kulbersh BD, King T, Chaudhuri TR, Zinn KR. Use of fluorescent labeled anti-epidermal growth factor receptor antibody to image head and neck squamous cell carcinoma xenografts. Mol Cancer Ther 2007;6:1230–8.

50. Noura S, Ohue M, Seki Y, Tanaka K, Motoori M, Kishi K, et al. Feasibility of a lateral region sentinel node biopsy of lower rectal cancer guided by indocyanine green using a near-infrared camera system. Ann Surg Oncol 2010;17:144–51.

51. Heath CH, Deep NL, Sweeny L, Zinn KR, Rosenthal EL. Use of panitumumab-IRDye800 to image microscopic head and neck cancer in an orthotopic surgical model. Ann Surg Oncol 2012;19:3879–87.

3

II

Preclinical validation of fluorescence-guided surgery

CHAPTER 4

Intraoperative fluorescence delineation of head and neck cancer with a fluorescent anti-epidermal growth factor receptor nanobody

Pieter B.A.A. Van Driel[1], Joost R. van der Vorst[2], Floris P.R. Verbeek[2], Sabrina Oliveira[3,4], Thomas J.A. Snoeks[1], Stijn Keereweer[5], John V. Frangioni[6,7], Paul M.P. van Bergen en Henegouwen[3], Alexander L. Vahrmeijer[2], Clemens W.G.M. Löwik[1]

1. Department of Radiology and Molecular Imaging, Leiden University Medical Center, Leiden, The Netherlands
2. Department of Surgery, Leiden University Medical Center, Leiden, The Netherlands
3. Division Cell Biology, Department of Biology, Utrecht University, Utrecht, The Netherlands
4. Department of Pathology, University Medical Center Utrecht, Utrecht, The Netherlands
5. Department of Otorhinolaryngology & Head and Neck Surgery, Erasmus Medical Center, Rotterdam, The Netherlands
6. Department of Medicine, Beth Israel Deaconess Medical Center, 330 Brookline Avenue, Boston, MA 02215
7. Department of Radiology, Beth Israel Deaconess Medical Center, 330 Brookline Avenue, Boston, MA 02215

ABSTRACT

Background

Intraoperative near-infrared (NIR) fluorescence imaging is a technology with high potential to provide the surgeon with real-time visualization of tumours during surgery. This study explores the feasibility for clinical translation of an epidermal growth factor receptor (EGFR) targeting nanobody for intraoperative imaging and resection of orthotopic tongue tumours and cervical lymph node metastases.

Methods

The anti-EGFR nanobody 7D12 and the negative control nanobody R2 were conjugated to the NIR fluorophore IRDye800CW (7D12-800CW and R2-800CW). Orthotopic tongue tumours were induced in nude mice using the OSC-19-luc2-cGFP cell line. Tumour bearing mice were injected with 25μg 7D12-800CW, R2-800CW or 11μg 800CW. Subsequently, other mice were injected with 50 μg or 75 μg of 7D12-800CW. The FLARE imaging system and the IVIS spectrum were used to identify, delineate and resect the primary tumour and cervical lymph node metastases.

Results

All tumours could be clearly identified using 7D12-800CW. A significantly higher tumour-to-background ratio (TBR) was observed in mice injected with 7D12-800CW compared to mice injected with R2-800CW and 800CW. The highest average TBR (2.00 ± 0.34 and 2.72 ± 0.17 for FLARE and IVIS spectrum, respectively) was observed 24 hours after administration of the EGFR-specific nanobody. After injection of 75 μg 7D12-800CW cervical lymph node metastases could be clearly detected.

Conclusion

Orthotopic tongue tumours and cervical lymph node metastases in a mouse model were clearly identified intraoperatively using a recently developed fluorescent EGFR targeting nanobody. Translation of this approach to the clinic would potentially improve the rate of radical surgical resections.

4

Introduction

In oncology, a range of noninvasive imaging modalities, including X-ray, ultrasonography, computed tomography (CT) and magnetic resonance imaging (MRI), enable early detection, staging, and treatment evaluation of cancer. However, in most cases surgeons still discriminate healthy tissue from cancerous tissue by means of visual inspection and palpation during surgery. Given the fact that adequate tumour free margins are of paramount importance for patient prognosis and outcome, and that irradical resections still frequently occur, novel imaging modalities are needed. Despite the primary objective of achieving macroscopic clearance of 1 cm in the surgical management of oropharyngeal or oral squamous cell carcinoma (OSCC), the presence of tumour positive margins has been reported in 16% of patients.[1] Numerous reports have indicated that involved margins imply deteriorated prognoses.[2] On the other hand, applying wider surgical margins will result in functional impairment in most cases.[3, 4] Therefore, clearer delineation of the tumour during surgery may improve the number of radical resections, thus increasing patients' survival rates while maintaining postoperative functionality. Near-infrared (NIR) fluorescence imaging is a novel imaging technique that provides the surgeon with real-time visualization of tumours during surgery.[5–7] In the NIR region (650 – 800 nm), less absorption of light by tissue components allows much deeper penetration of light. Furthermore, lower fluorescence from endogenous fluorophores decreases the nonspecific background signal. As the human eye is not sensitive to NIR fluorescent light, a specific NIR fluorescence imaging system is needed to visualize the fluorescence signal. At the same time, since NIR light is invisible to the human eye, it will not alter the surgical field.[8] One of the main challenges in intraoperative fluorescence imaging lies in the development, validation and clinical introduction of a tumour specific agent. Being widely overexpressed in OSCC, the epidermal growth factor receptor (EGFR) serves as an interesting target for intraoperative fluorescence imaging.[9, 10] The EGFR is a transmembrane glycoprotein that is involved in DNA synthesis and cell proliferation. Overexpression contributes to oncogenesis by proliferation, dedifferentiation, inhibition of apoptosis, invasiveness and lack of adhesion dependence.[11] Furthermore, EGFR overexpression is often associated with a poor prognosis for patients with OSCC.[12] For tumour targeting using molecular imaging techniques, antibodies are promising as they can be raised specifically against practically any molecular target. Nevertheless, due to their large hydrodynamic diameter, intact antibodies accumulate in the liver. Moreover, long halflife in the bloodstream and slow blood clearance via the liver results in high contrast images only several days after injection. A very appealing alternative is the use of nanobodies.[13] Nanobodies are the smallest functional antigen-binding fragments derived from naturallyoccurring heavy-chain only antibodies.[14] They show very specific binding to their targets and their size of approximately 15 kDa ensures efficient distribution and tissue penetration, as well as rapid clearance from the body.[15–17] This study

assesses the feasibility of intraoperative fluorescence delineation of orthotopic OSCC and microscopic lymph node metastases, using an anti-EGFR nanobody and a clinically available fluorescence camera system. For this, the anti-EGFR nanobody 7D12 was conjugated to the NIR fluorophore IRDye800CW[18], as previously described by Oliveira et al.[17]. Tumour accumulation and specificity of 7D12-800CW was compared to the negative control nanobody R2-800CW and to 800CW alone.

Material and Methods

Cell lines and culture

Two human cell lines were used. For the animal studies, the metastatic oral squamous cell carcinoma (OSCC) line OSC-19 was used. The OSC19 cell line was established in Japan with cells from a patient with a well-differentiated squamous cell carcinoma of the tongue that metastasized to a cervical lymph node.[19] Luc2 luciferase from pGL4.10 plasmid (Promega, Madison, WI, USA) was cloned into the multiple cloning site (MCS) of the lentiviral vector pCDH-EF1-MCS-T2A-copGFP (Biocat, Heidelberg, Germany) using specific primers with the corresponding restriction sites. OSC-19 cells were transduced by self-inactivating lentiviral vectors as previously described[20] and positive cell clones selected by limit dilution to create a stable luciferase 2 (luc2) and green fluorescent protein (GFP) expressing OSC-19-Luc2-copGFP cell line. The cells were grown *in vitro* in Dulbecco's Modified Eagle's Medium (DMEM, Invitrogen, Carlsbad, CA, USA) containing 4.5 g DGlucose/L, 110 mg sodium pyruvate/L, 580 mg L-glutamine/L supplemented with 10% fetal bovine serum (FCS; Lonza, Basel, Swiss), 100 IU/mL penicillin, 100 µg/mL streptomycin (Invitrogen), 1× Minimal Essential Medium (MEM) Non-Essential Amino Acids solution and 1× MEM vitamin solution (Invitrogen). The human colorectal cancer cell line SW620 was used as an EGFR negative control. This cell line was cultured in Leibovitz's L-15 medium (Invitrogen) containing 300 mg L-glutamine/L supplemented with 10% FetalClone II (Hyclone, Logan, UT, USA) 100 IU/mL penicillin, 100 µg/mL streptomycin (Invitrogen) and 20 mM HEPES (Invitrogen). All cell lines were grown in a humidified incubator at 37°C and 5% CO_2. Cells were regularly checked for *Mycoplasma* infection by PCR.

Nanobodies and Conjugation to IRDye800CW

Two nanobodies were used: 7D12 and R2. The EGFR specific nanobody 7D12 binds to the ectodomain of the EGFR.[18, 21] EGFR specificity of 7D12-800CW *in vitro* and *in vivo* was reported earlier.[17] The nanobody R2 was used as a non-EGFR specific control.[22, 23] Both nanobodies have a molecular weight of approximately 15 kDa and show similar *in vivo* biodistribution.[17, 18, 24] The generation of the nanobodies 7D12 and R2 was described previously.[18, 22] Induction of protein expression and purification of nanobodies from the periplasmic space of *Escherichia coli* were performed as described by Roovers et al.[25] Conjugation of both nanobodies to the NIR fluorophore IRDye800CW was performed as described by Oliveira et al.[17] Briefly, the IRDye800CW N-hydroxysuccinimide ester (LICOR, Lincoln, NE, USA) was added to the protein in a 4-fold molar excess and was incubated for two hours at room temperature. Removal of the unconjugated fluorophore was accomplished by using two Zeba Spin Desalting columns

(Thermo Fisher Scientific, Perbio Science Nederland B.B., Ettenleur, the Netherlands) per protein in two sequential steps. The fluorescent nanobodies, i.e. 7D12-800CW and R2-800CW, were characterized as previously described[17], namely for their conjugation efficiency and these parameters were in agreement with previous values, i.e. 0.5 and 1.1, respectively.

EGFR expression

OSC-19 and SW620 cells were cultured until subconfluence. Cells were detached with trypsin and adjusted at 1×105 cells/tube in ice cold PBS, 10% FCS (Lonza, Basel, Swiss) and 1% sodium azide. The anti-EGFR monoclonal antibody sc-120 alexa fluor 647 (Santa Cruz biotechnology, Santa Cruz, CA, USA) or non-specific normal mouse IgG2a alexa fluor 647 (Santa Cruz) were added and cells were incubated in the dark on ice for 30 minutes. After incubation, cells were washed three times in ice cold PBS and resuspended in ice cold PBS, containing 10% FCS (Lonza) and 1% sodium azide. Flow cytometry of alexa fluor 647 labeled cells was performed using the BD LSR II (BD biosciences, San Jose, CA, USA). EGFR expression was estimated as the geometric mean of fluorescence intensity measured in 10.000 viable cells. The experiment was performed in duplicate.

Binding study

A binding assay was performed to confirm the specificity of the EGFR binding of 7D12-800CW. A black 96-well plate (Greiner bio-one, Frickenhausen, Deutschland) was used in which 20.000 OSC-19-luc2-cGFP and SW620 cells were seeded per well. After one day, cells were washed with binding medium (DMEM supplemented with 25 mM Hepes and 1% BSA, at pH 7.2). 7D12-800CW (7D12), R2-800CW (R2) and IRDye800CW carboxylate (800CW, LI-COR, Lincoln, NE, USA) were added in triplicate in a concentration range of 0 to 50 nM. R2-800CW and IRDye800CW carboxylate were used as negative controls. The cells were incubated for 2 hours in the dark on a rocker at 4°C and afterwards washed two times with binding medium. Bound proteins were directly observed with the Odyssey scanner (LI-COR), scanning at 800 nm. Directly after these measurements cells were fixed with 4% paraformaldehyde and incubated with TO-PRO-3 (Invitrogen) at 1:5000 for 15 minutes. Again cells were washed twice and the plate was imaged using the 700nm channel of the Odyssey (LI-COR) to detect TO-PRO3 fluorescence. Nucleus staining was performed to correct the fluorescence signal for the amount of cells enabling direct comparison of fluorescence signal of both cell lines.

Fluorescence imaging systems

Real-time fluorescence imaging of primary tumour and lymph node metastases was performed using the FLARE imaging system.[26] Briefly, This imaging system consists of three wavelength-isolated light sources: a 400–650 nm light source generating 40.000 lux (white light), a 656–678

nm light source generating 4 mW/cm2 (700 nm) and a 745 – 779 nm light source generating 14 mW/cm2 (800 nm). The imaging head, attached to a flexible gooseneck arm, enables real-time image acquisition from all three cameras. Color, NIR fluorescence and pseudo-colored (lime green) merged images are displayed in real time. Next to the FLARE imaging system, the IVIS spectrum (Caliper Life Science, Hopkinton, MA, USA) was used to visualize primary tumours and metastases. Data analysis of FLARE and IVIS spectrum data was performed using image J and the *Living Image* software from xenogen version 3.2 (Caliper LS) respectively. Multiple regions of interest (ROI) were drawn in the tumour and in adjacent normal tissue of the tongue and divided by each other to calculate TBRs.

Animal model

Nude Balb/c female mice (Charles River laboratories, l'Arbresle, France), aged 4 – 6 weeks, were housed in individually ventilated cages and provided with food and sterilized water ad libitum. Animal experiments were approved by the local animal welfare committee of the Leiden University Medical Center. Orthotopic tongue tumours were submucosally induced in the tip of the tongue through injection of 40.000 OSC-19-luc2-cGFP cells, diluted in 20 μL phosphate-buffered saline (PBS). Mice body weight was monitored twice a week and tumour growth was monitored twice a week by bioluminescence (BLI) measurements and visual inspection of the tongue. BLI signal, being the most sensitive imaging method for the detection of tumour cells[27], served as an *in vivo* control for the tumour specific fluorescence of the nanobodies. Imaging procedures were performed under isoflurane gas anesthesia. Weight measurements and tongue inspections were performed to monitor general health during the experiments. Mice were sacrificed by injection of high doses ketamine/xylazine.

Fluorescence measurements

Twenty days after injection of tumour cells, mice (n = 9) were randomly divided into three groups and received a systemic injection of 25 μg 7D12-800CW (1.6 nmol, 64 nmol/kg), 25 μg R2-800CW (1.5 nmol, 60 nmol/kg) or 11 μg 800CW carboxylate (1 nmol, 40 nmol/kg, LI-COR). For the two nanobodies, a previous study reported 25 μg to be the optimal dose.[17] Fluorescent images were acquired at 0.5, 1, 2, 4, 8, 24 and 48 hours after injection. For the detection of microscopic cervical lymph node metastases two additional concentrations of 50 and 75 μg 7D12-800CW were injected (n = 4). Mice were sacrificed at 24 hours after injection and overlying skin of the cervical region was removed for gross examination. Whole-body fluorescence imaging was performed and the tongue and cervical lymph nodes were subsequently resected.

Histology and fluorescence microscopy

After ex vivo fluorescent measurements, the resected tongues were cut in two. One half was frozen on dry ice, the other half fixed in 4% formalin overnight and embedded in paraffin blocks. Cervical lymph nodes on both sides were resected. The left lymph node was frozen on dry ice, the right lymph node paraffin embedded and fixed in 4% formalin overnight. Tissue was sectioned at 10 μm and imaged using the Odyssey (LI-COR). All images were acquired using the same settings but the images (i.e. brightness and contrast) of the control probes were altered to show any fluorescence and emphasize the difference in localization between specific and non-specific probes. To confirm the presence of tumour cells, fluorescence microscopy (Nikon eclipse e800, Nikon, Amsterdam, the Netherlands) of the GFP fluorescence signal emitted by OSC-19-luc2-cGFP cells was performed on frozen tissue slices. Histologic sections were stained with standard hematoxylin-eosin stain (HE). As expected, fluorescence of GFP could not be detected in paraffin embedded sections. Therefore, the presence of smaller cervical lymph node metastases in paraffin sections was confirmed by staining the cervical lymph node sections with anti-human wide-spectrum cytokeratin staining (Abcam inc., Cambridge, MA, USA).

Statistical analysis

For statistical analysis, SPSS statistical software package (Version 16.0, Chicago, IL) was used. TBR's were calculated by dividing the fluorescent signal of the tumour by fluorescent signal of surrounding tissue. TBR was reported in mean and standard deviation. To compare TBR between dose groups and time points, and to assess the relation between dose and time, a mixed model analysis was used. When a significant difference was detected, a one-way ANOVA was used to post-test for differences between separate dose groups and/or time points. The one-way ANOVA was corrected using the Bonferroni correction. $P < 0.05$ was considered significant. Differences between the FLARE and IVIS imaging systems were tested with an unpaired T-test.

Results

In vitro results

The specificity of the EGFR targeting nanobody for the squamous cell carcinoma of the tongue, that metastasizes to cervical lymph nodes, was first validated *in vitro*. For that purpose, we started with the evaluation of the EGFR expression in the OSC-19-luc2-cGFP cell line. Direct staining of the cell surface epitope of the EGFR of OSC-19-luc2-cGFP cells caused an increase in fluorescence intensity, as shown by a shift to the right through flow cytometry analyses, compared to the non-specific antibody (Fig 1A). Next, as a control to the EGFR overexpressing OSC-19-luc2-cGFP cell line, we assessed the EGFR expression in the human colon carcinoma cell line SW620, a cell line that has no overexpression of the EGFR. In contrast to OSC-19-luc2-cGFP, the FACS data of this cell line revealed no increase in fluorescence intensity, thus confirming the absence of EGFR expression in the SW620 cell line (Fig 1B). Both these cell lines were employed to confirm the specificity of the EGFR targeting nanobody 7D12-800CW, which was compared to the non-EGFR specific nanobody R2-800CW and to 800CW alone. The IRDye800CW-conjugated probes were produced and characterized as described by Oliveira et al.[17] Consistently, after purification of the conjugates through removal of unconjugated fluorophores, a small percentage of the 800CW unconjugated fluorophore (less than 7.5 % of the 800CW conjugated fraction) was still present (data not shown) and the fluorophore to protein molar ratio of 7D12-800CW and R2-800CW after random conjugation was 0.5 and 1.1 respectively. The cell assay, performed at 4C to prevent internalization and investigate binding only, clearly demonstrated an EGFR specific binding of 7D12-800CW in OSC-19-luc2-cGFP cells that proved to be concentration dependent (Fig 1C). With R2-800CW and 800CW, although slightly concentration dependent, significantly less fluorescence intensity was observed (Fig 1C). In the EGFR negative cell line no significant differences in fluorescence intensity between 7D12-800CW and R2-800CW were observed. Altogether, these results confirm the specificity of 7D12-800CW for binding to EGFR and show that both the negative control R2-800CW and the 800CW alone do not associate with these cells (Fig 1C and 1D).
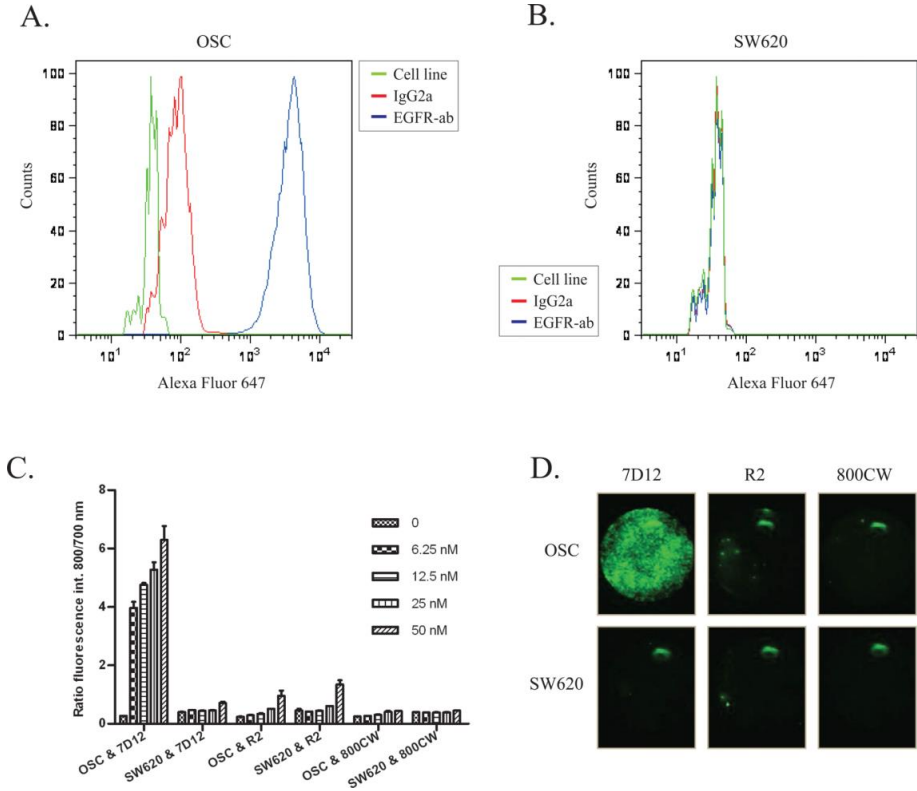
Figure 1. EGFR expression and binding assay

Flow cytometry was performed using OSC-19-luc2-cGFP and SW620 without antibody (green), with an EGFR specific antibody conjugated to alexa fluor 647 (blue) and with an isotype control normal mouse IgG2a conjugated to alexa fluor 647 (red). 7D12-800CW binds to human epidermal growth factor receptor expressed on OSC19-luc2-cGFP cells. A. The EGFR is highly expressed on the surface of OSC-19-luc2-cGFP cells. B. No expression of EGFR was found on the surface of SW620 cells. C. The human EGFR expressing OSC cells and EGFR negative SW620 cells were incubated with different concentrations of 7D12-800CW, R2-800CW and 800CW. The ratio of the fluorophore bound protein and the fluorescence intensity of TO-PRO-3 was plotted to correct for the amount of cells. Every concentration was performed in triplicate. Error bars indicate the standard deviation. D. Images were acquired with the Odyssey Scanner (LICOR). OSC and SW620 cells were incubated with 50 nM 7D12, R2 and 800CW. OSC = OSC-19-luc2-cGFP.

Animal model

Within three weeks after orthotopic inoculation of OSC-19-luc2-cGFP cells in the tip of the tongue, all mice developed a primary tongue tumour and cervical lymph node metastases (a typical example is shown in Fig 2A), observed during regular visual inspection and confirmed by the increase in mean bioluminescence signal (Fig 2B)
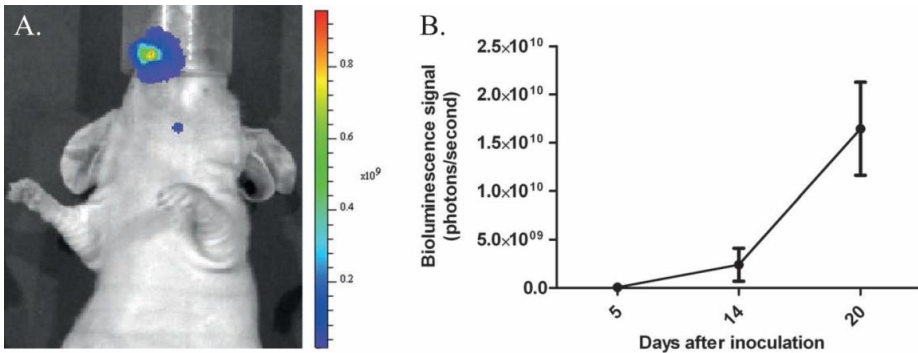

Figure 2. Tumour growth followed by imaging bioluminescence

A. Bioluminescent image after injection of OSC-19-luc2-cGFP cells. Primary tongue tumour and lymph node metastasis are shown. B. Increase of tumour growth (measured in bioluminescence signal) as a function of time.

In vivo NIR Fluorescence Imaging of primary tumours

Three weeks after tumour cell inoculation, mice were injected intravenously with 25 μg of 7D12-800CW, R2-800CW or 11 μg 800CW (for equivalent fluorescence to 7D12-800CW). To assess the feasibility of a possible clinical translation, fluorescence images were taken with both the preclinical, highly sensitive IVIS spectrum camera as well as with the FLARE intraoperative imaging system. As demonstrated in Figure 3A, all tumours of the animals that were injected with 7D12-800CW could be clearly identified through NIR fluorescence using both imaging modalities. No adequate tumour-to-background ratios were observed in the control mice injected with R2-800CW or 800CW (Fig 3B), which is in agreement with the results obtained in vitro (Fig 1).
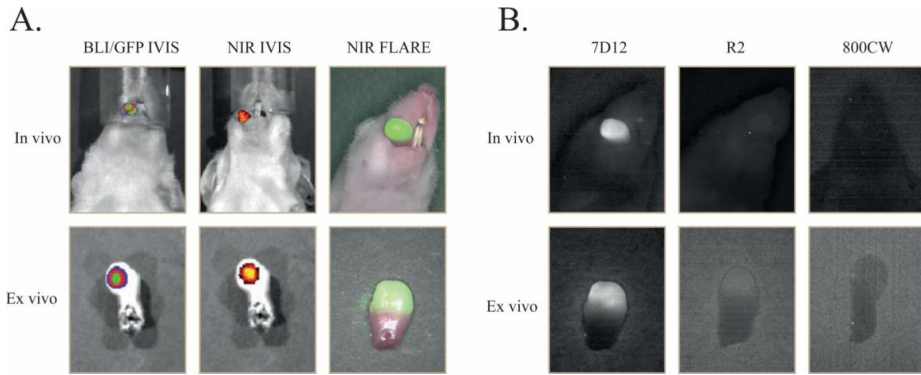
Figure 3. Multimodal *in vivo* and *ex vivo* imaging of an orthotopic tongue tumour

7D12 is specifically taken up in the oral squamous cell carcinoma of the tongue. Mice bearing OSC-19-luc2-cGFP human xenografts were intravenously injected with 25μg of 7D12, R2 and 800CW. After 24 hours fluorescent images were obtained with the IVIS spectrum and the intraoperative camera system (FLARE). A. *In vivo:* bioluminescence brightfield merge image (left), NIR fluorescence brightfield merge IVIS image of 7D12-800CW (middle) and NIR fluorescence color merge FLARE image (right) *Ex vivo*: GFP brightfield merge image (left), NIR fluorescence brightfield merge IVIS image of 7D12-800CW (middle) and NIR fluorescence color merge FLARE image (right) B. *In vivo*: Fluorescent imaging of a tongue tumour 24 hours after administration of 7D12-800CW (left), R2-800CW (middle) and 800CW (right). *Ex vivo*: Fluorescent imaging of a tongue tumour 24 hours after administration of 7D12-800CW (left), R2-800CW (middle) and 800CW (right). Images were obtained with the intraoperative camera system (FLARE)

Using the IVIS imaging system, a mixed model showed significant differences in TBRs between three study groups and between time points ($p < 0.0001$ and $p < 0.0001$, respectively) (Fig 4A). Post-testing using a one-way ANOVA showed significant differences between the 7D12-800CW and the R2-800CW ($p < 0.0001$) study groups and between the 7D12-800CW and 800CW ($p < 0.0001$) study groups. No significant difference was found between R2-800CW and 800CW ($p > 0.999$). The highest TBR (2.72 ± 0.17) was measured at 24 hours after administration of 7D12-800CW. Using the FLARE imaging system, a mixed model showed significant differences in TBRs between the three study groups and between time points ($p = 0.041$ and $p < 0.0001$, respectively) (Fig 4B). Post-testing using a one-way ANOVA showed significant differences between the 7D12-800CW and the R2-800CW study groups ($p = 0.05$) and between the 7D12-800CW and 800CW study groups ($p = 0.002$). No significant difference was found between R2-800CW and 800CW ($p = 0.77$). The highest TBR (2.00 ± 0.34) was measured at 24 hours after administration of 7D12-800CW. The highest TBR measured with the IVIS imaging system was significantly higher compared to the highest TBR measured with the FLARE imaging system ($p = 0.03$).
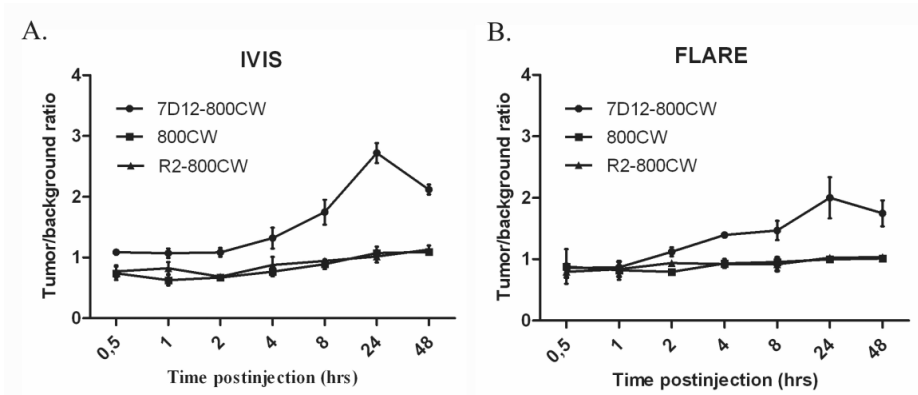
Figure 4. Intraoperative tumour to background ratios over time

The tumour to background ratio of 7D12-800CW is significantly higher compared to those of R2-800CW and 800CW. Tumour to background ratios were calculated from 0.5 hours to 48 hours after injection. Error bars indicate the standard deviation. Tumour to background ratios were plotted for the IVIS-Spectrum (A) and the FLARE imaging system (B).

Ex vivo fluorescence imaging and histology of primary tumours

In cryo sections, fluorescent imaging of the GFP that was transduced in the OSC-19 cells confirmed the presence of tumour cells in the tongue (Fig 5). After fluorescent imaging (GFP and NIR fluorescence), sections were stained with HE. Even sub-millimeter islands of tumour cells, confirmed with GFP fluorescence, co-localized with the fluorescence of 7D12-800CW, as measured with the Odyssey Scanner (Fig 5). No co-localization was observed in the tongue specimens of mice injected with R2-800CW or 800CW, which is in agreement with our observations in vivo (Fig 3B).
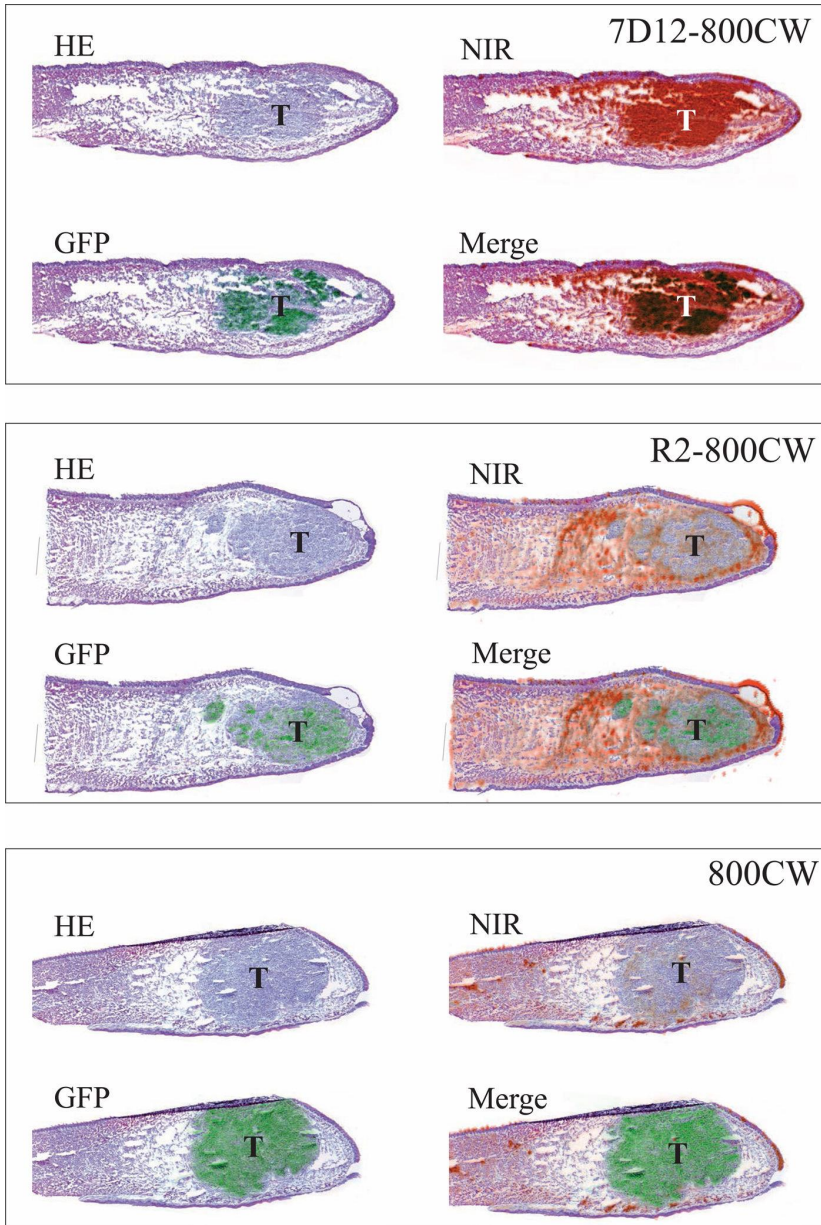
Figure 5. Histology and fluorescence imaging of orthotopic primary tongue tumours

Shown are hematoxylin and eosin (HE) stainings, HE and GFP fluorescence overlays, HE and NIR fluorescence overlays and HE, NIR and GFP fluorescence overlays. In the 7D12-800CW tissue specimen, a clear overlap between NIR and GFP (indicating tumour cells) fluorescence was observed. In the R2-800CW and 800CW specimens, no overlap between NIR and GFP fluorescence was observed. Brightness and contrast of the images of R2-800CW and 800CW was altered to show fluorescence and emphasize the localization in tissue.

4

In vivo and *ex vivo* fluorescence imaging and histology of cervical lymph nodes

In contrast to the primary tumour, microscopic cervical lymph node metastases were not grossly visible. In fact, a dose of 75 µg of 7D12-800CW only gave a weak fluorescence signal through the skin using the IVIS, but, importantly, a strong fluorescence with both imaging systems could be detected when the skin was removed (Fig 6). This highlights the potential of this imaging modality in the intraoperative context. During *ex vivo* imaging, the fluorescence of GFP that was transfected in the OSC-19-luc2-cGFP cells confirmed the presence of cervical lymph node metastases in the tissue specimen and could be colocalized to the fluorescent signal of 7D12-800CW. As expected, due to bleaching and the washing steps, no GFP fluorescence was found in the paraffin sections of the cervical lymph nodes. Nevertheless, immunohistochemical analysis, using a wide spectrum anti-cytokeratin staining, confirmed the presence of tumour cells. As shown in Figure 6, the fluorescence signal of 7D12-800CW co-localizes with the tumour cells in the cervical lymph node.
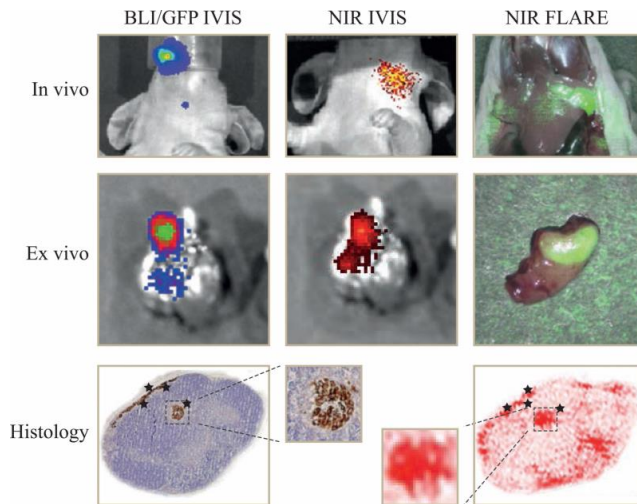
Figure 6. *In vivo, ex vivo* and histological fluorescence imaging of cervical lymph nodes

*In vivo: b*ioluminescence brightfield merge image (left), NIR fluorescence brightfield merge IVIS image of 7D12-800CW (middle) and NIR fluorescence color merge FLARE image (right) *Ex vivo*: GFP brightfield merge image (left), NIR fluorescence brightfield merge IVIS image of 7D12-800CW (middle) and NIR fluorescence color merge FLARE image (right) *Histology*: Shown are a hematoxylin and eosin (HE) staining combined with a cytokeratin staining (left) and NIR fluorescence image (right) of a cervical lymph node of a mice injected with 7D12-800CW. A clear overlap between NIR fluorescence and the brown cytokeratin staining (indicating tumour cells) was observed.

Discussion

In the present study, the EGFR targeting nanobody conjugated to 800CW was used to delineate orthotopic OSCC tumour margins during surgery. After 2 hours post injection tumours could already be clearly delineated. The highest TBR was obtained 24 hours after injection. Furthermore, a significant difference in TBR was observed between mice injected with 7D12-800CW, and mice injected with the control nanobodyR2-800CW or with 800CW alone. NIR fluorescent optical imaging is an imaging technique with high potential to obtain realtime information about the presence, location and dimensions of tumour tissue so that adequate tumour free margins can be obtained after resection[28–30]. Although the first clinical trial has recently been performed[29], it remains challenging to find a suitable fluorescent probe which can be detected with a sensitive NIR-fluorescent imaging system. The first challenge to NIR fluorescence imaging is the optimal fluorescent probe. An ideal fluorescent probe should distribute well, have a high affinity towards its target and a fast clearance from the bloodstream, to allow efficient accumulation at the tumour and rapid acquisition of images with high contrast. Furthermore, no accumulation in the liver is desirable and the ability to adequately penetrate the tissue of interest is of great importance. The EGFR serves as a very interesting target in head and neck cancer as the majority of these cancers overexpress this receptor.[10, 31] In a previous study we used recombinant human EGFR ligands conjugated to 800CW to target head and neck tumours.[32] Although efficient in targeting head and neck tumours, recombinant human EGFR ligands can potentially activate this receptor, which promotes its malignant phenotype. In other studies, cetuximab conjugated to Cy5.5 and panitumumab conjugated to 800CW are used to image head and neck tumours.[9,33] Conventional antibodies, however, show slower blood clearance (up to several days), higher accumulation in the liver and limited tumour penetration compared to nanobodies.17 For these reasons, we have selected a nanobody as our probe for this study. Next to the ideal probe, the extent to which a tumour can be visualized during surgery is highly depending on the NIR fluorescent imaging system. Gioux et al.[34] have reviewed the technical requirements for an intraoperative imaging system. To assess the feasibility of translating our results into clinical experiments, we used the clinically available FLARE™ imaging system. This system is able to adequately detect microscopic disease intraoperatively and has proven its clinical use in over 25 clinical trials.[26, 35] Using the IVIS spectrum we were able to measure bioluminescence and confirm the presence of tumour cells ex vivo, by imaging GFP fluorescence of the transfected OSC-19-luc2-cGFP cells. Furthermore, fluorescence measurements obtained with the IVIS spectrum, i.e. a closed ('black box') preclinical imaging system, were compared with the measurements of the clinically available FLARE™ imaging system. This comparison showed a significant difference in TBR favoring the IVIS spectrum on the optimal imaging time point (24hr post injection). This difference can be explained by the fact

that the IVIS spectrum is, in contrary to the FLARE imaging system, a 'black box' imager with less daylight interfering and subsequently less background fluorescence. However, since this device obviously cannot be used intraoperatively, the FLARE imaging system is an adequate alternative as the average TBR was over 2. In previous studies, we used the EGFR targeted nanobody 7D12 conjugated to 800CW to image subcutaneous A431 tumour xenografts, which have high EGFR expression.[17] Undoubtedly, the host microenvironment has great influence on tumour biology that affects parameters such as angiogenesis, growth, invasion, metastasis and lymphangiogenesis. Therefore, an orthotopic model is clinically a more relevant model with great importance to assess the ability of a probe for fluorescence delineation of tumours and its possible translation to the clinic. In this study, we successfully tested the potentiality of intraoperative fluorescence delineation of orthotopic OSCC and microscopic lymph node metastases using a clinically available fluorescence imaging system. Based on these results we conclude that clinical translation of 7D12-800CW may be possible, using the FLARE imaging system in the intraoperative set-up. A sufficient TBR is required to distinguish tumour from normal tissue[30] The small molecular weight of 7D12 allows fast detection of the tumour due to rapid distribution and fast clearance of unbound molecules. Oliveira et al.[17] reported tumour detection from 30 minutes after injection onwards. In the present study, using both the FLARE and IVIS spectrum, the tumour could be sufficiently detected 2 hours post injection. The use of an orthotopic model in the tongue that differs in angiogenesis, lymphangiogenesis and interstitial pressure from a subcutaneous A431 tumour, could perhaps explain these variations. Nevertheless, the highest average tumour to background ratio (2.72 IVIS spectrum vs 2.0 FLARE) was obtained 24 hours after injection, which is in agreement with what was previously reported in the subcutaneous tumour model.[17] Although nanobodies distribute and bind to their targets very rapidly, the background signal is relatively high during the first hours. Monovalent nanobodies are not efficiently internalized and therefore bound nanobody can un-bind over a certain period of time.[36] The 7D12-800CW washout from normal tissue occurs faster than the release from its receptor in the tumour. As a result the TBR will increase over time until an optimal TBR is reached. After that, release of nanobody from its receptor will result in a decrease in TBR. A decreased TBR in our study was seen after 48 hours. Cryosections of the tongue confirmed the tumour specific fluorescence by colocalization of the fluorescent signal of 7D12-800CW and the fluorescence of the GFP transfected OSC-19 cells. In the cryosections of mice injected with R2-800CW some fluorescence was detected, but there was no colocalization of NIR and GFP fluorescence. R2-800CW fluorescence mainly originated from the area surrounding the tumour. A possible explanation for the non- EGFR specific presence of R2-800CW could be the enhanced permeability and retention that is seen in many tumours.[37] Fluorescence could not be detected in the cryo sections of tongues of mice injected with 800CW alone. When translating 7D12-800CW to the clinic, the specific binding of the nanobody to human EGFR could result in

higher background fluorescence and therefore lower contrast. Importantly, Oliveira et al.[17] demonstrated the ability of 7D12-800CW to distinguish between different expression levels of EGFR *in vitro*. This implies that 7D12 could differentiate tumour tissue with high EGFR expression from normal tissue without overexpression of EGFR. The prognosis of patients with head and neck cancer is largely dependent on lymph node involvement.[38, 39] A sentinel lymph node (SLN) procedure could prevent elective neck dissections that are frequently performed for adequate staging and local control. Furthermore, despite the analysis by a trained pathologist, (micro) metastases and occult tumour cells in lymph nodes can be missed by standard histopathological examination. Limited examination of one lymph node could increase the accuracy of staging in head and neck cancer. Recently van der Vorst et al.[40] demonstrated the feasibility to detect draining lymph nodes in head and neck cancers using the nonspecific fluorescent tracer ICG:HSA. The fluorescent tracer however, quickly migrated to lymph nodes beyond the SLN. This present study demonstrates the feasibility of specific targeting of cervical lymph node metastases. A dose of 75 μg of 7D12-800CW clearly allowed delineation of the primary tumour and identification of the cervical lymph node metastases after removal of the skin. Histology showed clear co-localization of the NIR fluorescence of 7D12-800CW and the cytokeratin staining, that confirmed the presence of tumour cells. Compared to the primary tumour however, an increase of nonspecific background signal was observed. Also, the smaller the tumour or metastases, the lower the fluorescent signal. Furthermore, the influence of optical properties on the light propagation through tissue can result in a blurred delineation of smaller tumours. Altogether, these aspects rendered visualization of the metastases slightly difficult, which was significantly improved by removal of the skin. Further research is needed to explore which is the minimum size of lymph node metastases that can be detected using 7D12-800CW. Intraoperative detection of lymph node metastases would be a better alternative to the non-specific SLN procedure. First, the efficiency of an intraoperative histopathological diagnosis on fresh-frozen sections could be increased by examination of the fluorescence positive lymph node. Eventually, the procedure might even prevent intraoperative pathologic analysis of fresh-frozen tissue sections.

In conclusion, the present study reports a recently developed fluorescent EGFR targeting nanobody, which clearly allowed the identification of orthotopic tongue tumours and cervical lymph node metastases in a mouse model. These results highlight the potential of this nanobody for clinical translation in the context of surgical management of oropharyngeal or OSCC.

Acknowledgments

4

Conflicts of interest and source of funding

FLARE™ technology is owned by Beth Israel Deaconess Medical Center, a teaching hospital of Harvard Medical School. Dr. Frangioni has started three for-profit companies, Curadel, Curadel Res Vet Imaging, and Curadel Surgical Innovations, which has optioned FLARE™ - technology for potential licensing from Beth Israel Deaconess Medical Center.

4

References

1. McMahon J, O'Brien CJ, Pathak I, Hamill R, McNeil E, Hammersley N, Gardiner S, Junor E. Influence of condition of surgical margins on local recurrence and disease-specific survival in oral and oropharyngeal cancer. Br J Oral Maxillofac Surg. 2003; 41:224–231. [PubMed: 12946663]

2. Iseli TA, Lin MJ, Tsui A, Guiney A, Wiesenfeld D, Iseli CE. Are wider surgical margins needed for early oral tongue cancer? J Laryngol Otol. 2012; 126:289–294. [PubMed: 22258616]

3. Looser KG, Shah JP, Strong EW. The significance of "positive" margins in surgically resected epidermoid carcinomas. Head Neck Surg. 1978; 1:107–111. [PubMed: 755803]

4. Loree TR, Strong EW. Significance of positive margins in oral cavity squamous carcinoma. Am J Surg. 1990; 160:410–414. [PubMed: 2221245]

5. Weissleder R, Pittet MJ. Imaging in the era of molecular oncology. Nature. 2008; 452:580–589. [PubMed: 18385732]

6. Frangioni JV. New technologies for human cancer imaging. J Clin Oncol. 2008; 26:4012–4021. [PubMed: 18711192]

7. Keereweer S, Kerrebijn JD, van Driel PB, Xie B, Kaijzel EL, Snoeks TJ, Que I, Hutteman M, van der Vorst JR, Mieog JS, Vahrmeijer AL, van de Velde CJ, et al. Optical image-guided surgery-- where do we stand? Mol Imaging Biol. 2011; 13:199–207. [PubMed: 20617389]

8. Adams KE, Ke S, Kwon S, Liang F, Fan Z, Lu Y, Hirschi K, Mawad ME, Barry MA, Sevick-Muraca EM. Comparison of visible and near-infrared wavelengthexcitable fluorescent dyes for molecular imaging of cancer. J Biomed Opt. 2007; 12:024017. [PubMed: 17477732]

9. Heath CH, Deep NL, Sweeny L, Zinn KR, Rosenthal EL. Use of panitumumab-IRDye800 to image microscopic head and neck cancer in an orthotopic surgical model. Ann Surg Oncol. 2012;19:3879–3887. [PubMed: 22669455]

10. Pomerantz RG, Grandis JR. The epidermal growth factor receptor signaling network in head and neck carcinogenesis and implications for targeted therapy. Semin Oncol. 2004; 31:734–743. [PubMed: 15599851]

11. Yarden Y. The EGFR family and its ligands in human cancer. signalling mechanisms and therapeutic opportunities. Eur J Cancer. 2001; 37(Suppl 4):S3–S8. [PubMed: 11597398]

12. Laimer K, Spizzo G, Gastl G, Obrist P, Brunhuber T, Fong D, Barbieri V, Jank S, Doppler W, Rasse M, Norer B. High EGFR expression predicts poor prognosis in patients with squamous cell carcinoma of the oral cavity and oropharynx: a TMA-based immunohistochemical analysis. Oral Oncol. 2007; 43:193–198. [PubMed: 16854613]

13. Muyldermans S, Atarhouch T, Saldanha J, Barbosa JA, Hamers R. Sequence and structure of VH domain from naturally occurring camel heavy chain immunoglobulins lacking light chains. Protein Eng. 1994; 7:1129–1135. [PubMed: 7831284]

14. Hamers-Casterman C, Atarhouch T, Muyldermans S, Robinson G, Hamers C, Songa EB, Bendahman N, Hamers R. Naturally occurring antibodies devoid of light chains. Nature. 1993; 363:446–448. [PubMed: 8502296]

15. Cortez-Retamozo V, Lauwereys M, Hassanzadeh GhG, Gobert M, Conrath K, Muyldermans S, De Baetselier P, Revets H. Efficient tumour targeting by single-domain antibody fragments of camels. Int J Cancer. 2002; 98:456–462. [PubMed: 11920600]

16. De Genst E, Saerens D, Muyldermans S, Conrath K. Antibody repertoire development in camelids. Dev Comp Immunol. 2006; 30:187–198. [PubMed: 16051357]

17. Oliveira S, van Dongen GA, Stigter-van Walsum M, Roovers RC, Stam JC, Mali W, van Diest PJ, van Bergen en Henegouwen PM. Rapid visualization of human tumour xenografts through optical imaging with a near-infrared fluorescent anti-epidermal growth factor receptor nanobody. Mol Imaging. 2012; 11:33–46. [PubMed: 22418026]

18. Gainkam LO, Huang L, Caveliers V, Keyaerts M, Hernot S, Vaneycken I, Vanhove C, Revets H, De Baetselier P, Lahoutte T. Comparison of the biodistribution and tumour targeting of two 99mTclabeled anti-EGFR nanobodies in mice, using pinhole SPECT/micro-CT. J Nucl Med. 2008; 49:788–795. [PubMed: 18413403]

19. Yokoi T, Yamaguchi A, Odajima T, Furukawa K. Establishment and characterization of a human cell line derived from a squamous cell carcinoma of the tongue. Tumour Research. 1988; 23:43–57.

20. Carlotti F, Bazuine M, Kekarainen T, Seppen J, Pognonec P, Maassen JA, Hoeben RC. Lentiviral vectors efficiently transduce quiescent mature 3T3-L1 adipocytes. Mol Ther. 2004; 9:209–217. [PubMed: 14759805]

21. Roovers RC, Vosjan MJ, Laeremans T, El Khoulati R, de Bruin RC, Ferguson KM, Verkleij AJ, van Dongen GA, van Bergen En Henegouwen PM. A biparatopic anti-EGFR nanobody efficiently inhibits solid tumour growth. Int J Cancer. 2011; 129:2013–2024. [PubMed: 21520037]

22. Dolk E, van Vliet C, Perez JM, Vriend G, Darbon H, Ferrat G, Cambillau C, Frenken LG, Verrips T. Induced refolding of a temperature denatured llama heavychain antibody fragment by its antigen. Proteins. 2005; 59:555–564. [PubMed: 15778955]

23. van der Linden R, de Geus B, Stok W, Bos W, van Wassenaar D, Verrips T, Frenken L. Induction of immune responses and molecular cloning of the heavy chain antibody repertoire of Lama glama. J Immunol Methods. 2000; 240:185–195. [PubMed: 10854612]

24. Oliveira S, Cohen R, Walsum MS, van Dongen GA, Elias SG, van Diest PJ, Mali W, van Bergen En Henegouwen PM. A novel method to quantify IRDye800CW fluorescent antibody probes ex vivo in tissue distribution studies. EJNMMI research. 2012; 2:50. [PubMed: 23009555]

25. Roovers RC, Laeremans T, Huang L, De Taeye S, Verkleij AJ, Revets H, de Haard HJ, van Bergen en Henegouwen PM. Efficient inhibition of EGFR signaling and of tumour growth by antagonistic anti-EFGR Nanobodies. Cancer Immunol Immunother. 2007; 56:303–317. [PubMed: 16738850]

26. Troyan SL, Kianzad V, Gibbs-Strauss SL, Gioux S, Matsui A, Oketokoun R, Ngo L, Khamene A, Azar F, Frangioni JV. The FLARE intraoperative near-infrared fluorescence imaging system: a first-in-human clinical trial in breast cancer sentinel lymph node mapping. Ann Surg Oncol. 2009; 16:2943–2952. [PubMed: 19582506]

4

27. Kim JB, Urban K, Cochran E, Lee S, Ang A, Rice B, Bata A, Campbell K, Coffee R, Gorodinsky A, Lu Z, Zhou H, et al. Non-invasive detection of a small number of bioluminescent cancer cells in vivo. PloS one. 2010; 5:e9364. [PubMed: 20186331]

28. Mieog JS, Hutteman M, van der Vorst JR, Kuppen PJ, Que I, Dijkstra J, Kaijzel EL, Prins F, Lowik CW, Smit VT, van de Velde CJ, Vahrmeijer AL. Image-guided tumour resection using realtime near-infrared fluorescence in a syngeneic rat model of primary breast cancer. Breast Cancer Res Treat. 2011; 128:679–689. [PubMed: 20821347]

29. van Dam GM, Themelis G, Crane LM, Harlaar NJ, Pleijhuis RG, Kelder W, Sarantopoulos A, de Jong JS, Arts HJ, van der Zee AG, Bart J, Low PS, et al. Intraoperative tumour-specific fluorescence imaging in ovarian cancer by folate receptoralpha targeting: first in-human results. Nat Med. 2011; 17:1315–1319. [PubMed: 21926976]

30. Keereweer S, Sterenborg HJ, Kerrebijn JD, Van Driel PB, Baatenburg de Jong RJ, Lowik CW. Image-guided surgery in head and neck cancer: current practice and future directions of optical imaging. Head Neck. 2012; 34:120–126. [PubMed: 21284051]

31. Grandis JR, Tweardy DJ. Elevated levels of transforming growth factor alpha and epidermal growth factor receptor messenger RNA are early markers of carcinogenesis in head and neck cancer. Cancer Res. 1993; 53:3579–3584. [PubMed: 8339264]

32. Keereweer S, Kerrebijn JD, Mol IM, Mieog JS, Van Driel PB, Baatenburg de Jong RJ, Vahrmeijer AL, Lowik CW. Optical imaging of oral squamous cell carcinoma and cervical lymph node metastasis. Head Neck. 2012; 34:1002–1008. [PubMed: 21987435]

33. Gleysteen JP, Duncan RD, Magnuson JS, Skipper JB, Zinn K, Rosenthal EL. Fluorescently labelled cetuximab to evaluate head and neck cancer response to treatment. Cancer Biol Ther. 2007; 6:1181–1185. [PubMed: 17637562]

34. Gioux S, Choi HS, Frangioni JV. Image-guided surgery using invisible near-infrared light: fundamentals of clinical translation. Mol Imaging. 2010; 9:237–255. [PubMed: 20868625]

35. Mieog JS, Troyan SL, Hutteman M, Donohoe KJ, van der Vorst JR, Stockdale A, Liefers GJ, Choi HS, Gibbs-Strauss SL, Putter H, Gioux S, Kuppen PJ, et al. Toward optimization of imaging system and lymphatic tracer for near-infrared fluorescent sentinel lymph node mapping in breast cancer. Ann Surg Oncol. 2011; 18:2483–2491. [PubMed: 21360250]

36. Heukers R, Vermeulen JF, Fereidouni F, Bader AN, Voortman J, Roovers RC, Gerritsen HC, van Bergen En Henegouwen PM. EGFR endocytosis requires its kinase activity and N-terminal transmembrane dimerization motif. Journal of cell science. 2013

37. Keereweer S, Mol IM, Kerrebijn JD, Van Driel PB, Xie B, Baatenburg de Jong RJ, Vahrmeijer AL, Lowik CW. Targeting integrins and enhanced permeability and retention (EPR) effect for optical imaging of oral cancer. J Surg Oncol. 2012; 105:714–718. [PubMed: 21952950]

38. Leemans CR, Tiwari R, Nauta JJ, van der Waal I, Snow GB. Regional lymph node involvement and its significance in the development of distant metastases in head and neck carcinoma. Cancer. 1993; 71:452–456. [PubMed: 8422638]

39. Layland MK, Sessions DG, Lenox J. The influence of lymph node metastasis in the treatment of squamous cell carcinoma of the oral cavity, oropharynx, larynx, and hypopharynx: N0 versus N+ Laryngoscope. 2005; 115:629–639. [PubMed: 15805872]

40. van der Vorst JR, Schaafsma BE, Verbeek FP, Keereweer S, Jansen JC, van der Velden LA, Langeveld AP, Hutteman M, Lowik CW, van de Velde CJ, Frangioni JV, Vahrmeijer AL. Nearinfrared fluorescence sentinel lymph node mapping of the oral cavity in head and neck cancer patients. Oral Oncol. 2013; 49:15–19. [PubMed: 22939692]

CHAPTER 5

EpCAM as multi-tumour target for near-infrared fluorescence-guided surgery

Pieter B.A.A. Van Driel[1,2], Mark C. Boonstra[3], Henriette A.J.M. Prevoo[3], Martijn van de Giessen[4], Thomas J.A. Snoeks[1], Quirijn R.J.G. Tummers[3], Stijn Keereweer[5], Robert A. Cordfunke[6], Boudewijn P.F. Lelieveldt[4], Jouke Dijkstra[4], Cornelis J.H. van de Velde[3], Peter J.K. Kuppen[3,7], Alexander L. Vahrmeijer[3], Clemens W.G.M. Löwik[1], Cornelis F.M. Sier[3,7]

1. Department of Radiology, division of Molecular Imaging, Leiden University Medical Centre, Leiden, The Netherlands.
2. Percuros BV, Enschede, The Netherlands
3. Department of Surgery, Leiden University Medical Centre, Leiden, The Netherlands
4. Department of Radiology, division of image processing, Leiden University Medical Centre, Leiden, the Netherlands.
5. Department of Otorhinolaryngology & Head and Neck Surgery, Erasmus Medical Centre, Rotterdam, The Netherlands
6. Department of Immunohematology and Blood Transfusion, Leiden University Medical Centre, Leiden, The Netherlands
7. Antibodies for Research Applications BV, Gouda, The Netherlands

ABSTRACT

Evaluation of resection margins during cancer surgery can be challenging, often resulting in incomplete tumour removal. Fluorescence-guided surgery (FGS) aims to aid the surgeon to visualize tumours and resection margins during surgery. FGS relies on a clinically applicable imaging system in combination with a specific tumour-targeting contrast agent.

In this study EpCAM (epithelial cell adhesion molecule) is evaluated as target for FGS in combination with the novel Artemis imaging system. The NIR fluorophore IRDye800CW was conjugated to the well-established EpCAM specific monoclonal antibody 323/A3 and an isotype IgG1 as control. The anti-EpCAM/800CW conjugate showed to be stable in serum and showed preserved binding capacity as evaluated on EpCAM positive and negative cell lines using flow cytometry and cell-based plate assays. Four clinically relevant orthotopic tumour models, i.e. colorectal cancer, breast cancer, head and neck cancer, and peritonitis carcinomatosa, were used to evaluate the performance of the anti-EpCAM agent with the clinically validated Artemis imaging system. The Pearl Impulse small animal imaging system was used as reference. The specificity of the NIRF signal was confirmed using bioluminescence imaging and green-fluorescent protein.

All tumour types could clearly be delineated and resected 72 hours after injection of the imaging agent. Millimetre sized tumour nodules were detected that were invisible for the naked eye. Fluorescence microscopy demonstrated the distribution and tumour specificity of the anti-EpCAM agent.

This study shows the potential of an EpCAM specific NIR-fluorescent agent in combination with a clinically validated intraoperative imaging system to visualize various tumours during surgery.

Introduction

Curative intended oncologic surgery aims to completely resect all malignant cells. Discriminating tumour from healthy tissue during surgery is therefore of paramount importance [3]. As a consequence, clinically complete resected tumours frequently turn out to be pathological incompletely removed [4-6]. Therefore, novel intra-operative imaging modalities are needed that aid the surgeon in recognizing tumour spread and provide guidance during tumour removal. Fluorescence-guided surgery (FGS) is a technique based on near-infrared (NIR) light, which has been widely investigated for sentinel lymph node procedures, anastomosis and during cholecystectomies [7-9]. The advantage of NIR fluorescent light is the relatively deep tissue penetration and the minimal tissue auto fluorescence at these wavelengths. The tissue depth at which a fluorophore can be detected is dependent on the fluorophore (dose), tissue optical properties and the sensitivity of the imaging device. It has been estimated to be between 3 and 4 cm in intensified devices[10] and up to 2 cm in others[11]. Further, since NIR fluorescence light is invisible for the human eye, there is no alteration of the surgical field [12]. The major challenges for the routine introduction of FGS in the clinic comprise the availability of validated NIR fluorescence imaging systems in combination with a dedicated tumour-specific NIR fluorescence agent [13].

The first NIR imaging systems for clinical application proved the feasibility of the concept but were in fact more proto-types than standard clinical equipment. The next generation NIR imaging systems, as used in this study, are more versatile, smaller, cheaper, and more sensitive and should meet uniform standards warranting an exponential increase for clinical applications. Therefore, presently the biggest challenge for clinical introduction of FGS is the development of specific tumour targeting NIR fluorescent agents that comply with these second generation imagers. Various established membrane-bound tumour markers are under evaluation as targets for (NIR) fluorescence imaging in pre-clinical settings, such as EGFR, HER2/Neu, VEGF(R), folate receptor alpha, uPAR and various integrins [14-19]. Although these proteins have been successfully targeted in human tumours xenografted in animal models, none of them seems to be the universal target suited for the majority of tumour (types) in a clinical setting: These proteins are either present on the majority of tumours but only on a low percentage of tumour (stromal) cells, like VEGFR and $\alpha_v\beta_3$ integrin, or they are abundantly present in only a limited percentage of tumour (types), like folate receptor, EGFR and HER2.

In this study we evaluate Epithelial Cell Adhesion Molecule (EpCAM) as target for FGS. EpCAM is a transmembrane glycoprotein involved in cell-cell interactions and cell-stroma adhesion [20]. EpCAM expression is restricted to epithelial cells and is highly up-regulated in

virtually all epithelial carcinomas [21, 22]. EpCAM up-regulation is associated with cancer progression and EpCAM is found on circulating tumour cells and metastases. EpCAM overexpression in cancer cells was found to be 100- to 1000-fold higher compared to expression on normal breast cells resulting in 100,000 to 400,000 copies per cell [23]. Compared to an established tumour target like EGFR and Her2/Neu this number is only marginally less. But overexpression of EGFR and HER2/Neu in primary breast cancer is reported to be 0.8-14% and 15-20% respectively, whereas 40-98% of the primary breast tumours show enhanced EpCAM levels [22, 24]. For other epithelial cancers these figures are similar or favor the use of EpCAM as imaging target even more [22, 25-27]. These findings have led to the development of many EpCAM specific antibodies, from which some have been evaluated in phase I, II and III immunotherapeutic trials in various cancer types, such as ovarian, gastric and head-and-neck cancer [28, 29]. The results of these studies did not meet the high expectations for the therapeutic purpose and most of these investigations were aborted. Mild adverse effects like nausea, vomiting and elevation of pancreatic enzymes have been reported for therapeutic use, but are not expected in single dose imaging studies. The potential of EpCAM targeting has recently been re-discovered, as tumour specific imaging was demonstrated for SPECT imaging. A monoclonal antibody with medium high affinity for EpCAM, has been labelled with various radionuclides and has been extensively evaluated in several xenografted tumour models in mice [30, 31].

In the current study we conjugated the same monoclonal antibody 323/A3 to the clinically relevant NIR fluorescent dye IRDye800CW and evaluated this conjugate in tumour models of clinically relevant orthotopic colorectal, breast and head-and-neck cancer models. To simulate clinical conditions we evaluated the performance of the probe with the recently introduced commercially available Artemis imaging system [32] in comparison with the Pearl Impulse small animal imaging system, a standard apparatus for use in pre-clinical settings.

Material and Methods

Cell lines

For colorectal, breast and head-and-neck cancer, we selected two cell lines with different tumour characteristics (Table 1). Luciferase transfected cells were used to follow orthotopic tumour growth by bioluminescence imaging (BLI). MCF-7 and OSC-19 cells were transfected with Luciferase 2 and green fluorescent protein as described previously [33]. All cell lines were grown in a humidified incubator at 37°C and 5% CO_2. Cells were cultured for not more than 10 passages and regularly checked for *Mycoplasma* infection by PCR.

5

EpCAM expression

EpCAM expression of HT29(-/+)luc2, COLO320, OSC-19-luc2-cGFP, FaDu-luc2, MCF-7-luc2-cGFP and MDA-MB-231 cells was evaluated by flow cytometry. Cells were cultured until 90% confluence and detached with trypsin. Viability of the cells was evaluated using trypan blue. After adjusting the number of cells to 0.5 x 10^6 per tube in ice cold phosphate-buffered saline (PBS), they were incubated with 0.4 μg/ml 323/A3 anti-EpCAM antibody or isotype control MOPC21 for 30 minutes on ice. Then cells were washed three times in ice cold PBS and incubated with a goat anti-mouse IgG1-AF488 secondary antibody (Invitrogen, 2.5 μg/ml). The cells were washed three times in ice cold PBS and resuspended in 400 μL PBS containing propidium iodide to exclude dead cells from the analysis. Flow cytometry was performed using the LSRII (BD Biosciences). The experiments were performed in duplicate and EpCAM expression was estimated as the geometric mean of fluorescence intensity measured in 10,000 viable cells. For quantitative determination of EpCAM numbers per cell type the Qifikit (Dako) was used.

Antibodies and Conjugation to IRDye 800CW

EpCAM specific monoclonal chimeric antibody 323/A3 and the IgG_{1k} isotype control monoclonal antibody MOPC21 (BioXcell, West Lebanon, USA) were used [34]. Antibody 323/A3 has a medium high affinity ($K_a = 2$ x 10^9 M^{-1}) for EpCAM and is directed against the EGF-like domain I epitope on the extracellular domain of the EpCAM molecule, whereas MOPC21 has an unknown specificity after testing on human and rodent tissues [35-37]. Both antibodies were covalently conjugated to NIR fluorochrome IRDye 800CW (LI-COR, Lincoln, NE, USA). λex= 773 nm, λem= 792 nm) using N-hydroxysuccinimide ester chemistry as indicated by the manufacturer. Removal of unconjugated fluorophore was accomplished by using two Zeba Spin Desalting columns (Thermo Fisher Scientific, Perbio Science Nederland B.B., Etten-Leur, The Netherlands) per protein in two sequential steps. For comparison experiments, the two conjugates i.e. the EpCAM specific (323/A3-800CW) and control (MOPC21-800CW)

were complemented by the chemically inactive carboxylate version of IRDye 800CW, representing the fluorescent label without antibody control.

Serum stability

The stability of 323/A3-800CW in human serum was evaluated using HPLC (Biosep-SEC-s2000, Phenomenex, USA). Serum and sodium azide dilution were filtrated through a 0.22 μm filter in a 15 ml tube. A 24-wells plate (Greiner Bio-one, Germany) was prepared with 0.02% sodium azide and serum/probe in a ratio of 1:1 and PBS as control and incubated at 37°C under 5% CO_2. At 4, 24, 48 and 96 hours 20 μl of sample, diluted in 40 μL PBS was evaluated using HPLC in PBS at a flow rate of 0,5 ml/min for 60 minutes, detected at 2 channels, 280nm and 780nm.

Cell binding study

A cell binding assay was performed to confirm the EpCAM specificity of 323/A3-800CW. HT29-luc2 (40,000 cells), COLO320 (40,000 cells), OSC-19-luc2-cGFP (25,000 cells), FaDu-luc2 (35,000 cells), MCF-7-luc2-cGFP (40,000 cells) and MDA-MB-231 cells (40,000 cells) cells were seeded in a black 96-well plate (Greiner Bio-one, Germany). At ±90% confluence the cells were washed twice with PBS. 323/A3-800CW and MOPC21-800CW were added in a concentration range of 0-8 μg/ml and incubated for 1 hour at 37°C. After incubation, the cells were washed twice with culture medium without supplements. Bound antibody was imaged with an Odyssey scanner (LI-COR), scanning at the 800 nm channel. To correct the fluorescence signal for the number of tumour cells per well a cell nucleus staining was performed: The cells were fixed/permeabilized with acetone/methanol for 10 minutes, washed with PBS, and incubated with TO-PRO-3 (Invitrogen) at 1:1000 for 5 minutes at room temperature. After washing twice with PBS, the plate was imaged with the Odyssey scanner at the 700 nm channel to detect TO-PRO-3 fluorescence. The ratio of the 800 nm and 700 nm fluorescence was plotted. The experiments were performed in triplicate.

Animal models

Nude Balb/c female mice (Charles River laboratories, l'Arbresle, France), aged 4 – 6 weeks, were housed in individually ventilated cages and provided with food and sterilized water *ad libitum*. Their general health state was monitored by weight measurements throughout the experiments. Tumour growth was monitored longitudinally by visual inspection of the tumours, caliper measurements and/or by bioluminescence imaging. Bioluminescence imaging was performed by intraperitoneal injecting of 150 mg/kg of D-luciferin solution (SynChem, Inc, Elk Grove Village, IL) in PBS, in a total volume of 50 μL. After 10 minutes, mice were imaged with the IVIS Spectrum imaging system (PerkinElmer, Waltham, MA, USA). Imaging procedures were

performed under isoflurane gas anaesthesia. The local Animal Welfare Committee of the Leiden University Medical Centre approved all animal experiments.

Colon cancer models: To induce colon tumours, mice were subcutaneously injected at four sites with 5 x 10^5 HT29 cells in 40μL RPMI1640 medium. Tumour growth was followed by calliper measurements and after 10 days, when the tumours reached a volume of approximately 75 mm^3, imaging experiments started. Orthotopic HT29-luc2 tumours were induced as described previously[38].

Breast carcinoma model: To induce orthotopic breast tumours, 2.5 x 10^5 MCF-7-luc2-cGFP cells were inoculated in two contralateral mammary fat pads. Oestrogen pellets (17β-oestradiol, 0.36 mg/pellet, 60 day release) were implanted subcutaneously. Tumour growth was followed by visual inspection and bioluminescence measurements as described above.

Head-and-neck tumour model: Orthotopic tongue tumours were induced in the tip of the tongue through a submucosal injection of 4 x 10^4 OSC-19-luc2-cGFP cells. When tumours were visible and bioluminescence signal ranged between 5 x 10^9 and 1 x 10^{10} relative light units (RLU) imaging experiments started.

Peritonitis carcinomatosa: Multiple small MCF-luc2-cGFP tumours were induced in the peritoneum by intraperitoneal injection of 2.5 x 10^5 MCF-luc2-cGFP cells. Tumour growth was followed twice a week by bioluminescence as described above. Imaging experiments initiated when multiple tumour nodules were formed of various sizes.

NIR fluorescence imaging systems

Real-time NIR fluorescence imaging and operative resection of the tumours was performed using the next generation Artemis imaging system (Quest Medical Imaging, Middenmeer, the Netherlands). An earlier iteration of this system was extensively validated[32]. This system has a freely moveable handheld camera for simultaneous acquisition of visible light and NIR fluorescence. Since the system has been improved such that the camera can be fixed in a stable position with an arm, while both camera and arm are covered with a sterile drape. The illumination efficiency and homogeneity has been improved with a ring containing eight hemispheric illumination lenses centred around a wide field imaging lens for open surgery. Illumination is provided by four visible light sources with peaks centred in the blue, cyan, green and red and a NIR laser with a peak at 785 nm for fluorescence excitation. Reflected excitation light is blocked by a 750-800 nm notch filter. Captured visible and NIR light is split using a prism containing a dichroic coating (<785 mm). Visible light additionally passes through a low-pass filter (<640 nm) and the NIR emission light is filtered with a high pass filter (>808 nm). Exposure times and sensor gains are separately adjustable for both imaging channels. The visible light channel, the NIR fluorescence channel and an adjustable overlay of both channels are simultaneously presented during the procedures.

Next to the Artemis imaging system, the Pearl Impulse small animal imaging system (LI-COR) was used as a preclinical reference to visualize tumours and calculate the tumour-to-background ratios (TBRs). Data from the Artemis and Pearl imaging systems were analysed using imageJ (W. Rasband, Bethesda, Maryland) and the Pearl Cam Software, respectively.

NIR fluorescence measurements

Subcutaneous HT29 colon tumours were used to confirm *in vivo* EpCAM specificity of 323/A3-800CW and to measure fluorescence over time. When the subcutaneous HT29 colon tumours were 36 ± 6 mm², 1 nmol ($\approx 150\mu g$) of 323/A3-800CW (n=3), 1 nmol ($\approx 150\mu g$) MOPC-800CW (n=3) or 1 nmol (≈ 1.1 μg) of 800CW carboxylate was injected intravenously. NIR fluorescence signals were measured at 0, 4, 24, 48, 72 and 96 hours after injection using the PEARL small animal imaging system and the intraoperative Artemis imaging system after which TBRs were calculated. After *in vivo* confirmation of the EpCAM specificity and establishment of the optimal time frame for imaging with the subcutaneous model, the clinically more relevant orthotopic MCF-7-luc2-cGFP breast, OSC-19-luc2-cGFP tongue and HT29-luc2 colon tumours were evaluated. Hence, 1 nmol of 323/A3-800CW (n=3) or 1 nmol MOPC21-800CW (n=3) was intravenously injected in each group. Fluorescence imaging of mice bearing orthotopic tumours was performed 72 hours after administration for optimal TBR as determined in the subcutaneous HT29 colon carcinoma model. TBRs of orthotopic tumours were measured and tumours were resected under NIR fluorescence guidance using the Artemis imaging system. *Ex vivo*, fluorescent measurements of resected tissue were performed on a back table. Tumours were sliced and fluorescence measurements were performed on the sections to evaluate the distribution of the probe. Resected tumours from the head-and-neck cancer and breast cancer models were assessed by BLI imaging and GFP fluorescence imaging (OSC-19-luc2-cGFP and MCF-7-luc2-cGFP, IVIS spectrum). The MCF-luc2-cGFP peritonitis carcinomatosa tumour model was used to determine the minimal tumour sizes that could be detected by intra-operative fluorescence imaging using the EpCAM specific antibody 323/A3-800CW in combination with 2 imaging systems. Because an enhanced permeability and retention (EPR) effect in these micrometases is not expected as indicated recently by Hall et al.[36] no MOPC21-800CW control was used in this model. Mice were anesthetized 72 hours after intravenous injection of 323/A3-800CW (1 nmol, n = 3), as described above and fluorescence imaging using the Pearl and Artemis imaging system was performed. A midline abdominal incision was made and the abdominal skin was removed. Fluorescence imaging of the mice with both imaging systems was performed followed by resection of the peritoneum and again fluorescence images were taken. Fluorescence imaging of the abdominal area was performed to search for residual intraperitoneal tumour nodules. Presence of tumour nodules and tumour specific NIR fluorescence was confirmed by bioluminescence imaging and GFP fluorescence imaging, as described before. Receiver Operator

Curve (ROC) analysis was performed for the detection of micrometastases in the peritoneum. The overlay of BLI and GFP was used as the ground truth for tumour metastases and the ascending TBRs as positive cutoff criteria. The area under the curve (AUC) was computed and the sensitivity and specificity rates at the optimal TBR cutoff were found. The signals of NIR fluorescence and the overlay with BLI and GFP was confirmed against pathology in the primary tumour but not in the micrometastases. Multiple regions of interest were drawn in the tumour and in adjacent normal tissue and divided by each other to calculate TBRs. TBRs of subcutaneous colon and orthotopic breast tumours were calculated with skin overlying the tumour and adjacent normal tissue. Tongue tumours were imaged through an epithelial cell layer covering the tumour and normal tissue. For colon tumours the peritoneum was opened.

In vivo competition study

Three of the six nude Balb/C mice with bilateral orthotopic MCF-7-luc2-cGFP breast tumours were pre-injected with unconjugated 323/A3 antibody (1 mg, intraperitoneal, 100 μL). After 48 hours, all six mice were intravenously injected with 1 nmol 323/A3-800CW. Then, 72 hours after injection of 323/A3-800CW fluorescence imaging of all mice was performed using a Pearl imaging system. Mice were sacrificed and tumours were collected. Quantification of fluorescence was done as described before (Oliveira *et al.*, 2012). In brief, tumours were resected and lysed with a TissueLyser II system (Qiagen, Venlo, The Netherlands) using pre-cooled Eppendorf tube holders, 5-mm stainless steel beads, and RIPA buffer supplemented with a complete EDTA-free mini tablet protease inhibitor cocktail. Homogenates were serially diluted in 96-well plates, in parallel with a probe dilution. The fluorescence intensity of both series was detected at 800 nm using the Odyssey scanner. The concentration of probe in the homogenates was extrapolated from the calibration curves and the concentration values were used to calculate the injected dose per gram of tissue (% ID/g) with standard error of the mean (SEM) indicated per group, based on the volume of the homogenate and the weight of the tumours.

Histology and NIR fluorescence microscopy

After *ex vivo* fluorescence measurements, tumours were snap frozen in isopentane and kept at -80°C. Tissues were sectioned at 10 μm and fluorescence imaging was performed using the Odyssey imager. The presence of OSC-19-luc2-cGFP and MCF-7-luc2-cGFP tumour cells was confirmed by fluorescence microscopy (Nikon Eclipse e800). All histologic sections were stained with standard haematoxylin-eosin stain (HE) after acetone fixation. To confirm the presence of HT29 and HT29-luc2 cells, sections were stained with an anti-human wide-spectrum cytokeratin antibody (Abcam inc., Cambridge, MA, USA). Primary antibodies or controls were incubated for 60 minutes at room temperature. All slides were three times washed with PBS and incubated with Envision anti-rabbit (DAKO) for thirty minutes at room temperature. Subsequently, the slides

were washed with PBS and staining was visualized by using 3,3-diaminobenzidine. Sections were counterstained with haematoxylin, dehydrated and mounted with pertex. Frozen OSC-19-luc2-cGFP and MCF-7-luc2-cGFP tumours were stained with an anti-cGFP staining (Evrogen, Moscow, Russia). Sections stained with anti-cGFP were fixated with 4% formalin for 10 minutes. After washing with PBS, cells were treated with 0,1% saponin/PBS for 10 minutes and incubated with the anti-GFP antibody, diluted in 0,1% saponin/PBS for 60 minutes at room temperature. Adjacent sections were fixated with aceton for 10 minutes followed by three washes with PBS and stained for cytokeratin as described before.

Statistical analysis

For statistical analysis, SPSS statistical software package (version 20.0 for Windows, IBM SPSS Inc, Chicago, USA) was used. TBRs were calculated by dividing the fluorescent signal of the tumour by fluorescent signal of surrounding healthy tissue. TBRs are reported in mean and standard deviation. A two-way repeated measurement ANOVA was used to assess the relation between TBRs in the dose groups and time points. Furthermore a paired Student's t-test was used to calculate the overall difference between the EpCAM specific and control groups. The two-way repeated measurement ANOVA was corrected using the Bonferroni correction. A P-value equal or lower than 0.05 was considered significant.

Results

EpCAM expression on human cancer cell lines

The colon adenocarcinoma cell line HT29 showed intermediate high expression of EpCAM while COLO320 hardly had any EpCAM expression (200,000 versus <1000 EpCAM/cell), see Figure 1A). For MCF-7 breast cancer cells similar EpCAM over-expression was observed as for HT29, whereas considerably less expression was seen in MDA-MB-231 cells, as described previously (Figure 1B). For head-and-neck cancer cells, the human hypopharyngeal squamous cell carcinoma cell line FaDu-luc2 and the oral squamous cell carcinoma cell line OSC-19 showed similar intermediate EpCAM expression (Figure 1C). For all cancer cell lines the control antibody MOPC21 showed no significant signal. EpCAM expressing cell-lines MCF-7 and OSC-19 were transfected with GFP and luciferase and were, next to HT29-luc2 used for further *in vivo* experiments.
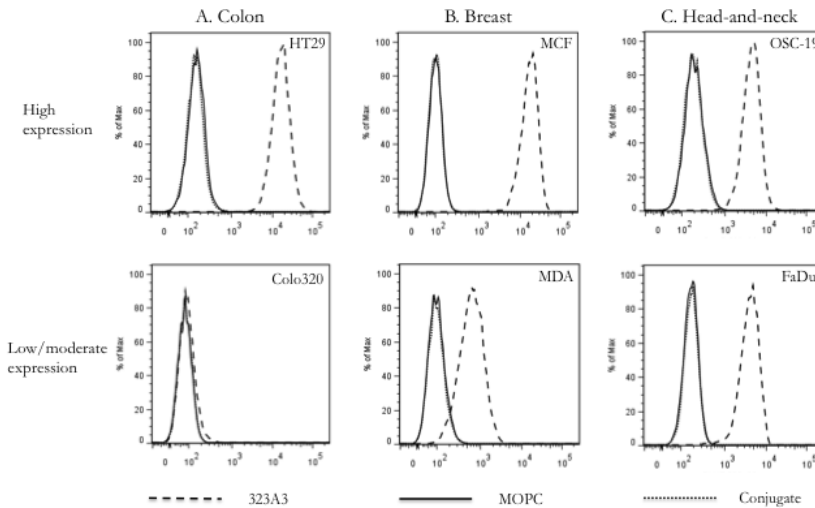
Figure 1 - EpCAM expression: EpCAM overexpression was present in all cell lines except in COLO320 cells. Expression of EpCAM was analyzed in human colon (A, HT29-luc2, COLO320), breast (B, MCF-7, MDA-MB231) and head & neck (C, OSC-19, FaDu-luc2) cancer. Cells were incubated with an anti-EpCAM antibody (323/A3) or an isotype normal mouse IgG (MOPC21). After washing, cells were incubated with fluorescein isothiocyanate (FITC)-conjugated anti-mouse IgG antibody. The anti-mouse antibody was solely used as a control (conjugate).

Conjugation, characterization and serum stability of 323/A3-800CW

Both the EpCAM specific (323/A3) and the control antibody (MOPC21) were labelled with IRDye 800CW (Figure 2A) in comparable mean dye:antibody ratios of respectively 2.6 ± 0.9 and 2.8 ± 0.9, as determined spectrophotometrically, according to the protocol of the manufacturer of the dye. Plate assays containing both high and low EpCAM expressing cell lines were utilized to confirm EpCAM specificity of 323/A3-800CW after conjugation. A significant ($p < 0.01$) difference was observed between 323/A3-800CW and MOPC21-800CW signals on MCF-7, HT29, OSC-19 and FaDu cells, but not on the low EpCAM expressing COLO320 and MB-
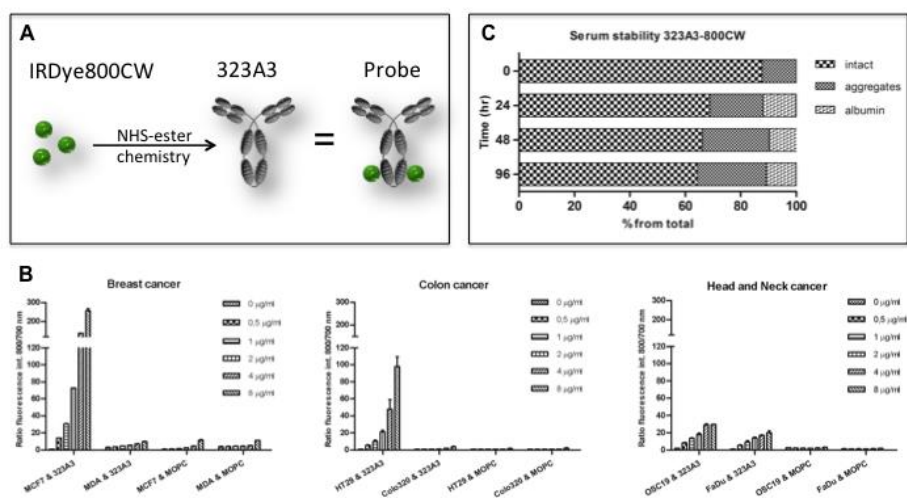
Figure 2 – Conjugation, serum stability and EpCAM specificity: Conjugation of IRDye 800CW to 323/A3 and MOPC21 was done through NHS ester conjugation. A mean labeling ratio of 2.6 ± 0.98 and 2.8 ± 0.99 was obtained for 323/A3 and MOPC21 respectively (A). EpCAM specificity of 323/A3 was confirmed after conjugation of IRDye 800CW on various cell types, corrected for cell number using the 800/700nm ratio (B). Experiments were done in human colon (HT29-luc2, COLO320), breast (MCF-7-luc2-cGFP, MDA-MB231) and head & neck (OSC-19-luc2-cGFP, FaDu-luc2) cancer. Cells were incubated with different concentrations of 323/A3-800CW or an isotype normal mouse IgG (MOPC21) conjugated to 800CW. To correct for the number of cells, the ratio of NIR fluorescence and the fluorescence intensity of TO-PRO-3 was plotted. 323/A3-800CW showed to be stable in human serum with more than 60% of the conjugate still free to bind EpCAM after 96 hours with the remaining 40% aggregated or bound to albumin (C).

MDA-231 cells (Figure 2B). The fluorescence intensity of MOPC21-800CW showed a slight concentration dependent increase as a result of non-specific binding. The results are in accordance to the EpCAM expression found using flow cytometry results of the antibodies without 800CW label, as shown in Figure 1. The increase in concentration resulted in a plateau in fluorescence intensity in MDA-MB-231, OSC-19 and FaDu cells. A further increase in concentration did not increase signal intensity. This phenomenon was not seen in MCF-7 and

HT29 cells, possibly due to the high EpCAM expression. The EpCAM specific conjugate showed to be stable in human serum with more than 60% of the conjugate still free to bind EpCAM after 96 hours with the remaining 40% aggregated or bound to albumin (Figure 2C).

Intra-operative NIR fluorescence tumour delineation and resection

In vivo specificity of 323/A3-800CW was shown by competition with unconjugated antibody. Pre-injection of 1 mg unconjugated 323/A3, resulted in a decrease of the percentage of injected dose per gram of tumour from 3.2 ± 0.9 % ID/g to 1.0 ± 0.1 % ID/g (p< 0.01, n=3 in both groups), see figure 3A.
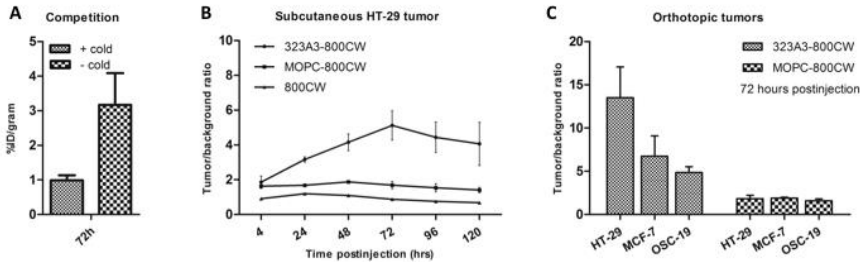
5

Figure 3 – EpCAM specificity and intra-operative tumour-to-background ratios (TBR's): Competition with 1 mg of cold 323/A3 antibody significantly decreased the percentage of injected dose 323/A3-800CW per gram tumour (%ID/gram) indicating *in vivo* tumour specificity (A). After development of subcutaneous HT29-luc2 tumours, 1 nmol (150ug) of 323/A3-800CW, MOPC21-800CW and IRDye 800CW was injected intravenously. TBR's were calculated from 4 hours to 120 hours after injection (B). Subsequently, 1 nmol (150ug) 323/A3-800CW and MOPC21-800CW was intravenously injected in mice bearing orthotopic colon (HT29-luc2), breast (MCF-7-luc2-cGFP) and tongue (OSC-19-luc2-cGFP) tumours (C). TBR's were calculated 72 hours post injection. TBR's of EpCAM specific antibody 323/A3-800CW in colon, breast and head & neck cancer are significantly higher compared to those of the control antibody MOPC21-800CW.

The HT29 subcutaneous tumour model was used to assess the feasibility of intraoperative fluorescence delineation using 1 nmol (150ug) intravenous 323/A3-800CW combined with the Artemis imaging system. Tumours could be clearly delineated from 4 hours post injection and an increase in TBR was seen with highest values at 72 hours post-injection (5.2 ± 0.7, Figure 3B). After 72 hours the TBR slightly decreased. Significant differences in TBR (p< 0.01) between EpCAM specific (323/A3-800CW) and non-specific control (MOPC21-800CW) could be observed from 24 hours post injection (TBR 3.2 ± 0.1 and 1.7 ± 0.2 respectively). MOPC21-800CW and IRDye 800CW showed a significantly lower TBR at all time points (p < 0.01). Based on the results from the subcutaneous tumour model an optimal incubation time of 72 hours was used to evaluate NIR fluorescence in clinically more realistic orthotopic mouse models for colon, breast and head-and-neck cancer. After exploration of the tumour, we assessed the feasibility of fluorescence-guided resection and chose suitable resection margins with the real-time NIR

fluorescence feedback of 323/A3-800CW and the Artemis imaging system. All tumours were radically resected as confirmed by BLI evaluation. Significant differences ($p < 0.01$) in TBRs were observed between the orthotopic colon (HT29) mice injected with 323/A3-800CW (TBR 13.5 ± 3.6) and MOPC21-800CW (TBR 1.8 ± 0.4) (Figure 3C). For the breast (MCF-7) and head-and-neck (OSC-19) cancer models, 323/A3-800CW showed TBRs of 6.7 ± 1.9 and 4.9 ± 0.7 respectively (Figure 3C). Significantly lower TBR values of 1.9 ± 0.1 and 1.6 ± 0.2 were observed for MOPC21-800CW in breast and head-and-neck cancer respectively ($p < 0.01$). Examples of *in vivo* and *ex vivo* images that were acquired with the Artemis imaging system after injection of 323/A3-800CW or MOPC21-800CW are shown for the orthotopic colon (Figure 4A & 4B), breast (Figure 4C) and head-and-neck cancer model (Figure 4D). Camera exposure time and gain were intra-operatively adjusted to obtain optimal image contrast. The most important factors influencing measured fluorescent intensities were sample fluorescence intensity, camera settings and the coupled distance to sample of both illumination source and camera. The Artemis camera is not calibrated for absolute intensity measurements (e.g. in lumen), hampering absolute intensity comparisons between images.
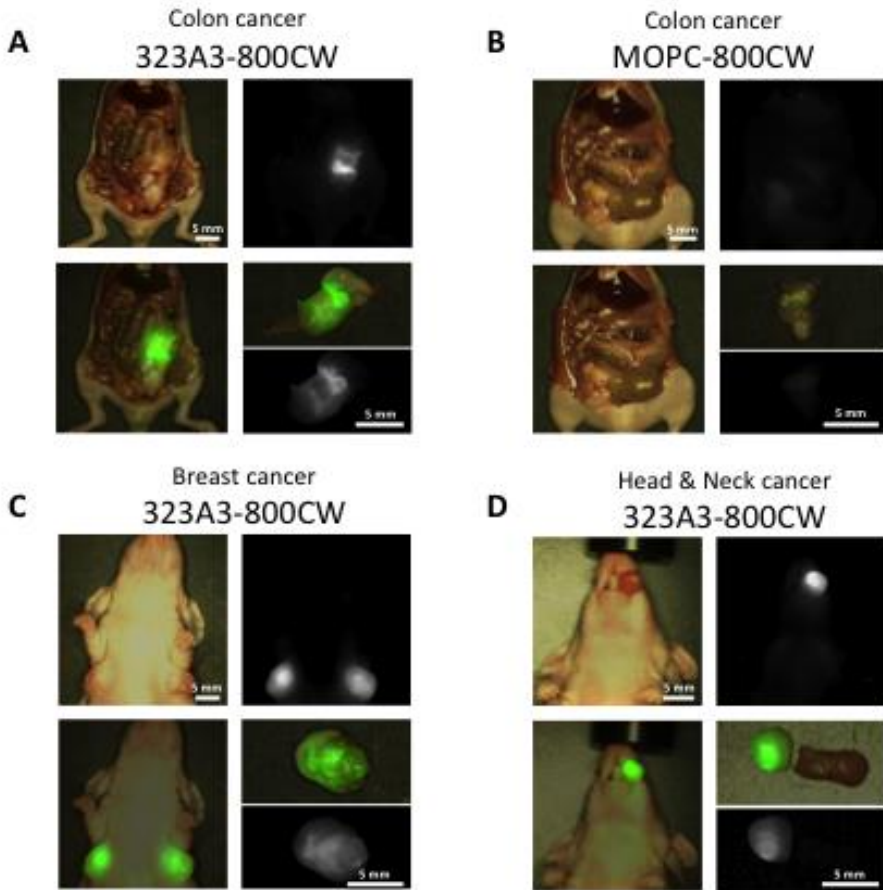
Figure 4 – Intra-operative NIR fluorescence delineation of colon, breast and Head & Neck cancer: Colon (A, B), breast (C) and head & neck tumours (D) could clearly be visualized during operation using EpCAM specific 323/A3-800CW (TBR colon 13.5, breast 6.7 and Head-and-neck 4.9) and the Artemis imaging system. 323/A3-800CW (A, C, D, 1 nmol) and the non-specific antibody MOPC21-800CW (B, 1 nmol) were intravenously injected. After an incubation of 72 hours NIR fluorescence imaging was performed. Depicted images are: bright light, fluorescence, overlay (fluorescence and bright light), ex vivo fluorescence and ex vivo overlay. Scale bars are 5 mm . Artemis fluorescence intensities were intra-operatively optimized for optimal contrast. Intensities can only be compared within images.

Detection of small tumour sizes

Four weeks after the intra-peritoneal injection of MCF-7-luc2-cGFP cells multiple tumours were observed by BLI imaging. Millimetre size tumour nodules located on the peritoneum, which were not visual by the naked eye, could be observed by NIR fluorescence imaging after injection of 1 nmol (150ug) 323/A3-800CW, using both the Pearl and Artemis imaging system (Figure 5). After the peritoneum was resected, BLI confirmed that intra-peritoneal metastases could be detected by NIR fluorescence imaging (Figure 5). As in Figure 4, camera exposure time and gain were adjusted to obtain optimal contrast. ROC curve analysis (Figure 5) showed an accuracy of 98% (area under the curve, $p < 0.0001$) for detecting micro metastases with a sensitivity of 93% and specificity of 92% at the curve's optimal TBR cutoff value. A cutoff value obtaining the highest sensitivity of 100% correlates with a specificity of 73%. A specificity of 100% on the other hand correlates with a sensitivity of 84%.
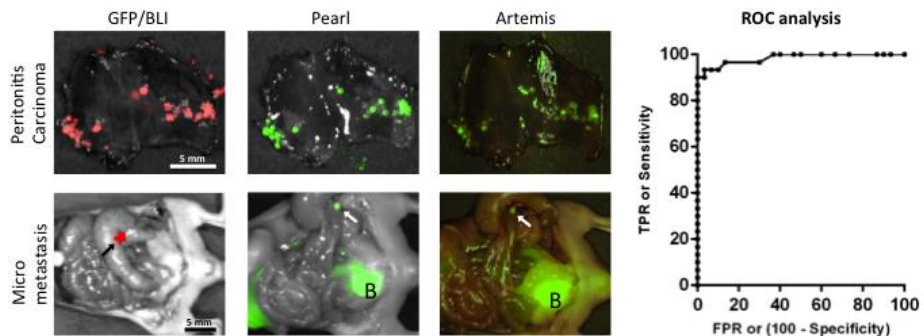
Figure 5 – tumour detection limit: Submillimeter sized intra-peritoneal metastases could clearly be visualized using EpCAM specific 323/A3-800CW and the Artemis system. MCF-7-luc2-cGFP cells were injected intraperitoneal. After the development of multiple tumours, 1 nmol (150ug) 323/A3-800CW was injected intravenously. NIR fluorescence imaging was performed after 72 hours of incubation using the Pearl and Artemis system. Confirmation of tumour tissue was performed by Green Fluorescent Protein (GFP) fluorescence imaging or Bioluminescence Imaging (BLI) using the IVIS spectrum. Micrometastases (arrow) of the colon could be discovered by NIR fluorescence imaging after resection of the peritoneum. ROC curve analysis of TBR of fluorescent spots in the peritoneum. True positive rate was plotted versus false-positive rate using ascending positive cutoff values. B = bladder. Scale bars are 5 mm. Artemis fluorescence intensities were intra-operatively optimized for optimal contrast. Intensities can only be compared within images.

Histology and Immunohistochemistry

Orthotopic tumour tissue was harvested 72 hours after injection of 323/A3-800CW, MOPC21-800CW and IRDye 800CW. In sections of cGFP transfected breast and tongue tumours, the presence of tumour tissue was confirmed by anti-cGFP immunohistochemical staining (brown colour, Figure 6C and D). Figure 6A clearly illustrates NIR fluorescence (indicated in red)
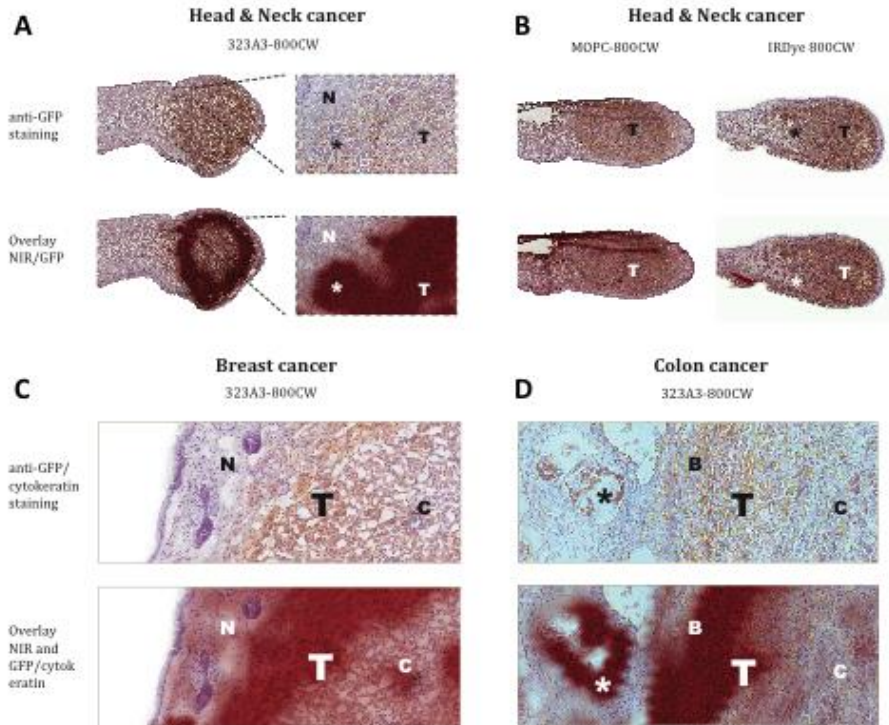
Figure 6 – Histology: 323/A3-800CW is specifically located in head-and-neck (A, B), breast (C), and colon (D) tumours. Tumour tissue was sectioned 72 hours after injection of 323/A3-800CW, MOPC21-800CW or IRDye 800CW. Shown are anti-GFP (brown, head-and-neck cancer, breast cancer) or cytokeratin (brown, colon cancer) immunohistochemistry stainings and overlays of NIR fluorescence (red) and anti-GFP/cytokeratin stainings. In all tissue a clear overlap is seen between NIR fluorescence from 323/A3-800CW and anti-GFP immunohistochemistry staining (indicating tumour). NIR fluorescence is mainly located in the border of tumours and even small tumour islands (*) are NIR fluorescent. A low, non specific fluorescence signal was observed in sections with MOPC21-800CW and IRDye 800CW (B). T = tumour; N = normal tissue; C = center tumour; B = tumour border. A and B 1x zoom; C and D 10x zoom

intensity and localization of 323/A3-800CW, MOPC-800CW and IRDye 800CW in tissue sections of tongue tumours, surrounded by normal tissue of the tongue. Fluorescence of 323/A3-800CW co-localized with the outer part of the tumour bulk and with small peninsulas of tumour cells (Figure 6A). Fluorescence intensity of MOPC21-800CW and IRDye 800CW was hardly visible and did not show association with tumour tissue (Figure 6B). In both, breast and colon cancer tissue sections NIR fluorescence appeared in the outer rim of tumour tissue. (Figure 6C and D). In colon cancer clear co-localization of small tumour islands and NIR fluorescence (indicated in red) was observed with 323/A3-800CW (Figure 6D). Cytokeratin staining (brown) was performed to confirm the presence of colonic tumour cells in sections of orthotopic colon tumours (Figure 6D).

Discussion

In this study we investigated an EpCAM-specific NIR-fluorescent agent using a state-of-the-art next generation clinical NIR imaging system. The recent technical developments stimulate the use of advanced but affordable imaging systems in the clinic. The Artemis imaging system simultaneously acquires NIR-fluorescent and visible light, generating a merged image in real-time. Systems like this will boost the demand for specific tumour probes dramatically.

The EpCAM directed antibody in this study has been extensively evaluated for imaging of various tumour models using radionuclides Technetium, Zirconium, Iodium and Rhenium [30, 31, 39]. Typically, in these experiments 15-20 μg of conjugate was used per mouse to obtain clear tumour signals in subcutaneous breast, colon and ovarian tumours. Using the same antibody but conjugated to a NIR dye and in combination with a state of the art NIR-fluorescence imager, we showed that 1 nmol (=150μg) clearly identified breast, colon and head-and-neck cancers, as well as micro-metastases in human orthotopic xenograft mouse models. The probe/system combination allowed an accurate demarcation of the tumours, the recognition of tumour margins, examination of malignant spread, and identification of micrometre sized metastasis or remnant disease.

A probe against a 'universal' target facilitates clinical usability, and prevents time consuming and costly development of multiple agents. Although EpCAM is considered to be a potential target for epithelial derived cancers, not all epithelial cancers over-express EpCAM enough to outflank adjacent normal tissue. But on the other hand not all tumours of mesenchymal origin are EpCAM negative. Over-expression of EpCAM was recently observed in all osteosarcomas, half of the angiosarcomas and 62.5% of the leiomyosarcomas, indicating the broad spectrum of tumours that might be targeted [40].

In breast cancer, 20% of tumours that seem radically resected during surgery turn out to be irradically removed in histologic analyses. Consequently, FGS in breast cancer could enhance the number of radical resections without increasing margins, thus improving patient's prognoses and cosmetic outcomes after lumpectomies and oncoplastic surgery [5, 41]. As pointed out earlier, in copies per cell EpCAM can probably not compete with Her2/Neu in the subpopulation of Her2 positive breast cancers, but in percentage of positive breast tumours EpCAM is clearly the more prevalent target. For head-and-neck cancer a relatively low percentage of tumours is irradically resected (16%). Due to the many vital structures in the surrounding tissue, resection margins should be small and FGS targeting would be of great clinical benefit. EpCAM overexpression is seen in 62.5% of tongue tumours [25, 42]. In colorectal cancers 80-100% overexpression of

EpCAM is found. Although irradical resections occur, the main problem is damage to vital structures in the lower abdomen. Ureteral injury is a rare but serious complication of lower abdominal surgery, with a reported incidence varying from 0.7 up to 10% [43]. EpCAM-based FGS of colorectal tumours in combination with FGS of the ureters could enhance the number of radical resections while preserving vital structures.

In our study, we performed a single injection of 1 nmol (150ug) of 323/A3-800CW to visualize tumours. This is the equivalent of 0.5 mg/kg for humans when converted using the body-surface-area method [44]. Using this dose, subcutaneously located colon tumours were clearly recognized from 4 hours after injection with optimal TBRs at 72 hours, showing the feasibility of the agent. The 72-hour time-point was utilized to perform surgery at the orthotopic colon, breast, and head-and-neck cancer models validating the results from the subcutaneous model in clinically more relevant models. At this time point the agent-imaging system combination was able to indicate small tumour nodules on the peritoneum or in the abdominal cavity that were otherwise only detectable by bioluminescence of these cells. Although we did not study the lower boundary of tumour size that could be detected, tumour nodules of 1 mm³ could clearly be visualized. Based on the number of cells in spheroids of that size, we estimate the minimal number of cells to be detectable above 50,000. Obviously this detection limit is depending on multiple factors like the imaging system, optical properties of overlying tissue and the probe. The ROC analysis for the detection of micrometastases showed an excellent sensitivity and specificity at the optimal TBR cutoff. Nevertheless, a remark has to be added that the ex vivo detection of micrometastases in the peritoneum is very opportune because almost no background fluorescence is observed in the peritoneum and the detection of metastases is not compromised by any tissue depth. Due to the lack of performance standards for clinically applicable imaging systems as well as imaging agents, at present, the combination of both is of major importance for a successful outcome [45, 46].

Although the anti-EpCAM/800CW conjugate performed well in various tumour types, this probe could still be optimized. The use of antibodies with relatively high affinity, like 323/A3, might culminate in heterogeneous tumour staining, concentrated around the tumour vascularization rather than homogeneous throughout the tumour. The use of an antibody with low or intermediate EpCAM affinity for EpCAM might promote a more homogenous distribution and avoid adverse effects at the cost of a lower total tumour uptake [31, 47]. An improvement in imaging accuracy without compromising the total tumour uptake could be expected by reducing Fc/FcγR interactions through deglycosylation of antibody-based imaging as recently demonstrated by Gao et al. [48]. Further, most EpCAM antibodies target actually the same EGF-like domain of EpCAM. Antibodies identifying other EpCAM domains, like the C-

domains might improve detection efficiency [49]. The use of any mouse-derived antibody, like 323/A3, will inevitably induce human anti-mouse antibodies. Although this is not disastrous for imaging purposes, where only one single dose is needed, a chimerized or humanized version with retained efficacy should be preferred [31]. Last but not least, fragments of antibodies like Fab or Fab2 could have higher penetration capabilities compared to full-size antibodies, as shown for several antibodies including anti-EpCAM [37, 39, 50]. Using antibody fragments would lead to shorter incubation times, making clinical translation more applicable. Moreover, recent developments have opened the way for hybrid molecules like immunoenzymosomes, consisting of liposomes equipped with 323/A3 Fab fragments for targeting [51]. Alternative probes for pre- and intraoperative imaging could also be generated by conjugation of the antibody with 2 different labels, one for PET/SPECT and one for NIRF imaging like has been done recently[36, 37, 52, 53].

In conclusion, FGS is a promising technique to ensure intra-operative fluorescence feedback of tumour margins. Clinical success is only achieved by using a dedicated camera system and tumour-specific agents. This study aimed to achieve complete preclinical validation of an EpCAM targeting fluorescence agent in combination with a next-generation Artemis imaging system. We showed the ability to visualize, primary tumours and millimetre sized tumour nodules and metastases that were otherwise invisible for the human eye. As a novel EpCAM specific optical agent can be used in a wide variety of tumours, together with the knowledge from previous clinical trials and the results from this study, this paves the way for a fast and cost effective clinical translation.

Acknowledgments

Conflicts of interest and source of funding

None.

5

References

1. Alexander, S. and P. Friedl, *Cancer invasion and resistance: interconnected processes of disease progression and therapy failure.* Trends in molecular medicine, 2012. **18**(1): p. 13-26.

2. Friedl, P. and S. Alexander, *Cancer invasion and the microenvironment: plasticity and reciprocity.* Cell, 2011. **147**(5): p. 992-1009.

3. Weissleder, R. and M.J. Pittet, *Imaging in the era of molecular oncology.* Nature, 2008. **452**(7187): p. 580-9.

4. Quirke, P., et al., *Local recurrence of rectal adenocarcinoma due to inadequate surgical resection. Histopathological study of lateral tumour spread and surgical excision.* Lancet, 1986. **2**(8514): p. 996-9.

5. Rizzo, M., et al., *The effects of additional tumour cavity sampling at the time of breast-conserving surgery on final margin status, volume of resection, and pathologist workload.* Ann Surg Oncol, 2010. **17**(1): p. 228-34.

6. Wong, L.S., et al., *Influence of close resection margins on local recurrence and disease-specific survival in oral and oropharyngeal carcinoma.* Br J Oral Maxillofac Surg, 2012. **50**(2): p. 102-8.

7. Xiong, L., et al., *Indocyanine green fluorescence-guided sentinel node biopsy: a meta-analysis on detection rate and diagnostic performance.* Eur J Surg Oncol, 2014. **40**(7): p. 843-9.

8. Verbeek, F.P., et al., *Optimization of near-infrared fluorescence cholangiography for open and laparoscopic surgery.* Surg Endosc, 2014. **28**(4): p. 1076-82.

9. Vahrmeijer, A.L., et al., *Image-guided cancer surgery using near-infrared fluorescence.* Nat Rev Clin Oncol, 2013. **10**(9): p. 507-18.

10. Sevick-Muraca, E.M., et al., *Imaging of lymph flow in breast cancer patients after microdose administration of a near-infrared fluorophore: feasibility study.* Radiology, 2008. **246**(3): p. 734-41.

11. Unno, N., et al., *Quantitative lymph imaging for assessment of lymph function using indocyanine green fluorescence lymphography.* Eur J Vasc Endovasc Surg, 2008. **36**(2): p. 230-6.

12. Keereweer, S., et al., *Optical image-guided cancer surgery: challenges and limitations.* Clin Cancer Res, 2013. **19**(14): p. 3745-54.

13. Gioux, S., H.S. Choi, and J.V. Frangioni, *Image-guided surgery using invisible near-infrared light: fundamentals of clinical translation.* Mol Imaging, 2010. **9**(5): p. 237-55.

14. Gong, H., et al., *A comparative study of affibody, panitumumab, and EGF for near-infrared fluorescence imaging of EGFR- and EGFRvIII-expressing tumours.* Cancer Biol Ther, 2014. **15**(2): p. 185-93.

15. Persson, M. and A. Kjaer, *Urokinase-type plasminogen activator receptor (uPAR) as a promising new imaging target: potential clinical applications.* Clin Physiol Funct Imaging, 2013. **33**(5): p. 329-37.

16.   Zielinski, R., et al., *Affibody-DyLight conjugates for in vivo assessment of HER2 expression by near-infrared optical imaging.* PLoS One, 2012. **7**(7): p. e41016.

17.   Paudyal, B., et al., *Detection of vascular endothelial growth factor in colon cancer xenografts using bevacizumab based near infrared fluorophore conjugate.* J Biomed Sci, 2014. **21**: p. 35.

18.   Lee, H., et al., *A folate receptor-specific activatable probe for near-infrared fluorescence imaging of ovarian cancer.* Chem Commun (Camb), 2014. **50**(56): p. 7507-10.

19.   Jin, Z.H., et al., *In vivo optical imaging of integrin alphaV-beta3 in mice using multivalent or monovalent cRGD targeting vectors.* Mol Cancer, 2007. **6**: p. 41.

20.   Winter, M.J., et al., *The epithelial cell adhesion molecule (Ep-CAM) as a morphoregulatory molecule is a tool in surgical pathology.* Am J Pathol, 2003. **163**(6): p. 2139-48.

21.   Went, P.T., et al., *Frequent EpCam protein expression in human carcinomas.* Hum Pathol, 2004. **35**(1): p. 122-8.

22.   Spizzo, G., et al., *Prognostic significance of Ep-CAM AND Her-2/neu overexpression in invasive breast cancer.* Int J Cancer, 2002. **98**(6): p. 883-8.

23.   Osta, W.A., et al., *EpCAM is overexpressed in breast cancer and is a potential target for breast cancer gene therapy.* Cancer Res, 2004. **64**(16): p. 5818-24.

24.   Gastl, G., et al., *Ep-CAM overexpression in breast cancer as a predictor of survival.* Lancet, 2000. **356**(9246): p. 1981-2.

25.   Laimer, K., et al., *EpCAM expression in squamous cell carcinoma of the oral cavity: frequency and relationship to clinicopathologic features.* Oral Oncol, 2008. **44**(1): p. 72-7.

26.   Fong, D., et al., *High expression of TROP2 correlates with poor prognosis in pancreatic cancer.* Br J Cancer, 2008. **99**(8): p. 1290-5.

27.   Goossens-Beumer, I.J., et al., *Clinical prognostic value of combined analysis of Aldh1, Survivin, and EpCAM expression in colorectal cancer.* Br J Cancer, 2014. **110**(12): p. 2935-44.

28.   Munz, M., et al., *Side-by-side analysis of five clinically tested anti-EpCAM monoclonal antibodies.* Cancer Cell Int, 2010. **10**: p. 44.

29.   Gires, O. and P.A. Bauerle, *EpCAM as a target in cancer therapy.* J Clin Oncol, 2010. **28**(15): p. e239-40; author reply e241-2.

30.   Meijs, W.E., et al., *Zirconium-labeled monoclonal antibodies and their distribution in tumour-bearing nude mice.* J Nucl Med, 1997. **38**(1): p. 112-8.

31.   Kievit, E., et al., *[186Re]-labeled mouse and chimeric monoclonal antibody 323/A3: a comparison of the efficacy in experimental human ovarian cancer.* Nucl Med Biol, 1998. **25**(1): p. 37-45.

32.   van Driel, P.B., et al., *Characterization and Evaluation of the Artemis Camera for Fluorescence-Guided Cancer Surgery.* Mol Imaging Biol, 2014.

33.   van Driel, P.B., et al., *Intraoperative fluorescence delineation of head and neck cancer with a fluorescent Anti-epidermal growth factor receptor nanobody.* Int J Cancer, 2013.

5

34.   Edwards, D.P., et al., *Monoclonal antibody identification and characterization of a Mr 43,000 membrane glycoprotein associated with human breast cancer.* Cancer Res, 1986. **46**(3): p. 1306-17.

35.   Velders, M.P., et al., *Immunotherapy with low and high affinity monoclonal antibodies 17-1A and 323/A3 in a nude mouse xenograft carcinoma model.* Cancer Res, 1995. **55**(19): p. 4398-403.

36.   Hall, M.A., et al., *Comparison of mAbs targeting epithelial cell adhesion molecule for the detection of prostate cancer lymph node metastases with multimodal contrast agents: quantitative small-animal PET/CT and NIRF.* J Nucl Med, 2012. **53**(9): p. 1427-37.

37.   Eder, M., et al., *68Ga-labelled recombinant antibody variants for immuno-PET imaging of solid tumours.* Eur J Nucl Med Mol Imaging, 2010. **37**(7): p. 1397-407.

38.   Tseng, W., X. Leong, and E. Engleman, *Orthotopic mouse model of colorectal cancer.* J Vis Exp, 2007(10): p. 484.

39.   Pak, K.Y., et al., *Evaluation of the 323/A3 monoclonal antibody and the use of technetium-99m-labeled 323/A3 Fab' for the detection of pan adenocarcinoma.* Int J Rad Appl Instrum B, 1991. **18**(5): p. 483-97.

40.   Ward, K., et al., *Epithelial cell adhesion molecule is expressed in a subset of sarcomas and correlates to the degree of cytological atypia in leiomyosarcomas.* Mol Clin Oncol, 2015. **3**(1): p. 31-36.

41.   McLaughlin, S.A., *Surgical management of the breast: breast conservation therapy and mastectomy.* Surg Clin North Am, 2013. **93**(2): p. 411-28.

42.   Yanamoto, S., et al., *Clinicopathologic significance of EpCAM expression in squamous cell carcinoma of the tongue and its possibility as a potential target for tongue cancer gene therapy.* Oral Oncol, 2007. **43**(9): p. 869-77.

43.   Verbeek, F.P., et al., *Near-infrared fluorescence imaging of both colorectal cancer and ureters using a low-dose integrin targeted probe.* Ann Surg Oncol, 2014. **21 Suppl 4**: p. 528-37.

44.   Reagan-Shaw, S., M. Nihal, and N. Ahmad, *Dose translation from animal to human studies revisited.* FASEB J, 2008. **22**(3): p. 659-61.

45.   Zhu, B. and E. Sevick-Muraca, *A review of performance of near-infrared fluorescence imaging devices used in clinical studies.* Br J Radiol, 2014: p. 20140547.

46.   Sevick-Muraca, E.M. and B. Zhu, *The need for performance standards in clinical translation and adoption of fluorescence molecular imaging.* Med Phys, 2013. **40**(4): p. 040402.

47.   Thurber, G.M., M.M. Schmidt, and K.D. Wittrup, *Antibody tumour penetration: transport opposed by systemic and antigen-mediated clearance.* Adv Drug Deliv Rev, 2008. **60**(12): p. 1421-34.

48.   Gao, P., et al., *Deglycosylation of mAb by EndoS for improved molecular imaging.* Mol Imaging Biol, 2015. **17**(2): p. 195-203.

49.   Takao, M., Y. Nagai, and T. Torii, *Cysteine-poor region-specific EpCAM monoclonal antibody recognizing native tumour cells with high sensitivity.* Monoclon Antib Immunodiagn Immunother, 2013. **32**(2): p. 73-80.

50.   Watanabe, R., et al., *Photoimmunotherapy targeting prostate-specific membrane antigen: are antibody fragments as effective as antibodies?* J Nucl Med, 2015. **56**(1): p. 140-4.

51.   Fonseca, M.J., et al., *Liposome-mediated targeting of enzymes to cancer cells for site-specific activation of prodrugs: comparison with the corresponding antibody-enzyme conjugate.* Pharm Res, 2003. **20**(3): p. 423-8.

52.   Boonstra, M.C., et al., *uPAR-targeted multimodal tracer for pre- and intraoperative imaging in cancer surgery.* 2015. 2015.

53.   Ghosh, S.C., et al., *Multimodal chelation platform for near-infrared fluorescence/nuclear imaging.* J Med Chem, 2013. **56**(2): p. 406-16.

5
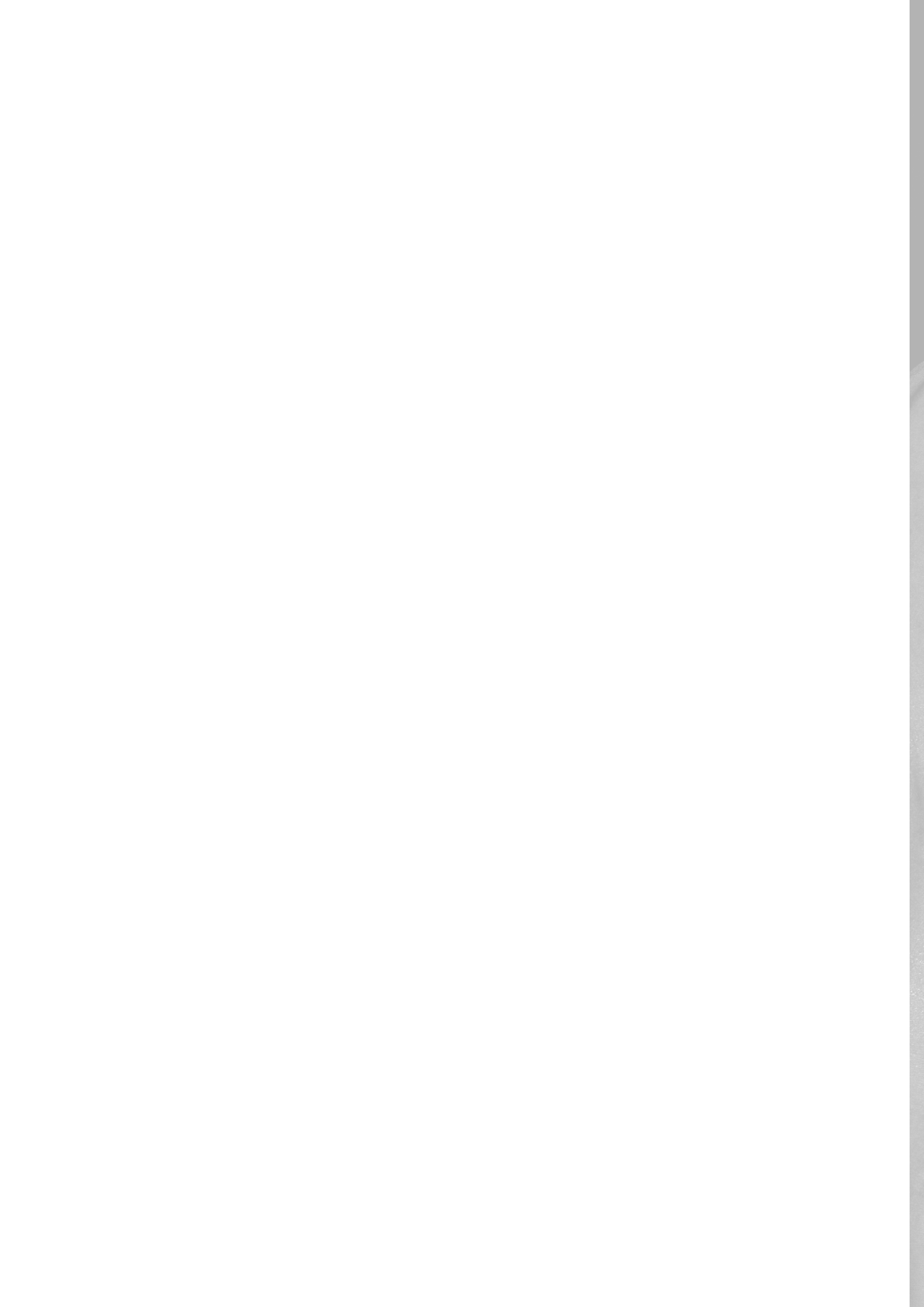
CHAPTER 6

Pieter B.A.A. Van Driel[1], Martijn van de Giessen[2], Martin C. Boonstra[3], Thomas J.A. Snoeks[1], Stijn Keereweer[4], Sabrina Oliveira[5,6], Cornelis J.H. van de Velde[3], Boudewijn P.F. Lelieveldt[2], Alexander L. Vahrmeijer[3], Clemens W.G.M. Löwik[1], Jouke Dijkstra[2]

1. Department of Radiology and Molecular Imaging, Leiden University Medical Center, Leiden, The Netherlands
2. Department of Image Processing, Leiden University Medical Center, Leiden, The Netherlands
3. Department of Surgery, Leiden University Medical Center, Leiden, The Netherlands
4. Department of Otorhinolaryngology & Head and Neck Surgery, Erasmus Medical Center, Rotterdam, The Netherlands
5. Division Cell Biology, Department of Biology, Utrecht University, Utrecht, The Netherlands
6. Department of Pathology, University Medical Center Utrecht, Utrecht, The Netherlands

ABSTRACT

Purpose

Near-infrared (NIR) fluorescence imaging can provide the surgeon with real-time visualization of, e.g., tumour margins and lymph nodes. We describe and evaluate the Artemis, a novel, handheld NIR fluorescence camera.

Procedures

We evaluated minimal detectable cell numbers (FaDu-luc2, 7D12-IRDye 800CW), preclinical intraoperative detection of sentinel lymph nodes (SLN) using indocyanine green (ICG), and of orthotopic tongue tumours using 7D12-800CW. Results were compared with the Pearl imager. Clinically, three patients with liver metastases were imaged using ICG.

Results

Minimum detectable cell counts for Artemis and Pearl were 2×10^5 and 4×10^4 cells, respectively. In vivo, seven SLNs were detected in four mice with both cameras. Orthotopic OSC-19-luc2-cGFP tongue tumours were clearly identifiable, and a minimum FaDu-luc2 tumour size of 1 mm3 could be identified. Six human malignant lesions were identified during three liver surgery procedures.

Conclusions

Based on this study, the Artemis system has demonstrated its utility in fluorescence-guided cancer surgery.

Introduction

In surgery, many non-invasive imaging modalities, such as computed tomography (CT), magnetic resonance imaging (MRI), single-photon emission computed tomography (SPECT), and positron emission tomography (PET), are used in a preoperative setting for the detection of tumours and for surgical planning. Translating these techniques to the operating room is challenging due to altered body positions and tissue manipulation. Therefore, the surgeon still mainly relies on visual inspection and tactile information during surgery. New intraoperative imaging modalities that support the surgeon in identifying vital structures and discriminating healthy from diseased tissues in real-time are needed, which is especially important for laparoscopic procedures where the surgeon lacks tactile information. Near-infrared (NIR) fluorescence-guided surgery (FGS) is such a novel technique [1, 2]. Compared to SPECT or PET, NIR fluorescence provides high-resolution images, can visualize microscopically tumour nodules, and can be tumourspecific due to targeted exogenous agents [3]. NIR light has the advantage of increased depth penetration and decreased autofluorescence compared to visible light [4, 5]. Furthermore, NIR light is invisible to the human eye and consequently does not alter the surgical field. The success of FGS in recognizing tumours and vital structures depends to a large extent on the imaging system used. In an excellent review, Gioux et al. [6] systematically described the required criteria to which a new clinically applicable NIR fluorescence camera system has to comply. These requirements are translated into a set of practical criteria. The most important criteria for practical application are the following: field of view, imaging distance to the patient, maneuverability, simultaneous imaging of near-infrared and visible light, real-time imaging, light intensity, sterility, and electrical safety. These criteria mainly affect the design choices of the following camera components: sensor, lens system, light source, and filters/dichroic mirrors. Currently, a small number of camera systems that fit most of the criteria above are clinically available [7]. The intraoperative Artemis imaging system is recently developed within the Center for Translational Molecular Medicine (CTMM) consortium. The system is developed in close collaboration with the clinic, which resulted in an easily maneuverable system (Fig. 1a) that acquires (NIR) fluorescence and white light images simultaneously allowing for a depicted overlay. Furthermore, the Artemis has an option to assemble a laparoscope to the camera head, allowing for minimally invasive surgery. The goal of this work was to evaluate the Artemis camera in two oncological procedures in which real-time NIR fluorescence could be of added value: (a) radical tumour resection and (b) the detection of sentinel lymph nodes, the first draining nodes from the tumour. Irradical tumour resections are a major problem in cancer surgery. At present, although tumours clinically appear to be radically resected, high percentages of microscopically irradical resections have been reported at pathological analysis [8, 9]. Such patients require adjuvant treatment and have higher risk of tumour recurrence [10, 11]. When performed with an exogenous tumour-specific ligand,

NIR FGS enables intraoperative guidance of tumour resections. This potentially decreases the relatively high percentages of irradical tumour resections and locoregional recurrences, which may lead to increased survival rates and decreased morbidity [8, 9]. The detection of the SLN is of vital importance for cancer staging and consequently influences the choice of therapy and therefore the survival rates. In breast cancer and melanoma surgery, the SLN procedure is presently the standard of care [12]. Currently, two exogenous contrast agents are clinically available: indocyanine green (ICG) (800 nm) and methylene blue (700 nm). Both non-specific contrast agents are used for the visualization of SLNs, vital structures, and various tumours in the clinic [12]. In this study, we performed a preclinical assessment of the sensitivity and intraoperative utility of the Artemis in the detection of head-and-neck tumours and SLNs preclinically in xenograft mouse models. Images were simultaneously acquired with the Pearl Impulse Small Animal Imager (LI-COR), an existing commercially available and commonly used imaging system. The Pearl system is expected to be an order of magnitude more sensitive than the Artemis, and therefore, these images serve as a ground truth comparison. The Pearl camera does not allow real-time imaging. The sample is shed from outside light imaging in a closed box. Although benefitting the image quality, the latter two characteristics prevent application of the Pearl for intraoperative (pre-)clinical imaging. The Artemis imaging system allows real-time imaging and free access to the sample, but imaging takes place at less ideal circumstances than in the Pearl. We report the first in-human study performed with the Artemis imaging system where colorectal liver metastases were visualized using ICG.
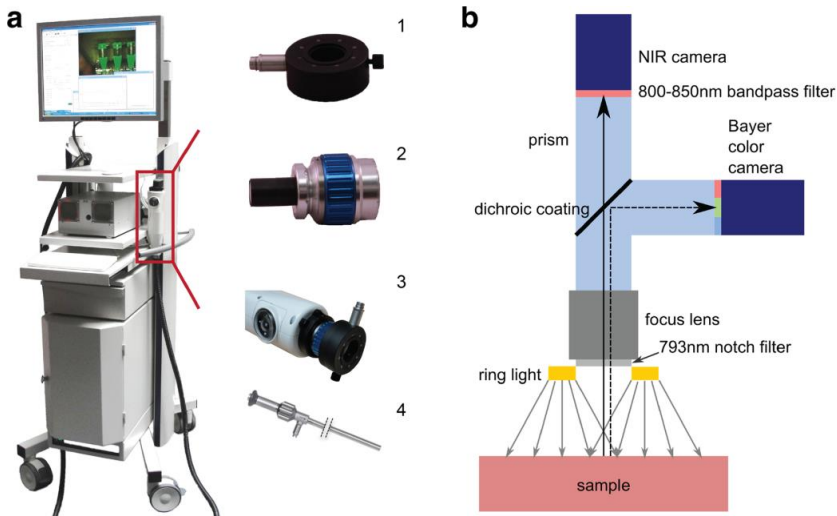
Figure 1 - Artemis NIR imaging system: a The NIR fluorescence imaging Artemis handheld system is positioned on a movable trolley. Ring light (1) and lens (2) have to be attached to the handheld camera (3) to obtain NIR fluorescence images. Instead of lens and ring light, a scope (4) can be attached to the handheld camera when minimal invasive surgery is applied. B Schematic representation of the Artemis camera with light path and filters. The sample is illuminated by a ring light around the camera lens.

Materials and Methods

Near-Infrared Camera Systems

The Artemis camera system was developed by Quest Medical Imaging and the Leiden University Medical Center (Fig. 1). Images were acquired using custom-designed cameras in a portable, freely moveable camera head. A wide field lens for open surgery was used. Samples were illuminated from a ring containing optical fibers (Fig. 1a-1) attached to the lens (Fig. 1a-2) during open surgery imaging. A Lumencor light engine was used containing four solid-state light sources for visible light illumination with peak intensities in the blue, cyan, green, and red. For NIR fluorescence imaging, an NIR laser with a peak intensity at 785 nm was used for the preclinical and at 793 nm for the clinical system. The intensities of the light sources could be controlled from the Artemis software. A sterilizable optical fiber was used to connect the light engine to the illumination ring. Reflected light was captured in the camera head as depicted in Fig. 1b. Reflected excitation light is blocked by a 750–800-nm notch filter. Subsequently, the light passes through a lens that could be used for focusing. The light then enters a prism containing a dichroic coating (G785 mm) in order to separate visible and NIR light. The visible light passes through a low-pass filter (G640 nm) and the NIR light through a high-pass filter (9808 nm). Both light beams are captured by a Sony ICX618 sensor with Bayer configuration having a 640×494 pixel grid. Exposure times and sensor gains were separately adjusted for both imaging channels, and acquisition was synchronized to the longest exposure time. The raw data of both sensors could be saved as individual snapshots or as a real-time movie. During procedures, the visible light channel, the NIR fluorescence channel, and an adjustable overlay are presented. The Pearl Impulse uses two lasers for excitation with a wavelength of 685 and 785 nm. In this work, only the 785-nm excitation light is used. The Pearl camera automatically optimizes exposure times. Imaging data is acquired with a thermoelectrically cooled CCD sensor.

Near-Infrared Probe(s)

The Artemis was evaluated in two imaging procedures in which fluorescence-guided surgery could be of added value. The clinically available ICG (Pulsion Medical Systems, Munich, Germany, λex= 780 nm, λem=820 nm) is frequently used in SLN mapping and for that the choice of dye in this study. IRDye 800CW (LI-COR, Lincoln, NE, USA, λex=774 nm, λem=789 nm) was chosen because it is one of two novel fluorophores in the process of clinical translation [2]. Two imaging procedures were evaluated because of the differences in fluorophores and mainly because fluorophore concentration differs at the side of interest. The near-tumoural injected ICG is highly concentrated compared to the intravenously injected IRDye 800CW conjugated to a targeting moiety. Furthermore, ICG and IRDye 800CW differ in excitation and emission spectra and have different quantum yields. ICG was resuspended in Cealb (20 % human

serum albumin, Sanquin, Amsterdam, The Netherlands) to obtain a dilution from 1 mM to 100 fM. Clinically, 25 mg ICG was resuspended in 10 ml of sterile water before injection obtaining a stock solution of 2.5 mg/ml (3.2 mM). Of this, 4 ml, corresponding to a dose of 10 mg, was administered intravenously. IRDye 800CW carboxylate was resuspended in phosphatebuffered saline to obtain a dilution from 1 μM to 100 fM. Tumourspecific imaging experiments were done using the epidermal growth factor receptor-specific nanobody 7D12 with the nonepidermal growth factor receptor (EGFR)-specific nanobody R2 as a control [13, 14]. The generation of the nanobodies 7D12 and R2 and the conjugation to the NIR fluorophore IRDye 800CW were done as described previously [15–17].

Cell Lines

Two human cancer cell lines were used: FaDu-luc2 (human hypopharyngeal squamous cell carcinoma) and OSC-19-luc2-Cgfp (metastatic oral squamous cell carcinoma). Both were cultured as previously described [1, 14].

Camera Characterization In Vitro

Calibration of Camera System

Concentration series of both NIR fluorophores were used to estimate the concentration-dependent sensitivity. ICG was dissolved in human serum albumin (HSA) in concentrations from 1 mM to 100 fM. HSA without ICG served as a control. IRDye 800CW was dissolved in PBS in concentrations of 1 μM to 100 fM. PBS without IRDye 800CW served as a control. One hundred microliters of each concentration was added to a 96-well plate and experiments were performed in duplicate. All series were imaged using both Pearl and the Artemis (with exposure times of 60 ms, to ensure real-time imaging).

Cell Experiments

FaDu-luc2 cells were cultured in T75 culture flasks until subconfluence. After washing with binding medium (MEM supplemented with 25 mM Hepes and 1 % BSA, at pH 7.2), 20 ml of binding medium with 50 nM 7D12-800CW was added. Cells were incubated in the dark, for 2 hours in a humidified incubator at 37 °C and 5 % CO_2. Cells were harvested with a solution of 10 % trypsin in PBS. Subsequently, cells were washed in medium and adjusted to a suspension containing 2×10^6 cells. This suspension was diluted ten times in a 1:2 ratio in medium and aliquoted in 500-μl tubes. Tubes were centrifuged with 13,000 rates per minute, and after the aspiration of medium, cell pellets were imaged with the Pearl and Artemis camera system. After imaging, cells were resuspended in 50 μl of PBS containing 2 μl of Dluciferin solution (Syncem, Inc. Elk Grove Village, IL) followed by bioluminescence imaging (BLI) using the IVIS Spectrum imaging system (Caliper Life Sciences). Quantification of the BLI signal was performed through

standardized regions of interest using Living Image software (Caliper Life Sciences). The experiment was performed in duplicate and cells incubated with medium served as a negative control [18]. The same dilutions of cells were made without incubation of 7D12-800CW to correlate the BLI signal to the number of cells (Fig. 2e).

Camera Characterization In Vivo

Animal Models

Animal experiments were performed in female nude Balb/c mice (Charles River laboratories, l'Arbresle, France) aged 4–6 weeks. Mice were housed in individually ventilated cages and provided with food and sterilized water ad libitum. During the experiments, general health was monitored by weight measurements and tongue inspections. Imaging procedures were performed under isoflurane gas anesthesia (5 % induction and 2 % maintenance). The local animal welfare committee of the Leiden University Medical Center approved the animal experiments. In order to induce subcutaneous xenografts of hypopharyngeal squamous cell carcinomas, mice were inoculated at four spots on the back with 1, 2, 3, and 4×10^{6} FaDu-luc2 cells, diluted in 50 µl PBS. Tumour growth was monitored twice a week with BLI. At day 10, mice were randomly allocated to injection with 7D12-800CW or R2-800CW. Orthotopic tongue tumours were induced in the tip of the tongue through a submucosal injection of 40,000 OSC-19-luc2-cGFP cells, diluted in 10 µl phosphate-buffered saline. Twice a week, mice body weight was monitored, tongues were inspected, and BLI was measured. At day 20, mice were randomly allocated to injection of 7D12-800CW or R2-800CW. BLI signals served as a control for the tumour specificity of the probe.

Sentinel Lymph Node Detection Using ICG

Precontrast images were taken with the Artemis and Pearl imaging systems to obtain background signal intensities of the tissue of interest. The Artemis was configured to image in real time (exposure time of 40 ms). After positioning of the mice (n=4), 10 µl of 100 µM ICG and HSA was injected submucosally in the tip of the tongue. NIR fluorescence imaging of ICG was performed at 0, 5, 10, 15, and 20 min after injection with both the Pearl and Artemis imaging systems. After 20 min, the skin of the cervical region was removed and images were taken. Subsequently, cervical lymph nodes were removed under NIR fluorescence guidance of the Artemis imaging system.

Tumour-Specific Imaging Using 7D12-800CW

FaDu-luc2 mice were randomly allocated to the intravenous injection of 7D12-800CW (3.2 nmol, n=4) or R2-800CW (3.0 nmol, n=3). After an incubation of 24 h, imaging was performed using both imaging systems. Tumours of mice injected with 7D12-800CW were excised with direct

guidance of the real-time fluorescence signal of the Artemis (exposure time 60 ms). All excised tumours were imaged ex vivo with both imaging systems, and tumour volume was determined by measuring the width (W), length (L), and height (H) of each tumour using a digital caliper. Tumour volume was calculated by using the ellipsoid volume formula $\pi/6 \times L \times W \times H$ [19]. Four tumours of mice injected with 7D12-800CW were cut in half and subsequently divided into halves until submillimeter tumour parts were obtained after which NIR fluorescence images were acquired. Muscle tissue was used as a control. When OSC-19-luc2-cGFP tumours were visible by the human eye and BLI signal ranged between 5×10^9 and 1×10^{10} relative light units (RLU), 7D12-800CW (3.2 nmol, n=3) or R2-800CW (3.0 nmol, n=3) was intravenously injected. Whole body fluorescence imaging with the Pearl and Artemis was performed after 24 h of incubation. Subsequently, all tongue tumours were resected under direct fluorescence guidance of the Artemis camera system.

Histology and Fluorescence Microscopy

The resected hypopharyngeal squamous cell carcinomas and tongue tumours were cut in two, one half was snap frozen in isopentane and stored at -80 °C. The other half was fixed in formalin overnight and embedded in paraffin. Frozen or paraffin tissue sections of 10µm were air-dried, and fluorescence imaging was performed using the Odyssey (LI-COR) to confirm tumour specificity of 7D12-800CW. Histologic sections were stained with standard hematoxylin–eosin stain (HE). The presence of OSC-19-luc2-cGFP and FaDu-luc2 cells was confirmed by staining the sections with antihuman wide spectrum cytokeratin staining (Abcam Inc., Cambridge, MA, USA).

Human Liver Metastases

Three patients with suspected colorectal liver metastases, based on a preoperative four-phase CT scan (Aquilion 64; Toshiba, Tokyo, Japan) of the thorax and abdomen, who were planned to undergo surgery with curative intent, were included. Exclusion criteria were pregnancy, lactation, or an allergy to iodine, shellfish, or ICG. Patients received 10 mg of ICG, diluted in 4 ml sterile water, as an intravenous bolus at 24 h prior to surgery. After exploration, the liver was first visually inspected and palpated then intraoperative ultrasound imaging was performed to locate the liver metastases. Subsequently, all liver segments were imaged using the Artemis imaging system. Patients were provided with informed consent, and the study was approved by the Local Medical Ethics Committee of the Leiden University Medical Center, Leiden, The Netherlands and was performed in accordance with the ethical standards of the Helsinki Declaration of 1975.

Statistical Analysis

All acquired images were analyzed by annotating regions of interest (ROI). During in vitro acquisitions, the background ROI was positioned at a location of homogeneous intensity without tissue. For the in vivo acquisitions, one background ROI was taken on the animal, next to the structures of interest. Furthermore, a ROI was drawn on a dark area outside the animal or sample for camera background correction. In each acquisition, mean foreground μ_f and background μ_b signals were measured within the ROIs. The camera noise σ_n was estimated as the standard deviation with the annotated homogeneous areas. Each acquisition is characterized by three measures: 1. Signal-to-noise ratio (SNR): μ_f / σ_n. This indicates how well signals of a particular intensity can be detected. 2. Contrast-to-noise ratio (CNR): $(\mu_f - \mu_b)/\sigma_n$. This indicates how well different regions can be identified. 3. Signal-to-background ratio (SBR): μ_f/μ_b. This measure is often reported in the literature to evaluate (tumour) marker specificity. In this work, CNR is mainly used to evaluate the Artemis camera system. This is different than the SBR used in many probebinding studies. While SBR is essentially a measure for the uptake of a probe, it does not measure how well a camera system is capable of capturing the contrast between tissues with different probe uptake. For the latter, it is essential to take the camera noise into account. A tumour with a high SBR may be almost invisible when imaged with a camera with high noise levels, while a very low SBR may be discernible very well when camera noise is low. Measurements with minimal CNR=2 were considered reliable. This corresponds to a limit of detection (LOD) defined as the control or background intensity plus two times the noise level. The SNR, CNR, and SBR for Pearl and Artemis were subjected to a Wilcoxon rank-sum test or U-test for non-normally distributed data.

Results

Camera Characterization In Vitro

Calibration of Camera System

Acquisitions of 96-well plates with concentration series of ICG and 800CW were compared between the Artemis and Pearl camera systems based on SNR (Fig. 2a, c) and SBR (Fig. 2b, d). CNR is in this experiment very similar to SNR. The SNR and SBR curves for ICG from the Pearl show an increase in SNR and SBR for increasing concentrations up to 10 μM. After this, peak quenching takes place, causing a decrease in intensity. The SNR and SBR for the Artemis peak earlier. This is, however, due to sensor saturation (i.e., values of 255, the high end of the dynamic range) for the fixed exposure time of 60 ms. For shorter exposure times, higher concentrations could be imaged within the dynamic range. For the lower concentrations, the SNR and SBR curves flatten off at a higher concentration than for the Pearl, indicating 10^{-2} μM as the lower boundary for reliable ICG detection. The SBR for low concentrations of ICG for the Artemis is about 100 instead of 1. This is due to bright reflections of the excitation light in the well plates that penetrates through the emission filter. These reflections were visible in wells with low concentrations of fluorophore as well as the control well and showed the eight bright spots that corresponded to the fiber ends in the illumination ring. The plot in Fig. 2a shows that within the dynamic range of the Artemis at 60 ms exposure time, SNRs are comparable between Artemis and Pearl. Pvalues for the U-test were P=0.75 and P=0.09, respectively. Figure 2c, d shows similar results for the 800CW concentration series as for the ICG concentration series. Bright reflections of the excitation light again cause high SNRs and SBRs for low 800CW concentrations, while the sensor was saturated for 10 μM of 800CW. The minimum detectable concentration of 800CW is again 10^{-2} μM. However, as for the ICG, the excitation light reflections may prevent detection of lower concentrations. P-values for the U-test were P=0.04 (SNR) and P=0.01 (SBR). These significant differences can be attributed to both a smaller dynamic range of the Artemis, as well as a higher minimally detectable concentration.
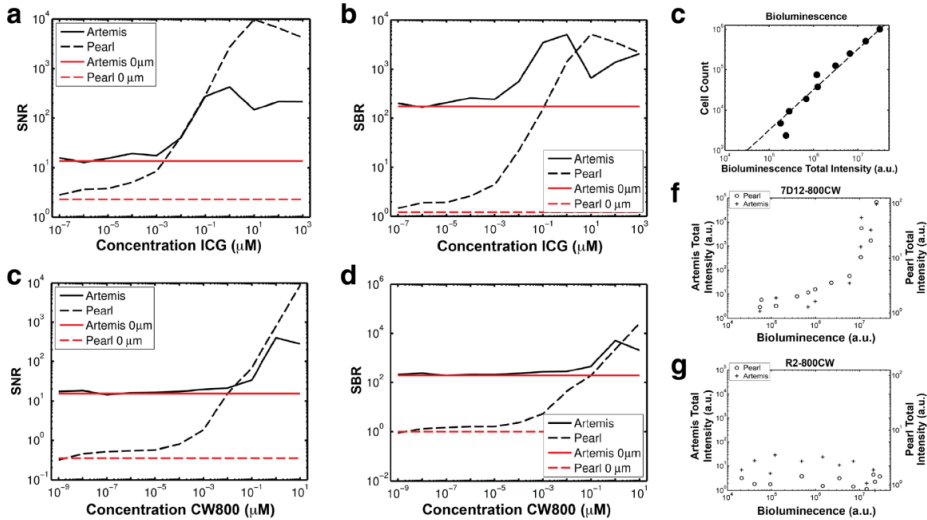
Figure 2 - Calibration of the Artemis system and minimal detection limit of hypopharyngeal tumour cells: a, c Signal-to-noise (SNR) and b, d signal-to-background (SBR) ratios of concentration ranges of a, b ICG and c, d CW800 imaged in 96-well plates. Measurements from control wells with 0 µM ICG and CW800 are shown as red horizontal lines. e Bioluminescence was correlated to the number of FaDu-luc2 cells. f FaDu-luc2 cells were incubated with the EGFR-specific nanobody 7D12-800CW and g non-specific nanobody R2-800CW for 2 hours. After incubation, cells were washed twice and cell pellets containing different amount of cells were imaged using the Artemis and Pearl imaging system.

Cell Line Experiments

Flow cytometry showed EGFR expression of FaDu-luc2 cells (data not shown). The experiment to determine the minimal detection limit of FaDu-luc2 cells was performed using the EGFR-specific nanobody 7D12-800CW and the non-EGFR-specific R2- 800CW as a control. The total intensities of fluorescence measured for 7D12-800CW show agreement between Artemis and Pearl (Fig. 2f). Also, although clearly not a linear relationship, both cameras measure an increased amount of total fluorescence for a larger number of cells, as indicated by a higher bioluminescent signal. For the nonspecific R2-800CW, both cameras show no relation between bioluminescence and total intensity (Fig. 2g). The Artemis total intensities were higher for the R2-800CW experiment than for the low bioluminescent cell pellets with 7D12-800CW, while Pearl total intensities are comparable. We attribute this (small) variation to variations in sample placement under the Artemis. The minimum amount of cells that could be detected with the Artemis was extrapolated from the bioluminescence signal (Fig. 2e) and proved to be approximately 2×10^5 cells and 4×10^4 cells using the Artemis and Pearl, respectively.

Camera Characterization In Vivo

Sentinel Lymph Node Detection

Using ICG Using both the Artemis and Pearl camera, seven SLNs were detected in vivo in four mice. All lymph nodes were visible within 10 min after injection. Massaging the injection spot could have expedited this process. After removal of the skin, all eight lymph nodes were visible. The initially invisible lymph node was covered by strongly absorbing tissue and was visible after removal of skin. Figure 3 shows NIR fluorescence images acquired with Artemis and Pearl after ICG injection in the tongue, as well as overlays with reflectance images. The distribution of ICG in the lymph node, as well as the lymphatic ducts, is clearly visible using both camera systems. CNRs are computed for each lymph node, where the background ROI is positioned between the front paws of the mouse. The mean CNR (Pearl 833, Artemis 225) and standard deviations (Pearl 584, Artemis 96) for the seven detected lymph nodes with closed skin are shown in Fig. 3. Signal-to-background ratios were 126 (standard deviation (SD) 59) for the Pearl and 1,260 (SD 691) for the Artemis. This difference was mainly due to low background signals, where the Pearl background was relatively higher. SBR is an unreliable measure when the background signal is low. The U-test P-values showed significant differences for both CNR (P=0.010) and SBR (PG0.001).
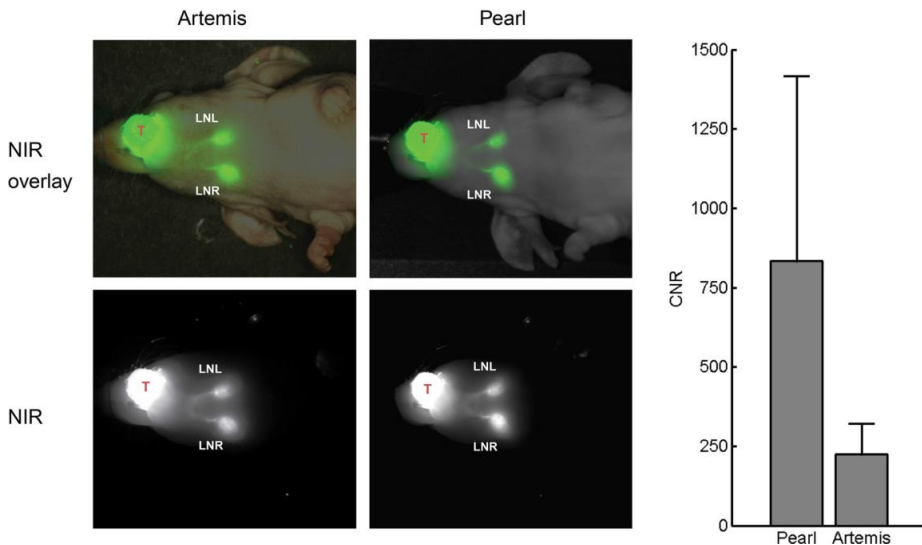

Figure 3 - Sentinel lymph node detection using indocyanine green: Cervical sentinel lymph nodes could clearly be identified after injection of 100 μM ICG (10 μl) in the tongue (T) using both the Artemis and Pearl imaging system within 10 min after injection. Contrast-to-noise ratios (CNR) of the Artemis and Pearl are shown. LNL = lymph node left; LNR = lymph node right.

Tumour-Specific Imaging Using 7D12-800CW, Tongue Tumour Model

Orthotopic EGFR-overexpressing (data not shown) OSC-19-luc2-cGFP tongue tumours were clearly identifiable using both Artemis and Pearl after injection of 7D12-800CW (Fig. 4). Bioluminescence confirmed the location of the tumour, and there was colocalization between fluorescence and bioluminescence signals. No fluorescence was observed with the control nanobody R2-800CW. CNRs for both Artemis and Pearl are 101 (SD 55) and 143 (SD 15) for 7D12-800CW, while a low fluorescence signal was detected for R2-800CW with CNRs 12 (18) and 18 (25) for Artemis and Pearl, respectively. The larger standard deviation in CNR of 7D12-800CW for the Artemis than for the Pearl could be attributed to inhomogeneous lighting conditions in the Artemis camera setup. In an open camera setting, a lower amount of excitation light tends to reach the tissue of interest, leading to excitation of a lower amount of fluorophore resulting in a lower excitation fluorescence signal that can be detected [5]. The large standard deviation is reflected in the differences in CNR of 7D12-800CW and R2-800CW between the Artemis and Pearl with P=0.7 and P=0.4, respectively. The CNR between 7D12-800CW and R2-800CW was statistically significantly different for the Pearl (P=0.017) but not for the Artemis (P=0.13). The larger standard deviation in CNR of 7D12-800CW for the Artemis could partly be attributed to inhomogeneous lighting conditions in the Artemis camera setup. Furthermore, due to short acquisition times in an intraoperative imaging setting, a smaller amount of fluorescent photons are captured per acquired frame, leading to noisier images. Lastly, the Artemis system does not have a cooled camera,

increasing sensitivity to thermal noise.
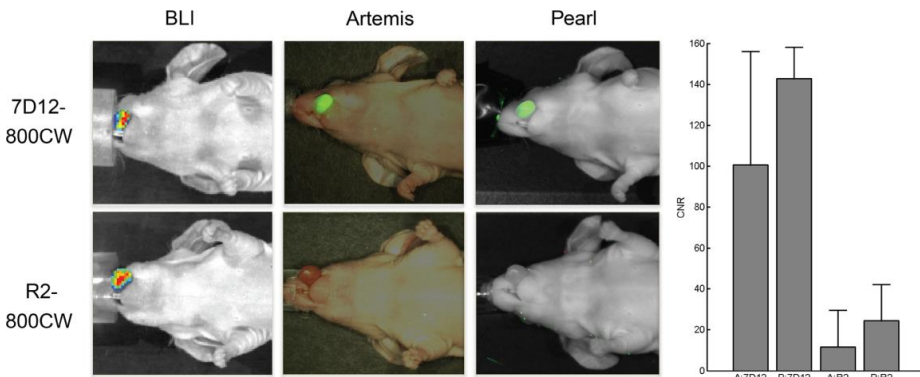
Figure 4 - Near-infrared fluorescence delineation of orthotopic tongue tumours: OSC-19-luc2-cGFP tongue tumours could clearly be identified after injection of the epidermal growth factor receptor-specific nanobody 7D12-800CW (50 µg) using both the Artemis and Pearl. No fluorescence could be observed after injection of 50 µg of control nanobody R2-800CW. Contrast-to-noise ratios (CNR) calculated by using the Artemis and Pearl are shown. A = Artemis; P = Pearl.

Tumour-Specific Imaging Using 7D12-800CW, Hypopharyngeal Tumour Model

Subcutaneous FaDu-luc2 tumours could be clearly imaged with both the Artemis and Pearl camera after injection of 7D12-800CW. Histology confirmed tumour specificity of 7D12-800CW (Supplementary Fig. 1). Figure 5 shows the bioluminescent signal (a) that confirms the tumour presence and overlays from the Artemis (b) and Pearl (c). The Artemis overlay shows a high signal between the kidneys, while the Pearl overlay does not show this signal. In contrast to the Artemis, for the Pearl, the overlay can be adjusted to show that the tumours fluoresce stronger than the center of the back of the mouse where scattering increases fluorescence signal next to the kidneys.
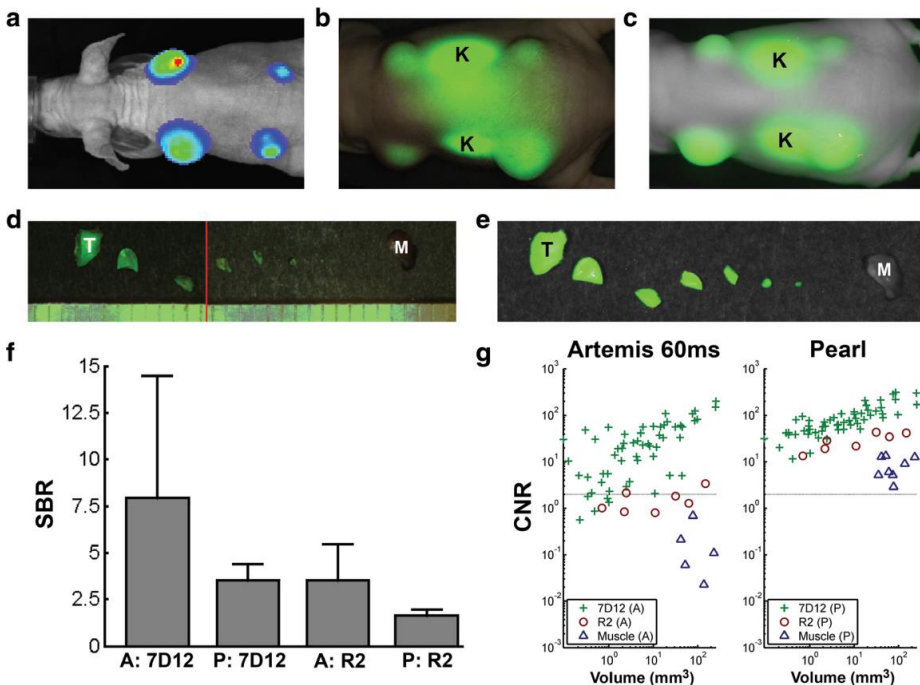
Figure 5 - Tumour detection limit: Hypopharyngeal FaDu-luc2 tumours of different sizes visualized using bioluminescence imaged by a the IVIS Spectrum system could clearly be delineated in vivo using both b the Artemis and c Pearl. fIn vivo tumour signal-tobackground ratios (SBR) were calculated. Twenty-four hours after injection of 7D12-800CW and R2-800CW, all tumours were repeatedly halved until submillimeter size. Tumour pieces were measured using the d Artemis and e Pearl. g Contrast-to-noise ratios (CNR) were plotted against the volume of the tumour pieces. Ruler lines denote millimeters. K = kidney; T = tumour; M = muscle; A = Artemis; P = Pearl.

For the Artemis, the large spatial variation in illumination intensity caused a non-significant difference between SBRs for tumours with 7D12-800CW and R2-800CW (P=0.09), while the difference for the Pearl was significant (PG0.001) (Fig. 5f). Figure 5d, e show an example of a

halved tumour with 7D12-800CW imaged with both Artemis (d) and Pearl (e). In the Artemis overlay, part of a ruler is visible. For each tumour piece, the volume is estimated and the relation between CNR and volume is shown in Fig. 5g. Muscle tissue was included as an additional control. A clear relation between tumour volume and CNR is visible for 7D12-800CW for both Artemis and Pearl, where the Pearl in general showed a higher CNR and the Artemis a larger spread. The CNRs were significantly different for both 7D12-800CW (P≤0.001) and R2-800CW (P≤0.001). Fluorescence of tumour pieces with a CNR below 2 is practically invisible by eye (depicted by the gray horizontal line). Five tumour pieces were below this line for the Artemis, while these tumour pieces were hardly visible with the Pearl. The tumour pieces missed by the Artemis had an average size in the order ≤1 mm3 . Although smaller pieces in general had a lower CNR, a size of 1 mm3 should be considered as the lower boundary, as the majority of tumour pieces of this size were visible by both cameras. Contrast-to-noise ratios are significantly different between specific and non-specific probes for both Artemis (P≤0.001) and Pearl (P≤0.001).

Human Liver Imaging

Three patients with liver metastases were imaged using the Artemis camera system during surgery. All three patients had metastases from colon tumours near or at the liver surface. Figure 6 illustrates the combination of images such as presented to the surgeon: visible light (Fig. 6a), NIR fluorescence signal (Fig. 6b), and a real-time overlay (Fig. 6c). The metastases in this example are recognizable due to their fluorescent rim. Benign lesions could be differentiated from malignant lesions by a lack of this fluorescent rim around the tumour, as was confirmed by pathologic analysis [20]. A total of six lesions with fluorescent rim were identified during surgery with NIR fluorescence, and all showed to be malignant after pathologic evaluation. No false-negative nodules were found. One lesion in segment 6 of the liver was initially missed by eye but was clearly visualized using the Artemis system.
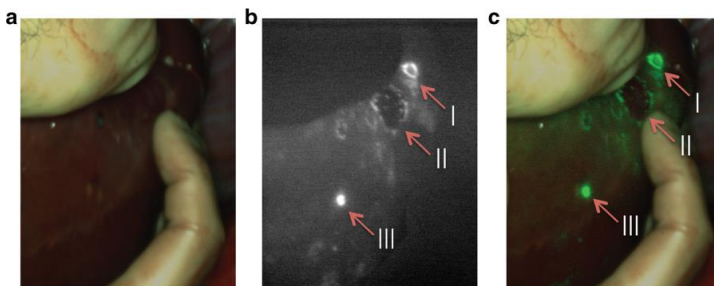

Figure 6 - Near-infrared fluorescence imaging of colorectal liver metastases: 24 h after injection of 10 mg indocyanine green, colorectal liver metastases could clearly be identified by a rim around the tumour (I and II). Benign lesion (III) could be identified by fluorescence without the rim. Images are depicted in a visible light, b NIR fluorescence signal, and c a real-time overlay.

Discussion

Fluorescence-guided surgery is a high potential imaging technique that provides surgeons with real-time information about vital structures, tumour margins, and regional disseminated disease. By real-time feedback of tumour margins and vital structures, tumours could be radically resected while healthy tissue can be preserved. A dedicated NIR fluorescence camera is vital as NIR light is invisible to the human eye. In this study, we evaluated the Artemis NIR fluorescence camera system. Its performance in detecting ICG and IRDye 800CW was assessed and was put in perspective by comparison with the preclinical Pearl imaging system. Furthermore, we demonstrated its utility in detecting and guiding resection of cervical SLNs using ICG, as well as primary tongue tumours and hypopharyngeal tumours using an EGFR-targeting nanobody conjugated to IRDye 800CW. Next, first in-human clinical data using the Artemis was shown by the detection of liver metastases using ICG. The efficacy of NIRF camera systems and the final realtime fluorescence imaging results are dependent on multiple factors. These factors include the interplay between the type of probe or fluorophore used, probe concentration injected, concentration of probe at the location of interest, tumour size, optical properties, and the camera system. The Artemis was evaluated for the use in two frequently used FGS procedures because there is a major difference in dye and in concentration of dye at the site of interest between both procedures. The near-tumoural injected ICG in SLN mapping is highly concentrated compared to the intravenously injected conjugate of IRDye 800CW and a targeting moiety in tumourspecific imaging. Furthermore, ICG and IRDye 800CW differ in excitation spectra, emission spectra, and quantum yield. In general, imaging results are more adequate when a fluorophore has a high quantum yield and there is a high concentration at the site of interest. The second variable that intervenes with the efficacy of a NIRF camera is the injected concentration of probes. For the experiments in vivo, the optimal concentration was chosen. The optimal concentration of ICG was extrapolated from the ICG dilution series in vitro. In the choice of the injected dose in vivo (100 µM), dilution of ICG after intratumoural injection was taken into consideration. Concentrations of 7D12-800CW (50 µM) and R2-800CW (µM) were chosen from earlier studies [14]. Next, the size of the tumour determines the imaging results. We assessed the detection limit of a FaDu-luc2 tumour nodule size that could be detected using the nanobody 7D12-800CW. For that, tumour pieces were subdivided into halves until submillimeter size. Since 7D12-800CW is homogenously distributed throughout the tumour [13, 14] (Supplementary Fig. 1), subdivision was justified. A size of 1 mm3 could be considered as the lower boundary of detection, as the majority of tumour pieces of this size were visible. A tumour size of 1 mm3 is considered to contain around three million tumour cells. Using this setup, lower amount of cells that could be clinically significant would not be detected. Obviously, a detection limit is dependent on multiple factors like the probe that is used, the observer, the concentration and

pharmacokinetics of the probe, the target that is chosen, and the amount of receptors in the tissue of interest. Furthermore, in vivo, the optical properties of the tissue of interest and overlaying tissue determine in a great extent what size of tumour tissue can be detected. Again, results were compared to the Pearl to validate the Artemis data. Despite successful utility of the Artemis in our preclinical experiments and the successful utility of the Artemis in a clinical setting, several improvements can be made to increase the applicability and imaging reliability. First, the illumination intensity as projected by the Artemis sharply decreases near the edge of the imaged field. This causes the apparent fluorescence intensity to have a strong dependence on the location in the image. In the experiment using cell lines in vitro, we showed that both the Artemis and Pearl were able to image the same relationship between number of cells and intensity for the tumour-specific 7D12-800CW probe. For the non-specific R2-800CW, both cameras showed a flat profile. The Artemis signal was less consistent than that of the Pearl for low cell counts with 7D12-800CW and for the cells with R2-800CW. This can be attributed to a less inhomogeneous illumination of the sample than for the Pearl. Precise positioning of the sample when comparing fluorescence intensities is thus essential for the Artemis while less critical for the Pearl. This spatial illumination variation is also visible in Fig. 5f, as a large standard deviation on the SBRs for the in vivo tumours resulting in a non-significant difference between SBRs for tumours with 7D12-800CW and R2-800CW (P=0.09). Second, a possible improvement lies in filtering the excitation light. The filters that are intended to block the excitation light do not block most specular reflections. If available, filters with a higher optical density would solve this problem or cross-polarization could be used. Results of the impairment in blocking reflections can be seen in the baseline experiment for evaluating the sensitivity of the Artemis system that consisted of measuring the signal from fluorophores in concentration series. For the real-time setting of 60 ms exposure time per image, the Artemis was able to measure concentrations of both ICG and 800CW of $10-2$ µM and higher. The control Pearl camera showed that fluorophores were present in wells with lower concentrations. This lower boundary was not solely due to sensitivity limits of the Artemis camera but also due to reflected excitation light that was not sufficiently filtered out. For concentrations smaller than $10-2$ µM, these reflections were stronger than the fluorescence signal. Third, the current camera has a rather low depth of field. Since the camera does not have an autofocus mechanism, this requires frequent adjustment of the focus. An additional problem with the current Artemis camera systems is a focal length difference between the visible light and near-infrared channels. This requires changing the focus between a sharp visible light and near-infrared fluorescence image at close imaging distances (G15 cm). A last possible improvement is the dynamic range of the camera. This lack of range is visible in the images with concentration ranges; only a few concentrations are between the lower detection boundary and the saturation boundary. Although such a wide variation in concentrations is not to be expected in clinical applications and overexposure is not a

big issue, large variations in working distance during surgery also lead to large intensity variations of the fluorescence signal. The visible light channel also tended to be overexposed, even at the least sensitive camera settings.

Conclusion

NIR fluorescence-guided surgery could aid surgeons in real-time visualization of tumours, SLNs, and vital structures to ensure a radical resection, adequate staging, and minimize damage to normal tissue. In this study, we evaluated the Artemis system and assessed the minimal detection limit of tumour-specific imaging using an EGFR-targeting nanobody. Furthermore, we demonstrated the possibility of fluorescence-guided resection of head and neck tumours and sentinel lymph nodes. At last, we demonstrated the use of the Artemis system for the detection and fluorescence-guided resection of liver metastases in a first in-human clinical trial. Based on this study, although improvements can be made, we think the Artemis system has demonstrated its utility in fluorescence-guided cancer surgery.

6

Acknowledgments.

Conflict of Interest.

The authors report no conflicts of interest

6

References

1. Keereweer S, Mol IM, Vahrmeijer AL et al (2012) Dual wavelength tumour targeting for detection of hypopharyngeal cancer using nearinfrared optical imaging in an animal model. Intl J Cancer 131:1633–1640

2. Vahrmeijer AL, Hutteman M, Van Der Vorst JR et al (2013) Imageguided cancer surgery using near-infrared fluorescence. Nat Rev Clin Oncol 10:507–518

3. Frangioni JV (2008) New technologies for human cancer imaging. J Clin Oncol 26:4012–4021

4. Adams KE, Ke SK et al (2007) Comparison of visible and near-infrared wavelength-excitable fluorescent dyes for molecular imaging of cancer. J Biomed Opt 12:024017

5. Keereweer S, Van Driel PB, Snoeks TJ et al (2013) Optical imageguided cancer surgery: challenges and limitations. Clin Cancer Res 19:3745–3754

6. Gioux S, Choi HS, Frangioni JV (2010) Image-guided surgery using invisible near-infrared light: fundamentals of clinical translation. Mol Imaging 9:237–255

7. Schaafsma BE, Mieog JS, Hutteman M et al (2011) The clinical use of indocyanine green as a near-infrared fluorescent contrast agent for image-guided oncologic surgery. J Surg Oncol 104:323–332

8. Mcmahon J, O'Brien CJ, Pathak I et al (2003) Influence of condition of surgical margins on local recurrence and disease-specific survival in oral and oropharyngeal cancer. Brit J Oral Maxillofac Surg 41:224–231

9. Huston TL, Simmons RM (2005) Locally recurrent breast cancer after conservation therapy. Am J Surg 189:229–235

1. Meric F, Mirza NQ, Vlastos G et al (2003) Positive surgical margins and ipsilateral breast tumour recurrence predict diseasespecific survival after breast-conserving therapy. Cancer 97:926–933

10. Rusthoven KE, Raben D, Song JI et al (2010) Survival and patterns of relapse in patients with oral tongue cancer. J Oral Maxillofac Surg 68:584–589

11. Schulze T, Bembenek A, Schlag PM (2004) Sentinel lymph node biopsy progress in surgical treatment of cancer. Arch Surg 389:532–550

12. Oliveira S, Van Dongen GA, Stigter-Van Walsum M et al (2012) Rapid visualization of human tumour xenografts through optical imaging with a near-infrared fluorescent anti-epidermal growth factor receptor nanobody. Mol Imaging 11:33–46

13. Van Driel PB, Van Der Vorst JR, Verbeek FP et al (2013) Intraoperative fluorescence delineation of head and neck cancer with a fluorescent anti-epidermal growth factor receptor nanobody. Intl J Canc

14. Dolk E, Van Vliet C, Perez JM et al (2005) Induced refolding of a temperature denatured llama heavy-chain antibody fragment by its antigen. Proteins 59:555–564

15. Gainkam LO, Huang L, Caveliers V et al (2008) Comparison of the biodistribution and tumour targeting of two 99mTc-labeled anti-EGFR nanobodies in mice, using pinhole SPECT/micro-CT. J Nucl Med: Off Publ Soc Nucl Med 49:788–795

16. Roovers RC, Laeremans T, Huang L et al (2007) Efficient inhibition of EGFR signaling and of tumour growth by antagonistic anti-EFGR nanobodies. Cancer Immunol Immunother: CII 56:303–317

17. Mieog JS, Vahrmeijer AL, Hutteman M et al (2010) Novel intraoperative near-infrared fluorescence camera system for optical imageguided cancer surgery. Mol Imaging 9:223–231

18. TomaykoMM, Reynolds CP (1989) Determination of subcutaneous tumour size in athymic (nude) mice. Cancer Chemother Pharmacol 24:148–154

19. Van Der Vorst JR, Schaafsma BE, Hutteman M et al (2013) Nearinfrared fluorescence-guided resection of colorectal liver metastases. Cancer 119:3411–3418

6

III

Future of fluorescence-guided therapy in oncology, theranostics
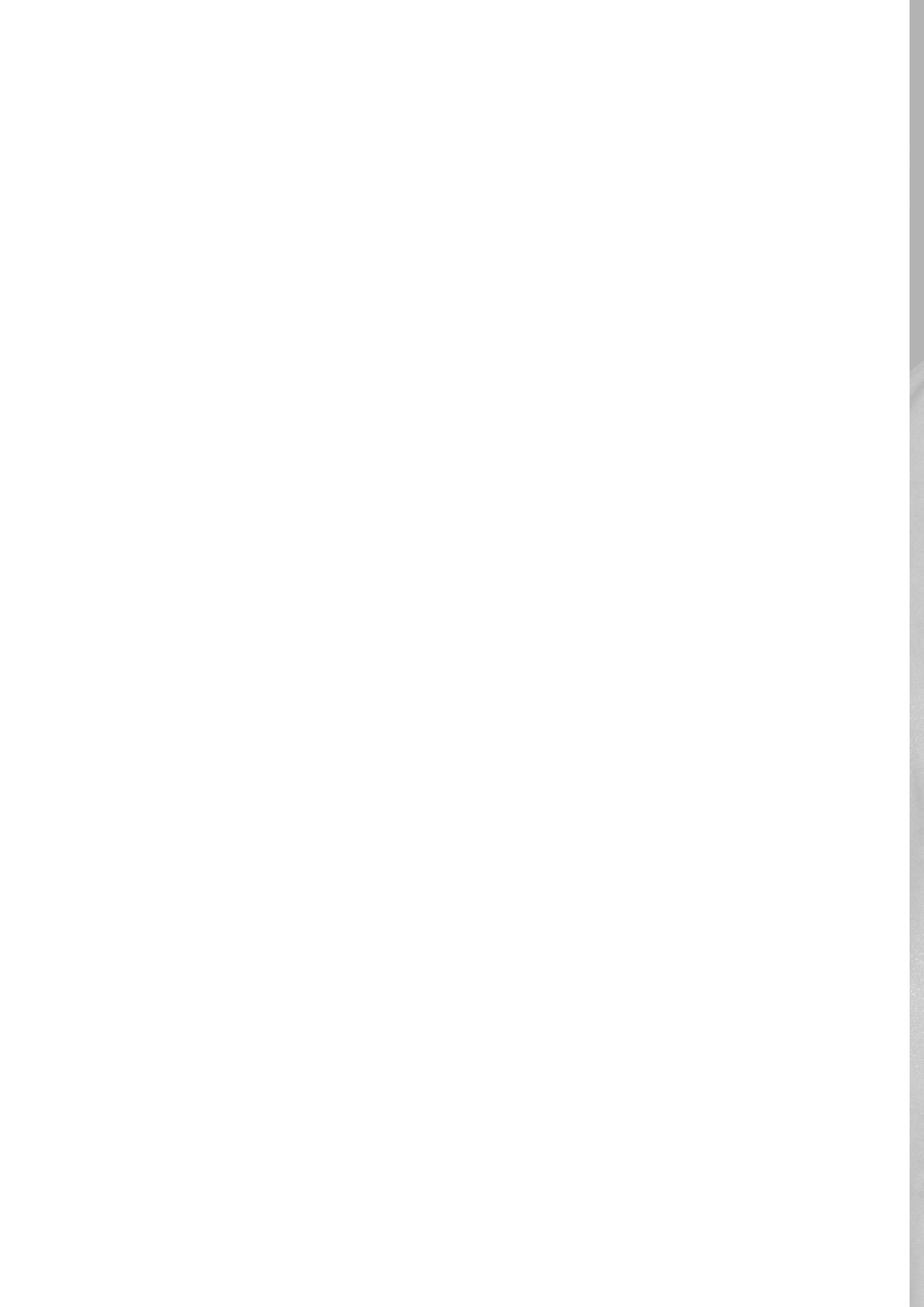
CHAPTER 7

Shifting focus in fluorescence-guided surgery

Stijn Keereweer[1,2], Pieter B.A.A. van Driel[2], Dominic J. Robinson[3], Clemens W.G.M. Löwik[1]

1. Department of Molecular Imaging, Leiden University Medical Center, Leiden, The Netherlands.
2. Department of Otorhinolaryngology Head and Neck Surgery, Erasmus Medical Center, Rotterdam, The Netherlands.
3. Center for Optical Diagnostics and Therapy, Postgraduate School of Molecular Medicine, Department of Dermatology, Erasmus Medical Center, Rotterdam, The Netherlands

ABSTRACT

Cancer patients could benefit from a surgical procedure that helps the surgeon to determine adequate tumour resection margins. Systemic injection of tumour-specific fluorescence agents with subsequent intraoperative optical imaging can guide the surgeon in this process. However, tumour heterogeneity hampers tumour-specific targeting. In addition, determination of adequate resection margins can be very challenging due to invasive tumour strands that are difficult to resolve and because of the confounding effect of variations in tissue optical properties in the surgical margin. We provide an overview of the "classic approach" of imaging tumour-specific targets or tumour-associated pathophysiological processes, and explain the limitations of these targeting strategies. It is proposed that problems of tumour heterogeneity can theoretically be circumvented by shifting focus of tumour targeting towards the follicle-stimulating hormone receptor (FSHR). Furthermore, we discuss why objective determination of resection margins is required to improve resection of the invasive strands, a goal that may be achieved by targeting the FSHR. When invasive strands would nevertheless extend beyond such a standardized resection margin, we suggest that adjuvant photodynamic therapy would be a very suitable therapeutic regimen. Finally, we describe how point optical spectroscopy can be used to scrutinize suspect tissue that is difficult to differentiate from normal tissue by measuring the local tissue optical properties to recover a local intrinsic fluorescence measurement.

Introduction

Despite the technological advancements of preoperative imaging techniques, clinical outcome of cancer surgery for most cancer types has only gradually improved over the last 3 decades. Introduction of real-time optical imaging could revolutionize the intraoperative approach to cure cancer by providing the surgeon with direct feedback on histopathologic markers. This intraoperative tissue characterization could improve surgical outcome, local control, and disease-free survival. In addition, it enables better preservation of healthy tissue, which is critical to postoperative functionality and quality of life. In optical imaging, tumour-specific fluorescent agents can be systemically injected to guide the surgeon in adequately determining resection margins. Although feasibility of intraoperative tumour-specific nearinfrared (NIR) fluorescence imaging was demonstrated in humans [1], cancer targeting with high sensitivity and specificity remains challenging. The continuous quest for a universal tumour-specific target has not yet been successful and the growing insight in cancer invasion is increasingly pointing toward multifactorial processes [2, 3]. There are many general aspects involved in making a tumour-specific targeting agent suitable for in vivo use, including high affinity of the agent with low non-specific binding, abundance of the target receptors or epitopes [4], biodistribution of the agent to the target, sufficient contact time with the target for binding to occur, retaining of the agent while non-bound agents are cleared from the circulation and toxicity issues [5]. These aspects have been extensively reviewed elsewhere [5–8]. Although an extensive amount of work is still needed to consider these issues, we anticipate that the next generations of fluorescent agent design will continue to improve these aspects. However, we have identified the three fundamental challenges that will remain to contribute to the conundrum of optical image-guided cancer surgery: dealing with tumour heterogeneity, obtaining adequate resection margins that include invasive tumour strands, and managing the confounding effects of differences and variations in optical tissue properties (Fig. 1). This review aims to explain the limitations of the "classic approach" of (combined) imaging of tumour-specific cell-surface receptors and tumour-associated pathophysiological processes. Next, we suggest that shifting focus to the follicle-stimulating hormone receptor (FSHR) could theoretically circumvent the problems of tumour heterogeneity. Furthermore, we advocate the need for objective intraoperative determination of resection margins to improve resection of the invasive strands and explain how this may be achieved by targeting the FSHR. If invasive strands would extend beyond the resection margin, we propose that photodynamic therapy (PDT) is the ideal adjuvant therapeutic regimen that is likely to play an increasingly important role in optical image-guided cancer therapy. Finally, the confounding effects of differences in tissue optical properties impede the ability to differentiate between areas of healthy and tumour tissue, particularly in the surgical margin where fluorescent signals can be

lower. We describe how point reflectance and fluorescence spectroscopy using fiber optic probes can be used to overcome these effects.
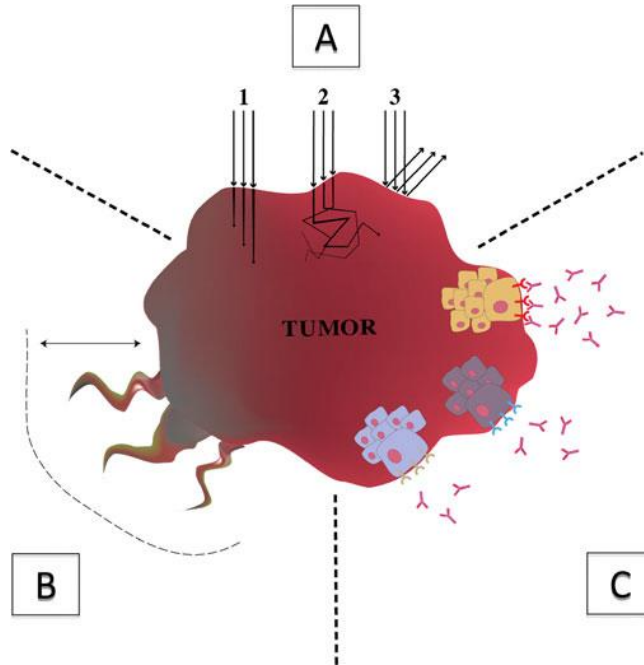
Figure 1; Schematic illustration of the three fundamental problems in optical image-guided cancer surgery. a How to deal with differences in optical properties that influence propagation of light in tissue (1–3): Absorption by tissue components that influences the optical path length (1), scattering by tissue components that influences the spatial distribution of light (2), and specular reflection at the tissue surface (3). b How to obtain adequate resection margins that include invasive tumour strands that extend beyond the (visible) tumour border. c How to cope with tumour heterogeneity that results in variability in expression of surface receptors, hampering target-specific imaging.

Challenges of Tumour-Specific imaging

Imaging Tumour Heterogeneity

The first problem that is currently challenging tumour-specific imaging is tumour heterogeneity. Different populations of tumour cells within a tumour display variable phenotypes such as the ability to metastasize or to survive chemo- or radiotherapy. This intra-tumour phenotypic diversity results from genetic and epigenetic heterogeneity, a consequence of genomic instability combined with high cell turnover, aswell as fromdifferences in the tumour microenvironment [9]. Improved molecular understanding of cancers has resulted in identification of targets for diagnostic and therapeutic interventions. However, the concept of tumour heterogeneity explains why tumour-specific imaging based on these targets is limited in many cases [9, 10].

Invasive Tumour Strands

The second factor that fluorescence-guided tumour resection has to deal with is the problem on how to include invasive tumour strands into the resection margin. Invasive tumour strands are crucial for the development of regional and distant metastasis. Moreover, invasive strands are less sensitive to adjuvant therapy due to adaptive responses to different types of therapy-induced stress inducing tumour cell survival [2]. This reactive resistance to adjuvant therapy emphasizes the importance of radical surgical resection that includes invasive strands [2, 3]. In addition, the pattern of tumour invasion at the invasive front may be indicative for tumour behavior [11]. However, it remains to be determined whether high-risk tumours require greater margin distances than low-risk tumours [12]. In conventional surgery, an extra resection margin around the tumour mass is removed in order to include potential invasive strands and to compensate for inaccurate determination of the tumour border. Because it is practically infeasible to objectively determine a consistent margin, for instance of 1 cm, using a caliper in all dimensions around the tumour, the resection margin is subjectively assessed by the surgeon, resulting in intersurgeon variability [13]. This interferes with standardized oncologic care and hampers complete surgical resection in some cases. Although optical imaging techniques can provide the surgeon with direct feedback on histopathological markers, it is impossible to image individual invasive strands under many circumstances. To detect invasive strands, fluorescent agents would require very high affinity for these thin layers of cancer cells. However, as will be explained below, the influence of differences in background optical properties of tissue and their spatial heterogeneity would regularly prevent detection or detailed imaging. The inability to identify individual invasive strands dictates a new approach to consistently include an objective resection margin into the surgical resection.

Optical Tissue Properties

Finally, tumour-specific imaging and subsequent imageguided surgical resection is strongly influenced by the background tissue optical properties. The basic geometry of optical imaging requires excitation light from an external light source that travels through the imaged tissue and excites the fluorophore inside the tissues [5, 7]. After excitation, the fluorescent light travels back through the tissues and is detected outside the body by a dedicated camera system. The path that these photons travel is influenced by the optical properties of the tissues at the excitation and emission wavelength. Scattering can change the direction of part of the photons and multiple consecutive scatter events will result in diffuse light; a gradual randomization of the propagation direction [5, 7, 14, 15]. Additionally, photons can be absorbed by various components in the tissue. Consequently, fluorescence images will display intensities that are strongly influenced by varying absorption properties of the tissue and the images may be blurred due to the scattering of

light. The problem with targeting invasive tumour strands could be as follows: invasive strands can be very thin, limiting the amount of tumour-specific fluorescent agent that is bound or activated. This results in a relatively low amount of fluorescent photons that are subsequently influenced by scattering and absorption. Imaging of strands that are invading the surrounding tissues will result in blurry images with very low intensity. Various groups have developed imaging systems that incorporate tissue attenuation correction algorithms that have been validated using phantoms [16–18]. Although improved margin delineation and quantification is reported, it is unlikely that such estimations or more sensitive detectors will be able to completely resolve the effects caused by optical properties and autofluorescence in vivo, because of the heterogeneous composition of the tissue and differences in autofluorescence intensity in location and over time [7].

Current Strategies of Tumour-Specific imaging

Imaging The "Classic Approach": Targeting of Tumour-Specific Cell Surface Receptors

Themost often approach employed for tumour-specific targeting is to conjugate a fluorophore to a tumour-specific antibody or peptide targeting a receptor. The limitless replicative potential of tumour cells, a key feature of carcinogenesis, offers useful targets because it is facilitated by increased metabolism, high expression of growth-signalling receptors, and increased tumour angiogenesis to supply sufficient oxygen and nutrients [19]. Many of these hallmarks of cancer have been a target for antibody-derivatives, peptides, or small molecules conjugated to a fluorophore [20]. For instance, promising results have been reported in preclinical experiments that target growth-signalling receptors [1, 21–23]. However, these preclinical models mostly include homogeneous tumours, and antibody-specific targeting is likely to be limited when tumours become increasingly heterogeneous. Moreover, these models are often formed using human xenografts that are targeted by human antibody derivatives, resulting in zero background signal. Sustained angiogenesis has been imaged by targeting integrins; specific cell-surface markers of tumour angiogenesis [24, 25], which results in the imaging of tumour vasculature. Although this strategy could strongly reduce the problem of tumour heterogeneity, studies have shown that these agents are taken up by cancer cells in vitro, improving their tumour-specific fluorescence signal but increasing variability of this signal due to tumour heterogeneity [25]. Moreover, this targeting strategy does not include an objective standardized resection margin, which is required because targeting of angiogenesis will not image strands that are not (yet) supported by new sprouting vessels, such as solid strands that can be found in basal and squamous cell carcinomas [3].

Targeting Tumour-Associated Pathophysiological Processes

To reduce the problem of tumour heterogeneity and find a more universal tumour-specific target, the approach changed from targeting cell surface receptors to targeting tumour-associated pathophysiological processes. The best-known example of such a process is the degradation of the extracellular matrix, which is required for tumour growth andmetastasis. By targeting enzymes that are involved in these general processes, the tumour border is imaged, independent from the type of receptors that are expressed by the cancer cells [19, 21, 26, 27]. Targeting of proteolytic enzymes results in imaging of the invasive tumour front where these enzymes are abundant. Therefore, surgical resection guided by the enzyme-specific fluorescence signal could be sufficient for radical resection including invasive tumour strands. To further improve sensitivity, different tumour-specific characteristics have been targeted simultaneously. These different targets can be imaged at different wavelengths, allowing separate analysis of different cancer features [21]. The use of a "cocktail" of fluorescent agents that target different tumour markers could reduce the effect of tumour heterogeneity. Although this may seem a feasible approach, it is difficult to assess in advance what percentage of the tumour would be "covered" by this mixture of tumour targets. As an alternative, the biologic tumour markers for each individual tumour could be determined preoperatively, which would require representative samples and complex biochemical analyses. Both approacheswillmost likely not be cost-effective compared to the use of a single universal targeting agent. Moreover, although targeting of cancer cell surface receptors, either or not in combination with simultaneous imaging of tumour-specific pathophysiological processes, seem to solve most of the aforementioned limitations while imaging with high specificity, a closer look into its basic principles reveal that fundamental limitations remain equally existent. First, targeting tumour-associated pathophysiological processes goes at the expense of sensitivity and specificity of the imaging technique. Although imaging of tumour-associated pathophysiological processes is not affected by phenotypic heterogeneity of cell-surface receptors, there is still heterogeneity in the behavioral features of the tumour that influences sensitivity. For example, proteolytic activity may be reduced at the invasive front in less invasive tumours with fewer tendencies towards metastasis, or in cases of encapsulated tumours, reducing the sensitivity of this target. On the other hand, specificity of the target is limited due to the regular expression of these enzymes in healthy tissues and increased expression in inflammatory tissues [26, 28]. Second, a resection margin as indicated by fluorescent agents that target tumour-associated pathophysiological processes would be inconsistent as a result of the variability of proteolytic activity due to phenotypic heterogeneity and regular expression in inflammatory tissues. Although it is expected that proteolytic activity would be increased in regions where invasive strands are found, this approach does not incorporate a standardized objective resection margin. Consequently, the resection margin could be too small in slow-growing tumours or too large in tumours that are surrounded by

inflammatory tissue. Third, with either of the two targeting strategies, it is even more important to consider the influence of the tissue optical properties (absorption and scattering) in the tumour margin which are themselves likely to be altered differently by the presence of an invasive front or at the boundary of an encapsulated tumour. Consequently, smaller lesions and invasive strands may be very difficult to detect, and a basic understanding of the optical physics is required for the surgeon to adequately interpret the acquired images.

Shifting Focus in Optical Image-Guided Therapy

To establish a definite role for optical image-guided therapy into clinical practice, it is necessary to be able to identify the tumour with high sensitivity and specificity, and to remove the complete tumour mass including invasive tumour strands. In the following section, we propose that a shift in focus is required to deal with the three challenges that were identified: tumour heterogeneity, obtaining adequate resection margins that include invasive tumour strands, and managing and ultimately correcting for the effects of tissue optical properties during the surgical resection.

Circumventing the Problems of Tumour Heterogeneity

Recently, a new potential target was identified with the finding of expression of FSHR in tumour blood vessels of a wide range of different cancer types [29]. Expression was found from 5 mm within the tumour to 9 mm outside of the tumour and was not located in healthy tissue more than 10 mm from the tumour (Fig. 2). Although the exact pathogenic mechanism of expression of FSHR is yet unknown, this finding introduces new opportunities for image-guided cancer surgery: resection of tumour margin guided by an FSHR-specific signal may prove to be sufficient to completely remove the tumour. Because expression of the FSHR was found in a wide range of different cancer types that have different cellsurface receptors and variable malignant behavior, sensitivity is not influenced by tumour phenotypic or behavioural heterogeneity. Moreover, expression of the FSHR was found in tumour blood vessels and not in cancer cells. The specificity of this target is very high, as the FSHR is expressed only in the granulosa cells of the ovary and the Sertoli cells of the testis in adult humans. Hence, targeting of the FSHR would result in very low non-specific binding. Although the amount of FSHRs might be lower in smaller tumours, Radu et al. calculated that the volume that consists of blood vessels that have FSHR-expressing endothelial cells represents a substantial fraction of the tumour volume (e.g., in a tumour with a 2-cm diameter, a 3- mm-thick peripheral layer inside the tumour accounts for 66 % of its volume) [29].
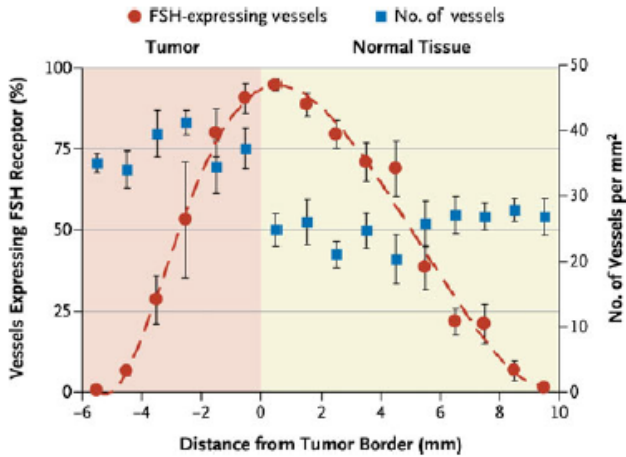
Figure 2; FSHR expression according to vessel location. The blood vessels were visualized with the use of anti-von Willebrand factor antibodies followed by Alexa-488 dye secondary antibodies, and FSHR-stained vessels were visualized by the FSHR323 antibody followed by Alexa-555 dye-labeled secondary antibodies. The vessels were counted on 148 microscopical digital images of tumours obtained from five patients. Zero (0) indicates the border of the tumour, the negative numbers indicate the interior of the tumour, and the positive numbers indicate the exterior of the tumour. The red circles and dashed line represent the percentage of FSHRexpressing vessels. The blue squares indicate the total number of vessels per square millimeter; the mean number was higher in the interior of the tumour than in the exterior (37±2 vs. 25±1 vessels/mm2, PG0.001 with the use of a twotailed t test). I bars denote standard errors. Reproduced with permission from Radu et al., [29], Copyright Clearance Center Rightslink.

This example excludes the additional number of FSHR-expressing vessels that co-exist up to 10 mm outside the tumour border. Expression has been described even in early T1 tumours and in tumour metastases, illustrating the full potential of this target for image-guided cancer therapy. Development of a fluorescently labeled FSHR target is currently still in the experimental phase and future studies on pharmacodynamics, pharmacokinetics, and toxicity (including side effects on the reproductive system) are required for FDA approval. A possible drawback of this target could be that identification of tumours by targeting the FSHR is only feasible after formation of tumour blood vessels. In the prevascular phase, tumour volume is limited to 2–3 mm3 , a size that is usually clinically undetectable [30]. After the angiogenic switch has occurred, neovascularization permits tumours to grow and metastasize, which heralds the onset of symptoms [30, 31]. Because surgery is performed only on clinically detectable lesions that have given symptoms in most cases, neovascularization will always be present and expression of the FSHR can be used as an imaging target for optical image-guided surgery. In addition, most injectable agents have additional "tumour binding" through the nonspecific effect of enhanced permeability and retention (EPR) that is present in many tumours [32, 33]. Non-specific retention of the agent in the tumour (periphery) could have a positive effect by increasing the

fluorescent signal, but on the other hand could reduce the exact specificity of margin delineation by the tumour-specific agent. Preclinical studies have demonstrated clear differences in tumour-specific binding localization [25] and intensity [17] between non-specific EPR and tumour-specific targeting. Finally, similar to targeting of growth factor receptors, injection of contrast agents that target hormone receptors heralds a risk of potentially harmful effects such as tumour proliferation. In longitudinal animal studies on fluorescent agents targeting the epidermal growth factor receptor (EGFR) in prostate cancer, no tumour-promoting effects were found [34]. In contrast to prostate cancer cells that express EGFR, FSHR-expression was only found in the tumour vasculature and not in cancer cells [29], but it is currently unknown if stimulation of the FSHR has effects on tumour growth. As long as these agents are used solely for guidance of tumour resection, the agents would be injected preoperatively and such potentially proliferative effects would be limited to the tumour that is directly removed, provided that regional or distant metastasis are non-existent. Nevertheless, this aspect requires attention in the evaluation of the clinical feasibility of an FSHR-specific fluorescent agent.

Dealing with Undetectable Invasive Tumour Strands

The high recurrence rates in many cancer types warrant a new approach to the inability to identify individual invasive tumour strands. Optical imaging would allow consistent inclusion of an objective resection margin into the surgical resection by targeting of the FSHR. Because FSHR expression was found up to 9 mm outside the tumour border, a resection guided by an FSHR-specific fluorescence signal would include a consistent resection margin and would theoretically include invasive tumour strands in the vast majority of resectable tumours. Even with a highly specific targeting agent available, the fundamental problems associated with detecting weak fluorescence signals in an environment dominated by heterogeneous optical absorption may sometimes prevent undisputable identification of the border of the fluorescent resection margin [7, 8, 15, 35]. Furthermore, high-risk pathological characteristics could imply that adjuvant therapy may still be required to completely treat the cancer [11]. In these selected cases, PDT may be very suitable for adjuvant therapy after optical imageguided cancer surgery for various important reasons. In PDT, photosensitizers are used that produce cytotoxic reactive oxygen species after excitation by light with a specific wavelength. As a result, cancer cells are killed by apoptosis and/or necrosis, and tumour microvasculature is obliterated [36, 37]. Specific damage of the tissue of interest is obtained by local illumination. Furthermore, the very short half-life of cytotoxic reactive oxygen species ensures that damage only occurs in the immediate vicinity of its formation. Although conventional adjuvant treatments (i.e., radiotherapy, chemotherapy, or a combination) can induce immunosuppression, PDT-induced immunogenic cell death induces a local inflammatory reaction and stimulates the host immune system [37]. In addition, formation of a tumourspecific immune response (e.g., production of tumour-specific

cytotoxic T-cells) offers opportunities to treat distant metastases [37]. Preclinical studies showed possibilities of boosting the immune response by the adjuvant use of an oncolytic vaccine virus resulting in effective inhibition of distant metastatic spread [38]. Compared to other adjuvant therapeutic modalities, PDT has the potential to induce low toxicity in normal tissue, produce negligible systemic effects, and reduce acute and long-term morbidity [36]. Furthermore, PDT does not compromise future treatment options for patients with residual or recurrent disease and can be repeated with perpetual efficacy. However, due to limited light penetration depth (G1 cm), PDT is only applicable for superficial lesions, unless the tumour is accessible for insertion of fibers into the tumour to deliver the light. In larger tumours that are inaccessible, debulking of the tumour mass is therefore preferred before adjuvant PDT could be performed [39]. Wavelength-specific excitation of photosensitizers could technically be performed using the same imaging systems as those used for optical image-guided surgery, emphasizing its practical advantages as an adjuvant therapeutic modality in the surgical theatre. In order to fully exploit the advantages of both modalities, a tumour-specific NIR fluorescent photosensitizer is required [40, 41]. A tumour-specific photosensitizer has the potential to be much more efficient and cause less damage to surrounding normal tissue than a non-specific photosensitizer [40, 41]. The increasing amount of photosensitizer that is expected to accumulate in the tissue of interest ensures that less light is required to induce a cytotoxic reaction. Consequently, even light that penetrates deeper into tissue (>1 cm) will result in specific damage of tumour cells that are deeper located. Moreover, such an agent could be used for both NIR fluorescence image-guided surgery and adjuvant PDT (i.e., a "theranostic"). Thereby, a targeting moiety and photosensitizer conjugate can be chosen that accumulates at a location in the cell that is favourable for eliciting a specific cellular or host response (e.g., apoptosis or an immune response)[36]. Recent studies report of tumour-specific PDT that could potentially be performed using heptamethine cyanine dyes that have been shown to specifically target cancer cells in vivo through internalization into the cell by the organic anion transporting polypeptide [42]. Because these agents have shown photosensitizing properties, they are nominated as promising theranostics for future NIR fluorescence imageguided surgery with adjuvant PDT [43]. A second approach could be to design a construct that is a combination of a fluorophore and photosensitizer conjugated with a tumourspecific target. The use of nanotechnology may circumvent some of the negative physio-chemical properties of photosensitizer conjugates [44] and a photosensitizer.

Managing and Correcting for the Effects of Optical Tissue Properties

As we have described above, a current approach to tumourspecific imaging results in fluorescence signals that are strongly influenced by the background tissue optical properties of the tissue under investigation. Given the nature of the fluorescence signals, we propose a shift of focus in optical image-guided cancer therapy towards intraoperative quantitative intrinsic

fluorescence measurements. While various groups have developed imaging systems that incorporate tissue attenuation correction algorithms [16–18], other approaches are aimed at performing truly quantitative in vivo fluorescence measurements [45]. To perform truly quantitative intrinsic fluorescence measurements, the research field of biomedical optics has mainly focused on the use of optical techniques in which the path length of light in tissue can be controlled. This generally involves placing a fiber optic probe on the surface of the tissue, through which light enters the tissue and is subsequently collected from a known distance inside the tissue. The use of a known distance between light source and light detection is important for two reasons. First, it determines the volume over which optical signals are averaged, which is an important consideration for the interrogation of tumour, tumour margin, and the surrounding normal tissue. Second, using a known separation distance between the light source and the light detection, theoretical models can be built to describe the complex interaction of light with tissue over this distance. By applying these theoretical models to the light measured by the fiber optic probe, the tissue optical properties can be quantified. The use of a fiber optic probe also facilitates the acquisition of spectrally resolved fluorescence with a high signal-to-background ratio. Spectral deconvolution allows intrinsic fluorophore fluorescence to be distinguished from the tissue autofluorescence and residual excitation light. Recently, the use of a single fiber optic probe for the delivery and collection of light has been described; single fiber reflectance spectroscopy (SFR) [46]. Mathematical models have been developed to describe the underlying interaction of light with tissue [47, 48]. The sampling volume can be tailored to a specific clinical application or suited to the intraoperative need by varying the diameter of the optical fiber(s) that are used (range in sampling depth 0.1–1 mm). Using knowledge of the sampling volume, algorithms have been developed that can be used to perform quantitative reflectance and fluorescence spectroscopy [45, 49]. By utilizing two or more fiber diameters in a single fiber optic probe, SFR spectroscopy enables a complete determination of tissue optical properties [49, 50]. This technique, termed multi-diameter single fiber reflectance spectroscopy (MDSFR), can then be used to recover a fully quantitative measure of intrinsic fluorescence [51]. In MDSFR spectroscopy, an overlap exists in delivery and collection of light, which provides information on the distribution of angles at which the light scatters [52, 53]. Preclinical studies have suggested that measuring these types of scattering properties may have diagnostic value [54]. This approach yields the quantification of intrinsic fluorescence, given as the product of the tissue fluorophore absorption coefficient at the excitation wavelength. Recently, the first promising results were reported in neurosurgical and gastrointestinal applications using similar approaches [55, 56]. The use of a fiber optic probe has some disadvantages; the point measurement technique needs to be incorporated into the procedure of image-guided surgery and it is not ideal for covering a large proportion of the tumour margin. In addition, true real-time acquisition is not possible, because the measurements take a few seconds to produce at each measurement location. Future

developments in the clinical implementation of MDSFR such as the use of larger coherent fiber bundles [57] could allow this fiber-based technique to approach the resolution and speed of optical imaging. It is also important to consider how point spectroscopic information and optical imaging might be registered most optimally. The acquisition of point measurements as an adjuvant intraoperative optical imaging technique to fluorescenceguided surgery is clearly not limited to the use of reflectance and fluorescence spectroscopy. Other spectroscopic approaches such as Raman spectroscopy have significant potentials [58] but spectral analysis of a tumour margin during fluorescence-guided surgery may be hampered by the presence of the exogenous fluorophores. In addition, although these techniques are rapidly improving, the acquisition time of a representative Raman spectrum is currently too long to be used intraoperatively. Given the potential of the approaches that we have presented, we advocate the use of fluorescence-guided surgery for resection of the gross tumour mass, followed by point spectroscopic fluorescence measurements of suspect tumour margins.

The Paradigm of Field Cancerization

An interesting problem for optical image-guided cancer therapy is introduced with the concept of field cancerization that suggests that achieving histological adequate margins may not be sufficient in some cases [59]. Squamous cell carcinomas develop within preoplastic fields of mucosal epithelium made up of genetically altered cells. However, these precursor changes in the mucosa may have a macroscopically normal appearance. Therefore, preoplastic lesions can be found in parts of the surrounding mucosal epithelium [59] and can extend into the surgical margins when tumours are excised [60] causing local recurrences and second primary tumours. The relation between dysplastic changes surrounding tumours and the rate of local recurrences and multiple primary tumours in cancer has been reviewed extensively [59, 60]. An important aspect of the genetic basis of multi-step progression from normal mucosa to squamous cell carcinoma is found in the role of p53 [61] and loss of heterozygosity of specific chromosomes [59, 60, 62]. Although the cancerization process can be clearly identified genetically, no specific targeting agents have thus far been found for identification of preoplastic lesions. An important reason is that preoplastic fields have much more biological similarities with normal mucosa than with tumour, making array and proteomic studies very difficult. The paradigm of field cancerization poses a problem for identification of tumour-free margins using optical imaging. Considering the surrounding preoplastic lesions and their relevance for local recurrence rates, it might not be sufficient to completely remove the tumour at its borders. At present, no literature exists that is able to guide a surgeon towards adequate margins in the setting of field cancerization [12]. However, the potential extent of this problem emphasizes the necessity to include a consistent objective resection margin as would be indicated by targeting of the FSHR.

Conclusion

Although the introduction of optical imaging techniques for intraoperative applications has great potential to improve assessment of tumour margins during surgery, optimizing sensitivity and specificity remain challenging because of tumour heterogeneity. In addition, results of optical imageguided surgery are potentially limited due to difficulty in including invasive tumour strands in the resection margin and dealing with the influences that optical tissue properties have on the image. We review three new concepts that could deal with these challenges. First, expression of the FSHR provides an ideal target for cancer imaging and could theoretically circumvent the problems of tumour heterogeneity. Next, the inability to identify individual invasive strands dictates a new approach to consistently include an objective resection margin into the surgical resection. The FSHR positive margin would provide such a consistent objective resection margin. Extension of invasive strands beyond such a standardized resection margin could ideally be treated with adjuvant photodynamic therapy. And finally, the confounding effects of variable background tissue optical properties can be overcome by combining fluorescence-guided surgery with quantitative optical spectroscopy of the tumour margin. We anticipate that these promising concepts will play an elementary role in the next generation of optical image-guided cancer therapy.

Acknowledgments.

7

Conflict of interest.

The authors declare that they have no conflicts of interest.

References

1. van Dam GM, Themelis G, Crane LM et al (2011) Intraoperative tumourspecific fluorescence imaging in ovarian cancer by folate receptor-alpha targeting: first in-human results. Nat Med 17:1315–1319

2. Alexander S, Friedl P (2012) Cancer invasion and resistance: interconnected processes of disease progression and therapy failure. Trends Mol Med 18:13–26

3. Friedl P, Alexander S (2011) Cancer invasion and the microenvironment: plasticity and reciprocity. Cell 147:992–1009 S.

4. Hilderbrand SA, Weissleder R (2010) Near-infrared fluorescence: application to in vivo molecular imaging. Curr Opin Chem Biol 14:71–79

5. Frangioni JV (2003) In vivo near-infrared fluorescence imaging. Curr Opin Chem Biol 7:626–634

6. Gioux S, Choi HS, Frangioni JV (2010) Image-guided surgery using invisible near-infrared light: fundamentals of clinical translation. Mol Imaging 9:237–255

7. Keereweer S, Van Driel PB, Snoeks TJ et al (2013) Optical imageguided cancer surgery: challenges and limitations. Clinical Cancer Research 19(14):3745–54

8. Weissleder R, Pittet MJ (2008) Imaging in the era of molecular oncology. Nature 452:580–589

9. Marusyk A, Almendro V, Polyak K (2012) Intra-tumour heterogeneity: a looking glass for cancer? Nat Rev Cancer 12:323–334

10. Gerlinger M, Rowan AJ, Horswell S et al (2012) Intratumour heterogeneity and branched evolution revealed by multiregion sequencing. New England J Med 366:883–892

11. Li Y, Bai S, Carroll W et al (2012) Validation of the risk model: highrisk classification and tumour pattern of invasion predict outcome for patients with low-stage oral cavity squamous cell carcinoma. Head Neck Pathol 7(3):211–23

12. Hinni ML, Ferlito A, Brandwein-Gensler MS et al (2012) Surgical margins in head and neck cancer: a contemporary review. Head Neck 35(9):1362–70

13. Martling A, Cedermark B, Johansson H et al (2002) The surgeon as a prognostic factor after the introduction of total mesorectal excision in the treatment of rectal cancer. Br J Surg 89:1008–1013

14. Chance B (1998) Near-infrared images using continuous, phasemodulated, and pulsed light with quantitation of blood and blood oxygenation. Ann N Y Acad Sci 838:29–45

15. Ntziachristos V (2010) Going deeper than microscopy: the optical imaging frontier in biology. Nat Methods 7:603–614

16. Valdes PA, Leblond F, Jacobs VL et al (2012) Quantitative, spectrallyresolved intraoperative fluorescence imaging. Sci Rep 2:798

17. Zhu B, Wu G, Robinson H, et al. (2013) Tumour margin detection using quantitative NIRF molecular imaging targeting EpCAM validated by Far Red Gene Reporter iRFP. Molecular Imaging and Biology : MIB

18. Themelis G, Yoo JS, Soh KS et al (2009) Real-time intraoperative fluorescence imaging system using light-absorption correction. J Biomed Opt 14:064012

19. Keereweer S, Kerrebijn JD, van Driel PB et al (2011) Optical imageguided surgery–where do we stand? Mol Imaging Biol 13:199–207

20. Van Driel PBAA, Keereweer S, Snoeks TJA, Lowik CWGM (2013) Fluorescence-Guided Surgery: A Promising Approach for Future Oncologic Surgery. In Comprehensive Biomedical Physics. Elsevier, Oxford

21. Keereweer S, Mol IM, Vahrmeijer AL et al (2012) Dual wavelength tumour targeting for detection of hypopharyngeal cancer using nearinfrared optical imaging in an animal model. Int J Cancer 131(7):1633– 40

22. Mieog JS, Hutteman M, van der Vorst JR et al (2011) Image-guided tumour resection using real-time near-infrared fluorescence in a syngeneic rat model of primary breast cancer. Breast Cancer Res Treatment 128:679–689

23. Kovar JL, Volcheck W, Sevick-Muraca E et al (2009) Characterization and performance of a near-infrared 2-deoxyglucose optical imaging agent for mouse cancer models. Analytical Biochemistry 384:254–262

24. Kossodo S, Pickarski M, Lin SA et al (2010) Dual in vivo quantification of integrin-targeted and protease-activated agents in cancer using fluorescence molecular tomography (FMT). Mol Imag Biol: MIB : official publication Acad Mol Imag 12:488–499

25. Keereweer S, Mol IM, Kerrebijn JD et al (2011) Targeting integrins and enhanced permeability and retention (EPR) effect for optical imaging of oral cancer. J Surg Oncol 105(7):714–8

26. Weissleder R, Tung CH, Mahmood U, Bogdanov A Jr (1999) In vivo imaging of tumours with protease-activated near-infrared fluorescent probes. Nat Biotechnol 17:375–378

27. Blum G, von Degenfeld G, Merchant MJ et al (2007) Noninvasive optical imaging of cysteine protease activity using fluorescently quenched activity-based probes. Nat Chem Biol 3:668–677

28. Keereweer S, Mieog JS, Mol IM et al (2011) Detection of oral squamous cell carcinoma and cervical lymph node metastasis using activatable near-infrared fluorescence agents. Arch Otolaryngol Head Neck Surg 137:609–615

29. Radu A, Pichon C, Camparo P et al (2010) Expression of folliclestimulating hormone receptor in tumour blood vessels. New England J Med 363:1621–1630

30. Folkman J (1995) Angiogenesis in cancer, vascular, rheumatoid and other disease. Nat Med 1:27–31

31. Hanahan D, Folkman J (1996) Patterns and emerging mechanisms of the angiogenic switch during tumourigenesis. Cell 86:353–364

32. Fang J, Nakamura H, Maeda H (2011) The EPR effect: unique features of tumour blood vessels for drug delivery, factors involved, and limitations and augmentation of the effect. Adv Drug Deliv Rev 63:136–151

33. Maeda H (2010) Tumour-selective delivery of macromolecular drugs via the EPR effect: background and future prospects. Bioconjugate Chem 21:797–802

34. Kovar JL, Johnson MA, Volcheck WM et al (2006) Hyaluronidase expression induces prostate tumour metastasis in an orthotopic mouse model. American J Pathol 169:1415–1426

35. Chance B (1998) Near-infrared images using continuous, phasemodulated, and pulsed light with quantitation of blood and blood oxygenation. Annals New York Acad Sci 838:29–45

7

36. Agostinis P, Berg K, Cengel KA et al (2011) Photodynamic therapy of cancer: an update. CA Cancer J Clin 61:250–281

37. Castano AP, Mroz P, Hamblin MR (2006) Photodynamic therapy and anti-tumour immunity. Nat Rev Cancer 6:535–545

38. Gil M, Bieniasz M, Seshadri M et al (2011) Photodynamic therapy augments the efficacy of oncolytic vaccinia virus against primary and metastatic tumours in mice. Br J Cancer 105:1512–1521

39. Hendren SK, Hahn SM, Spitz FR et al (2001) Phase II trial of debulking surgery and photodynamic therapy for disseminated intraperitoneal tumours. Annals Surg Oncol 8:65–71

40. Schmitt F, Juillerat-Jeanneret L (2012) Drug targeting strategies for photodynamic therapy. Anticancer Agents Med Chem 12:500–525

41. Bugaj AM (2011) Targeted photodynamic therapy–a promising strategy of tumour treatment. Photochemical Photobiological Sciences 10:1097– 1109

42. Yang X, Shi C, Tong R et al (2010) Near IR heptamethine cyanine dyemediated cancer imaging. Clin Cancer Res 16:2833–2844

43. Tan X, Luo S, Wang D, Su Y, Cheng T, Shi C (2012) A NIR heptamethine dye with intrinsic cancer targeting, imaging and photosensitizing properties. Biomaterials 33:2230–2239

44. Kepczynski M, Dzieciuch M, Nowakowska M (2012) Nanostructural hybrid sensitizers for photodynamic therapy. Curr Pharm Des 18:2607– 2621

45. Amelink A, Kruijt B, Robinson DJ, Sterenborg HJ (2008) Quantitative fluorescence spectroscopy in turbid media using fluorescence differential path length spectroscopy. J Biomed Optics 13:054051

46. Kanick SC, Sterenborg HJ, Amelink A (2009) Empirical model of the photon path length for a single fiber reflectance spectroscopy device. Optics Express 17:860–871

47. Kanick SC, Sterenborg HJ, Amelink A (2008) Empirical model description of photon path length for differential path length spectroscopy: combined effect of scattering and absorption. J Biomed Optics 13:064042

48. Kanick SC, Robinson DJ, Sterenborg HJ, Amelink A (2009) Monte Carlo analysis of single fiber reflectance spectroscopy: photon path length and sampling depth. Phys Med Biol 54:6991–7008

49. Kanick SC, Robinson DJ, Sterenborg HJ, Amelink A (2011) Method to quantitate absorption coefficients from single fiber reflectance spectra without knowledge of the scattering properties. Optics Lett 36:2791– 2793

50. Kanick SC, Gamm UA, Sterenborg HJ et al (2011) Method to quantitatively estimate wavelength-dependent scattering properties from multidiameter single fiber reflectance spectra measured in a turbid medium. Optics Lett 36:2997–2999

51. Kanick SC, Robinson DJ, Sterenborg HJ, Amelink A (2012) Extraction of intrinsic fluorescence from single fiber fluorescence measurements on a turbid medium. Optics Lett 37:948–950

52. Gamm UA, Kanick SC, Sterenborg HJ et al (2012) Quantification of the reduced scattering coefficient and phase-function-dependent parameter gamma of turbid media using multidiameter single fiber reflectance spectroscopy: experimental validation. Optics Lett 37:1838– 1840

53. Kanick SC, Gamm UA, Schouten M et al (2011) Measurement of the reduced scattering coefficient of turbid media using single fiber reflectance spectroscopy: fiber diameter and phase function dependence. Biomed Opt Express 2:1687–1702

54. van Leeuwen-van ZF, Gamm UA, van Driel PB et al (2013) In vivo quantification of the scattering properties of tissue using multi-diameter single fiber reflectance spectroscopy. Biomed Opt Express 4:696–708

55. Valdes PA, Leblond F, Kim A et al (2011) Quantitative fluorescence in intracranial tumour: implications for ALA-induced PpIX as an intraoperative biomarker. J Neurosurg 115:11–17

56. Roy HK, Backman V (2012) Spectroscopic applications in gastrointestinal endoscopy. Clin Gastroenterol Hepatol 10:1335–1341

57. Hoy CL, Gamm UA, Sterenborg HJ et al (2012) Use of a coherent fiber bundle for multi-diameter single fiber reflectance spectroscopy. Biomed Opt Express 3:2452–2464

58. Nijssen A, Koljenovic S, Bakker Schut TC et al (2009) Towards oncological application of Raman spectroscopy. J Biophotonics 2:29–36

59. Braakhuis BJ, Tabor MP, Kummer JA et al (2003) A genetic explanation of Slaughter's concept of field cancerization: evidence and clinical implications. Cancer Res 63:1727–1730

60. Graveland AP, Golusinski PJ, Buijze M et al (2011) Loss of heterozygosity at 9p and p53 immunopositivity in surgical margins predict local relapse in head and neck squamous cell carcinoma. Int J Cancer 128:1852–1859

61. Califano J, van der Riet P, Westra W et al (1996) Genetic progression model for head and neck cancer: implications for field cancerization. Cancer Res 56:2488–2492

62. Leemans CR, Braakhuis BJ, Brakenhoff RH (2011) The molecular biology of head and neck cancer. Nat Rev Cancer 11:9–22

CHAPTER 8

EGFR targeted nanobody-photosensitizer conjugates for photodynamic therapy in a pre-clinical model of head and neck cancer.

Pieter B.A.A. van Driel[1,2], Martin C. Boonstra[3], Maxime D. Slooter[1,2], Raimond Heukers[4], Marieke A. Stammes[1,2], Thomas J.A. Snoeks[1], Henriette S. de Bruijn[5], Paul J. van Diest[6], Alexander L. Vahrmeijer[3], Paul M.P. van Bergen en Henegouwen[4], Cornelis J.H. van de Velde[3], Clemens W.G.M. Löwik[1], Dominic J. Robinson[5], Sabrina Oliveira[4]

1. Department of Radiology, Division of Molecular Imaging, Leiden University Medical Center, Leiden, The Netherlands
2. Percuros BV, Enschede, The Netherlands
3. Department of Surgery, Leiden University Medical Center, ZA Leiden, The Netherlands
4. Molecular Oncology, Cell Biology Division, Department of Biology, Faculty of Science, Utrecht University, Utrecht, The Netherlands
5. Department of Otorhinolaryngology & Head and Neck Surgery, Center for Optical Diagnostics and Therapy, Erasmus Medical Center, Rotterdam, The Netherlands
6. Department of Pathology, University Medical Center Utrecht, Utrecht, The Netherlands

ABSTRACT

Photodynamic therapy (PDT) induces cell death through local light activation of a photosensitizer (PS) and has been used to treat head and neck cancers. Yet, common PS lack tumour specificity,which leads to collateral damage to normal tissues. Targeted delivery of PS via antibodies has pre-clinically improved tumour selectivity.However, antibodies have long half-lives and relatively poor tissue penetration, which could limit therapeutic efficacy and lead to long photosensitivity. Here, in this feasibility study, we evaluate at the pre-clinical level a recently introduced format of targeted PDT,which employs nanobodies as targeting agents and awater-soluble PS (IRDye700DX) that is traceable through optical imaging. In vitro, the PS solely binds to cells and induces phototoxicity on cells overexpressing the epidermal growth factor receptor (EGFR), when conjugated to the EGFR targeted nanobodies. To investigatewhether this new format of targeted PDT is capable of inducing selective tumour cell death in vivo, PDTwas applied on an orthotopic mouse tumour model with illumination at 1 h post-injection of the nanobody–PS conjugates, as selected from quantitative fluorescence spectroscopymeasurements. In parallel, and as a reference, PDTwas appliedwith an antibody–PS conjugate, with illumination performed 24 h post-injection. Importantly, EGFR targeted nanobody–PS conjugates led to extensive tumour necrosis (approx. 90%) and almost no toxicity in healthy tissues, as observed through histology 24 h after PDT. Overall, results showthat these EGFR targeted nanobody–PS conjugates are selective and able to induce tumour cell death in vivo. Additional studies are now needed to assess the full potential of this approach to improving PDT.

Introduction

Cancers of the head and neck region are the sixth most common cancers in the world [1]. In spite of recent advances in surgery and radiotherapy, increasing incidences and moderate survival rates are reported [2]. Photodynamic therapy (PDT) is a promising minimally invasive approach that is being used for the local treatment of premalignant and malignant lesions in the head and neck region [3,4]. Despite the potential advantages of PDT, collateral damage to normal tissue remains a significant side effect, particularly in the treatment of large tumours [5]. Targeted PDT, in which photosensitizers (PS) are selectively delivered to the tumour, could greatly enhance the results of PDT in head and neck cancer. PDT makes use of three essential elements to induce localized (tumour) cell death: a PS, light of a particular wavelength, and oxygen [3]. Although each of these individual components is not toxic, together they induce local toxicity through the formation of toxic reactive oxygen species, notably singlet oxygen ($1O_2$), damaging proteins, lipids and/or nucleic acids. The lifetime and diffusion distance of $1O_2$ are very short [6], consequently, the localization of PS at the time of the illumination is a critical factor in the selectivity of PDT. The overall localization of the PS at the tumour and the surrounding normal tissues is determined by the pharmacokinetics of the PS (i.e. its absorption, distribution, metabolism, and excretion). The generation of $1O_2$ in the target tissue results in cell death through apoptosis and/or necrosis. Necrotic cell death can be induced either by a direct effect on tumour cells or indirectly through a shutdown of tumour vasculature. An important additional mechanism of action in PDT is derived from a robust inflammatory response that can lead to development of systemic immunity [3]. Clinically available PSs can be categorized as derivatives of three major families: porphyrins (e.g. Photofrin), chlorins (e.g. Foscan) and phthalocyanines (e.g. Photosense) [7]. In general, most PSs are rather hydrophobic which promotes cell binding, but provides no specificity. As a result, 2 to 4 days are generally necessary between injection of the PS and illumination, in order to favor clearance of PS from normal tissues and to promote some tumour specificity [7]. Alternatively, light can be applied earlier after PS administration, with the particular intention to induce vascular damage [3]. In addition, patients generally show skin photosensitivity for long periods of time (2–6 weeks) [3,8]. Therefore, efforts have been made to render PS more hydrophilic and to target these molecules more selectively to tumours, through chemical modifications, delivery systems, and/or targeting molecules [9–13]. The targeting of PS through the use of monoclonal antibodies (mAbs), which is termed photoimmunotherapy [11], has shown promising results [14,15]. Nevertheless, due to their large molecular weight (150 kDa), mAb–PS conjugates have a limited capability of penetrating into the interior of large tumours [16,17]. Moreover, the larger size of mAbs–PS conjugates (~15 nm) may impede the generation of $1O_2$ within the outer cell membrane of targeted cells and affect the therapeutic efficacy. The location of lipophilic photosensitisers within the plasma membrane

has previously been shown to influence in vitro and in vivo efficacy [18]. Furthermore, because of long half-lives of mAbs in the bloodstream, time is needed for tumour accumulation and development of sufficient tumour-to-background ratios (TBR) to protect healthy tissues. As many of these disadvantages are related to the size of mAbs, some studies reported the use of smaller mAb fragments such as F(ab')2 and scFv conjugated to a PS [19–24]. Recently, we have introduced an alternative approach for targeted PDT employing nanobodies conjugated to awater-soluble and traceable PS, leading to encouraging results in vitro [25]. Nanobodies are the smallest naturally derived antigen-binding fragments that consist of the variable domain of heavy chain antibodies, whichwere first discovered in dromedaries in 1993 [26]. Nanobodies bind specifically and with high affinities to their antigens [26,27], they are stable and soluble in aqueous solutions, can be chemically modified, and have low immunogenic potential [28]. Importantly, with a molecular weight ten times smaller than conventional antibodies (15 kDa vs 150 kDa) [29] and high binding affinities, tumour penetration of nanobodies is greatly enhanced, and occurs more rapidly [27,30,31] (this is in line with the modeling of Schmidt and Wittrup [32]). In addition, the rapid clearance through the kidneys accelerates the acquisition of imageswith sufficient TBR, as demonstrated in our previous studies in which a nanobody was compared to an antibody for optical molecular imaging [30,31]. The nanobodies that we used for PDT, i.e. the monovalent 7D12 [31,33] and the biparatopic 7D12-9G8 [34], specifically targeted the epidermal growth factor receptor (EGFR). With more than 83% of all head and neck squamous cell carcinomas overexpressing EGFR [35], it serves as a promising target in head and neck cancer patients. In fact, increased levels of EGFR are associated with poor prognosis by locoregional failure and decreased survival [36]. The PS that we conjugated to the nanobodies was IRDye700DX, which is a water-soluble silicon-phthalocyanine derivative, that has a strong absorption band in the near-infrared region of the spectrum (690 nm) and is also traceable through optical imaging [15,37]. Our previous studies showed that, in vitro, the nanobody–PS conjugates (i.e. 7D12–PS and 7D12-9G8–PS) bound specifically to EGFR, allowing the distinction of cell lines with different expression levels of EGFR. Notably, the conjugates specifically induced cell death of EGFR overexpressing cells in low nanomolar concentrations. Importantly, the biparatopic conjugate (i.e. 7D12-9G8–PS) was more toxic, as it could deliver more PS intracellularly [25], via the clustering induced endocytosis of EGFR [38]. These encouraging results have stimulated further investigation of these conjugates in an in vivo setting. The aim of the present study is to investigate the therapeutic potential of nanobody–PS conjugates for targeted PDT, i.e. to determine whether these conjugates are capable of inducing selective tumour cell death in vivo, in a pre-clinical head and neck tumour model. First, the nanobody–PS conjugates are characterized for their specificity and phototoxicity in vitro employing the EGFR overexpressing oral squamous cell carcinoma cell line OSC-19-luc2-cGFP (OSC). Subsequently, this cell line is grown as an orthotopic model in the tongue of mice to

allow pre-clinical evaluation through histological analysis post-PDT. As a reference or positive control, and for validation of themodel and analysis procedure employed in this feasibility study, Cetuximab–PS was employed as Mitsunaga et al. [15] have described the use of their mAb–PS conjugates. To determine the best time point for illumination after intravenous injection of the nanobody–PS conjugates, quantitative fluorescence spectroscopy is employed. This is a method that has been developedwithin our group and is currently being evaluated in the clinic for guiding PDT applications, as it provides insights in the pharmacokinetics (through local distribution) of the PS. Thereafter, PDT is applied in this orthotopic tumour model and the efficacy is evaluated in vivo by histological analysis. Our data show that nanobody–PS conjugates are selective and able to induce specific tumour cell death in a pre-clinical model of head and neck cancer.

8

Materials and Methods

2.1. Nanobodies and PS conjugation

Nanobodies 7D12, R2, and 7D12-9G8 were produced as described previously, i.e. His-tagged nanobodies were produced in E. coli and purified from the periplasmic space by TALON affinity purification [31, 34]. The nanobody 7D12 binds to the domain III of the EGFR, preventing EGF binding to the receptor [39]. The biparatopic nanobody 7D12-9G8 is composed of two nanobodies that bind to different epitopes on EGFR and that cannot bind simultaneously to the same receptor, therefore being able to create clusters of receptors [39]. The irrelevant nanobody R2 is employed as a control and was specifically selected to bind to the azo dye Reactive Red 6 [40,41]. The photosensitizer IRDye700DX (here named PS) was purchased from LI-COR (LI-COR Biosciences, Lincoln, Nebraska) as an N-hydroxysuccinimidine (NHS) ester. Conjugation of the PS to the nanobodies was performed as described in Heukers et al. [25], except that the molar ratio for conjugation was 1 to 4 for 7D12–PS and 1 to 2 for R2–PS and 7D12-9G8–PS. After 2 h at room temperature, the conjugates were separated from free PS by size exclusion chromatography using Zebra Spin Desalting columns (Thermo Fisher Scientific, Perbio Science Nederland, Etten-Leur, The Netherlands), in three sequential steps. The degree of conjugation (DOC) was determined as recommended by the provider, by measuring the absorbance at 280 nmand 689nmusing a NanoDrop spectrophotometer (NanoDrop Technologies,Wilmington, Delaware, USA). Purity and integrity of the nanobody–PS conjugates were determined by molecular size separation through SDS-PAGE using 15% gels. Immediately after running the gels, these were imaged on an Odyssey Infrared scanner (LI-COR Biosciences) using the 700 nm channel to detect PS fluorescence. Thereafter, Coomassie Blue staining was performed and detected in the same way as the PS. Cetuximab–PSwas used as a reference or positive control in this study andwas obtained as described byMitsunaga et al. [15] for panitumumab.

2.2. Cell lines

Three human cell lines with different EGFR expressions were used. The well differentiated squamous cell carcinoma of the tongue OSC-19-luc2-cGFP (high EGFR overexpression) was cultured in Dulbecco's modified Eagle's medium (DMEM; Invitrogen, Carlsbad, CA) containing 4.5 g D-glucose/L, 110 mg sodium pyruvate/L, 580 mg L-glutamine/L supplemented with 10% fetal bovine serum (FCS; Lonza, Basel, Swiss), 400 IU/mL penicillin, 100 µg/mL streptomycin (Invitrogen) 1× Minimal Essential Medium (MEM) non-essential amino acids solution and 1× MEM vitamin solution (Invitrogen) [42]. The human cervical cancer cell line HeLa (intermediate EGFR expression) was cultured in DMEM (Gibco, Invitrogen, United Kingdom) supplemented with 8% FCS (v/v), 100 U/ml penicillin, 100 µg/ml streptomycin, and 2 mM L-glutamine (PAA, Germany) [25]. The human colorectal cancer cell line SW620 (low EGFR) was cultured in

Leibovitz's L-15 medium (Invitrogen) containing 300 mg L-tlutamine/L supplemented with 10% FetalClone II (Hyclone, Logan, UT), 100 IU/mL penicillin, 100 μg/mL streptomycin (Invitrogen) and 20 mM HEPES (Invitrogen) [42]. All cell lines were grown in ahumidified incubator at 37 °C and 5% CO2 andwere regularly checked for Mycoplasma infection by polymerase chain reaction.

2.3. Cell binding assay

A total of 8000 cells were seeded per well of a 96-wells plate (Nunc, Roskilde, Denmark) and allowed to adhere overnight. For the affinity determination, plates were placed at 4 °C and cells were washed with cold binding medium (1% BSA and 25 mM HEPES in DMEM without phenol red, pH 7.2). Subsequently, cells were incubated with a concentration range of nanobody–PS conjugates in binding medium for 2 h at 4 °C. Thereafter, cells were washed twice with cold binding medium and bound conjugates were detected though fluorescence imaging of the PS with the Odyssey Infrared scanner, using the 700 nm channel. Fluorescence intensities were plotted (in triplicate ± SEM) versus the concentrations. The resulting saturation curveswere used to determine the apparent affinity (kD) of the nanobody–PS conjugates, using the GraphPad Prism 5.02 software for Windows (GraphPad Software, San Diego, CA), and one-site specific binding, non-linear regression protocol. Experiments were repeated at least twice. For evaluation of the binding specificity by fluorescence microsocpy, cells were incubated with 25 nMof nanobody–PS as described above, followed by twowashing steps and incubation with calcein AM(0.5 μg/ml, Invitrogen) for detection of cells. This calcein incubation was not performed with OSC cell line as this one is GFP positive and thus already detectable through fluorescence microscopy. Imagingwas performedwith an EVOS Microscope (Advanced Microscopy Group, AMG, Thermo Fischer Scientific) equipped with 10× objective (Plan Fluor, 10×, NA 0.3, Air and working distance 8.3 mm, AMG) and the following LED-based fluorescence light cubes: GFP (Cat. no. 12-563-470) and Cy5 (for PS detection, Cat. no. 12-563-475) (fromWestover Scientific Inc., AMG). Overlays of the separate imageswere also generatedwith the EVOS Microscope software (AMG).

2.4. Steady-state fluorescence and absorption measurements

The fluorescence quantum yields (ΦF) of the nanobody/antibody conjugates were determined using a relative method in PBS (pH 7.4) [43] using Chlorin e6 (Ce6) in the same buffer as a reference. At pH 7.4 the fluorescence quantum yield of Ce6 is 0.18 [44,45]. The absorption spectrum of Ce6 and conjugates (concentration 1×10^{-6} M) was recorded in Shimadzu spectrophotometer (UV-2101 PC, Duisburg, Germany). The fluorescence emission of PS was recorded in a Perkin-Elmer spectrofluorometer (LS 50B, Massachusetts, USA). Ce6 and conjugates fluorescence spectra were acquired under 630 nm and 660 nm excitation respectively

at an OD lower than 0.1. Calculations ofΦF was accompanied by careful consideration of the differences in photon number at different wavelengths.

2.5. Singlet oxygen quantum yield measurements

Photo-oxidation of Singlet Oxygen Sensor Green Reagent (SOSGR) (Molecular Probes, NL) was used to determine the singlet oxygen formation by the nanobody–PS conjugates. This reagent was used because of its high selectivity for singlet oxygen and lowsensitivity to hydroxyl radicals/superoxides [46]. Stock solution of SOSGR (5 mM) was prepared in methanol. The final concentration of SOSGR within the PS solution in PBS pH 7.4 was 1 µM. Solutions of PS and nanobody–PS or antibody–PS conjugates were prepared in PBS pH 7.4. The concentration of PS were adjusted so that all absorb the same number of photonswithin the irradiated region (O.D.=0.014 at the λirr.=660nm(Spectra Physics, NL). Data was acquired in quartz cuvettes in aerobic conditions using stirring under uniform,measured fluence rate at 5 mW/cm2. At intervals, the cuvette was removed from magnetic stirrer and absorption and fluorescence emission spectrum (λexc = 405 nm) acquired. The singlet oxygen quantum yields (ΦD) of conjugates in PBS were determined in duplicate by a relative method [47] with a ΦD = 0.64 of Ce6 in the PBS at pH 7.4 as reference [48].

2.6. In vitro PDT

One day after seeding 8000 cells per well of 96-wells plates (Greiner Bio-One, Alphen a/d Rijn, The Netherlands), cells are washed once with PDT medium (DMEM without phenol red supplemented with 8% FCS (v/v), 100 U/ml penicillin, 100 µg/ml streptomycin, and 2 mM L-glutamine). Then, a dilution range of nanobody–PS conjugates was added to the cells and incubated for 30 min at 37 °C. After the incubation (also referred to as pulse), cells were washed twice with PDT medium. Immediately after, the fluorescence intensity of the conjugates bound to and/or internalized by the cells was detected with the Odyssey scanner and the cells were illuminated immediately after. Plates were illuminated with ~4 mW/cm2 fluence rate (measured with an Orion Laser power/energy monitor, Ophir Optronics LTD, Jerusalem, Israel), for a total dose of 10 J/cm2, using a device consisting of 96 LED lamps (670 ± 10 nm, 1 LED per well) described in [49,50]. After illumination, cells were placed back into the incubator, unless mentioned otherwise. In all experiments, a number of wells were covered during llumination as internal negative control. Experiments were repeated at least twice.

2.7. Cell viability assays

After overnight incubation of the cells treated as described above, cells were incubated with the Alamar Blue reagent, according to the manufacturer's protocol (AbD Serotec, Oxford, United Kingdom), i.e. 10 μl of Alamar Blue was added into each well and mixed with the 100 μl of medium present in the wells. After an incubation of 1 h at 37 °C, fluorescence intensity was measured on a FluoStar Optima fluorescent plate reader (BMG Labtech GmbH, Ortenberg, Germany). Values of fluorescence intensities obtained fromwells only containing medium and Alamar bluewere taken as background,whilewells containing cells that were covered during illumination and that were not treated with nanobody–PS conjugates were set to 100% cell viability. Results are expressed as cell viability in percentage (%), thus relatively to the untreated cells, and the half maximal inhibitory concentration (IC50) are determined using the GraphPad Prism 5.02 software.

2.8. Co-culture assay

A mixture consisting of 50% of HeLa and 50% of OSC cell lines was seeded in 96-wells plates (Greiner), pulsed with 25 nM of nanobody– PS and followed by 10 J/cm2 of light dose. After overnight incubation (~16 h), dead cellswere distinguished fromliving cells by propidiumiodide (1 μg/ml, Invitrogen) and calcein AM(0.5 μg/ml, Invitrogen) staining, according to the manufacturers' protocol. Cells were imaged with an EVOS Microscope equipped with 10× objective and the following LED-based fluorescence light cubes: GFP for calcein AM and RFP (Cat. no. 12-563-471) for propidium iodide. Phase contrast images were also taken. Overlays of the separate images were generated with the EVOS Microscope software.

2.9. Animal model

Nude Balb/c female mice (Charles River laboratories, l'Arbresle, France), aged 4–6 weeks, were housed in individually ventilated cages and provided with food and sterilized water ad libitum. Animal experiments were approved by the local animal welfare committee of the Leiden University Medical Center. Orthotopic tongue tumours were submucosally induced in the tip of the tongue through injection of 40,000 OSC-19-luc2-cGFP cells, in suspension in 20 μl PBS. General health was monitored twice a week by weight measurements and inspection of the tongue. Tumour growth was monitored twice a week by bioluminescence (BLI) measurements and visual inspection of the tongue. Mice were sacrificed by injection of high-doses ketamine/xylazine.

2.10. Quantitative fluorescence spectroscopy

Quantitative fluorescence spectroscopy, which fully corrects for the differences in tissue optical properties, was performed as described previously [51]. White light reflectance and fluorescence

spectra were acquired using a single probe that contained two fibers of 0.4 and 0.8 mm. The 0.8 mm fiber was used for both fluorescence and reflectance spectroscopy while the 0.4 mm fiber was used to perform reflectance spectroscopy. The end of the fiber probe in contactwith the tissue was polished to an angle of 15° tominimize the collection of specular reflection. To obtain a reflectance spectrum, light froma tungsten halogen lamp was directed on the tissue through a probe containing 2 single fibers with diameters of 0.4 and 0.8 mm. This choice of fiber diameters was dictated by the intention to optically sample a representative proportion of the tumour and normal tissue under interrogation. The photon path length and therefore the sampling volume is on the order of the fiber diameter which means that approximately 1/3 of the tumour volume is interrogated by the smallest fiber diameter. After these sequential reflectance measurements, a single fiber fluorescence spectroscopy (SFF) spectrum was acquired using the 0.8 mm fiber and 660 nm laser light. This wavelength was chosen to optimally separate IRDye700DX (PS) fluorescence from background autofluorescence. The reflectance and fluorescence spectra were detected by three spectrometers, one for each fiber to measure reflectance and one to measure fluorescence where a 675 nm notch filter was used to block scattered excitation light. The spectrometers, light sources and shutters were controlled by a custom made LabView program (National Instruments LabView 7.1) on a notebook computer. A single combined multi-diameter optical fiber (MDSFR)/SFF measurement took approximately 3 s. The fiber probe was removed from the tissue and replaced to perform repeated measurements. Three spectra were acquired from each tissue type, and the average and standard deviation of these measurements were reported.

2.10.1. Data analysis

To calculate the intrinsic fluorescence, the raw fluorescence signals were corrected for the effects of absorption and scattering using the optical properties obtained from the MDSFR reflectance spectra. A detailed mathematical description of the recovery of the tissue optical properties from an MDSFR spectrum and their use in determining the intrinsic SFF from a raw fluorescence spectrum has been described previously [52]. The result of this analysis is a calibrated, corrected fluorescence spectrum expressed as the wavelength-dependent intrinsic fluorescence, where $Q(l)\mu_f$ is the quantum efficiency of the fluorophore at each emission wavelength. This spectrum is then integrated over the emission bandwidth of the fluorophore IRDye700DX (PS) to yield the intrinsic fluorescence $Q \cdot \mu_{f\,a,x}$ where Q is now the fluorescence quantum yield of the PS.

2.10.2. Fluorescence spectral analysis

The fluorescence spectra, corrected for the influence of tissue optical properties, were then analyzed to determine the contribution from the tissue autofluorescence, and that from PS. A skewed Gaussian was used to fit the autofluorescence while the basis spectra for PS conjugated

to each antibody/nanobody were isolated from an average of representative in-vivo spectra after subtraction of the autofluorescence [53]. We note that the width and peak of PS fluorescence was slightly different for each antibody/nanobody conjugate.

2.10.3. Calibration of the MDSFR/SFF system

Before each set ofmeasurements a careful calibration procedurewas performed as described previously [54] consisting of an integrating sphere calibration, a measurement of a calibrated light source, and measurements in water in a dark container and in a liquid phantom containing 1.32% Intralipid with a known reduced scattering coefficient ($\mu s'$ at 800 nm=1.2 mm−1). This procedure accounts for variations in the output powers of the light sources and the spectral transmission and sensitivity of the system.

2.10.4. Quantitative fluorescence spectroscopy in vivo

When OSC tumours were visible by the human eye and the BLI signal ranged between 5×10^9 and 1×10^{10} relative light units (RLU), mice were randomly divided into three groups and received an intraveneous injection of 200 µg of 7D12–PS, 7D12-9G8–PS, or R2–PS, eachmouse receiving approximately 6 nmol of PS to allow comparison. Quantitative fluorescence spectroscopy measurements were performed 0.5, 1, 2, 4, 6, 8 and 24 h after injection of the conjugates. Cetuximab–PS was employed as other mAb–PS were described in [15] (i.e. 300 µg and also approximately 6 nmol of PS per mouse) and measurements were only performed at 24 h p.i., which corresponded to the selected illumination time point.

2.11. Tumour specificity and distribution

Tumour specificity of 7D12–PS and 7D12-9G8–PS was explored by optical imaging in vivo and fluorescence imaging of tissue sections. At 1 h after injection of 7D12–PS, 7D12-9G8–PS and R2–PS (200 µg), mice were imaged (n = 2) with the Pearl imaging system (LI-COR), while kept under isoflurane anesthesia. In parallel, other mice injectedwith each of the nanobody–PS conjugates (n=1) had their tongues resected, fixed overnight in 4% formalin and embedded in paraffin blocks. Tissue was sectioned at 10 µm and fluorescence imaging was performed using the Odyssey. All images were acquired using the same settings. Further, sectionswere processed for hematoxylin and eosin (H&E) staining.

2.12. Photodynamic therapy

When OSC-19-luc2-cGFP tumourswere visible by the human eye and the BLI signal ranged between 5×10^9 and 1×10^{10} relative light units (RLU), mice (n=4 per group)were randomly divided into three groups and received an intraveneous injection of 200 µg 7D12–PS, 7D12-9G8–PS, R2–PS, or 300 µg cetuximab–PS. Based on the quantitative fluorescence spectroscopy

measurements, 1 h post-injection (p.i.) was chosen to apply the light. Thus at this time after nanobody–PS administration, or 24 h p.i. of cetuximab–PS injection, mice received painkillers, were put under isoflurane anesthesia, and their tumours were then illuminated using a 690 nm diode laser (Modulight, Tampere, Finland). The power at the end of the optic fiber was calibrated with a power meter (Gigahertz optic, Turkenfeld, Germany). Light was delivered via a 600 μmoptic fiberwith a fluence rate of 50mW/cm2 and a homogenous treatment area with the largest diameter of the tumour was used. The exposure time was adjusted to obtain a fluence of 100 J/cm2. Mice were sacrificed 24 h after illumination, tongues were collected and frozen on dry ice for subsequent processing for histological analysis of tissue damage.

2.13. Histological assessment post-PDT

To assess whether nanobody-targeted PDT is capable of inducing selective tumour cell death in vivo, and using antibody-targeted PDT as a positive control, tongues of mice were collected 24 h after application of light for PDT. Thereafter, tongues were sectioned and processed for H&E staining and for CD31 staining of blood vessels. Briefly, for the CD31 staining, sections were subjected to 10 mM tris/EDTA at 96 °C for 20 min. Thereafter, endogene peroxidase was blocked with a solution of 3% hydrogen peroxide. Blocking of aspecific staining was performed with a solution of 5% low fat milk, for 30 min. Then, the primary antibody rabbit anti-CD31 (Abcam, Cambridge, UK) and the secondary antibody goat-anti rabbit biotin (Dako, Heverlee, Belgium) were employed, followed by streptavidin-HRP (Southern Biotech, Birmingham, AL) and the final development of the brown color with DAB, and counterstained with hematoxylin. Pictures were taken with an Olympus microscope equipped with a 4×, 10× or 20× objectives. Two independent researchers scored the damage on H&E tissue sections in percentage (%) of necrosis and scored phototoxicity of normal epithelium, muscle cells, and endothelium (blood vessels), as well as edema, from 0 or 1+ to 3+ by observation of the tumour, and of the blood vessels or themuscle cells, either in close proximity or distant to the tumour. The CD31 staining was employed to score the damage of blood vessels in the tumour area by absence of the brown color. An experienced pathologist was the first observer and was responsible for the training of the second observer. At least 3 sections at different depths were analyzed per tumour. The second observer made use of the Image J software to determine % of necrosis, by drawing regions of necrosis and comparing to the overall region of the tumour. At the end, a consensus was reached on the final score.

2.14. Statistical analysis

Data was analyzed using the GraphPad Prism 5.02 software for Windows (GraphPad Software, San Diego, CA). To compare responses to PDT treatment in vitro, analysis of significance was performed through unpaired t-tests. Intrinsic fluorescence values are reported as mean and standard deviation. Statistical analysis of spectroscopy was performed through a two way ANOVA with the Bonferroni correction. As for the effect in vivo, analysis of significance was performed through Mann–Whitney test because of the non-normal distribution of the data. In all cases, p b 0.05 was considered significant.

8

Results and discussion

Targeted PDT aims to increase tumour specificity of the PS, in order to enhance the therapeutic effect and spare surrounding normal tissue. In this study, we evaluate the recently introduced nanobody–PS conjugates for their potential to induce specific tumour cell death in vivo.

3.1 Characterization and EGFR-specific binding of the nanobody–PS conjugates

The nanobodies targeting EGFR used in this study are the monovalent 7D12 [31,33] and the internalizing, biparatopic 7D12-9G8 [34]. In addition, the irrelevant nanobody R2 [40,41] is used as a negative control. These nanobodies were conjugated to the PS (IRDye700DX) via random NHS-mediated coupling to lysine amino acids, similarly to the previous study [25]. After removal of unconjugated PS, SDS-PAGE was used to verify the conjugation. The molecularweights of the fluorescent nanobody–PS conjugates, as detected by fluorescence imaging (top gel, red bands, Fig. 1A), were similar to those of the nanobodies, as demonstrated by the post-Coomassie Blue stained SDS-PAGE gel (bottom gel, black bands, Fig. 1A). Furthermore, very little unconjugated PS was detectable at the front of the gel (Fig. 1A), which rendered the conjugates suitable for both in vitro and in vivo studies. The PS-to-protein molar ratios (or degree of conjugation, DOC) of 7D12–PS, 7D12-9G8–PS and R2–PS after random conjugation were on average 0.5, 1.0 and 0.5, respectively. Compared to our previous study, these are different ratios or DOC, except for 7D12–PS. In fact, 0.5 is the highest DOC this nanobody–PS can have while maintaining its low nanomolar binding affinity. For the negative control R2–PS, we chose to use the same DOC as for 7D12–PS (i.e. 0.5, instead of 1.0). To enable the comparison of the therapeutic potential in vivo, theDOCof7D12-9G8–PS was also decreased and used as twice the DOC of 7D12–PS (i.e. 1.0, instead of 1.5). This particular choice wasmade aiming at themost effective delivery of the drug, i.e. the PS, by the least amount of carrier needed, i.e. protein, in a manner that would allow normalization of PS dose administered in vivo. Thus,with the selected DOCs, the in vivo administration of equal amounts of protein (i.e. nanobody, in micrograms), result in the administration of equal molar amounts of PS, allowing a better comparison of the therapeutic potential. These two nanobody formats (i.e. 7D12–PS and 7D12-9G8–PS) are two independent carriers used for PS delivery,which are here investigated side-by-side, as it is difficult to anticipate which format is the most promising for in vivo application. Next, the specificity of 7D12–PS and 7D12-9G8–PS for binding to EGFR was demonstrated. For that, besides the human oral squamous cell carcinoma cell line OSC (Fig. 1B), two human control cell lines were employed: the cervical cancer cell line HeLa and the colon cancer cell line SW620 (Fig. 1C). These three cell lines express high, intermediate (or normal), and very low levels of EGFR, respectively. Binding assays were performed at 4 °C to solely explore the binding of conjugates to

EGFR. Fluorescence intensities of the bound conjugates correlated well with the level of EGFR expression, i.e. OSC N HeLa N SW620. Moreover, the approximately 2-fold difference in fluorescence intensity observed between the two EGFR targeted nanobody–PS conjugates correlated well with the difference in DOC. Binding affinities of 7D12–PS and 7D12-9G8–PS to high EGFR expressing OSC cells were 1.9 $\pm$ 0.4 nM and 1.0 $\pm$ 0.1 nM, respectively; and to intermediate EGFR expressing HeLa cellswere 0.7$\pm$0.3 nMand0.5$\pm$0.07nM, respectively.Hardly any fluorescence, and thus binding, was observed for 7D12–PS and 7D12-9G8–PS to low EGFR expressing SW620 cells, and for R2–PS and PS to any of the cell lines. To emphasize the specific binding of the nanobody–PS conjugates to EGFR, fluorescence microscopy was performed (Fig. 1D). Among the three cell lines, binding of 7D12–PS and 7D12-9G8–PS was mainly observed in the high EGFR expressing OSC cells (Fig. 1D). As for R2–PS and PS, no fluorescence was observed in any of the three cell lines. Overall, comparable to our previous study, both 7D12–PS and 7D12-9G8–PS target EGFR specifically. Importantly, this water-soluble PS (IRDye700DX) has no cell binding capacity, unless it is conjugated to the EGFR targeted nanobodies. These facts together could guarantee tumour-specific PDT.

8
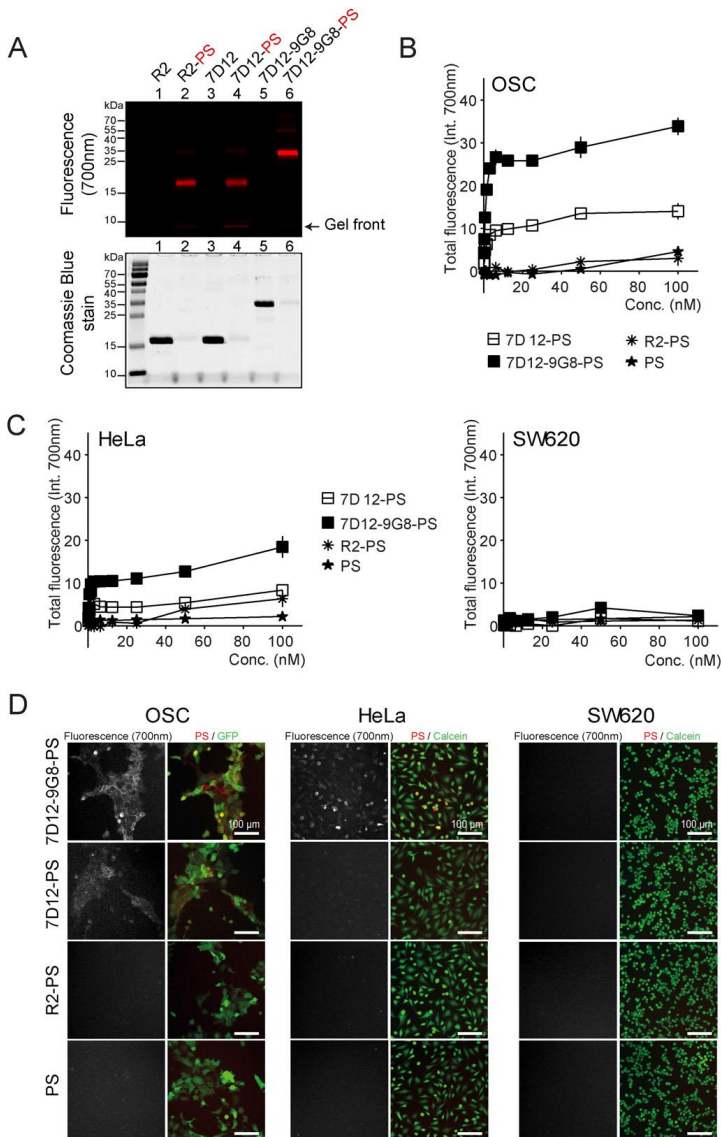
Figure 1; Purity and specificity of nanobody–PS conjugates. (A) Nanobodies and the respective nanobody–PS conjugates are separated by SDS-PAGE, with the following order (numbered 1–6): R2, R2–PS, 7D12, 7D12–PS, 7D12-9G8, and 7D12-9G8–PS. Prior to the Coomassie stain, the fluorescence of the PS is detected (depicted in red, top gel); after the Coomassie stain, the proteins are visualized (depicted in black, bottom gel). (B) Fluorescence intensities of cell bound conjugates are plotted after incubation of OSC cells or (C) the control cell lines HeLa and SW620 with varying concentrations of the EGFR targeted conjugates 7D12–PS and 7D12-9G8–PS, or the controls R2–PS and PS. EGFR expression levels: OSC N HeLa N SW620. (D) Fluorescent microscopy depicting the fluorescence of the nanobody–PS bound to cells (in white, left panels) and that (in red, right panels) overlayed with either GFP (OSC cell line) or calcein staining (HeLa, SW620) for cell visualization (in green, right panels).

3.2. Singlet oxygen quantum yield and in vitro efficacy of nanobody–PS conjugates

To determine the relative potency of these nanobody–PS conjugates, singlet oxygen quantum yields ($\phi\Delta$) were measured in test tubes. For that, first, fluorescence quantum yields were determined using a relative method in PBS and Chlorin e6 as a reference. The fluorescence quantum yields of PS, 7D12–PS and 7D12-9G8–PS were 0.15 ± 0.03, 0.14±0.03 and 0.16±0.03, respectively. Interestingly, the determined $\phi\Delta$ differed significantly between photosensitizer and conjugates: for PS it was determined to be 0.19 ± 0.06, for 7D12–PS 0.25 ± 0.06, and for 7D12-9G8–PS 0.42±0.07. Previous studies have also documented variations in fluorescence and singlet oxygen quantum yields for free PS and conjugates with different DOC [55]. The differences in $\phi\Delta$, for the two nanobody–PS conjugates, may be related to variations in amino acids to which the PS is conjugated, thus affecting the environment surrounding PS molecules. Although the efficient generation of singlet oxygen is an important factor in the induction of phototoxic effects, the localization of the PS, and variables determining this localization, also influence significantly the overall therapeutic effect. The phototoxicity of different concentrations of these conjugates was assessed in vitro following an incubation time of 30 min. This time period was based on previous work, in which we reported saturable binding of nanobody–PS conjugates after 30 min of incubation [25]. The EGFR targeted nanobody–PS conjugate 7D12-9G8–PS showed to be a very potent PDT agent on OSC cells with an IC50 value of 2.2 ± 0.97 nM (Fig. 2A). As for 7D12–PS, cell viability was decreased by 32.3% at 50 nM, suggesting an IC50 higher than 50 nM, though likely belowthe micromolar range. No reduction of cell viabilitywas observed after illumination of cells incubated with R2–PS or PS alone, indicating the need of specific targeting to induce cell damage (Fig. 2A). The difference in phototoxicity between 7D12–PS and 7D12-9G8–PS in vitro is larger than the difference in fluorescence intensity of the conjugates associatedwith the cells just before illumination (Supplementary Material, Fig. S1). This could partially be explained by the higher singlet oxygen quantum yield of 7D12-9G8–PS. Furthermore, several studies pointed to an intracellular localization of the PS as important to increase the phototoxicity of mAbs–PS [56–58]. In fact, aswe showed in our previous study, more 7D12-9G8–PS is delivered intracellularly compared to 7D12–PS,which has been described to be via clustering induced endocytosis of EGFR [25]. Thus, both aspects are likely to explain the higher potency of 7D12-9G8–PS in vitro. Our previous study showed even lower IC50 values for 7D12–PS and 7D12-9G8–PS, though that can be partly justified by a lower DOC for 7D12-9G8–PS in the current study, and also by the different EGFR expression levels of the cell lines employed. In our previous study, A431 and 14C cell lineswere employedwhich have higher EGFR expression than the OSC cells. Here, to confirm that the phototoxicity is indeed dependent on the EGFR level, toxicity was also assessed on cell lines with different EGFR expression levels (Fig. 2B, i.e. HeLa and SW620), and indeed the phototoxicitywas lower than the values obtainedwith OSC cells,which related to the extent of conjugate bound to cells

(Supplementary Material, Fig. S1), and correlated to the EGFR expression as demonstrated in Fig. 1B and C. The IC50 on HeLa cells was 33.5 ± 1.4 nM for 7D12- 9G8–PS, while 7D12–PS induced almost no effect in the concentration range here tested (i.e. highest concentration 50 nM). These are significantly lower toxicities than observed in high EGFR expressing OSC cells.No IC50 could be calculated for SW620 cells indicating the absence of cell damage on low EGFR expressing cells (Fig. 2B). Co-culture experiments were performed to assess the selectivity of these nanobody–PS conjugates toward OSC cells overexpressing EGFR, among intermediate EGFR expressing HeLa cells (Fig. 2C). In these cocultures, HeLa and OSC cells could be distinguished by the differences in morphology and GFP fluorescence imaging of cGFP transfected OSC cells (i.e. OSC-19-luc2-cGFP). 7D12–PS and 7D12-9G8–PS induced phototoxicity only to OSC cells, as indicated by the propidium iodide staining (indicative of dead cells, Fig. 2C) that coincides with GFP fluorescence. Also here, 7D12-9G8–PS showed to be more toxic than 7D12–PS, as illustrated by the higher number of dead cells. No PS nor phototoxicity was observed under the same conditions on HeLa cells (See Supplementary Material for similar treatment on these two cell lines separately, Fig. S2).
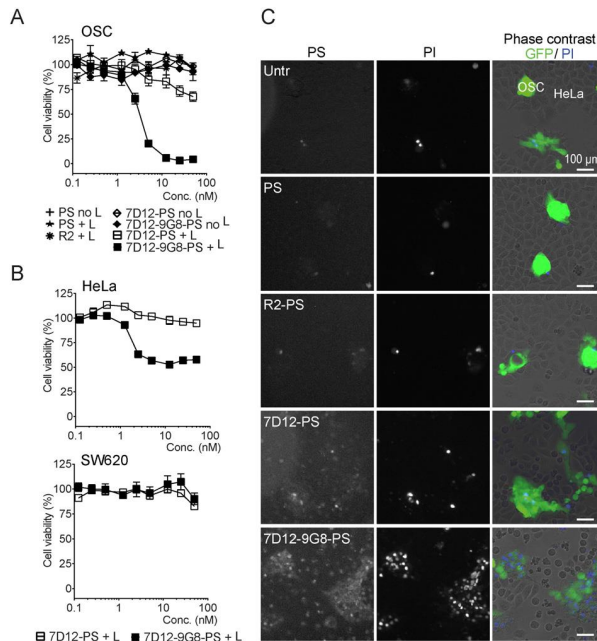
Figure 2; Nanobody–PS are phototoxic to EGFR overexpressing cells. Phototoxicity of nanobody–PS conjugates and controls in (A) OSC, (B) HeLa andSW620 cells presented as percentage (%) of cell viability after a 10 J/cm2 light dose. Data depicted as means± SEM. (C) Fluorescence and phase contrast images of co-cultures of HeLa and OSC cells after PDT with nanobody–PS conjugates or the controls R2–PS and PS. Left panel depicts PS fluorescence,middle panel propidiumiodide (PI) to identify dead cells, and right panel the overlay of PI with both GFP and phase contrast to visualize cells. Cells can be differentiated by morphology and fluorescence of the GFP (green) positive OSC cells.

3.3. Pharmacokinetics and macroscopic localization of nanobody–PS conjugates

To investigate the selectivity and potency of these nanobody–PS conjugates in a pre-clinical model of head and neck cancer, the OSC cell line was inoculated and grown orthotopically in tongues of nude mice. Being the first pre-clinical study, we have decided to use a reference for validation of the procedure here employed: we used Cetuximab–PS as Mitsunaga et al. [15] have described the use of their mAb–PS conjugates, i.e. with a DOC of 3.0 and injecting a dose of 300 μg permouse,which are equivalent to approximately 6 nmol of PS. With these particular conditions, we expected to induce tumour cell death and subsequently validate the procedure selected for analysis. Based on the selected DOC of the different nanobody–PS, the dose of protein to be injected was calculated so that it was normalized for the amount of drug carried, i.e. PS. For an effective PDT without damage to normal tissue, light should be applied locally at the most favorable time point post-injection (p.i.) of the nanobody–PS conjugates. This is when the highest dose of PS is located at the tumour, and the lowest dose in the surrounding tissues. In practice, this generally corresponds to a balance between the dose of PS at the tumour and a sufficient tumour-to-background ratio (TBR). As the nanobody–PS conjugates are traceable through optical imaging, wide field fluorescence imaging gives insights into their tumour specificity and distribution in vivo. However, the differences in optical properties of different tissues greatly influence the number of collected fluorescent photons. Alternatively, determining the intrinsic fluorescence enables a quantitative comparison of fluorescence's pharmacokinetics locally in tissues with different and/or varying optical properties (such as in tumour, normal tongue, and skin). Our group has been investigating the use of empiricalmodeling and point reflectance spectroscopy with multi-diameter optical fibers (MDSFR) combined with single fiber fluorescence spectroscopy (SFF) to measure the tissue optical properties μ_a, μ'_s, and thereby recovering the intrinsic fluorescence fromthe interrogated volume [52]. This approach is particularly important when the optical properties of tumour and normal tissue are known to be significantly different [51]. Using this method, the quantitative fluorescence pharmacokinetics were assessed for the PS (IRDye700DX) in each conjugate. The intrinsic fluorescence reported in this study, defined as $Q_f \mu_a^f$, is the product of the fluorescence quantum yield of the PS and its absorption coefficient at 660 nm.While reliable estimates of Q_f and the in vivo extinction spectrum of the PS would allow for the quantitative determination of its concentration in vivo, we considered it sufficient for this study to determine the intrinsic fluorescence. No significant differenceswere observed in normal tongue tissue between all conjugates. At all time points, significantly less R2–PS was present in the tumour compared to 7D12–PS and 7D12-9G8–PS (p b 0.05 for all time point) (Fig. 3A). For 7D12–PS, more conjugate was present in the tumour compared to that in normal tongue tissue and skin, proving tumour specificity in vivo. Differences were statistically significant (p b 0,05) at time-point 0.5, 1, 6 and 24 h p.i. The maximum amount of 7D12–PS in the tumour was observed already at 30 min p.i., after which it

slowly decreased, correlating with our previous imaging study [31], and possibly related to the unbinding of non-internalized conjugates. However, a relatively high value of fluorescence was also present in normal tongue tissue at 30min p.i. At 1 h p.i. the fluorescence at the normal tongue tissue decreased slightly and a TBR of 1.8 ± 0.3 was obtained. Although at a later time point the TBR increased, such as to a value of 16.1 ± 4.5 at 24 h p.i. (Fig. 3B), the total fluorescence of 7D12–PS in the tumour at 24 h p.i. had already decreased 42% from the intrinsic fluorescence at 1 h p.i. Differences in TBR of 7D12–PS, compared to R2–PS, were statistically significant at 24 h p.i (p b 0.0001). Similar results were obtained for 7D12-9G8–PS, showing tumour specificity in vivo as significantly more conjugate was present in the tumour compared to that in normal tongue tissue and skin (p b 0.05 for all time points, except for 8 h p.i.). Unlike 7D12–PS, the highest intrinsic fluorescence at the tumour was observed for a longer period, i.e. during the first 4 h p.i., which is possibly related to a more pronounced internalization and less unbinding of non-internalized conjugate. Already at 1 h p.i. a TBR of 3.8 ± 0.5 was obtained. Also in this case, higher TBR could be obtained at later time points, such as 30.8 ± 0.9 at 24 h p.i. The differences in TBR of 7D12-9G8–PS, compared to R2–PS, were statistically significantly at both 1 and 24 h p.i. (p = 0.0024 and p b 0.0001, respectively). However 24 h p.i. the intrinsic fluorescence had also in this case decreased 39%, compared to 1 h after the injection. One could expect that high TBRs are needed to spare normal tissue, and to enable accurate tumour detection with fluorescence imaging (in the setting of image-guided PDT). Nevertheless, in principle, the actual amount of PS in the tissue predominantly determines the actual phototoxic effect. Therefore, in order to maximize the concentration of PS while retaining a suitable TBR, we decided to subsequently apply the light locally at the tumour 1 h p.i. of the nanobody–PS conjugates. Clear differences were observed on the values of intrinsic fluorescence of the two EGFR targeted nanobody–PS conjugates, where higher values were obtained for 7D12-9G8–PS in the tumour at all times, compared to 7D12–PS. Thus, 7D12-9G8–PS seems to be the best nanobody format to carry PS to the tumour. Although additional experiments are needed to further clarify these differences, at this pointwe can speculate that these could be related to the different nanobody formats, i.e.monovalent versus biparatopic, and their different distribution and binding in tumours. In fact, the enhanced internalization documented for 7D12-9G8 in vitro [25] could play an important role. We have observed more internalization of 7D12-9G8–PS than 7D12–PS, after 30 min incubation in vitro, thus at 1 h after i.v. injection it is well possible that the same trend can affect the results observed in vivo. In addition, differences are to some extent related to the different DOC of the nanobody–PS, as this was 0.5 for 7D12–PS and 1.0 for 7D12-9G8–PS. Although, the equal dose of protein given (in micrograms) allowed the injection of equal amounts of PS molecules per mouse, approximately half of the 7D12 molecules were conjugated to PS, whereas all molecules of 7D12-9G8 injected contained a PS. As a consequence, competition of conjugated 7D12–PS and unconjugated 7D12 for binding to the EGFR, could

A

⊖ Tumor   ⊟ Tongue   ▲ Skin
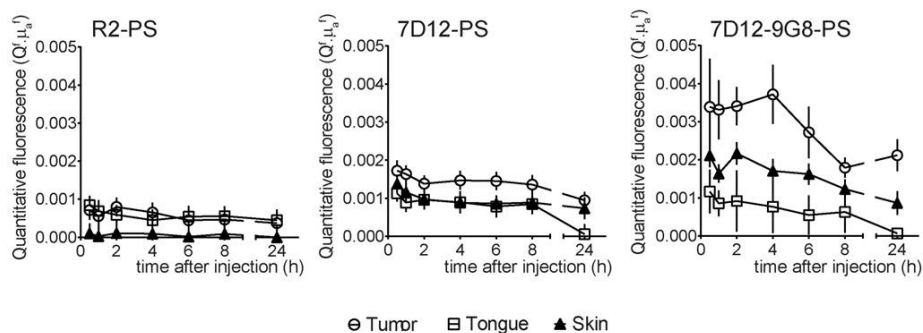
B
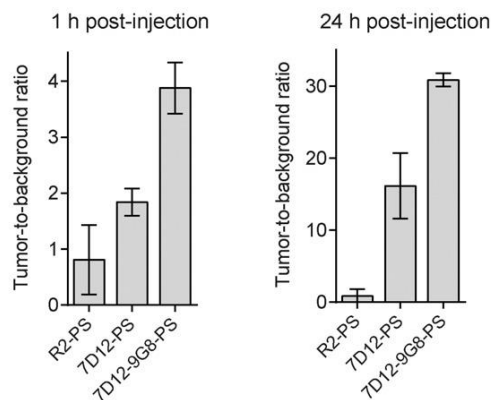
Figure 3; Quantitative fluorescence spectroscopy for selecting the illumination time point. (A) Local assessment of the intrinsic fluorescence of the nanobody–PS conjugates at the tumour, normal tongue and skin, as an indication of their pharmacokinetics. Intrinsic fluorescence, Qfμa f , is the product of the fluorescence quantum yield of the PS and its absorption coefficient at 660 nm. Average values of Qfμa f are calculated from 0 to 24 h after injection of nanobody–PS conjugates. (B) Tumour-to-background ratio (TBR) at 1 h and 24 h p.i. of the different nanobody–PS conjugates, calculated from intrinsic fluorescence measurements. Error bars represent the standard deviation of the calculated TBRs.

have contributed to the lower intrinsic fluorescence and TBRs of 7D12–PS, compared to 7D12-9G8–PS. In order to further elucidate the mechanism(s) underlying the efficacy of our conjugates compared to that of a mAb–PS conjugate, we also performed quantitative spectroscopy in animals 24 h after the injection of cetuximab–PS (which was the time point employed in previous studies for mAb–PSs [15], with DOC of 3.0, equivalent PS injected as the other mice). At this time point the average value of Qfμa f was 0.0374 ± 0.0045, 0.0057 ± 0.0019 and 0.0036 ± 0.0007, in tumour, normal tongue, and in skin, respectively, with a corresponding TBR of 6.5 ± 0.9. These tumour values for Qfμa f are significantly greater (~7.5-fold) than the maximum fluorescence intensity early after the injection of 7D12-9G8–PS and the TBR exceeds the TBR

found for 7D12-9G8–PS at 1 h p.i. Despite the same dose of PS had been injected with this mAb–PS as with the nanobody–PS conjugates, these results suggest that the mAb–PS is the most effective carrier for higher accumulation of PS at the tumour. This is likely a consequence of a combination of the longer half-life of cetuximab–PS in the blood stream, which leads to later accumulation of the conjugate at the tumour (i.e. 24 h instead of 1 h p.i.), and the higher DOC of cetuximab–PS. It is important to note that quantitative spectroscopy provides a volume average signal (over ~1 mm3) and does not retain any information on themicroscopic distribution of the conjugates. Therefore, additional studies are required to compare themicroscopic localization of the different conjugates.

To further validate the 1 h p.i. as being the optimal time point for illumination, a number ofmice (n=2)were subjected to in vivo optical imaging at that time point after injection of the different nanobody–PS conjugates. Clearly, very little fluorescence is observed at the tongue when R2–PS was injected, in contrast to the highly fluorescent tongues shown when mice were injected with either 7D12–PS or 7D12-9G8–PS (Fig. 4A). These images support the specificity documented earlier (Fig. 3). In parallel, tongues of mice were collected 1 h p.i. of the nanobody–PS conjugates and were processed for fluorescence imaging and histology. These analyses confirmed that both EGFR targeted conjugates are tumour specific. Already at 1 h p.i. of 7D12–PS and 7D12-9G8–PS, a clear colocalization of fluorescence and tumour could be observed, confirming tumour specificity (Fig. 4B). No tumour accumulation was observed in sections of tongues of mice injected with the control R2–PS. Importantly, nanobody–PS conjugates showed a homogenous distribution through the solid tumour,which is in agreement with our previous optical imaging study [31] and is expected to contribute to treatment efficacy.
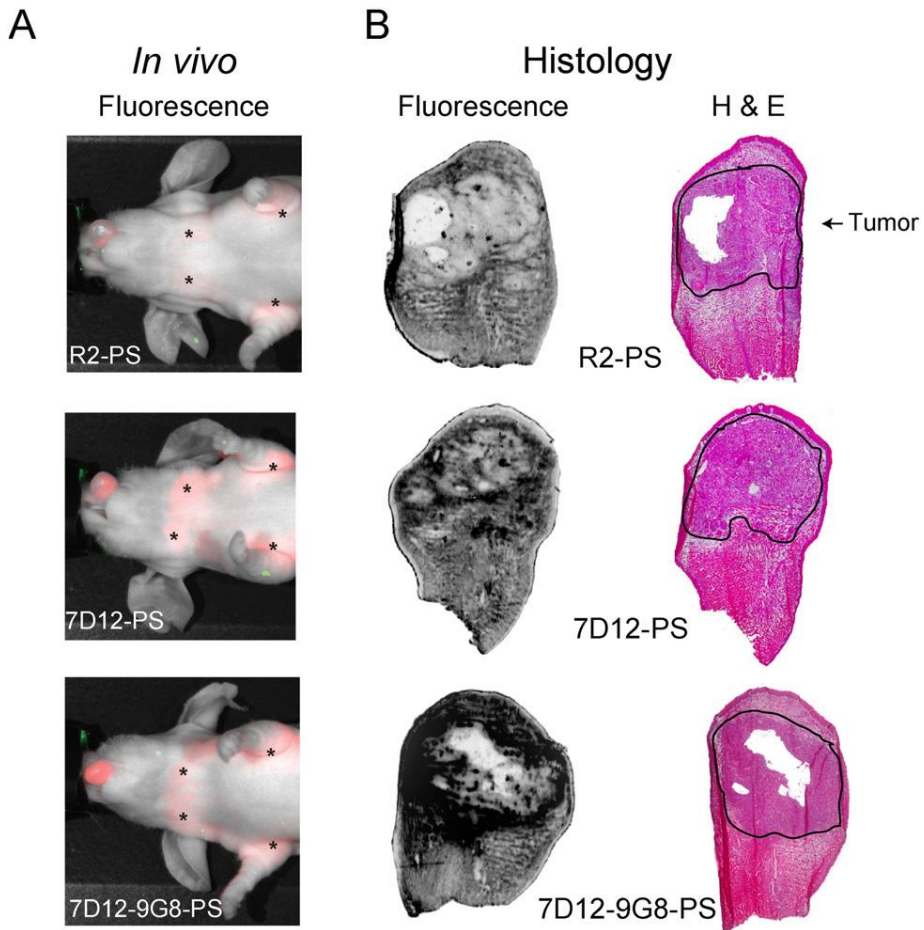
Figure 4; EGFR-targeted nanobody–PS conjugates specifically localize in tumours. (A) Optical imaging of mice 1 h p.i. of the nanobody–PS conjugates. Images were obtained with a Pearl imaging system. Brightness of individual illustrations is manually adjusted to highlight the location of the fluorescence. Asterisks (*) indicate lymph nodes. (B) Fluorescence imaging of the PS (in dark) and H&E staining of sections of tongues obtained from mice 1 h p.i. of the nanobody–PS conjugates. OSC tumours are distinguished at the higher half of the tongues, by a characteristic dense mass of tumour cells, delimited by a dark line.

3.4. In vivo evaluation of nanobody-targeted PDT

Besides the best time point for illumination (i.e. 1 h p.i.), an important consideration for optimizing the efficacy of the nanobody–PS conjugates in vivo is the choice of PDT illumination parameters: fluence and fluence rate. The latter was chosen to be 50 mW/cm2 to avoid any heating of the illuminated tissue and to maximize the ability of the tumour vasculature to supply oxygen during illumination. The former parameter, the therapeutic light fluence (or dose) was chosen to be 100 J/cm2 in order to maximize PDT efficacy, considering the penetration of the laser light (690 nm, which is the excitation maximum for this PS) in the tongue and the inevitable photobleaching of the PS during the illumination. It is important to note that this light fluence may be reduced, in the future, after a full optimization of the illumination parameters has been performed. Given the difficulty of light fluence (rate) treatment planning in mice, we chose to accept the potential overtreatment of the underlying normal tissue in the present study. Thus, 1 h p.i. of the nanobody–PS conjugates, illumination was performed superficially on the tongue of mice. As positive control for in vivo PDT, we injected mice with cetuximab–PS, which were then illuminated 24 h p.i., similar to the study of Mitsunaga et al. [15]. Thereafter, to determine whether the conjugates were capable of inducing selective tumour cell death in vivo, mice were sacrificed at 24 h post-PDT and their tongues were processed for histological analyses. All the controls, i.e. light only and R2–PS, 7D12–PS and 7D12-9G8–PS without application of light, presented a viable and dense tumour (H&E), as well as numerous blood vessels (CD31 staining), indicating that neither light alone, nor the nanobody–PS conjugates without light were capable of inducing damage (Fig. 5A). The antibody-targeted PDT led to tumour damage, which validates the model and procedure here employed, although with a broad variation of degree of necrosis, ranging from 25 to 70% (median 57.5%, Fig. 5A, B). Numerous blood vessels remained intact after this PDT, as observed in the corresponding CD31 staining. An unexpected mild to moderate tumour damage was obtained with R2–PS (median 42.5%, range 20–50% necrosis, Fig. 5B), likely a bystander effect due to vascular damage, as suggested by the heavily coagulated blood vessels observed just below the tip of the tongue and the absence of CD31 staining in the tumour area, though viable tumour is still observed (Fig. 5A, Table 1). Whether R2–PS is specifically associating with endothelial cells is not clear at this point in time, though this may be an explanation for these observations. On the contrary, for both nanobody formats targeting EGFR, a more homogenous damage to the tumour is observed, reaching even 90% of necrosis (Fig. 5A, B). In the case of 7D12–PS, a very localized and reproducible damage was induced at the tumour site (median 80%, range 80–90% necrosis), with minimal effect on the CD31 staining of blood vessels around the tumour (brown color present), whereas inside the tumour no CD31 staining was observed (Fig. 5A, Table 1). With 7D12-9G8–PS, some variation between mice was observed in the extent of damage induced (median 80%, range 60–90% necrosis), and slightly more coagulation was observed at the blood vessels surrounding the tumour (compared

to 7D12–PS) (Fig. 5A, Table 1). Notably, the two EGFR targeted nanobodyphotosensitizer conjugates were the only format of conjugates capable of inducing 90% necrosis (Fig. 5B). 7D12–PS induced significantly more necrosis compared to both R2–PS (p = 0.0256) and cetuximab–PS (p = 0.0265) (Fig. 5B). Due to the variation in effect induced in mice with 7D12-9G8–PS, the extent of necrosis was significantly higher compared to R2–PS (p = 0.0284), but not compared to cetuximab–PS (p = 0.1102) (Fig. 5B). Interestingly, although spectroscopy experiments showed a significantly higher concentration of cetuximab–PS at the time point of irradiation compared to 7D12-9G8–PS and 7D12–PS, significantly more necrosis was observed with the nanobody–PS conjugates. In fact, these in vivo results suggest that the most effective and reproducible treatment was obtained with the monovalent 7D12–PS conjugate. Importantly, we realize that at this point conclusions should be very carefully drawn as these are in fact three different antibody formats and thus three independent carrier systems for PS, here investigated side-by-side in very particular conditions. Nevertheless, these results are remarkable, in light of the observations obtained with quantitative fluorescence spectroscopy revealing a lower concentration of PS and lower TBR obtained with the 7D12–PS conjugate, compared to 7D12-9G8–PS or cetuximab–PS. Furthermore, while 7D12-9G8–PS was more toxic than 7D12–PS in vitro (Fig. 2), also in respect of induction of necrosis (Supplementary Material, Fig. S3), in vivo efficacy studies point to a higher phototoxicity induced by 7D12–PS. This increase in efficacy of themonovalent 7D12–PS could be due to its small size,which likely enables better penetration into the interior of tumours and a more homogenous distribution. It is well accepted that the diffusion of molecules from the blood vessels and their subsequent penetration through tissues is influenced by factors such as molecular weight, size, charge, affinity, and antigen expression among others [59,60]. Furthermore, using small nanobodies, the PS is in closer proximity to the cell membrane which could increase phototoxicity. More studies are certainly needed to better understand the differences observed in PDT efficacy between 7D12–PS and 7D12-9G8–PS in vivo, and future studies will also demonstratewhether the significant differences in necrosiswill result in differences in survival. However, at this point, it is clearly suggested that the overall amount of PS accumulated in the tumour is not per se the limiting factor for efficacy, but theway it is distributed is likely very critical. The more homogenous and reproducible degree of damage induced by 7D12–PS, as compared to cetuximab–PS, is in agreement with our former study showing differences in intratumoural distribution of 7D12 and cetuximab in A431 xenografts [31]. In a similar context, Watanabe et al. [24] have recently compared a mAb–PS (150 kDa) with a minibody–PS (80 kDa) and a diabody–PS (50 kDa), where the PS was IRDye700DX, and found that the use of the smallest fragment (in this case a diabody) resulted in the shortest time interval between injection and light exposure without compromising therapeutic efficacy. These results differ from ours, in that we found a difference in phototoxicity with our nanobody–PS conjugates (15 or 30 kDa), to the advantage of the smaller nanobody–PS conjugates compared to

the antibody–PS conjugate. The disparity between these results could be explained by the differences in format and/or size of diabody–PS and nanobody–PS conjugates. Besides the extent of damaged tumour, damage to the epithelium and other features were also scored (Table 1, with examples given in Fig. 5C). Overall, no significant damage to the epithelium was induced by any of the treatments, other than the damage likely associated with handling of the tongues with a pincette. Damage to muscle cells was common to all treatments on the cells nearest to the tumour, but absent in muscle cells away from the tumour. Blood vessel damage varied for the different groups, although the trend was a more pronounced damaged in the tumour or in blood vessels surrounding the tumour and no damage further away from the tumour. Due to necrosis, the damage to muscle cells and blood vessels inside the tumour was not possible to score accurately from H&E sections. Edema was always present, while the extent of infiltration of neutrophils or mast cells varied, suggesting that PDT mediated by this PS (IRDye700DX) is also capable of recruiting immune cells. Future studies will have to prove how these inflammatory responses affect overall treatment efficacy. Vascular targeted PDT is very dependent on the time interval between PS administration and illumination. Here, we have selected 1 h p.i. for the nanobody–PS conjugates and 24 h p.i. for cetuximab–PS, to promote tumour targeted PDT. Shorter intervals could possibly lead to more vascular damage, also risking damage to normal tissues. Clearly, the time point selected was appropriate for 7D12–PS and 7D12-9G8–PS as this resulted in minimal damage of blood vessels and normal muscle cells around the tumour and no damage of blood vessel and normal muscle cells away from the tumour area. These details also indicate that high TBRs are not a requirement, in this particular form of PDT, to damage the tumour and spare normal tissue (TBRs obtained were 1.8 ± 0.3 for 7D12–PS and 3.8 ± 0.5 for 7D12-9G8–PS). This is an interesting observation that could have important implications for the PDT field. Possibly, it is an effect of this particular PS, as this PS does not lead to any damage unless it is conjugated to a targeting molecule (nanobody) that binds to cells. Furthermore, the observation of minimal damage around the tumour also suggests appropriate selection of the fluence for the illumination. In fact, as much as the laser was pointed to the tumour, normal tissue surrounding it was certainly also exposed to the illumination to some extent. Additionally, the light only control (Fig. 5A) also proved that the selected parameters are safe for normal tissues. Further in vivo research focused on varying nanobody–PS conjugate dose, illumination time point, and fluences for shorter treatment times, could optimize this protocol further. In such protocol optimization, quantitative fluorescence spectroscopy may be of substantial benefit, allowing patient- and tumour-specific planning for illuminations. The considerable efforts made in the field to render PDT tumour specific [14,61–63] have recently resulted in first-in-human trials, such as NCT02422979 (clinicaltrials.gov), which is testing an antibody–PS conjugate composed of cetuximab and IRDye700DX. This trial will certainly have an impact in the field and hopefully stimulate additional trials that will encourage the use of targeted PDT as a standard

treatment in the clinic. Even though antibody-targeted PDT has now entered a clinical trial, as demonstrated in this study, nanobody-targeted PDT has the potential to even further improve clinical PDT: through rapid accumulation and fast clearance of the conjugates, enabling light application very shortly after conjugate administration and minimizing possible photosensitivity. Thesewould likely bring benefits in respect of hospital management and costs involved per treatment. In fact, nanobodytargeted PDT has great potential to be translated to the clinic. First, because the PS investigated here is already being employed in a clinical trial, and second, because nanobodies have been in clinical trials for several years in areas other than oncology (e.g. antithrombotic nanobody [64]). The possibility for clinical translation surely should encourage additional research to further explore this approach of nanobody-targeted PDT.

Table 1
Several features are scored to characterize the damage observed in Fig. 5.

	Controls	R2–PS	Cet–PS	7D12–PS	7D12-9G8–PS
Edema	+	++	++	++	++/+++
Presence of mast cells	+	+/++	+	+	+
Presence of neutrophils	−	+/++	+++	++	+/++
Damage to muscle cells					
Around the tumor	−	+	+	+/++	+
Away from tumor	−	−	−	−	−
Damage to epithelium	−	5–10%	5–10%	5–10%	5%
Damage to blood vessels (H&E)					
Around the tumor	−	++	+	+/++	++
Away from tumor	−	−	−	−	−
Absence of CD31 stain					
Inside the tumor	−	++/+++	++/+++	+++	++/+++
Around the tumor	−	+	+	+	+
Away from the tumor	−	−	−	−	−
Remarks	−	Coagulation	−	−	−

8
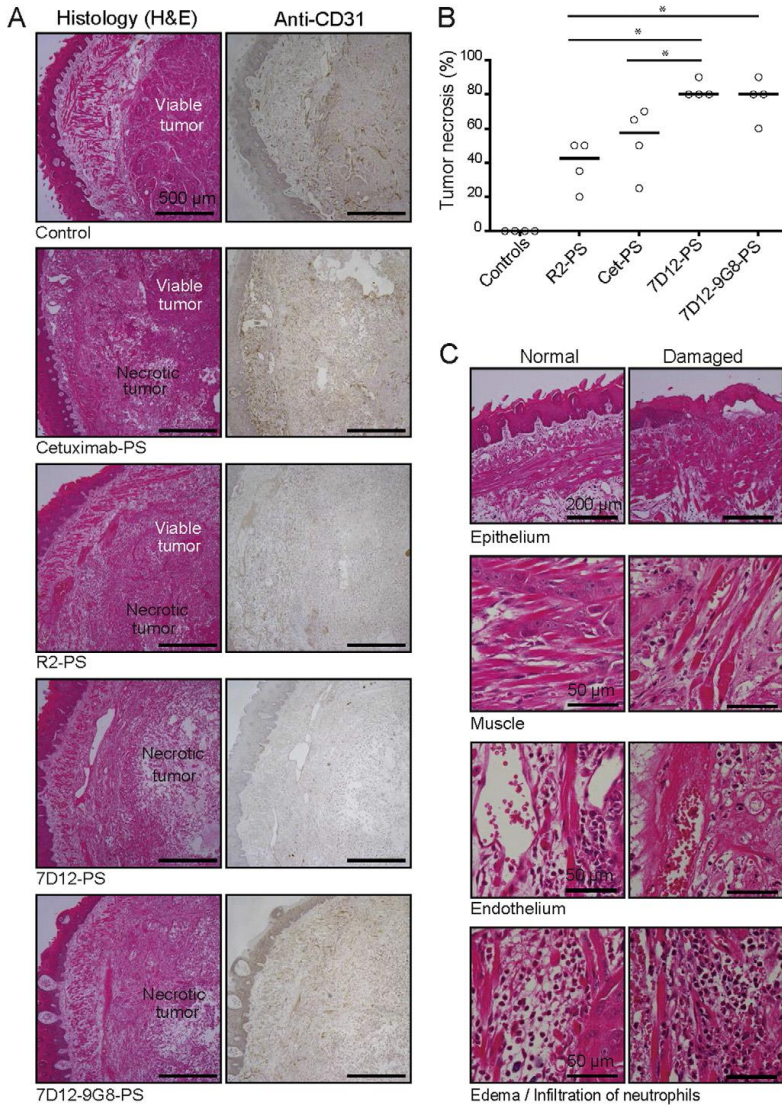
Figure 5; In vivo tumour specific phototoxicity of nanobody–PS conjugates. (A) Sections of tongues of mice collected 24 h post-PDT, processed for histology (H&E) and anti-CD31 staining to assess phototoxicity of the different treatments: intravenous administration of R2–PS, 7D12–PS or 7D12-9G8–PS followed by illumination 1 h p.i., or cetuximab–PS followed by illumination 24 h p.i. These are compared to the controls: light alone or each nanobody–PS conjugate without illumination. Each image is representative of the results obtained for that group. Areas of viable or necrotic tumour are indicated and blood vessels are highlighted by the anti-CD31 staining (in brown). (B) Percentages (%) of tumour necrosis obtained for each single treatment are depicted together with the median value. (C) Representative examples of damage to the epithelium, muscle cells, endothelium, and of edema and infiltration of neutrophils indicating recruitment of immune cells.

Conclusions

Overall, the EGFR targeted nanobody–PS conjugates 7D12–PS and 7D12-9G8–PS are selective and potent PDT agents that specifically accumulate in tumours in vivo. Upon local illumination within 1 h after administration, these conjugates lead to pronounced tumour necrosis and to the infiltration of immune cells. This study highlights the therapeutic potential of these novel nanomedicines and stimulates further research, contributing to the exploration of nanobody-targeted PDT.

8

Acknowledgements

Conflict of interest.

The authors declare that they have no conflicts of interest.

8

References

1   I.A.f.R.o.C.W.H. Organisation, Globocan 2012: Estimated Cancer Incidence,Mortatlity and Prevalence Worldwide in 2012, 2012.

2   L.A. Torre, F. Bray, R.L. Siegel, J. Ferlay, J. Lortet-Tieulent, A. Jemal, Global cancer statistics, 2012, CA Cancer J. Clin. 65 (2015) 87–108.

3   P. Agostinis, K. Berg, K.A. Cengel, T.H. Foster, A.W. Girotti, S.O. Gollnick, S.M. Hahn, M.R. Hamblin, A. Juzeniene, D. Kessel, M. Korbelik, J. Moan, P. Mroz, D. Nowis, J. Piette, B.C. Wilson, J. Golab, Photodynamic therapy of cancer: an update, CA Cancer J. Clin. 61 (2011) 250–281.

4   B. Green, A.R. Cobb, C. Hopper, Photodynamic therapy in themanagement of lesions of the head and neck, Br. J. Oral Maxillofac. Surg. 51 (2013) 283–287.

5   B. Karakullukcu, H.J. Nyst, R.L. van Veen, F.J. Hoebers, O. Hamming-Vrieze, M.J. Witjes, S.A. deVisscher, F.R.Burlage,P.C. Levendag, H.J. Sterenborg, I.B.Tan,mTHPCmediated interstitial photodynamic therapy of recurrent nonmetastatic base of tongue cancers: development of a new method, Head Neck 34 (2012) 1597–1606.

6   A.E. O'Connor,W.M. Gallagher, A.T. Byrne, Porphyrin and nonporphyrin photosensitizers in oncology: preclinical and clinical advances in photodynamic therapy, Photochem. Photobiol. 85 (2009) 1053–1074.

7   R.R. Allison, G.H. Downie, R. Cuenca, X.H. Hu, C.J. Childs, C.H. Sibata, Photosensitizers in clinical PDT, Photodiagn. Photodyn. Ther. 1 (2004) 27–42.

8   R.R. Allison, C.H. Sibata, Oncologic photodynamic therapy photosensitizers: a clinical review, Photodiagn. Photodyn. Ther. 7 (2010) 61–75.

9   C.J. Gomer, Preclinical examination of first and second generation photosensitizers used in photodynamic therapy, Photochem. Photobiol. 54 (1991) 1093–1107.

10   A.S. Derycke, P.A. de Witte, Liposomes for photodynamic therapy, Adv. Drug Deliv. Rev. 56 (2004) 17–30.

11   G.A. van Dongen, G.W. Visser, M.B. Vrouenraets, Photosensitizer–antibody conjugates for detection and therapy of cancer, Adv. Drug Deliv. Rev. 56 (2004) 31–52.

12   S.A. Sibani, P.A. McCarron, A.D.Woolfson, R.F. Donnelly, Photosensitiser delivery for photodynamic therapy. Part 2: systemic carrier platforms, Expert Opin. Drug Deliv. 5 (2008) 1241–1254.

13   W.M. Sharman, J.E. van Lier, C.M. Allen, Targeted photodynamic therapy via receptor mediated delivery systems, Adv. Drug Deliv. Rev. 56 (2004) 53–76.

14   N.S. Soukos, M.R. Hamblin, S. Keel, R.L. Fabian, T.F. Deutsch, T. Hasan, Epidermal growth factor receptor-targeted immunophotodiagnosis and photoimmunotherapy of oral precancer in vivo, Cancer Res. 61 (2001) 4490–4496.

15   M. Mitsunaga, M. Ogawa, N. Kosaka, L.T. Rosenblum, P.L. Choyke, H. Kobayashi, Cancer cell-selective in vivo near infrared photoimmunotherapy targeting specific membrane molecules, Nat. Med. 17 (2011) 1685–1691.

16   R.A. Beckman, L.M. Weiner, H.M. Davis, Antibody constructs in cancer therapy: protein engineering strategies to improve exposure in solid tumours, Cancer 109 (2007) 170–179.

17   G.M. Thurber, S.C. Zajic, K.D.Wittrup, Theoretic criteria for antibody penetration into solid tumours and micrometastases, J. Nucl. Med. 48 (2007) 995–999.

18   I. Bronshteint, S. Aulova, A. Juzeniene, V. Iani, L.W. Ma, K.M. Smith, Z. Malik, J.Moan, B. Ehrenberg, In vitro and in vivo photosensitization by protoporphyrins possessing different lipophilicities and vertical localization in the membrane, Photochem. Photobiol. 82 (2006) 1319–1325.

19   L.R. Duska,M.R. Hamblin,M.P. Bamberg, T. Hasan, Biodistribution of charged F(ab')2 photoimmunoconjugates in a xenograft model of ovarian cancer, Br. J. Cancer 75 (1997) 837–844.

20   M.K. Kuimova,M. Bhatti,M. Deonarain, G. Yahioglu, J.A. Levitt, I. Stamati, K. Suhling, D. Phillips, Fluorescence characterisation of multiply-loaded anti-HER2 single chain Fv-photosensitizer conjugates suitable for photodynamic therapy, Photochem Photobiol. Sci. 6 (2007) 933–939.

21   C. Staneloudi, K.A. Smith, R. Hudson, N.Malatesti, H. Savoie, R.W. Boyle, J. Greenman, Development and characterization of novel photosensitizer: scFv conjugates for use in photodynamic therapy of cancer, Immunology 120 (2007) 512–517.

22   M. Bhatti, G. Yahioglu, L.R. Milgrom, M. Garcia-Maya, K.A. Chester, M.P. Deonarain, Targeted photodynamic therapy with multiply-loaded recombinant antibody fragments, Int. J. Cancer 122 (2008) 1155–1163.

23   L.R. Milgrom, Towards recombinant antibody-fragment targeted photodynamic therapy, Sci. Prog. 91 (2008) 241–263.

24   R. Watanabe, H. Hanaoka, K. Sato, T. Nagaya, T. Harada, M. Mitsunaga, I. Kim, C.H. Paik, A.M. Wu, P.L. Choyke, H. Kobayashi, Photoimmunotherapy targeting prostate-specific membrane antigen: are antibody fragments as effective as antibodies? J. Nucl. Med. 56 (2015) 140–144.

25   R. Heukers, P.M. van Bergen En Henegouwen, S. Oliveira, Nanobody-photosensitizer conjugates for targeted photodynamic therapy, Nanomed.: Nanotechnol., Biol. Med. 10 (2014) 1441–1451.

26   C. Hamers-Casterman, T. Atarhouch, S. Muyldermans, G. Robinson, C. Hamers, E.B. Songa, N. Bendahman, R. Hamers, Naturally occurring antibodies devoid of light chains, Nature 363 (1993) 446–448.

27   S. Oliveira, R. Heukers, J. Sornkom, R.J. Kok, P.M. van Bergen En Henegouwen, Targeting tumours with nanobodies for cancer imaging and therapy, J. Control. Release 172 (2013) 607–617.

28   S. Muyldermans, Nanobodies: natural single-domain antibodies, Annu. Rev. Biochem. 82 (2013) 775–797.

29   S. Muyldermans, T. Atarhouch, J. Saldanha, J.A. Barbosa, R. Hamers, Sequence and structure of VH domain from naturally occurring camel heavy chain immunoglobulins lacking light chains, Protein Eng. 7 (1994) 1129–1135.

30   M. Kijanka, F.J. Warnders, M. El Khattabi, M. Lub-de Hooge, G.M. van Dam, V. Ntziachristos, L. de Vries, S. Oliveira, P.M. van Bergen En Henegouwen, Rapid optical imaging of human breast tumour xenografts using anti-HER2 VHHs site-directly conjugated to IRDye 800CW for image-guided surgery, Eur. J. Nucl. Med.Mol. Imaging 40 (2013) (1718-1729).

31   S. Oliveira, G.A. van Dongen,M. Stigter-vanWalsum, R.C. Roovers, J.C. Stam,W. Mali, P.J. van Diest, P.M. van Bergen en Henegouwen, Rapid visualization of human tumour xenografts through optical imaging with a near-infrared fluorescent anti-epidermal growth factor receptor nanobody, Mol. Imaging 11 (2012) 33–46.

8

32   M.M. Schmidt, K.D.Wittrup, Amodeling analysis of the effects ofmolecular size and binding affinity on tumour targeting, Mol. Cancer Ther. 8 (2009) 2861–2871.

33   L.O. Gainkam, L. Huang, V. Caveliers, M. Keyaerts, S. Hernot, I. Vaneycken, C. Vanhove, H. Revets, P. De Baetselier, T. Lahoutte, Comparison of the biodistribution and tumour targeting of two 99mTc-labeled anti-EGFR nanobodies in mice, using pinhole SPECT/micro-CT, J. Nucl. Med. 49 (2008) 788–795.

34   R.C. Roovers, M.J. Vosjan, T. Laeremans, R. el Khoulati, R.C. de Bruin, K.M. Ferguson, A.J. Verkleij, G.A. van Dongen, P.M. van Bergen en Henegouwen, A biparatopic anti-EGFR nanobody efficiently inhibits solid tumour growth, J. Int. Cancer 129 (2011) 2013–2024.

35   J.R. Grandis, D.J. Tweardy, Elevated levels of transforming growth factor alpha and epidermal growth factor receptor messenger RNA are early markers of carcinogenesis in head and neck cancer, Cancer Res. 53 (1993) 3579–3584.

36   K.K.Ang, B.A. Berkey, X. Tu,H.Z. Zhang,R.Katz, E.H. Hammond, K.K. Fu, L.Milas, Impact of epidermal growth factor receptor expression on survival and pattern of relapse in patients with advanced head and neck carcinoma, Cancer Res. 62 (2002) 7350–7356.

37   X. Peng, D.R. Draney, W.M. Volcheck, G.R. Bashford, D.T. Lamb, D.L. Grone, Y. Zhang, C.M. Johnson, Phthalocyanine dye as an extremely photostable and highly fluorescent near-infrared labeling reagent, 2006 (pp. 60970E-60970E-60912).

38   R. Heukers, J.F. Vermeulen, F. Fereidouni, A.N. Bader, J. Voortman, R.C. Roovers, H.C. Gerritsen, P.M. van Bergen En Henegouwen, Endocytosis of EGFR requires its kinase activity and N-terminal transmembrane dimerization motif, J. Cell Sci. 126 (2013) 4900–4912.

39   K.R. Schmitz, A. Bagchi, R.C. Roovers, P.M. van Bergen en Henegouwen, K.M. Ferguson,Structural evaluation of EGFR inhibition mechanisms for nanobodies/VHH domains, Structure 21 (2013) 1214–1224.

40   L.G. Frenken, R.H. van der Linden, P.W. Hermans, J.W. Bos, R.C. Ruuls, B. de Geus, C.T. Verrips, Isolation of antigen specific llama VHH antibody fragments and their high level secretion by Saccharomyces cerevisiae, J. Biotechnol. 78 (2000) 11–21.

41   E. Dolk, C. van Vliet, J.M. Perez, G. Vriend, H. Darbon, G. Ferrat, C. Cambillau, L.G. Frenken, T. Verrips, Induced refolding of a temperature denatured llama heavychain antibody fragment by its antigen, Proteins 59 (2005) 555–564.

42   P.B. van Driel, J.R. van der Vorst, F.P. Verbeek, S. Oliveira, T.J. Snoeks, S. Keereweer, B. Chan, M.C. Boonstra, J.V. Frangioni, P.M. van Bergen en Henegouwen, A.L. Vahrmeijer, C.W. Lowik, Intraoperative fluorescence delineation of head and neck cancer with a fluorescent anti-epidermal growth factor receptor nanobody, Int. J. Cancer 134 (2014) 2663–2673.

43   J. Lakowicz, Principles of Fluorescence Spectroscopy, third ed. Springer, New York, 2006. E. Zenkevich, E. Sagun, V. Knyukshto, A. Shulga, A.Mironov, O. Efremova, R. Bonnett, S.P. Songca, M. Kassem, Photophysical and photochemical properties of potential porphyrin and chlorine photosensitizers for PDT, J. Photochem. Photobiol. B Biol. 33 (1996) 171–180.

44   M.V. Parkhots, V.N. Knyukshto, G.A. Isakov, P.T. Petrov, S.V. Lepeshkevich, A. Ya, Khairullina, B.A. Dzhagarov, Spectral-luminescent studies of the "Photolon" photosensitizer in model media and in blood of oncological patients, J. Appl. Spectrosc. 70 (2003) 921–926.

45   Invitrogen, Molecular Probes Product Information, 2004.

46   F.W.Wilkinson,W.P. Helman, A.B. Ross, Quantumyields for the photosensitized formation of the lowest electronically excited singlet state of molecular oxygen in solution, J. Phys. Chem. 22 (1993) 113–262.

47   R.W. Redmond, J.N. Gamlin, A compilation of singlet oxygen yields from biologically relevant molecules, Photochem. Photobiol. 70 (1999) 391–475.

48   C.J. Rijcken, J.W. Hofman, F. van Zeeland, W.E. Hennink, C.F. van Nostrum, Photosensitiser-loaded biodegradable polymeric micelles: preparation, characterization and in vitro PDT efficacy, J. Control. Release 124 (2007) 144–153.

49   J.W. Hofman,M.G. Carstens, F. van Zeeland, C. Helwig, F.M. Flesch,W.E. Hennink, C.F. van Nostrum, Photocytotoxicity of mTHPC (temoporfin) loaded polymeric micelles mediated by lipase catalyzed degradation, Pharm. Res. 25 (2008) 2065–2073.

50   F. van Leeuwen-van Zaane, U.A. Gamm, P.B. van Driel, T.J. Snoeks, H.S. de Bruijn, A. van der Ploeg-van den Heuvel, I.M. Mol, C.W. Lowik, H.J. Sterenborg, A. Amelink, D.J. Robinson, In vivo quantification of the scattering properties of tissue using multi-diameter single fiber reflectance spectroscopy, Biomed. Opt. Expr. 4 (2013) 696–708.

51   F. van Leeuwen-van Zaane, U.A. Gamm, P.B. van Driel, T.J. Snoeks, H.S. de Bruijn, A. van der Ploeg-van den Heuvel, H.J. Sterenborg, C.W. Lowik, A. Amelink, D.J. Robinson, Intrinsic photosensitizer fluorescence measured using multi-diameter singlefiber spectroscopy in vivo, J. Biomed. Opt. 19 (2014) 15010.

52   S. Brooks, C.L. Hoy, A. Amelink, D.J. Robinson, T.E. Nijsten, Sources of variability in the quantification of tissue optical properties by multidiameter single-fiber reflectance and fluorescence spectroscopy, J. Biomed. Opt. 20 (2015) 57002.

53   C.L. Hoy, U.A. Gamm, H.J. Sterenborg, D.J. Robinson, A. Amelink, Method for rapid multidiameter single-fiber reflectance and fluorescence spectroscopy through a fiber bundle, J. Biomed. Opt. 18 (2013) 107005.

54   S.L. Rakestraw,W.E. Ford, R.G. Tompkins, M.A. Rodgers,W.P. Thorpe, M.L. Yarmush, Antibody-targeted photolysis: in vitro immunological, photophysical, and cytotoxic properties of monoclonal antibody-dextran-Sn(IV) chlorin e6 immunoconjugates, Biotechnol. Prog. 8 (1992) 30–39.

55   D.Mew, C.K.Wat, G.H. Towers, J.G. Levy, Photoimmunotherapy: treatment of animal tumours with tumour-specific monoclonal antibody-hematoporphyrin conjugates, J. Immunol. 130 (1983) 1473–1477.

56   M. Carcenac,M. Dorvillius, V.Garambois, F. Glaussel, C. Larroque, R. Langlois,N.E.Hynes, J.E. van Lier, A. Pelegrin, Internalisation enhances photo-induced cytotoxicity of monoclonal antibody-phthalocyanine conjugates, Br. J. Cancer 85 (2001) 1787–1793.

57   M.B. Vrouenraets, G.W. Visser, F.A. Stewart, M. Stigter, H. Oppelaar, P.E. Postmus, G.B. Snow, G.A. van Dongen, Development of meta-tetrahydroxyphenylchlorinmonoclonal antibody conjugates for photoimmunotherapy, Cancer Res. 59 (1999) 1505–1513.

58   A.I. Minchinton, I.F. Tannock, Drug penetration in solid tumours, Nat. Rev. Cancer 6 (2006) 583–592.

8

59   M.E. Ackerman, D. Pawlowski, K.D. Wittrup, Effect of antigen turnover rate and expression level on antibody penetration into tumour spheroids, Mol. Cancer Ther. 7 (2008) 2233–2240.

60   M.D. Savellano, T. Hasan, Targeting cells that overexpress the epidermal growth factor receptor with polyethylene glycolated BPD verteporfin photosensitizer immunoconjugates, Photochem. Photobiol. 77 (2003) 431–439.

61   M.D. Savellano, T. Hasan, Photochemical targeting of epidermal growth factor receptor: a mechanistic study, Clin. Cancer Res. 11 (2005) 1658–1668.

62   A.O. Abu-Yousif, A.C.Moor, X. Zheng,M.D. Savellano,W. Yu, P.K. Selbo, T. Hasan, Epidermal growth factor receptor-targeted photosensitizer selectively inhibits EGFR signaling and induces targeted phototoxicity in ovarian cancer cells, Cancer Lett. 321 (2012) 120–127.

63   O. Muller, J. Bartunek, M. Hamilos, C.T. Berza, F. Mangiacapra, A. Ntalianis, K. Vercruysse, C. Duby, W. Wijns, B. De Bruyne, G.R. Heyndrickx, M. Vanderheyden, J.B. Holz, E. Barbato, von Willebrand factor inhibition improves endothelial function in patients with stable angina, J. Cardiovasc. Transl. Res. 6 (2013) 364–370.

CHAPTER 9

Towards a successful clinical implementation of fluorescence-guided surgery

Thomas J.A. Snoeks, Pieter B.A.A. van Driel[1,2], Stijn Keereweer, S. Aime, K.M. Brindle, Gooitzen .M. van Dam, Clemens W.G.M. Löwik, Vasilis Ntziachristos, Alexander L. Vahrmeijer

1. Department of Radiology, Division of Molecular Imaging, Leiden University Medical Center, Leiden, The Netherlands
2. Department of Otorhinolaryngology & Head and Neck Surgery, Center for Optical Diagnostics and Therapy, Erasmus Medical Center, Rotterdam, The Netherlands
3. Deparment of Molecular Biotechnology and Health Sciences, University of Torino, Torino, Italy
4. Deparment of Biochemistry, University of Cambridge, Cambridge, United Kingdom
5. Department of Surgery, University Medical Center Groningen, Groningen, The Netherlands
6. Institute for Biological and Medical Imaging, Technische Universität München and Helmholtz Zentrum München, Neuherberg, Germany
7. Department of Surgery, Leiden University Medical Center, Leiden, The Netherlands

ABSTRACT

During the European Molecular Imaging Meeting (EMIM) 2013, the fluorescence-guided surgery study group held its inaugural session to discuss the clinical implementation of fluorescence-guided surgery. The general aim of this study group is to discuss and identify the steps required to successfully and safely bring intraoperative fluorescence imaging to the clinics. The focus group intends to use synergies between interested groups as a tool to address regulatory and implementation hurdles in Europe and operates within the intraoperative focus group of the World Molecular Imaging Society (WMIS) that promotes the same interests at the WMIS level. The major topics on the critical path of implementation identified within the study group were quality controls and standards for ensuring accurate imaging and the ability to compare results from different studies, regulatory affairs, and strategies to increase awareness among physicians, regulators, insurance companies, and a broader audience. These hurdles, and the possible actions discussed to overcome them, are summarized in this report. Furthermore, a number of recommendations for the future shape of the fluorescence-guided study group are discussed. A main driving conclusion remains that intraoperative imaging has great clinical potential and that many of the solutions required are best addressed with the community working together to optimally promote and accelerate the clinical implementation of fluorescence imaging towards improving surgical procedures.

Introduction

The inaugural fluorescence-guided surgery study groupmeeting was held during the European Molecular Imaging Meeting (EMIM) 2013, organized by the European Society for Molecular Imaging (ESMI) in Turin, Italy. The group focuses on the propagation of fluorescence imaging in surgery, in particular for accelerating clinical propagation while promoting safety and the use of standards for ensuring the development of accurate fluorescence imaging systems and clinical acceptance of the best agents. Fluorescence guidance can assist the surgeon to "see" beyond the limitations of human vision by imparting molecular contrast, improve the detection sensitivity over white-light color imaging, and enable subsurface visualization [1–3]. Correspondingly, there is an emerging drive to ensure that this technology is accepted widely for clinical use to improve the surgical healthcare offered to patients. The goal of the study group meeting was to serve as a forum to openly discuss aspects and hurdles faced by different investigators and stakeholders and to suggest solutions. The study group also intends to discuss European-specific issues and relay them to the corresponding World Molecular Imaging Society study group. Major discussion points during the session revolved around regulatory and safety issues for clinical implementation, quality controls and standards, strategies to increase awareness for a wider acceptance of the technology, and the future shape of the fluorescence-guided surgery study group. In this report, these topics are summarized together with proposed actions. A general consensus has been that information exchange and a common action on large-scale issues, in particular (1) the use of accurate and appropriate fluorescence imaging technology held at a high standard, (2) the action plan on informing regulatory bodies and obtaining regulatory approvals, and (3) the responsibility to act in a safe and ethical manner are important issues that should be addressed as a community to ensure a pragmatic propagation of this technology for the benefit of the patient.

Ethics and Good Clinical Practice

The first clinical trial of fluorescence-guided surgery using targeted agents has been performed [4], and new trials are presently ongoing. However, there are still numerous hurdles to be addressed before new imaging devices and optical probes can actually be implemented in standard clinical care. These hurdles include not only the obvious bottlenecks such as costs and regulatory approval but also the less visible but more important issue of good clinical practice and good scientific practice. We have seen in other scientific fields, such as gene therapy, how unfortunate events can have devastating effects on the progress of an entire area of research [5]. As a result, there is a significant responsibility of all investigators involved with the clinical propagation of intraoperative imaging to conduct preliminary clinical studies and lengthier clinical trials at the highest level of ethical conduct and safety precautions.

Regulatory Affairs

The regulatory approval of an imaging agent and an imaging system presents complexities and has a direct effect on study design and data collection (and thus requires well-designed research protocols). The US Food and Drug Administration (FDA) and its European counterpart, the European Medicines Agency (EMA), have very similar guidelines for phases I and II clinical studies. A well-designed trial can thus be used in both the European and the US approval procedures. In Europe, however, approval is subject not only to European guidelines but also to additional regulatory bodies at a national level. All of these regional bodies come with their own specific set of regulations on top of the EMA framework. The trial design has a direct influence on the required toxicity tests, as these tests are dependent on variables like dosing, administration route, and number of administrations. Once these variables have been established, toxicity screening can be outsourced to dedicated commercial companies. Outsourcing prevents a lot of unnecessary work or delay and generates data in a format that is immediately ready for FDA and EMA filing. The execution of the clinical trial itself is complicated, as it requires close collaboration between multiple partners. This is especially the case for large multicentre trials performed in more than one country. It is during the setup of these trials that there is an important role for the European and worldwide intraoperative imaging study group in stimulating or even facilitating the exchange of knowledge on national regulatory issues and sharing experiences with trial design and approval procedures. Also, the study group can speed up the process of clinical implementation by making and distributing updated guidelines for good research practice, regulations, and study design.

Quality Control for Agent Production

The production of a fluorescence agent is also subject to extensive regulations. Minor chemical modifications such as coupling a dye to a targeting moiety are considered to be a manufacturing step and require approval as a new entity and corresponding production under good manufacturing practice (GMP) conditions, before clinical administration. Phase I clinical trials already require compounds produced to GMP standards. Currently, small GMP facilities are set up by research groups in order to produce probes for small inhouse trials. Running a GMP production facility is expensive and time-consuming, as it involves a lot of paperwork, regulations, and periodic inspections. However, it is advisable to start using GMP probes at a preclinical stage, as this can prevent problems introduced by changes in production procedures at a later point in time. Typical problems associated with switching to GMP production of compounds at a later time point include production and synthesis protocols in which one or more steps are not allowed under GMP regulations, insufficient purity of the manufactured agent, and difficulties in identifying the chemical characteristics of impurities. Increasing the

production scale of a probe is essential during the transition from preliminary to large clinical trials. Often, the small in-house facilities are not suitable for largescale production. Moreover, probe production for one multicentre trial is ideally performed within one production facility to prevent quality variation. There are a number of issues when switching to large-scale probe production. First of all, most antibody and peptide-based probes are notoriously difficult to produce. Even for a dedicated facility, setting up a large-scale production line is expensive and very time-consuming. Second, the probe and its activity should be reevaluated after optimizing the production protocols. Third, as part of the GMP process, there should be a quality control system in place in order to ensure production stability in terms of probe quality and purity over time. Finally, the probe should be well characterized in terms of shelf life, stability, and possible aggregation, as running large multicentre trials will involve increased transport and storage time. Multicentre trials are ideally dependent on one dedicated centralized production facility. This requires extensive collaboration between scientific groups designing probes and their production protocols, clinical researchers leading these trials, pharmaceutical formulation experts, and probe manufacturers. The fluorescence-guided surgery study group should take a leading role in maintaining information flow in regard to experiences gained in this process and the pitfalls to avoid when setting up of a GMP production of a new agent. The study group can further aid in coordinating actions directed to the EMA in order to provide a common framework for all investigators involved in translating intraoperative imaging.

Standardization of Fluorescence Cameras

A discussion ensued on whether clinical approval will be granted for probes and imaging devices independently or whether certain fixed probe–camera combinations will become eligible for approval. This is a very relevant question as a good probe can lead to adverse clinical results if the performance of the imaging device used is inadequate. In essence, the question touches upon the need for standardization in the assessment of imaging device performance. Standardization and quality control is an important matter in all radiological modalities but is particularly important in fluorescence imaging since there is no established fluorescence imaging standard. In addition, the signals recorded by fluorescence "photographic" imaging depend nonlinearly on tissue optical properties, which may lead to insufficient or erroneous detection of fluorescence in tissues and result in false negatives or positives [6–9]. There is currently no objective way of determining the performance of an imaging device as a whole. One can easily compare the resolution and sensitivity of the cameras used, but not the overall performance of an imaging device, i.e., its performance in relation to tissue optical properties, light illumination homogeneity, and several other features that may impact performance. The insensitivity of the fluorescence signal intensity to the (variation of) tissue optical properties and corresponding methods for overall noise reduction is of great importance in understanding and characterizing

an intraoperative imaging device that has been developed for medical use, rather than just simple technical-only parameters such as camera sensitivity or resolution [10]. One step towards accurate fluorescence imaging is the development of a standardized fluorescent phantom. Phantoms can be imaged for assessing the performance and accreditation of a system for clinical use. Possibly, phantoms may also be necessary for system calibration, as they are common for other imaging modalities such as nuclear imaging [11]. Again, community involvement in understanding and addressing these issues is required for devising appropriate standards and recommending their use.

Assessment of Imaging Agents

Not only are the imaging devices in need of a standardized measure of performance but also probes and the even more fundamental measurements of biomarker expression levels are in need of standardization. An illustrative example is the vascular endothelial growth factor (VEGF). Each of seven different VEGF antibodies gives different results in terms of staining intensity when used for immunohistochemistry performed by one person within one laboratory due to slight variations in the execution of the staining procedure, such as buffer handling, incubation times, and antibody handling. Matters become even more complicated as one specific antibody can give rise to completely different results in different laboratories or when handled by different people [12]. Yet, immunohistochemical staining is one of the typical experiments used in scientific publications to show and measure biomarker expression levels and to prove probe specificity. Consequently, it is actually very difficult to compare biomarker expression and probe performance between different studies. In order to address the issue of comparing probe performance and biomarker expression levels between studies, there is a need for the standardization of the antibodies used, the methods and lab protocols, the measuring/imaging devices used, and the methods of signal quantification. These standards must be set for each individual biomarker. Another solution to the problem might lie in the use of techniques like mass spectrometry and liquid chromatography–mass spectrometry (LC–MS) for the quantification of expression levels [13]. Setting these standards on European and worldwide levels will create great opportunities when it comes to selecting the most promising probes to enter a clinical phase.

Raising Wider Awareness

The field of intraoperative imaging is moving forward towards clinical implementation. As we may be approaching a period of large multicentre clinical trials, the research field will require relatively large investments and research budgets in the near future. Similar to other areas of medical research, investments can come either from the industry or from public funding agencies and governments. A particular case for intraoperative imaging is that it does not have a dedicated

"industry" space. It rather defines a new theranostic area that may generate its own industry. Many of the participants in the study group believe that this will be a sufficiently large field for imaging industries to enter; however, there is certain reluctance on their behalf, primarily due to the requirement for imaging agents, to enter a field where they do not have much experience. Intraoperative imaging is a field in great need of public funding. The benefits to the patient can be seen, but on the other hand, clinical translation is best handled today by clinical surgical departments with a clear view and understanding on how this field should move forward. This is a clear case of a "valley-of-death" scenario seen in clinical translation of promising technology that is best addressed by competitive publicly funded research to support clinical studies and to demonstrate the benefit of the technology. Such demonstration is then certain to attract industrial investment. The focus of research should lie on developing low-cost imaging systems and reagents in order to stimulate fast clinical translation of these systems. Furthermore, this field of development is consistent with the goals of the European community priority lists. Therefore, there is a further clear goal of the study group, and that is to promote a community approach to ensure sustainable funding that will enable the demonstration of promising agents and systems in the clinic, as an important remaining step towards wider clinical dissemination. Intraoperative imaging has great potential but requires support at a larger community level and beyond in reaching more widely the clinical communities and informing the general public and government regulatory and funding bodies of the opportunities and need for raising proper support.

The Future of the ESMI Fluorescence-Guided Surgery Study Group

Exchange of information and joint actions representing the community will be a major driving force during the implementation of intraoperative imaging. Therefore, the study group will foster synergies and scientific or regulationdriving alliances to focus on proper implementation of the technique in clinical practice. Through regular and ad hoc meetings, supported by ESMI and World Molecular Imaging Congress (WMIC) under the world focus group on intraoperative imaging, the European group aims to help investigators promote their interests in the field by addressing not only the common scientific challenges but also particular regulatory considerations associated with performing these studies in different European countries. It further aims to serve as a forum to compare "notes" and experiences in order to avoid the pitfalls and accelerate propagation of the technology. There is a need for a knowledge base where groups share relevant information on trial design, regulatory issues, and details of trials that are being performed. Sharing experiences on running trials, regulatory affairs, and possible pitfalls will prevent duplication of work and repetition of mistakes made by other groups. A field-wide collaboration on common challenges is the next logical step, especially as we stand on the brink of large multicentre trials of probes and imaging devices for certain specific indications. The study group can further play a key role in implementing standards for imaging devices, probe

performance, and biomarker expression, by synergizing, not only at a European level but also with all scientists under the WMIC focus group on intraoperative imaging to gain consensus on optimal guidelines. Setting these standards is of paramount importance, as it will create a reference frame within which data can be compared and this issue will remain on the agenda of future meetings with the aim of reaching a consensus on optimal imaging and targeting performance metrics. Finally, it is essential to develop means to communicate critical issues outside the research community. Awareness should be raised within three different target groups. First, surgeons, the future users of intraoperative imaging techniques, should be made aware of the technique and the possible implications for surgical oncology. This will create interest and possibilities for future cooperation within clinical trials and clinical implementation. Second, informing the general public via various media will increase the social support and understanding needed for the largescale public investments involved in the next stage of research. Finally, governments and funding bodies need to become aware of the particular benefits and challenges of the field, in order to offer valuable support in accelerating clinical propagation.

General Conclusion

Intraoperative imaging has great clinical potential. One investigator or group cannot address all the major challenges, neither it is reasonable that each interested party will have to overcome the same hurdles in a repetitive manner. Instead, there are grand challenges that need to be addressed at the community level, for example reaching out to regulatory bodies, raising awareness of the field, and in reaching a consensus on standards. The European study group will continue its role in offering a forum for discussion and coordinating actions with the ultimate goal of aiding in the establishment of guidelines and optimal practices and bringing the community together on critical issues. By creating an environment in which communication is stimulated and participants can engage in action groups with common benefits, the study group wishes to aid in the process of safe clinical implementation.

9

References

1. Keereweer S, Kerrebijn JD, van Driel PB et al (2011) Optical imageguided surgery–where do we stand? Mol Imaging Biol 13:199–207

2. Vahrmeijer AL, Hutteman M, van der Vorst JR et al (2013) Imageguided cancer surgery using near-infrared fluorescence. Nature Rev Clin Oncology 10:507–518

3. Weissleder R, Pittet MJ (2008) Imaging in the era of molecular oncology. Nature 452:580–589

4. van Dam GM, Themelis G, Crane LM et al (2011) Intraoperative tumourspecific fluorescence imaging in ovarian cancer by folate receptor-alpha targeting: first in-human results. Nature Med 17:1315–1319

5. Check E (2002) A tragic setback. Nature 420:116–118

6. Li XD, O'Leary MA, Boas DA, Chance B, Yodh AG (1996) Fluorescent diffuse photon density waves in homogeneous and heterogeneous turbid media: analytic solutions and applications. Appl Optics 35:3746–3758

7. Ntziachristos V, Ripoll J, Wang LV, Weissleder R (2005) Looking and listening to light: the evolution of whole-body photonic imaging. Nature Biotechnol 23:313–320

8. Taroni P, Pifferi A, Torricelli A et al (2003) In vivo absorption and scattering spectroscopy of biological tissues. Photochem Photobiol Sci 2:124–129

9. Ntziachristos V, Yoo JS, van Dam GM (2010) Current concepts and future perspectives on surgical optical imaging in cancer. J Biomed Opt 15:066024

10. Keereweer S, Van Driel PB, Snoeks TJ et al (2013) Optical imageguided cancer surgery: challenges and limitations. Clin Can Res 15:3745–3754

11. MacFarlane CR, American College of R (2006) ACR accreditation of nuclear medicine and PET imaging departments. J Nuclear Med Technol 34:18–24

12. Taylor CR (2000) The total test approach to standardization of immunohistochemistry. Archives Pathology Laboratory Med 124:945–951

13. Aebersold R, Mann M (2003) Mass spectrometry-based proteomics. Nature 422:198–207

IV
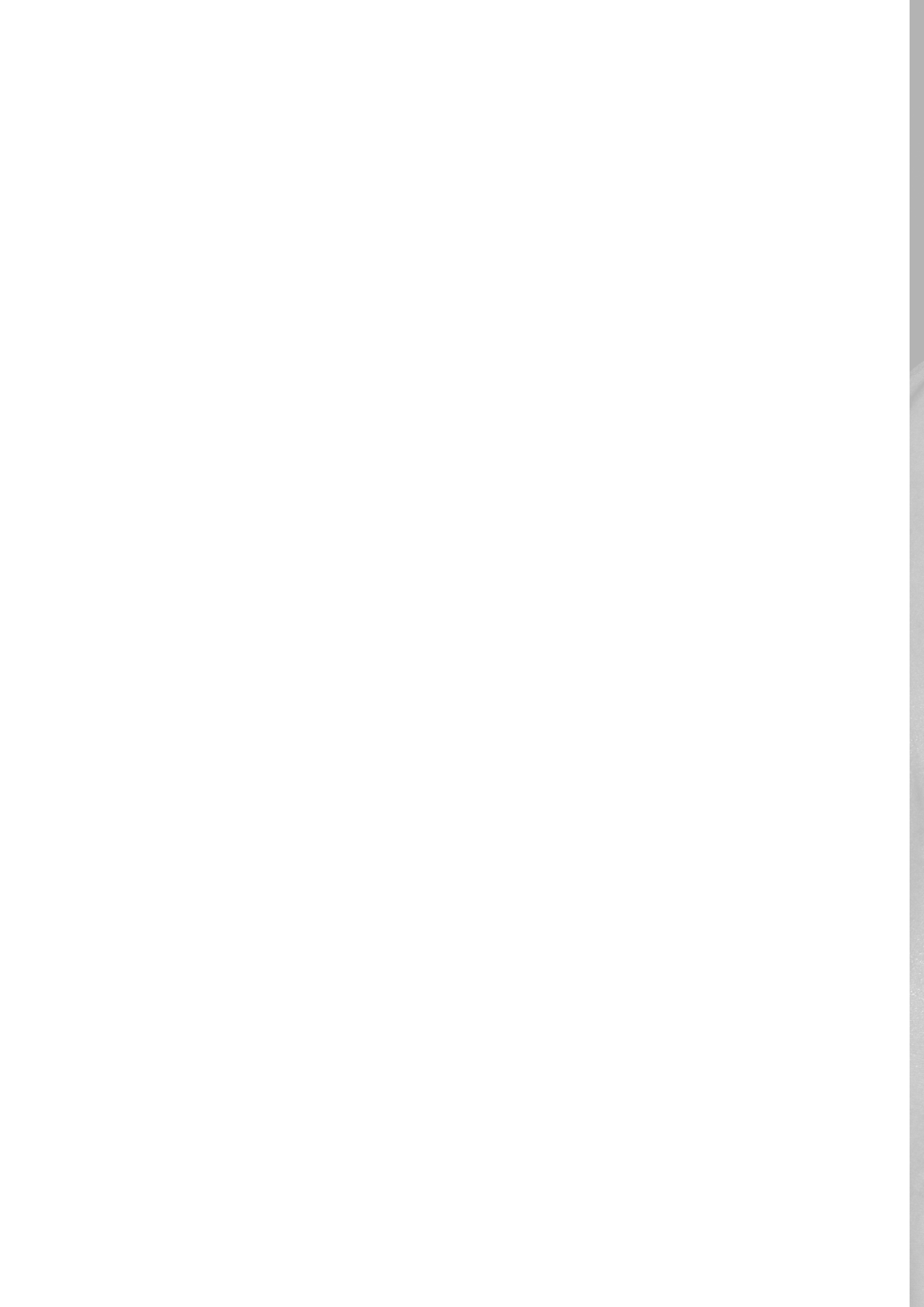
CHAPTER 10

Summary, Discussion and Future perspectives
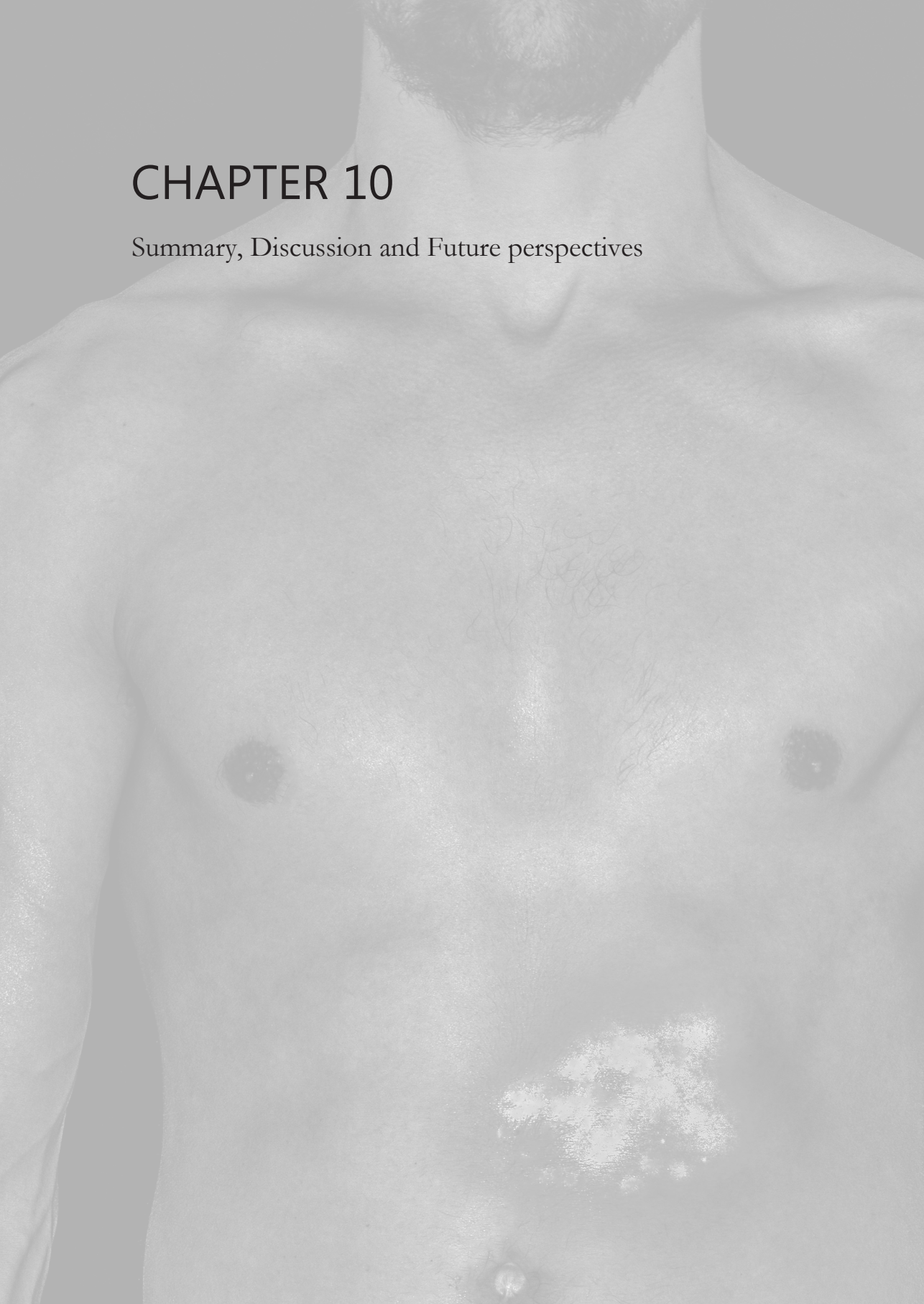
Summary

Over the last century, pre- and postoperative imaging for early detection, staging and treatment evaluation have been a major part of oncological surgery. Nevertheless, during surgery, surgeons mostly discriminate healthy tissue from cancerous tissue by means of visual inspection and palpation. Consequently, incomplete tumour resections are still encountered even though intra-operatively these tumours seem radically resected. Providing the surgeon with intra-operative visual feedback on tumour margins may promise an improvement in radical resections of tumours, thus increasing patients' survival rates.

Fluorescence-guided surgery (FGS) is a technique based on near-infrared (NIR) light that provides the surgeon with real-time visualization of tissues of interest. Although initially not very appealing for clinical use, this radically changed with the discovery of NIR light. Using NIR light tissue penetration was higher and autofluorescence decreased significantly. The high potential of FGS for surgical oncology increased the amount of research in this relatively new field of optical imaging exponentially. Currently, FGS has been widely investigated for sentinel lymph node procedures, evaluation of perfusion of anastomosis and cholangiography during cholecystectomies. An increasing amount of clinical trials are performed studying targeted FGS to discriminate cancerous tissue from healthy surrounding tissue during surgery. Nevertheless, targeting cancer remains challenging, mostly because of a great extent of intra- and intertumoral heterogeneity of the targeted receptors. Further, optical properties of tissue hamper the detection of a single tumour cell potentially leaving residual tumour cells in situ after a NIR fluorescence-guided resection.

The aim of this thesis was to validate two probes and the newly designed Artemis camera for NIR FGS preclinically to pave the way for a clinical implementation. In the last part, the first steps were made to combine targeted NIR imaging and photodynamic therapy. A potential treatment combination to treat the last residual tumour cells.

In **part I** the current modalities of fluorescence-guided surgery and the challenges in optical imaging were reviewed. **Chapter 2** gives an extensive overview of the preclinical and clinical data in targeted fluorescence-guided oncologic surgery to reflect its current status. In particular, it focuses on specific targeting of primary tumours by organic fluorescent agents that target the alterations in cell physiology involved in cancer. **Chapter 3** describes the fundamental basic principles of NIR fluorescence imaging. Here, the consequences of these principles on FGS and the influence on clinical decision-making are discussed in more detail. The technique can be a

very powerful tool in guiding the surgeon to radical tumour resections, as long as the intrinsic limitations are taken into account.

Preclinical studies were shown in **part II**. Here, two preclinical studies are performed using probes that target two important receptors in oncology. The first target that was explored is the epidermal growth factor receptor (EGFR) in **chapter 4**. The EGFR is a transmembrane glycoprotein that is involved in DNA synthesis and cell proliferation. Overexpression contributes to oncogenesis. Being widely overexpressed in oral squamous cell carcinomas (OSCC) we used an orthotopic OSCC of the tongue that metastasises to the cervical lymph nodes. Here, a nanobody was conjugated to the fluorophore IRDye-800CW. A nanobody is the smallest functional antigen-binding fragment derived from naturally occurring heavy-chain-only antibodies. They show very specific binding to their targets and their size ensures efficient distribution and tissue penetration, as well as rapid clearance from the body. All tumours could be clearly identified using the FLARE NIR fluorescence camera. From two hours after injection of 7D12-800CW a significantly higher tumour-to-background ratio (TBR) was observed compared to the control nanobody. A higher dose was needed to detect cervical lymph node metastases. Using an orthotopic tumour model and a clinically available NIR camera system this study showed the true potential of a nanobody based imaging agent in FGS. In search for a more universal receptor we evaluated the epithelial cell adhesion molecule in **chapter 5**. EpCAM is a transmembrane glycoprotein involved in cell-cell interactions and cell-stroma adhesion. Its expression is restricted to epithelial cells and is highly up-regulated in virtually all epithelial carcinomas. To assess the value of this target in FGS we conjugated the monoclonal chimeric antibody 323/A3 to the IRDye 800CW. The anti-EpCAM/800CW conjugate showed to be stable in serum and showed preserved binding capacity as evaluated on EpCAM positive and negative cell lines using flow cytometry and cell-based plate assays. Four clinically relevant orthotopic tumour models, i.e. colorectal cancer, breast cancer, head and neck cancer, and peritonitis carcinomatosa were used to evaluate the performance of the anti-EpCAM agent with the clinically validated Artemis imaging system. All tumour types could clearly be delineated and resected 72 hours after injection of the imaging agent. Millimetre sized tumour nodules were detected that were invisible for the naked eye. Fluorescence microscopy demonstrated the distribution and tumour specificity of the anti-EpCAM agent. This study showed the potential of EpCAM as a target in FGS in a versatile of orthotopic tumour models paving the way for clinical translation. Next, the use of the new Artemis NIR fluorescence camera was reported for the first time in literature. **In chapter 6** we evaluated the performance of the new Artemis camera preclinically as well as clinically. The minimal detectable dose of pure ICG and IRDye 800CW was determined *in vitro*. The lower limit of cells targeted by the EGFR targeting nanobody 7D12-800CW that could be detected was 2×10^5 and 4×10^4 for the Artemis and preclinical camera

10

(Pearl) respectively. *In vivo,* the camera was evaluated in two procedures namely sentinel lymph node imaging and tumour specific FGS. Two head and neck cancer cell lines were used in combination with 7D12-800CW. Orthotopic OSC-19-luc2-cGFP tongue tumours were clearly visible and a minimum FaDu-luc2 tumour size of 1 mm3 could be identified. Further, for the first time, clinical evaluation of cancer patients using the NIR Artemis camera was described. Six human malignant lesions were identified during three liver surgery procedures.

In **part III** we focussed on the future of fluorescence-guided surgery. In **chapter 7** three major challenges in FGS were described and subsequently possible solutions were postulated. The challenges in FGS described here comprise imaging tumour heterogeneity, invasive tumour strands and dealing with the tissue optical properties. Tissue optical properties ensure that it is most unlikely that the last residual tumour cells will be visualized using FGS. Mainly in invasive tumour strands this could hamper radical tumour resections. To overcome the hurdle of optical properties, intrinsic fluorescence measurements can be performed intra-operatively. We described how point reflectance and fluorescence spectroscopy using fiber optic probes can be used to overcome the effects of tissue optical properties and detect residual fluorescent signal. A second promising solution to treat the remaining tumour cells is adjuvant photodynamic therapy. PDT is a promising minimally invasive approach that is being used for the local treatment of premalignant and malignant lesions. Compared to other adjuvant therapeutic modalities, PDT has the potential to induce low toxicity in normal tissue, produce negligible systemic effects, and reduce acute and long-term morbidity. Furthermore, PDT does not compromise future treatment options for patients with residual or recurrent disease and can be repeated with perpetual efficacy. More importantly PDT and NIR FGS can be combined in one theranostic probe. In **chapter 8** we explored the feasibility of tumour specific photodynamic therapy and NIR fluorescence imaging. Despite the potential advantages of PDT, collateral damage to normal tissue remains a significant side effect, particularly in the treatment of large tumours. Targeted PDT, in which photosensitizers (PS) are selectively delivered to the tumour, could greatly enhance the efficacy of PDT and simultaneously reducing damage to normal tissue. Here, in this feasibility study, we conjugated the photosensitizer IRDye700DX to the EGFR targeting nanobody 7D12 and explored the selectivity and phototoxicity in an orthotopic head and neck cancer model. *In vitro*, the EGFR specific IRDye700DX conjugates solely binded to cells overexpressing the EGFR. Further, phototoxicity was only induced in cells that were bound by the conjugate. Importantly, EGFR targeted nanobody–PS conjugates led to extensive tumour necrosis (approx. 90%) *in vivo* and almost no toxicity in healthy tissues was observed through histology 24h after PDT. Overall, results showed that these EGFR targeted nanobody–PS conjugates are selective and able to induce tumour cell death in vivo. In **chapter 9** we identified the steps required to successfully and safely bring intraoperative fluorescence imaging to the

clinics. The major topics on the critical path of implementation were identified and the possible actions discussed to overcome them. A main overall conclusion remained that intraoperative fluorescence imaging has great clinical potential and that with the community working together the clinical implementation of FGS could be substantially accelerated.

This thesis demonstrates the use of fluorescence-guided therapy in oncology. First it shows the preclinical validation of two different targets and probes for fluorescence-guided surgery, results that pave the way towards clinical implementation. Next, the utility of the NIR fluorescence Artemis camera is described. Lastly, the first steps are made towards fluorescence theranostics in oncology: NIR fluorescence-guided surgery and intra-operative targeted photodynamic therapy.

10

Discussion and Future perspectives

Target

Over the past decade, an important driver in the field of fluorescence-guided therapy was to identify a universal tumour-specific target with optimal tumour-to-background ratio. A probe against a 'universal' target facilitates clinical usability, and prevents time consuming and costly development of multiple agents. However, the continuous quest for a universal tumour-specific target has not yet been successful and the growing insight in cancer invasion is increasingly pointing towards multifactorial processes[1,2]. Next, cancer targeting with high sensitivity and specificity remains challenging, mostly related to issues with intra- and intertumoral heterogeneity.
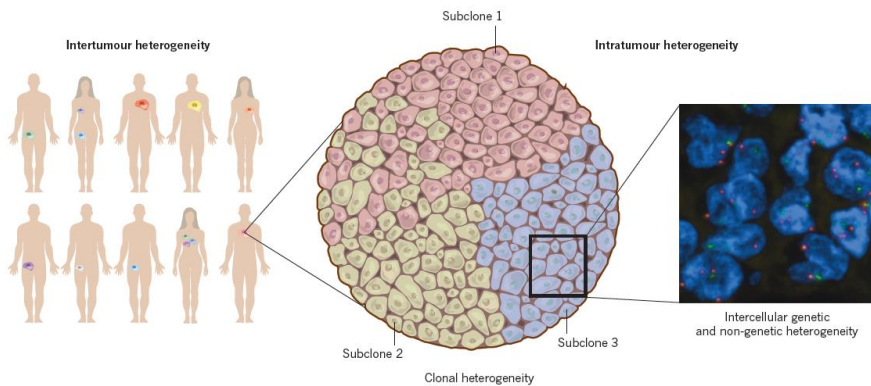
Figure 1 | Intertumoral and intratumor heterogeneity.

Extensive genetic and phenotypic variation exist between tumours that originate from different tissues and cell types. They are even observed between tumours that originate from the same tissue and cell type (Figure 1). This intertumoral heterogeneity occurs probably because genetic events of transformation interact with cell-intrinsic biological properties[3]. Furthermore, genetic diversity in population of tumours cells is induced by genomic instability and the fact that a large number of proliferation cycles is needed for a macroscopic tumour to grow. Subsequently, subclones of cells within a tumour are formed by somatic evolution (Figure 1). The result is diversity in the expression of biomarkers in each tumour and even in subclones within a tumour. Therefore, complete imaging of the tumour border by a single target will be challenging. This suggests that a personalized approach to individual patients may be required where multiple targets per patient are selected to completely image the tumour border during surgery. Costly developments of tumour specific agents hamper a rapid clinical implementation of multiple

agents. Until surgeons will have access to a variety of agents, the first developments of agents will focus on the most universal targets or targets that can be used in a greater subset of tumours. An adequate target for NIR fluorescence imaging is defined by the exclusive upregulation on tumour cells compared to adjacent normal tissue cells, the localization on the cell membrane, the number of targeted proteins available per cell and the distribution of target expressing cells within the tumour[4]. The EGFR studied in chapter 4 is upregulated in most cancer types and serves as an interesting target that is used in therapeutic and imaging studies[4]. Being widely overexpressed in head and neck cancer the target served as a logical choice for our study. The second target studied in chapter 6 is the Epithelial Cell Adhesion Molecule (EpCAM). EpCAM is a transmembrane glycoprotein involved in cell-cell interactions and cell-stroma adhesion[5]. EpCAM certainly holds as an universal target for epithelial tumours as its expression is restricted to epithelial cells and is highly up-regulated in virtually all epithelial carcinomas[6,7]. Both targets proved their usability in preclinical experiments results from clinical trials have to be awaited. (NCT03282461, NCT03154411, NCT03134846,)

10

Probe

Research into the development of probes for optical imaging has been preceded by decades of research into therapeutic antibodies[8]. Many of the research done in therapeutic antibody (fragments) can be extrapolated to optical imaging. For instance, the challenge of immunogenicity of murine antibodies in patients and the development of humanized or fully human antibodies. Further research on antibody-drug conjugates brought attention to conjugation methods and site-specific conjugation[9]. Although antibodies became the mainstay of biotherapeutics, treatment of solid tumours remained difficult because of limited tumour penetration. One of the most important variables that determine penetration is the molecular radius. Therefore, development of tumour targeting molecules focused on making smaller fragments including 7 kDa affibodies[10], 12-15 kDa nanobodies[11], 27kDa ScFvs[12], 50 kDa Fabs and 80 kDa minibodies[13].

The desired requirements for therapeutic and optical agents differ significantly. Contrary to therapeutic antibodies where effector functions are desirable, optical agents have to be biologically inert to reduce the risk of unwanted side effects. Furthermore, therapeutic antibodies require significant concentrations in target tissue over time whereas optical imaging agents need to achieve high contrast at early times. Early imaging is practical and cost-effective in surgical practice because patients do not have to be admitted to the hospital days before surgery. In NIR FGS, where the tumour border is of main concern, it is still questionable whether penetration of solid tumours is of that much importance.

In search of the optimal probe size we need to find out what the influence is of size on the targeting properties of the agent. In a study by Schmidt et al.[14] a mechanistic model was developed that predicted the complex interplay between molecular size, affinity, and tumour uptake. In this study empirical relationships between molecular radius, capillary permeability, interstitial diffusivity, available volume fraction, and plasma clearance were obtained using data in the literature. Intermediate sized targeting agents (molecular weight approximately 25 kDa) seemed to have the lowest tumour uptake and similar peak tumour levels were predicted using small and large proteins. Contrary to large proteins, smaller proteins achieve high tumour levels rapidly but need a high affinity to be retained[14]. An increase in tumour penetration ensures a more homogenous distribution of smaller proteins in solid tumours.

In this thesis two different sized tumour targeting agents were used: the 15kDa 7D12-800CW nanobody (chapter 4, 6 and 8) and the 150 kDa 323/A3-800CW antibody (chapter 5). Nanobodies are the smallest functional antigen-binding fragments derived from naturally occurring heavy-chain only antibodies. They bind specifically and with high affinities to their antigens[15, 16], they are stable and soluble in aqueous solutions, can be chemically modified, and have low immunogenic potential[17]. Further, with a molecular weight ten times smaller than conventional antibodies (15 kDa vs 150 kDa) and high binding affinities, tumour penetration of nanobodies is greatly enhanced, and occurs more rapidly[18]. Therefore, nanobodies seem a logical choice for FGS. Nevertheless, the wide clinical experience and known safety of antibodies allows for a faster and safe clinical translation.

Next to the targeting moiety, the fluorophore is one of the key factors in FGS. When all vairables (NIR wavelength, quantum yield, photobleaching, clearance, nonspecificity, solutibliy and toxicity)of the fluorophore are optimal, still tissue penetration will be relatively limited to a maximum of approximately 1 cm. Imaging in the NIR2 spectrum (1000 – 1700 nm) is an interesting alternative option to increase tissue penetration because of reduced tissue scattering and negligible tissue autofluorescence[19]. A second, promising imaging tool to increase tissue penetration is photoacoustic imaging. Here, light of short laser pulses is absorbed by an exogenous contrast agent and converted into heat leading to ultrasonic emission. The photoacoustic waves can be detected by ultrasound transducers. Less scattering of soundwaves results in a high tissue penetration compared to NIR fluorescence imaging[20].

An interesting new area of imaging is multimodal imaging. Pre-operative tumour staging, intra-operative imaging and post-operative pathologic examination can be achieved by one probe in multimodal imaging[19]. Here, preoperative imaging techniques (SPECT/PET) are combined with intraoperative fluorescence optical guidance. Postoperatively, fluorescence imaging guides the

pathologic examination. Next to multimodal imaging, the theranostic concept (simultaneous diagnosis and treatment) can be applied to FGS when it is combined with tumour targeted therapy. One of the promising fields in theranostics is the combination of NIR fluorescence imaging and photodynamic therapy[20]. Residual tumour cells located in the wound bed after FGS can be treated by intra-operative PDT, potentially reducing local recurrence[21].

Imaging systems

The success of FGS in recognizing tumours and vital structures depends to a large extent on the imaging system used. The most important criteria for practical application of an imaging system are the field of view, imaging distance to the patient, manoeuvrability, simultaneous imaging of near-infrared and visible light, real-time imaging, light intensity, sterility, and electrical safety[24]. The criteria that mainly affect the design choices of the camera components are the sensor, lens system, light source, and filters/dichroic mirrors. The last decade several research groups and industrial companies designed and developed NIR fluorescence imaging systems of which a small number fit most of the criteria above and are clinically available[25]. Further, for an adequate clinical translation and widespread clinical use it is of importance that the imaging systems are not overprized. The first NIR fluorescence intraoperative imaging systems were developed for open surgery and recently several became available for clinical trials[25]**.** Over the past decades, significant progression has been made towards minimally invasive surgery to reduce pain, haemorrhaging and to shorten recovery times. As fluorescence guided surgery could certainly be of major benefit in this emerging field of surgery, NIR imaging options were incorporated in laparoscopy, thoracoscopy and robotic systems[25].

A system that can be used for both open and laparoscopic surgery is the Artemis system. In Chapter 6 we evaluated the Artemis NIR imaging system in two oncological procedures in which real-time NIR fluorescence could be of added value: radical tumour resection and the detection of sentinel lymph nodes. Based on the results of this study, it was concluded that the Artemis system demonstrated its utility for fluorescence-guided cancer surgery preclinically and clinically but improvements had to be made. Many of the desired improvements that were suggested in chapter 6 have been implemented in the next generation Artemis system.

Two major challenges in the development of imaging systems are the correction for the influence of optical properties and autofluorescence. Signal to background ratios can be increased drastically if the influence of these factors can be reduced. As widely discussed in chapter 3, two possible solutions could be a correction scheme for light intensity variations in tissues[26] and spectral unmixing[27]. For both, dedicated systems were developed[26,27]. Further, multiple imaging

systems have been developed for photoacoustic imaging that has the major advantage of an increased tissue penetration compared to NIR fluorescence imaging[28].

Nevertheless, the future of imaging systems predominantly lies in multimodal imaging and theranostics. If multiple targets are selected in personalized FGS, several excitation wavelengths need to be incorporated in one imaging system to detect multiple probes simultaneously. Further, hybrid tracers like ICG and ^{99m}Tc-nanocolloid need a hybrid modality that is capable of detecting both gamma and fluorescence signals[29]. Lastly, a logical development for the use in FGS combined with intra-operative targeted PDT is a multimodal system capable of imaging and treatment[30].

Adjuvant photodynamic therapy

Although in 10 years even a single cell can be imaged on the surface using fluorescence imaging, optical properties will probably hamper detection of cancer cells situated under the surface. Consequently, tumor cells could be left in situ after the tumor seems radically resected by fluorescence navigation. This may require the need of adjuvant therapy. Here, intra-operative targeted PDT could be of great value.

Like in FGS, intra- and intertumoral heterogeneity are important challenges in targeted PDT and a personalized approach to individual patients may be required. Next, the photosensitizer (PS) is a major challenge. Most PS's are rather hydrophobic which promotes cell binding, but provides no specificity. Therefore, efforts have been made to render PS more hydrophilic and to target these molecules more selectively to tumors, through chemical modifications, delivery systems, and/or targeting molecules[31-34]. The PS that we conjugated to the nanobodies was IRDye700DX, which is a water-soluble silicon-phthalocyanine derivative that has a strong absorption band in the near-infrared region of the spectrum (690 nm) and is also traceable through optical imaging. Although a major advantage, the use of a single agent for both FGS and PDT holds some limitations. When a chromophore absorbs a photon it will result in fluorescence or the formation of reactive oxygen species. Thus, a single agent will not have an optimal fluorescence- and triplet state quantum yield.

But several advantages favor the use of targeted PDT as an adjuvant treatment. Targeted PDT has the advantage of low toxicity in normal tissue, negligible systemic effects and it induces a local inflammatory reaction that stimulates the host immune system[35,36]. All are major advantages compared to other adjuvant therapeutic modalities like radiotherapy and/or chemotherapy. As demonstrated in chapter 8, a multimodal agent can be used for both FGS and intra-operative

targeted PDT. In contrast to optical imaging where excited and emitted photons encounter the challenge of optical properties, in targeted PDT only excited photons are relevant. Consequently, tissue penetration increases. When PDT is used as adjuvant treatment after surgical resection, residual tumor will be situated directly under the surface of the tumor bed, lowering the need for a high tissue penetration of light. Furthermore, wavelength-specific excitation of photosensitizers (PS) could technically be performed using the same imaging systems as those used for FGS, emphasizing its practical advantages as an adjuvant therapeutic modality in the surgical theatre.

Fluorescence guided therapy in oncology; one probe that allows NIR fluorescence guided resection of a tumor and intra-operative PDT of residual tumor cells.

10

References

1.   Alexander, S. and P. Friedl, *Cancer invasion and resistance: interconnected processes of disease progression and therapy failure.* Trends Mol Med, 2012. **18**(1): p. 13-26.

2.   Friedl, P. and S. Alexander, *Cancer invasion and the microenvironment: plasticity and reciprocity.* Cell, 2011. **147**(5): p. 992-1009.

3.   Burrell, R.A., et al., *The causes and consequences of genetic heterogeneity in cancer evolution.* Nature, 2013. **501**(7467): p. 338-45.

4.   Boonstra, M.C., et al., *Selecting Targets for Tumor Imaging: An Overview of Cancer-Associated Membrane Proteins.* Biomark Cancer, 2016. **8**: p. 119-133.

5.   Winter, M.J., et al., *The epithelial cell adhesion molecule (Ep-CAM) as a morphoregulatory molecule is a tool in surgical pathology.* Am J Pathol, 2003. **163**(6): p. 2139-48.

6.   Went, P.T., et al., *Frequent EpCam protein expression in human carcinomas.* Hum Pathol, 2004. **35**(1): p. 122-8.

7.   Spizzo, G., et al., *Prognostic significance of Ep-CAM AND Her-2/neu overexpression in invasive breast cancer.* Int J Cancer, 2002. **98**(6): p. 883-8.

8.   Scott, A.M., J.D. Wolchok, and L.J. Old, *Antibody therapy of cancer.* Nat Rev Cancer, 2012. **12**(4): p. 278-87.

9.   Agarwal, P. and C.R. Bertozzi, *Site-specific antibody-drug conjugates: the nexus of bioorthogonal chemistry, protein engineering, and drug development.* Bioconjug Chem, 2015. **26**(2): p. 176-92.

10.   Strand, J., et al., *Gallium-68-labeled affibody molecule for PET imaging of PDGFRbeta expression in vivo.* Mol Pharm, 2014. **11**(11): p. 3957-64.

11.   Bannas, P., et al., *In vivo near-infrared fluorescence targeting of T cells: comparison of nanobodies and conventional monoclonal antibodies.* Contrast Media Mol Imaging, 2014. **9**(2): p. 135-42.

12.   Kim, H.Y., et al., *Discovery of hapten-specific scFv from a phage display library and applications for HER2-positive tumor imaging.* Bioconjug Chem, 2014. **25**(7): p. 1311-22.

13.   Tavare, R., et al., *Engineered antibody fragments for immuno-PET imaging of endogenous CD8+ T cells in vivo.* Proc Natl Acad Sci U S A, 2014. **111**(3): p. 1108-13.

14.   Schmidt, M.M. and K.D. Wittrup, *A modeling analysis of the effects of molecular size and binding affinity on tumor targeting.* Mol Cancer Ther, 2009. **8**(10): p. 2861-71.

15.   Hamers-Casterman, C., et al., *Naturally occurring antibodies devoid of light chains.* Nature, 1993. **363**(6428): p. 446-8.

16.   Oliveira, S., et al., *Targeting tumors with nanobodies for cancer imaging and therapy.* J Control Release, 2013. **172**(3): p. 607-17.

17.   Muyldermans, S., *Nanobodies: natural single-domain antibodies.* Annu Rev Biochem, 2013. **82**: p. 775-97.

18. Kijanka, M., et al., *Rapid optical imaging of human breast tumour xenografts using anti-HER2 VHHs site-directly conjugated to IRDye 800CW for image-guided surgery.* Eur J Nucl Med Mol Imaging, 2013. **40**(11): p. 1718-29.

19. Welsher, K., Sherlock, S.P., Dai, H., *Deep-tissue anatomical imaging of mice using carbon nanotube fluorophores in the second near-infrared window.* Proc Natl Acad Sci USA, 2011. 31;108(22):8943-8

20. Weber, J., Beard, P.C., Bohndiek, S.E. *Contrast agents for molecular photoacoustic imaging.* Nat Methods. 2016. 28;13(8):639-50

21. Boonstra, M.C., et al., *uPAR-targeted multimodal tracer for pre- and intraoperative imaging in cancer surgery.* Oncotarget, 2015. **6**(16): p. 14260-73.

22. van Dongen, G.A., G.W. Visser, and M.B. Vrouenraets, *Photosensitizer-antibody conjugates for detection and therapy of cancer.* Adv Drug Deliv Rev, 2004. **56**(1): p. 31-52.

23. Maawy, A.A., et al., *Photoimmunotherapy lowers recurrence after pancreatic cancer surgery in orthotopic nude mouse models.* J Surg Res, 2015. **197**(1): p. 5-11.

24. Gioux, S., H.S. Choi, and J.V. Frangioni, *Image-guided surgery using invisible near-infrared light: fundamentals of clinical translation.* Mol Imaging, 2010. **9**(5): p. 237-55.

25. Zhang, R.R., et al., *Beyond the margins: real-time detection of cancer using targeted fluorophores.* Nat Rev Clin Oncol, 2017. **14**(6): p. 347-364.

26. Themelis, G., et al., *Real-time intraoperative fluorescence imaging system using light-absorption correction.* J Biomed Opt, 2009. **14**(6): p. 064012.

27 Mansfield, J.R., *Distinguished photons: a review of in vivo spectral fluorescence imaging in small animals.* Curr Pharm Biotechnol, 2010. **11**(6): p. 628-38.

28. Valluru, K.S., Willmann, J.K., *Clinical photoacoustic imaging of cancer.* Ultrasonography, 2016. 35(4):267-80

29. van den Berg, N.S., et al., *First-in-human evaluation of a hybrid modality that allows combined radio- and (near-infrared) fluorescence tracing during surgery.* Eur J Nucl Med Mol Imaging, 2015. **42**(11): p. 1639-1647.

30. de Boer, E., et al., *A standardized light-emitting diode device for photoimmunotherapy.* J Nucl Med, 2014. **55**(11): p. 1893-8.

31. Gomer, C.J., *Preclinical examination of first and second generation photosensitizers used in photodynamic therapy.* Photochem Photobiol, 1991. **54**(6): p. 1093-107.

32. Derycke, A.S. and P.A. de Witte, *Liposomes for photodynamic therapy.* Adv Drug Deliv Rev, 2004. **56**(1): p. 17-30.

33. Sibani, S.A., et al., *Photosensitiser delivery for photodynamic therapy. Part 2: systemic carrier platforms.* Expert Opin Drug Deliv, 2008. **5**(11): p. 1241-54.

34. Sharman, W.M., J.E. van Lier, and C.M. Allen, *Targeted photodynamic therapy via receptor mediated delivery systems.* Adv Drug Deliv Rev, 2004. **56**(1): p. 53-76.

10

35.   Agostinis, P., et al., *Photodynamic therapy of cancer: an update.* CA Cancer J Clin, 2011. **61**(4): p. 250-81.

36.   Castano, A.P., P. Mroz, and M.R. Hamblin, *Photodynamic therapy and anti-tumour immunity.* Nat Rev Cancer, 2006. **6**(7): p. 535-45.

Nederlandse Samenvatting

Pre- en postoperatieve beeldvorming is gedurende de afgelopen eeuw een belangrijk onderdeel van de oncologische chirurgie geworden. In de klinische praktijk worden verscheidene beeldvormende modaliteiten zoals echografie, röntgen, CT, MRI, PET en SPECT gebruikt voor de vroegtijdige opsporing van tumoren, adequate stadiering en evaluatie van de behandeling. Hoewel er vele mogelijkheden van beeldvorming beschikbaar zijn preoperatief, is de chirurg peroperatief afhankelijk van zijn handen en ogen om tumor weefsel te onderscheiden van gezond weefsel. Hoewel de chirurg macroscopisch het idee kan hebben dat de tumor radicaal is verwijderd, blijkt toch dat de patholoog microscopisch een hoog percentage irradicaal verwijderde tumoren ziet. Het onvermogen de rand van de tumor te kunnen zien peroperatief kan van invloed zijn op het hoge percentage irradicaal verwijderde tumoren. Intra-operatieve beeldvorming waarmee de tumor onderscheiden kan worden van het omliggende gezonde weefsel kan ervoor zorgen dat het percentage radicaal verwijderde tumoren en daarmee de overleving van de patiënt toeneemt.

Fluorescentie geleide chirurgie (FGS) is een techniek die gebruik maakt van nabij-infrarood licht. Het geeft de chirurg peroperatieve visuele feedback over het weefsel van interesse. Nabij infrarood licht is noodzakelijk voor klinisch gebruik doordat dit licht het weefsel dieper penetreert en er bij deze golflengte geen verstoring is van autofluorescentie. FGS is uitgebreid onderzocht bij schildwachtklier procedures, anastomosen en cholecystectomiën. Het zou van grote waarde zijn als de chirurg door middel van fluorescentie tumor weefsel kan onderscheiden van gezond weefsel gedurende de operatie. De bewustwording van de potentie van FGS zorgde voor een exponentiele groei van het onderzoek dat vervolgens resulteerde in een groeiend aantal klinische trials. Echter blijft het targeten van tumoren een grote uitdaging, in het bijzonder vanwege de grote intra- en intertumorale heterogeniteit. Optische eigenschappen van weefsel maken daarnaast dat het detecteren van een enkele tumorcel een grote uitdaging zal blijven. Het doel van deze thesis is de preklinische validatie van twee nieuwe probes en de Artemis camera. Daarnaast zijn de eerste stappen gemaakt richting fluorescentie geleide peroperatieve fotodynamische therapie. Een behandeling waarmee gedurende de operatie eventuele overgebleven tumorcellen na chirurgische resectie kunnen worden behandeld.

In **deel 1** geven we een overzicht van de huidige status van FGS in de literatuur en kijken we naar de uitdagingen die het veld moet aangaan voor een succesvolle klinische introductie. In **hoofdstuk 2** wordt een uitgebreide uiteenzetting gegeven van de literatuur over preklinische en klinische fluorescentiegeleide chirurgie. In het bijzonder richtten we ons hier op tumor specifieke targeting van primaire tumoren door organische fluorescente probes. Na de uiteenzetting van de

10

huidige literatuur in hoofdstuk 2, gaat **hoofdstuk 3** terug naar de fundamentele basis principes van de optische beeldvorming. Hier worden de consequenties van deze principes voor FGS bediscussieerd en bekijken we welke invloed ze hebben op de klinische besluitvorming. We laten zien dat er beperkingen zitten aan de techniek maar vooral ook dat het een krachtig instrument kan zijn om de chirurg bij te staan en het aantal radicale tumor resecties te verhogen.

In <u>deel 2</u> vervolgen we met de preklinische studies. In dit deel onderzoeken we een tweetal probes die aangrijpen op twee interessante receptoren binnen de oncologie. Het eerste target in **hoofdstuk 4** is de epidermale groei factor receptor (EGFR). De EGFR is een transmembraan glycoproteine die is betrokken bij DNA synthese en cel proliferatie en waarbij overexpressie bijdraagt aan oncogenese. De EGFR komt veelal tot overexpressie bij orale plaveiselcelcarcinomen (OSCC). Om de EGFR specifieke probe te testen hebben we gekozen voor een orthotoop OSCC model van de tong die metastaseert naar de cervicale lymfklieren. In deze studie werd een nanobody geconjugeerd aan de fluorescente stof IRDye-800CW. Een nanobody is het kleinste antigen-bindende deel van een natuurlijk antilichaam met 1 zware keten. Ze binden zeer specifiek en de grootte van een nanobody zorgt voor een efficiënte distributie en weefsel penetratie, evenals een snelle klaring uit het lichaam. De FLARE NIR fluorescentie camera werd gebruikt in deze studie en vergeleken met preklinische camera's. Twee uur na injectie van 7D12-800CW waren de tumoren duidelijk zichtbaar. De tumor tot achtergrond ratio was significant hoger dan die van de controle probe. Een hogere dosis was nodig om lymfklier metastasen te zien. In deze studie lieten we de potentie zien van een nanobody in fluorescentie geleide chirurgie door gebruik te maken van een orthotoop tumor model en een klinische camera. Het target dat misschien nog interessanter is vanwege de expressie die verhoogd is in een groter aantal tumoren, is de EPCAM receptor in **hoofdstuk 5**. EpCAM is een transmembraan glycoproteïne die betrokken is bij de cel-cel interacties en cel-stroma adhesie. De expressie is beperkt tot epitheliale cellen en is verhoogd in nagenoeg alle epitheliale tumoren. Om de waarde van dit target binnen de FGS te bekijken conjugeerden we het monoclonale antilichaam 323/A3 aan IRDye 800CW. Dit conjugaat bleek stabiel in serum en specifiek te binden aan de EpCAM receptor, gemeten met flow cytometrie en plaat assays. Vier klinisch relevante orthotopische tumor modellen (peritonitis carcinomatosa en colorectale-, borst- en hoofd/hals- tumoren) werden gebruikt om deze probe samen met de Artemis camera te valideren. Alle tumoren waren goed te onderscheiden en konden met behulp van fluorescentie worden gereseceerd. Millimeter grootte tumoren werden gevonden die niet met het blote oog konden worden gezien. Tumor specificiteit werd bekeken met fluorescentie microscopie. In deze studie bewees EpCAM zich als universeel target binnen de FGS en werd een stap gezet naar klinische translatie. Uiteindelijk in deel twee, **hoofdstuk 6**, evalueren we de nieuwe Artemis camera in een preklinische en klinische setting. Als eerste in de literatuur wordt de Artemis camera klinisch gebruikt. We onderzoeken

preklinisch wat de minimale dosis ICG en IRDye 800CW is die de Artemis nog kan detecteren. Het minimum aantal cellen, geïncubeerd met 7D12-800CW, dat nog detecteerbaar was met de Artemis camera is 2x 10^5 versus 4 x 10^4 met de preklinische Pearl camera. Verder onderzoeken we de prestatie van de Artemis camera in relatie met de poortwacht klier procedure en tumor specifieke FGS. Hiervoor gebruiken we twee hoofd-hals kanker tumoren in combinatie met de probe 7D12-800CW. FaDu-luc2 tumoren vanaf 1 mm^3 konden gedetecteerd worden met de probe 7D12-800CW en de Artemis. De Artemis camera wordt in dit artikel klinisch gebruikt voor de detectie van levermetastases waarbij zes maligne tumoren werden ontdekt.

In **deel 3** ligt de focus op de toekomst van de fluorescentie geleide chirurgie. We onderzoeken hoe we tot een succesvolle klinische implementatie van FGS kunnen komen en of we ons doel van radicale tumor resecties behalen met een enkele tumor specifieke probe. **Hoofdstuk 7** beschrijft 3 grote uitdagingen binnen de FGS waarbij we vervolgens kijken naar de mogelijke oplossingen. De uitdagingen zijn tumor heterogeniteit, invasief groeiende tumoren en de optische eigenschappen van weefsel. De optische eigenschappen van weefsel zorgen ervoor dat het detecteren van een enkele tumor cel zeer onwaarschijnlijk zal zijn. Voornamelijk bij invasief groeiende tumoren kan dit ervoor zorgen dat tumoren irradicaal worden verwijderd. Het meten van de intrinsieke fluorescentie kan hiervoor een oplossing zijn. We beschrijven hoe punt reflectie en fluorescentie spectroscopie met het gebruik van fiber optische probes kan corrigeren voor het effect van de optische eigenschappen van weefsel. Zodoende zou een enkele tumorcel kunnen worden gedetecteerd. Een tweede oplossing is niet de detectie maar behandeling van de laatste tumorcellen met fotodynamische therapie (PDT). PDT wordt al gebruikt voor de behandeling van premaligne en maligne laesies. Vergeleken met andere adjuvante therapeutische modaliteiten, heeft PDT het voordeel dat er relatief weinig schade is aan normaal weefsel en er geen nadelige systemische effecten zijn. Verder beïnvloed PDT het effect van andere behandelingen niet en kan het herhaald worden indien nodig. Belangrijker echter is dat PDT gecombineerd kan worden met FGS waarbij er maar één probe gebruikt hoeft te worden. In **hoofdstuk 8** Onderzoeken we de mogelijkheden van tumor specifieke PDT en FGS. Tumor specifieke PDT kan het effect van de PDT enorm vergroten en de schade aan normaal weefsel nog meer reduceren. In deze preklinische studie kijken we naar het effect van PDT met de EGFR specifieke nanobody 7D12 geconjugeerd aan de water oplosbare fotosensitizer IRDye 700DX. Het construct is eveneens detecteerbaar met fluorescentie beeldvorming. We kijken naar de selectiviteit en fototoxiteit gebruik makende van een orthotopisch hoofd-hals tumor model. Het construct bindt specifiek aan cellen met een expressie van de EGFR en zorgt na belichting voor specifieke schade. Nog belangrijker zien we in deze studie dat er tot 90% schade optreedt in een muismodel waarbij er geen schade aan normaal weefsel ontstaat. De resultaten in deze studie laten zien dat het construct specifiek is en specifieke schade geeft aan tumoren met een over

10

expressie van de EGFR. In **hoofdstuk 9** bespreken we de stappen die nodig zijn om FGS succesvol en veilige naar de kliniek te brengen. De conclusie was dat FGS groot klinisch potentieel heeft en dat de klinische implementatie versneld kan worden als het veld samenwerkt.

Dit proefschrift onderzoekt het gebruik van fluorescentie geleide therapie binnen de oncologie. Initieel beschrijven we de preklinische validatie van twee targets en stoffen voor fluorescentie geleide chirurgie. Resultaten die de weg vrij maken voor een klinische translatie. Verder onderzoeken we de werkzaamheid van de nieuwe Artemis camera in een preklinische en klinische setting. Als laatste zetten we de eerste stappen richting een peroperatieve, multimodale fluorescentie geleide behandeling binnen de chirurgische oncologie met behulp van tumor specifieke fotodynamische therapie.

Een woord van dank

Professor Lowik, beste Clemens,

Een ontdekker puur sang. Het is absoluut een gave om buiten de kaders te denken en verschillende wetenschappelijke werelden bij elkaar te brengen. Jouw hunkering naar nieuwe ontdekkingen gecombineerd met je opportunisme en enthousiasme is wat mij betreft een enorme kwaliteit. Een korte vraag aan jou eindigde meestal in een college van 3 uur waarbij ik ondergedompeld werd in de wondere wereld van de moleculaire biologie. Ik ben zeer dankbaar dat je mij de kans hebt gegeven de wereld van de wetenschap te ontdekken. De avonden in het LUMC met wetenschap, pizza en bier zal ik nooit vergeten. We hebben de wetenschap kunnen combineren met vele borrels, congressen en ski-trips. Het heeft even geduurd, maar ik wil je bedanken voor een fenomenale tijd.

Alexander Vahrmeijer, beste Lex,

Het LUMC is een voorloper van de fluorescentie geleide chirurgie door jouw wetenschappelijke inspanning en ambitie. De klinische vertaalslag is inmiddels ruimschoots ingezet en hopelijk zal de fluorescentie geleide chirurgie zich de komende jaren klinisch bewijzen. Je weet continu een gezellige green light groep om je heen te verzamelen met een hoog wetenschappelijk niveau. Heel veel succes en bedankt voor een mooie samenwerking en de begeleiding gedurende mijn onderzoek.

Stijn Keereweer, Stinjo

Onderzoek doen met een goede vriend als jij was absoluut een zegen. Wij wisten als geen ander de wetenschap te combineren met plezier. Van bier en pizza in het LUMC tot wetenschappelijke discussies in de kroeg of in de sportschool. Juist deze discussies maakten de wetenschap levendig en vertaalden het preklinische onderzoek naar een klinische toepassing. "Denk in artikelen" is het eerste dat je me leerde, of in ieder geval dat ik heb onthouden. Je hebt de gave om rauwe natuurkundige en moleculair biologische materie op een heldere manier aan een breed klinisch publiek te presenteren. Een echte, kritische wetenschapper die ook nog eens enorm sociaal vaardig is, kan verbinden en onwaarschijnlijk scherp kan schrijven. De wetenschap samen was een mooi avontuur en ik hoop dat dit nog voort mag blijven duren. Je wordt een hele grote binnen de hoofd-hals chirurgie.

Thomas Snoeks,

Tijdens mijn wetenschapsstage en in het begin van dit promotieonderzoek was jij mijn houvast in de nieuwe wereld van de moleculaire biologie. Ik wil je bedanken voor een kritische blik en vooral mooie tijd.

Sabrina Oliveira,

De introductie met nanobodies die een belangrijk deel van mijn promotie vormden heb ik aan jou te danken. Als gedreven en zeer integere wetenschapper heb je mij naar een hoger niveau getild. Bedankt voor een vruchtbare samenwerking.

Dominic Robinson,

Met de introductie van fotodynamische therapie in mijn onderzoek kwam een mooie samenwerking tot stand met het Erasmus MC onder leiding van jou. Het was interessant en inspirerend om de natuurkundige kant van het onderzoek met licht te ontdekken. Ik heb enorm veel van je mogen leren. Succes met het vervolg onderzoek naar de combinatie van fluorescentie geleide chirurgie en fotodynamische therapie.

Mark Boonstra, Bony

De preklinische wetenschapper van de green light groep. De vele dagen in het muizen lab, in ons huis en avonden in de kroeg hebben de laatste jaren van mijn promotie zowel wetenschappelijk als persoonlijk veel moois gebracht. Ik heb enorm veel respect voor jouw discipline en doorzettingsvermogen. Dank voor een mooie en intense tijd.

Christian van Gaalen, fluim

Hoewel je bijnaam anders doet vermoeden bleek daar bij de hulp bij dit proefschrift niets van. Als 'native' heb je elke Engelse zin met veel interesse gelezen en met nog veel meer plezier gecorrigeerd als het naar jouw idee niet geheel correct was. Het was uitkijken naar het commentaar in de zijlijn dat ik elke keer lachend heb gelezen. Door de jaren heen ben je inmiddels ook medische inhoudelijk geschoold.. Dank voor een zeer waardevolle vriendschap die ik zal blijven koesteren.

Pien van Vierssen Trip & Joost von Schmidt auf Altenstadt, Pien & Joost

Een bijzondere eenheid en enorm (h)echte vriendschap. Zo waardevol en eentje die ik niet meer kan missen. Bedankt voor een onmisbare tijd en alvast voor alles wat gaat volgen de rest van ons leven.

Steef, Thomas, Frank, Kaz, Mark

We zijn een hecht jaar, zeer verschillend maar juist ook daarom is de vriendschap zo waardevol. Bedankt voor een hele mooie tijd, de steun tijdens mijn promotie en de herhaaldelijke vraag wanneer mijn verdediging eindelijk plaats zou vinden.

Wout, Dalibor, Leon, Henri, Thomas

Een vriendengroep als deze die bestaat sinds onze pubertijd en zo vanzelfsprekend is koester ik dierbaar.

Bart, Edin, Tomek, Maks

Wat was/is het een avontuur tijdens mijn opleiding en leven in Amsterdam. Een waardevolle en blijvende vriendschap.

Mijn ouders

Lieve pap en mam, wie ik ben heb ik in alles te danken aan jullie en de bagage die jullie me mee hebben gegeven. Ik ben enorm dankbaar voor jullie onvoorwaardelijke steun en interesse en kan me geen betere ouders wensen. Er komen nog veel mooie avonturen.

Zussen en broertje

Hoewel we aan de 4 uiteinden van het spectrum zitten is het een briljante eenheid. Lied, je bent zowel wetenschappelijk als persoonlijk een groot voorbeeld. Dierbare Charlot, door jouw tomeloze inzet is het een hechte eenheid. Art, broertje en beste vriend, je praatjes en intelligentie gaan je ver brengen.

Lieve Sanne

Ik ben dolblij dat jij in mijn leven bent gekomen en ben gek op je oprechtheid, temperament, eigenwijsheid, doortastendheid, moed en ambitie. Zonder je gaat niet meer.

Curriculum Vitae

Pieter Bastiaan Arie Antonius van Driel was born on May 18th 1985 in Arnhem, The Netherlands, as the first son of Antonius Hermanus Cornelis van Driel and Lydi Hendrina Irma Mathilde Zuiderent. In 2003 he graduated from Baudartius College, Zutphen, The Netherlands. In that same year he started his studies in psychology at Leiden University. In 2004 he switched to medical school at the Leiden University Medical Center. He did an internship family medicine in Curacao, at the Sentro Medico Stakamahachi, under supervision of Drs. Oleana-Ayoubi. During his studies he worked as a chief surgeon for non-heart beating bone and tendon explantations, at the foundation of Bio Implant Services in Leiden, The Netherlands. Next to this he worked for the council of Eurotransplant, Bio Implant Services and the Dutch Transplantation Foundation. After scientific research internship on photodynamic therapy, under the supervision of Prof. C.W.G.M. Löwik, PhD at Leiden University Medical Center, Pieter started in October 2010 as a PhD-student on the subject of Fluorescence-guided therapy at the deparment of Molecular Imaging at the Leiden University Medical Center and the Erasmus Medical Center. He was supervised byf Prof. C.W.G.M. Löwik, PhD, A.L. Vahrmeijer, MD, PhD and S. Keereweer, MD, PhD As a PhD student, Pieter initiated and participated in several research projects on the combination of photodynamic therapy and specific immunotherapy, multidiameter single fiber spectroscopy, fluorescence-guided surgery in orthopaedic oncology and fluorescence-guided imaging of the vascular supply to the meniscus with Prof F.A. Ossendorp, PhD, D.J. Robinson, PhD, Prof P.D.S. Dijkstra, MD, PhD and E.R.A. van Arkel, MD, PhD, respectively. Several of his studies were published in international medical journals and presented at international meetings on molecular imaging. In October 2013, he started as a clinical resident at the General Surgery department of the Sint Lucas Andreas Hospital, as the first part of the six-year trajectory to become an Orthopaerdic Surgeon. In April 2015 he continued with Orthopaedic surgery at the Haaglanden Medical Center and from April 2017 at the Leiden University Medical Center.

List of publications

Related to this thesis

Van Driel PBAA, Boonstra MC, Prevoo AJ, van de Giessen M, Snoeks TJ, Tummers QR, Keereweer S. Cordfunke RA, Lelieveldt BP, Dijkstra J, van de Velde CJ, Kuppen PJ, Vahrmeijer AL, Löwik CW, Sier CF. EpCAM as multi-tumour target for near-infrared fluorescence-guided surgery. BMC cancer, 2016 sept

van Driel PBAA, Boonstra MC, Slooter MD, Heukers R, Stammes MA, Snoeks TJ, de Bruijn HS, van Diest PJ, Vahrmeijer AL, van Bergen En Henegouwen PM, van de Velde CJ, Löwik CW, Robinson DJ, Oliveira S. EGFR targeted nanobody-photosensitizer conjugates for photodynamic therapy in a pre-clinical model of head and neck cancer. J Control Release. 2016 May 10;229:93-105.

van Driel PBAA, van de Giessen M, Boonstra MC, Snoeks TJ, Keereweer S, Oliveira S, van de Velde CJ, Lelieveldt BP, Vahrmeijer AL, Löwik CW, Dijkstra J. Characterization and evaluation of the artemis camera for fluorescence-guided cancer surgery. Mol Imaging Biol. 2015 Jun;17(3):413-23.

Snoeks TJ, **van Driel PBAA**, Keereweer S, Aime S, Brindle KM, van Dam GM, Löwik CW, Ntziachristos V, Vahrmeijer AL. Towards a successful clinical implementation of fluorescence-guided surgery. Mol Imaging Biol. 2014 Apr;16(2):147-51.

van Driel PBAA, van der Vorst JR, Verbeek FP, Oliveira S, Snoeks TJ, Keereweer S, Chan B, Boonstra MC, Frangioni JV, van Bergen en Henegouwen PM, Vahrmeijer AL, Lowik CW. Intraoperative fluorescence delineation of head and neck cancer with a fluorescent anti-epidermal growth factor receptor nanobody. Int J Cancer. 2014 Jun 1;134(11):2663-73.

Keereweer S, **van Driel PBAA**, Robinson DJ, Lowik CW. Shifting focus in optical image-guided cancer therapy. Mol Imaging Biol. 2014 Feb;16(1):1-9.

Keereweer S, **Van Driel PBAA**, Snoeks TJ, Kerrebijn JD, Baatenburg de Jong RJ, Vahrmeijer AL, Sterenborg HJ, Löwik CW. Optical image-guided cancer surgery: challenges and limitations. Clin Cancer Res. 2013 Jul 15;19(14):3745-54.

Other publications

S. Bosma, **P.B.A.A. van Driel**, P.C.W. Hogendoorn, P.D.S. Dijkstra, C.F.M. Sier
Introducing fluorescence-guided surgery into orthopaedic oncology: A systematic review of candidate protein targets for Ewing sarcoma. Submitted to Journal of Surgical Oncology

Boonstra MC, **van Driel PBAA**, Keereweer S, Prevoo HA, Stammes MA, Baart VM, Löwik CWGM, van de Velde CJH, Vahrmeijer AL, Sier CF. Preclinical uPAR-targeted multimodal imaging of locoregional oral cancer. Oral Oncol. 2017 Mar 66:1-8

Van Driel PBAA, van der Zwaal P. Een pijnlijke en gezwollen arm na krachttraining: verzuren tot aan rhabdomyolyse. Physios

Kleinovink JW, **van Driel PBAA**, Snoeks TJ, Prokopi N, Fransen MF, Cruz LJ, Mezzanotte L, Chan A, Löwik CW, Ossendorp F. Combination of Photodynamic Therapy and Specific Immunotherapy Efficiently Eradicates Established Tumours. Clin Cancer Res. 2016 Mar 15;22(6):1459-68.

Xie B, Stammes MA, **van Driel PBAA**, Cruz LJ, Knol-Blankevoort VT, Löwik MA, Mezzanotte L, Que I, Chan A, van den Wijngaard JP, Siebes M, Gottschalk S, Razansky D, Ntziachristos V, Keereweer S, Horobin RW, Hoehn M, Kaijzel EL, van Beek ER, Snoeks TJ, Löwik CW. Necrosis avid near infrared fluorescent cyanines for imaging cell death and their use to monitor therapeutic efficacy in mouse tumour models. Oncotarget. 2015 Nov 17;6(36):39036-49.

Boonstra MC, **van Driel PBAA**, van Willigen DM, Stammes MA, Prevoo HA, Tummers QR, Mazar AP, Beekman FJ, Kuppen PJ, van de Velde CJ, Löwik CW, Frangioni JV, van Leeuwen FW, Sier CF, Vahrmeijer AL. uPAR-targeted multimodal tracer for pre- and intraoperative imaging in cancer surgery. Oncotarget. 2015 Jun 10;6(16):14260-73.

van Leeuwen-van Zaane F, Gamm UA, **van Driel PBAA**, Snoeks TJ, de Bruijn HS, van der Ploeg-van den Heuvel A, Sterenborg HJ, Löwik CW, Amelink A, Robinson DJ. Intrinsic photosensitizer fluorescence measured using multi-diameter single-fiber spectroscopy in vivo. J Biomed Opt. 2014 Jan;19(1):15010.

van Leeuwen-van Zaane F, **van Driel PBAA**, Gamm UA, Snoeks TJ, de Bruijn HS, van der Ploeg-van den Heuvel A, Löwik CW, Sterenborg HJ, Amelink A, Robinson DJ. Microscopic

analysis of the localization of two chlorin-based photosensitizers in OSC19 tumours in the mouse oral cavity. Lasers Surg Med. 2014 Mar;46(3):224-34.

Keereweer S, **Van Driel PBAA**, Lowik CW. Preclinical studies on tumour-specific fluorescent targeting agents: the need for a gold standard of tumour localization. Mol Imaging Biol. 2014 Feb;16(1):10-2.

van Leeuwen-van Zaane F, Gamm UA, **van Driel PBAA**, Snoeks TJ, de Bruijn HS, van der Ploeg-van den Heuvel A, Mol IM, Löwik CW, Sterenborg HJ, Amelink A, Robinson DJ. In vivo quantification of the scattering properties of tissue using multi-diameter single fiber reflectance spectroscopy. Biomed Opt Express. 2013 Apr 9;4(5):696-708.

Van Driel PBAA, de Vos RJ, Thomassen BJW, van Arkel ERA. Resorptie van calcificaties bij een gluteus minimus tendinopathie na conservatieve behandeling. Nederlands Tijdschrift voor Orthopaedie.

Keereweer S, Mol IM, Vahrmeijer AL, **Van Driel PBAA**, Baatenburg de Jong RJ, Kerrebijn JD, Löwik CW. Dual wavelength tumour targeting for detection of hypopharyngeal cancer using near-infrared optical imaging in an animal model. Int J Cancer. 2012 Oct 1;131(7):1633-40.

Keereweer S, Kerrebijn JD, Mol IM, Mieog JS, **Van Driel PBAA**, Baatenburg de Jong RJ, Vahrmeijer AL, Löwik CW. Optical imaging of oral squamous cell carcinoma and cervical lymph node metastasis. Head Neck. 2012 Jul;34(7):1002-8.

Keereweer S, Mol IM, Kerrebijn JD, **Van Driel PBAA**, Xie B, Baatenburg de Jong RJ, Vahrmeijer AL, Löwik CW. Targeting integrins and enhanced permeability and retention (EPR) effect for optical imaging of oral cancer. J Surg Oncol. 2012 Jun 1;105(7):714-8.

Keereweer S, Mieog JS, Mol IM, **Van Driel PBAA**, Snoeks TJ, Baatenburg de Jong RJ, Vahrmeijer AL, Kerrebijn JD, Löwik CW. Detection of oral squamous cell carcinoma and cervical lymph node metastasis using activatable near-infrared fluorescence agents. Arch Otolaryngol Head Neck Surg. 2011 Jun;137(6):609-15.

Keereweer S, Sterenborg HJ, Kerrebijn JD, **Van Driel PBAA**, Baatenburg de Jong RJ, Löwik CW. Image-guided surgery in head and neck cancer: current practice and future directions of optical imaging. Head Neck. 2012 Jan;34(1):120-6.

Keereweer S, Kerrebijn JD, **van Driel PBAA**, Xie B, Kaijzel EL, Snoeks TJ, Que I, Hutteman M, van der Vorst JR, Mieog JS, Vahrmeijer AL, van de Velde CJ, Baatenburg de Jong RJ, Löwik CW. Optical image-guided surgery--where do we stand? Mol Imaging Biol. 2011 Apr;13(2):199-207.

PHD PORTFOLIO

Name PhD student:	Pieter Bastiaan Arie Antonius van Driel	
Erasmus Department:	Radiology, Optical Molecular Imaging	
PhD-period:	March 1st 2011- October 24 2018	
Promotor:	C.W.G.M. Löwik	
Co-promotor:	A.L. Vahrmeijer, S. Keereweer	

PhD training

Courses

	Animal experiments	2010
	Evidenced based Medicine	2015
	Basic course regulations and organization clinical researchers (BROK)	2015
	A multidisciplinary approach to the diagnosis of bone tumours	2017
	Clinical teaching	2017

Presentations

	European Molecular Imaging Meeting (EMIM)	1010-2014
	World Molecular Imaging Meeting (WMIC)	2013, 2015
	European Society of Molecular Imaging, winter conference, TOPIM	2011, 2013
	Congress of the European Society for Photobiology	2015

(Inter)national conferences

	European Molecular Imaging Meeting (EMIM)	2010 - 2013
	World Molecular Imaging Congress (WMIC)	2011, 2012, 2015
	European Society of Molecular Imaging, winter conference, TOPIM	2010-2014
	Surgical meeting, the Netherlands	2014
	Symposium Experimental Research Surgical Specialties (SEOHS)	2015

Teaching

	Supervising B. Sinterniklaas, bachelor thesis Biomedical Sciences	2012